Pharmaceutical polymorphism: An investigation using solid-state nuclear magnetic resonance spectroscopy

Susan Christina Campbell

Pharmaceutical Polymorphism: An Investigation Using Solid-State Nuclear Magnetic Resonance Spectroscopy

by

Susan Christina Campbell B.Sc. (Hons.), G.R.S.C., A.I.Mgt.

Trevelyan College

University of Durham

A thesis submitted in partial fulfilment of the requirements for the degree of Doctor of Philosophy

Department of Chemistry

University of Durham

1998

Pharmaceutical Polymorphism: An Investigation using Solid-state Nuclear Magnetic Resonance Spectroscopy

Susan C. Campbell B.Sc. (Hons.)

Submitted for the degree of Doctor of Philosophy

1998

Abstract

The study of two pharmaceutically active systems that each display polymorphism has provided a platform upon which to develop and apply solid-state NMR techniques in order to increase the understanding of the solid-state structure of small organic molecules. The multidisciplinary approach adopted has highlighted the advantages of solid-state NMR as a non-invasive probe of molecular conformation and crystallographic packing.

Carbon-13 CP/MAS spectra of the two polymorphs of BRL55834 - a fluorinated benzopyran derivative - immediately suggest the presence of one and three molecules in the asymmetric unit. A lack of crystals suitable for single-crystal XRD has catalysed the application of high-power powder X-ray diffraction studies. Subsequent attempts at structure solution using Genetic Algorithm techniques are showing preliminary results that reinforce predictions made from solid-state NMR. Novel triple-channel ^{19}F techniques have aided assignment and resolution of the complex ^{13}C CP/MAS spectra. Enrichment of the ^{15}N site appears to have resulted in the formation of a new polymorph. Techniques for the analysis of detection limits have been developed using solid-state Raman spectroscopy and chemometric analysis.

The aminoxanthine derivative, BRL61063, provides interesting inter-form variations in molecular disorder, solid-state packing, and hydrogen bonding. A previously basic understanding of the single-crystal XRD data has been further evaluated through the course of this Ph.D. and solid-state NMR spectral editing techniques have been developed and applied to identify these phenomena. Recrystallisation studies have produced two samples that appear to exist in an intermediate state between the rigid and mobile structural limits. Temperature variation causes interesting changes in the relaxation characteristics and natural abundance ^{15}N and ^{13}C CP/MAS spectra.

Residual dipolar coupling effects vary in their manifestation within the ^{13}C CP/MAS spectra of the polymorphic systems studied and comparison with the literature yields important information regarding molecular conformation. Nitrogen-15 enrichment and operation at higher magnetic field have been applied to reduce these second order effects. Finally, some distance has been travelled along the path towards decoupling ^{14}N. Future development of this technique holds potential for resolution enhancement in the solid state spectra of most naturally occurring, nitrogen-containing molecules.

Memorandum

The research presented in this thesis has been carried out in the Department of Chemistry, University of Durham, between October 1995 and September, 1998. Unless otherwise stated it is the original work of the author. None of this work has been submitted for any other degree.

Acknowledgements

First of all I would like to thank Professor Robin Harris for his support and open-mindedness, which have allowed me to cultivate an original approach to the Ph.D. and thus get so much more out of it all. Also, Martin Hardy of SmithKline Beecham Pharmaceuticals for giving up his time to impart valuable insight into the wider application of chemistry in the pharmaceutical industry.

During my research I have been fortunate to work with various people and benefit from their wide and varied areas of knowledge and expertise. At SmithKline Beecham these have included David Lee and David Busby (IR, Raman, DSC), Ute Gerhard (solution-state NMR), plus Geoff Badman (synthetic radioisotope chemistry). At Durham: Alan, Julia and Ian (solution-state NMR), David and Nicola (UDIRL solid-state NMR), Randal and Stella (IRC/ DSC) plus the crystallographers: Andres Goeta, Janet Moloney, Christian Lehman, and Andrei Batsanov, whose interest and enthusiasm, especially in the latter stages of my project has been greatly appreciated.

I am grateful for the funding that I have received from the EPSRC and SB including the opportunities to attend international conferences on both NMR and polymorphism, which have been very enjoyable and useful. I am particularly appreciative of the recent opportunity given to me by the RSC to attend the Nobel Laureates meeting in Lindau, Germany to 'mingle with the stars', an experience I'll certainly never forget!

The Durham 'NMR family' is a large and international one and I have enjoyed having the opportunity of working with these people: Gary (for the 'Scotland the Brave' flag), Gustavo and Claudia (for their Argentinian/Spanish teaching), Ulrich, Regis, Peter, Minoru, Marco, Shinji, Eric B., Philippe and Naser. Worth particular mention is Alison ('Big Al'), who provided so much theoretical and practical support (even in the times of undergraduate, broken-footed NMR); Eric H. and Barry, who have been so helpful throughout some of the more 'hair-raising' and 'hair-tearing' times of NMR experimentation; plus my fellow postgrads, Lindsey 'Stig' Crowe, Helen 'solution-state' Birkett, Stefan 'the curious' Reinsberg, and my two year-mates Julian ('Arnie') and Jon – thanks for the computer know-how and the sense-of-humour training, respectively!

For their sanity-retaining influence on the past three years of my life I'd like to mention people from Symphony Orchestra, the Graduate Ball Committee, the I.M. Certificate class, Gradsoc rowing club, and Trevelyan College (especially Julie Phipps and Judith Howard). Also Helen, Robbie, Swainey, Anna, Marie, Emma, Pete, Brian, Foggy, Mr. Gundy, Lise, Fiona, plus my various housemates at 'Eden cottage' including the more notable characters of Carrie, Andy, Angela, 'the Allisi' (Wiggy and Jonesy), Terry, Wod, Chris, Jon and Steve. I'd also like to mention Wiggy and Claire for that unforgettable mountain ascent – it's OK, I'll walk again!! For the madder moments when it was just necessary to restore sanity with a golf lesson or a trip to Newcastle, I'd like to thank Angela, my back-packing pal and fellow survivor of six years in Durham!

I would like to thank Romaan for his patience, and 'being there', especially at the times when it felt like nothing short of a miracle would be necessary to hit that deadline!

Finally I'd like to thank my whole family, especially Mum, Dad, Douglas, Jennifer, Hamish and Grandpa M for providing the foundation of love and support upon which all my achievements are based. Initially no one really understood what drove me towards the precipitous slope of chemistry and NMR, but maybe now if you read the first few pages of this thesis you'll see the connection. After spending almost 20 years of my life tormenting your eardrums by my various musical antics, I finally found a technique that would allow me to do, usefully, what the realms of music and only ten fingers could never permit ... hit all the 'notes' at the same time!

Supersoo

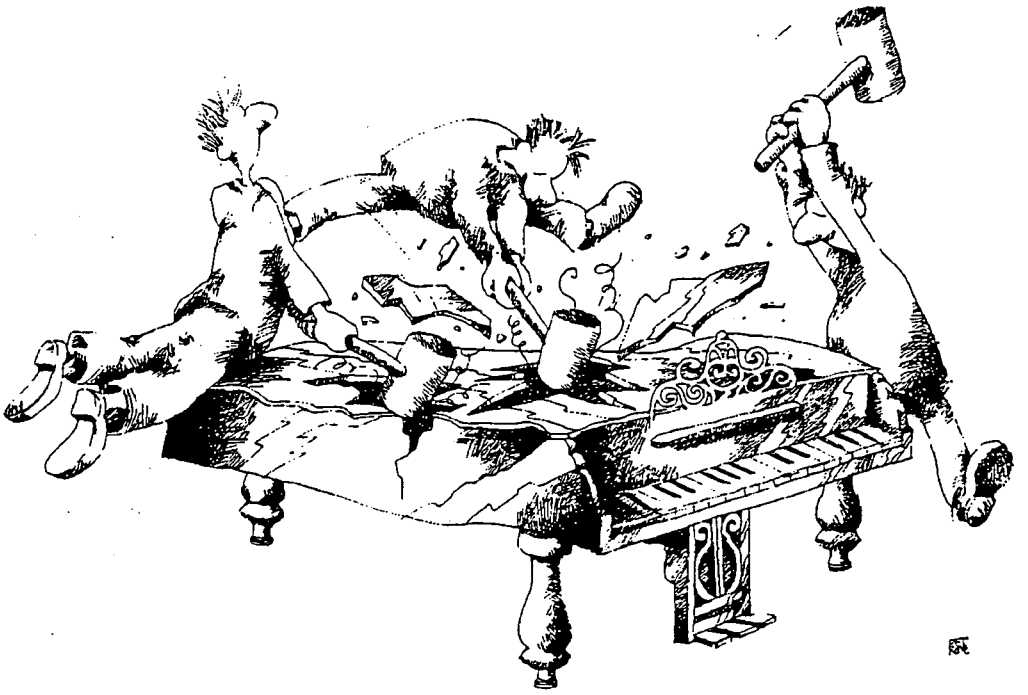

'Piano deconstruction' image and analogy to pulse FT-NMR reproduced with permission of Professor Ray Freeman

To my family

Table of Contents

Chapter 4

BRL55834 – A fluorinated organic compound

Chapter 6

Residual dipolar coupling and resolution enhancement

Abbreviations and symbols

NMR	Nuclear Magnetic Resonance
CSA	Chemical shift anisotropy
SA	Shielding anisotropy
CP	Cross polarisation
MAS	Magic-angle spinning
HH	Hartmann-Hahn
HPPD	High power proton decoupling
FT-IR	Fourier Transform Infra red
ATR	Attenuated total reflection
CRAMPS	Combined rotation and multiple pulse spectroscopy
DSC	Differential scanning calorimetry
T_1^x	Spin-lattice relaxation time of nucleus x
$T_{1\rho}^x$	Spin-locked relaxation time of nucleus x
T_{IS}	Cross polarisation time from the I to the S nucleus
T	Temperature
B_{1x}	Radiofrequency magnetic field associated with the x nucleus
B_o	The static magnetic field
BRL	Compound code prefix
CMX	Chemagnetics
AMT	Amplifier Technology
CE	Creative Electronics
UDIRL	University of Durham Industrial Research Laboratories
Kel-F	Proton-free polymer used in rotor accessories ~[CF2CFCl]~
Vespel	Fluorine-free polymer used in rotor accessories
FID	Free induction decay
PDMSO	Polydimethyldisiloxane
DMSO	Dimethylsulphoxide
TMS	Tetramethylsilane
DMF	Dimethylformamide
IPA	Isopropanol

BS	Bloch-Siegert
VT	Variable temperature
PTFE	Polytetrafluoroethylene (Teflon)
PXRD	Powder X-ray diffraction
XRD	X-ray diffraction
CW	Continuous wave
DEPT	Distortionless enhancement by polarisation transfer
COSY	Correlation Spectroscopy
HMBC	Heteronuclear multiple bond coherence
HMQC	Heteronuclear multiple quantum coherence
HETCOR	Heteronuclear Correlation
DQF	Double-quantum filtered
^{n}J	Scalar coupling constant through n bonds
SPE	Single pulse excitation
rf	Radiofrequency
TPPM	Two Pulse Phase Modulated decoupling
ϕ	Modulation angle of the decoupler in the TPPM sequence
τ_p	Pulse duration
τ_c	Cycle time
τ_r	Rotor period
r_{IS}	Distance (through space) between nucleus I and S
M_Z	Component of macroscopic magnetisation in the z direction
SB	SmithKline Beecham Pharmaceuticals
$P\bar{1}$, $P2_1/c$	Crystallographic space groups
FDA	Food and Drug Administration
ICH	International Conference for Harmonisation
PLS	Principle least squares analysis
PCR	Principle components regression analysis
DSA	Direct space approach
DARTS	Daresbury analytical research and technology service
GA	Genetic algorithm
SR	Synchotron radiation
RDC	Residual dipolar coupling

amu	Atomic mass unit
ppm	Parts per million
fwhh	Full width at half height
efg	Electric field gradient
APT	Attached proton test
NQS	Non-quaternary suppression
WISE	Wide line separation
SLF	Separated local field
Dipshift	Correlation of dipolar and chemical shift information
Cpflip	Cross polarisation with flip back
Cp4_pm	Cross polarisation with TPPM decoupling during acquisition
anDDecho	Dipolar dephasing with echo
uscp2dec	Cross polarisation with dual channel decoupling
sccslf3W	SLF with WAHUHA decoupling
1pulse	Single pulse with phase cycling
1pda	Single pulse with decoupling during acquisition
1pncyc	Single pulse with no phase cycling
gamircp	Inversion recovery cross polarisation
ant1rhohdec	Variable spin lock $T_{1\rho}$ experiment
t1xcp	CP version of the Freeman-Hill experiment to measure T_1^X
t1hcp	X-nucleus observed measurement of T_1^H
WAHUHA	Waugh-Huber-Haeberlen
BR-24	Burum-Rhim
MREV-8	Mansfield-Rhim-Elleman-Vaughan
DCP	Double cross polarisation
scchnhetcor	Version of DCP experiment allowing ^1H, ^{15}N correlation
rd	Recycle delay
ct	Contact time
ad	Acquisition delay
ppfn	Pulse program filename

I_j	Nuclear spin operator for nucleus j
χ	Quadrupolar coupling constant
D	Dipolar coupling constant
η	Asymmetry parameter
γ	Magnetogyric ratio
α^D, β^D	Euler angles
$\hat{H}$	Hamiltonian operator (subscripts indicate the nature of the operator)
θ	Angle between fixed molecular position and static magnetic field, B_o
β	Angle between rotor axis and B_o.
m	Magnetic quantum number
k	Boltmann constant
I	Spin quantum number
$\hbar$	Planck constant divided by 2π
ΔE	Energy difference
ν	Frequency / Hz
ω	Frequency / rad s^{-1}
n_α, n_β	Populations of the α and β spin states
e	Unit of elementary charge

Chapter 1

Introduction

1.1 Structure elucidation of solid-state pharmaceutical compounds

A large proportion of pharmaceuticals are administered or stored as solids in the form of tablets, powders or capsules. Since the solid-state structure of drug molecules plays a critical role in their function, efficiency and bioavailability, knowledge of the conformation and properties of the molecules in the finally-prescribed state is of prime importance to the manufacturer, drug regulatory authorities, and, of course, the patient!

It is the aim of the work presented in this thesis to use and develop the application of solid-state NMR as a structural analytical technique for organic, pharmaceutical compounds, particularly those that exhibit polymorphism[1].

In the process of carrying out this investigation, other techniques have been applied to the systems under study in order to explore the breadth of information available, and to support and reinforce the NMR results obtained. Techniques such as solid-state Raman spectroscopy, infrared spectroscopy, differential scanning calorimetry and X-ray diffraction have been used.

1.2 Polymorphism[2,3,4,5]

The ability of a molecule to crystallise in more than one form, exhibiting different crystals of the same substance with different unit cells and crystal packing arrangements is referred to as 'polymorphism'. For example, graphite, diamond and buckminsterfullerene are polymorphs (actually allotropes) of carbon. The ability of a molecule to crystallise in forms based upon the solvation state of the molecule is termed 'pseudopolymorphism'[6,7,8,9].

Polymorphs often possess differing physical and chemical properties. This has major implications for the pharmaceutical industry[10] since different polymorphic forms of drugs may possess very different bioavailabilities[1]. This may manifest itself in varying reactivity, solubility and transportation rates in the physiological conditions found within the body. Whilst a polymorph with low bioavailability may cause relatively little harm to a patient, the case in which the bioavailability of the polymorph is very great compared to the form prescribed may cause levels of the drug in the recipient's body to reach dangerously toxic levels thus potentially causing great harm: a highly undesirable result!

The drug 'chloramphenicol palmitate'[1] is an example of a drug that possesses polymorphs which differ enormously in their bioavailabilities. In this case the solubility is related to the rate of enzymatic attack on the solid.

It is therefore a major concern of many analytical techniques to be able to recognise any potential for polymorphism early on in the research and development process. This may then preclude ultimate tabletting, impurity and mixture problems that may lead to the resultant failure of the drug at a very late and thus expensive stage of development.

Stunning visible examples of the existence of polymorphism have been displayed by the tendency of some polymorphic forms to vary in their colour. This is exemplified by conformational polymorphism of 5-methyl-2-[(2-nitrophenyl)amino]-3-thiophenecarbonitrile[7]. This compound exists in five polymorphic forms including 'red', 'orange' and 'yellow', so-named due to the bright colour of their crystals. The colours may be attributed to the degree of electron delocalisation within the molecules, which is determined by the angles between the planes of the phenyl and the thiophene rings. These angles appear to correlate with the wavelength of the colour absorbed by each form. Colour polymorphism that is caused by differences in orientation and hydrogen-bonding characteristics has also been described by Fletton *et al*[11], who observed a yellow and a white form of 4-methyl-2-nitroacetanilide.

The formation of different polymorphs has also been related to the way in which the crystals form and the mode of nucleation. This can be influenced by solvent

composition, polarity, pH (especially for the formation of salts), or agitation, since hydrogen-bonding in aggregates in the solution can influence the initial nucleation state of the compound. Concentration or degree of saturation also affects which polymorph is formed. The supersaturation ratio may be taken as the ratio of the concentration of the solution to that of a saturated solution. When working on cimetidine, Sudo[12] showed that in isopropyl alcohol at high supersaturation ratio (greater than 3.6), form A crystallised spontaneously, or in the presence of seeds of A or B. However, in lower supersaturation ratios (less than 2) form A crystallised if there were A seeds present and form B if there were B seeds. This example also shows the influence of the addition or presence of seeds in the preparation solution.

Temperature effects including the cooling rate may also affect the polymorphic form produced. This is exemplified by the work of Kitamaru on L-glutamic acid. At 45 °C the α-form nucleates slowly, resulting in the growth of the β form. However, at 25 °C the α-form nucleates rapidly causing the α-form to be obtained.

Temperature-related studies have also been carried out to investigate the crystal growth and properties of paracetamol[13]. Results showed a variation in the thermodynamic and mechanical properties of the crystals.

Modern work (of York *et al.)* is using supercritical fluids in an attempt to control polymorph formation. Using a gas above its triple point as a solvent has the significant advantage of causing no solvent to remain once the sample has been cooled down, thus minimising the potential for any damaging formulation, pretreatment and product processing effects. The technique also appears to produce uniform samples that are particularly useful for inhalation delivery systems, as demonstrated by the direct preparation of microfine particles of pure forms of the polymorphs of salmeterol xinafoate for respiratory drug delivery[14].

Possession of a detailed knowledge and understanding of the presence of stable polymorphic forms of the drug in question makes it possible to obtain more accurate and comparable detail for the pure polymorphic forms themselves. This can be

especially advantageous if one particular polymorph has beneficial pharmaceutical properties.

An example of a positive result of early polymorphic recognition is the anti-ulcer drug 'Zantac' (Ranitidine), produced by Glaxo-Wellcome, which was the market leader in 1994, with sales of $3.657 billion US dollars[15]. The first thirteen batches that were created of this drug were form 1, following which form 2 was repeatedly created and form 1 could not be created again. This is a common complication with polymorphism issues[16].

The polymorphism issue is now having serious implications on patent law and intellectual property rights. A strategic approach[17] to the analysis of polymorphism has been published describing a conceptual approach to the characterisation of pharmaceutical solids. Through the use of flow charts, this article suggests a direct approach to the characterisation of pharmaceutical solids, with the ultimate aim of allowing faster approval of regulatory documents containing information on pharmaceutical solids.

Currently, ICH (the International Conference on Harmonisation of Technical Requirements for Registration of Pharmaceuticals for Human Use)[18] is working to bring together the regulatory authorities of the three main market regions of Europe, Japan and the US to define and standardise technical aspects of pharmaceutical product registration. Decision trees have been developed[18] describing how to detect whether a drug substance displays polymorphism, followed by a recommended approach for the analysis of the effects in a standard way.

Recently, large pharmaceutical companies have been able to take out subsidiary patents on desirable polymorphic forms to prolong the patent life of major products. In the case of Zantac, where the patent on the particular polymorph used may be held valid from 1995-2002 in many countries of the world, it can be appreciated that the financial incentives to investigate polymorphs are enormous.

This issue is particularly relevant with respect to the anti-ulcer drug 'Tagamet'[19] (cimetidine) produced by SmithKline Beecham Pharmaceuticals. This compound was identified as possessing two, and now four stable polymorphic forms, A, B, C and D.

1.3 Nuclear Magnetic Resonance – the technique

The NMR technique uses atomic nuclei as internal 'spies' to deduce information regarding structure, mobility and chemical reaction characteristics of molecules. These 'spies' use their highly sensitive nuclear magnetic moments to probe their environments whilst exerting negligible influence on the molecular properties that they interrogate.

There are three essential requirements for a NMR experiment: a strong static magnetic field (provided by a superconducting solenoid); a source of radiofrequency radiation to excite nuclei in the sample (generated by passing a sinusoidally oscillating current through a coil arranged round the sample which sits inside the magnet); and a method for detecting the NMR signal (incorporating a receiver coil, amplifier, and computer).

1.3.1 Basic principles of NMR

When a magnetic nucleus is placed in a magnetic field its nuclear magnetic moment causes it to adopt one of a small number of permitted orientations of different energy. In the case of this work, only spin-½ nuclei (^{13}C, ^{1}H ^{15}N and ^{19}F) have been observed which possess just two permitted orientations of the magnetic moment.

Spin angular momentum, **I**, is quantised by units of $\hbar = h/2\pi$ such that $|I| = [I(I+1)]^{1/2}\hbar$ where I is the spin quantum number. **I** is a vector quantity and has $2I+1$ projections onto the z axis. Thus the z component of **I** (I_z) is quantised, giving $I_z = m\hbar$ where m (the magnetic quantum number) has $2I + 1$ values in integral steps between +I and -I: m = I, I - 1, I - 2 ...- I..

The two states of the spin-½ nucleus, with permitted momentum components of $\pm ½ \hbar$, are separated by an energy, ΔE, which depends upon the interaction between the magnetic nucleus (i.e. the nuclear magnetic moment magnitude) and the magnetic field strength (see ***Figure 1***).

ΔE can be measured by applying electromagnetic radiation of frequency ν which causes the nuclei to 'flip' from the lower to the higher energy level, provided that the energy supplied satisfies the resonance condition of $\Delta E = h\nu$.

Every nucleus possesses a characteristic magnetic moment. Therefore ΔE, and thus the resonance frequency, are determined by the specific nucleus being observed as well as its chemical environment within the molecule. The chemical environment of specific nuclear sites is reflected in the 'chemical shift' of their associated resonances in the spectrum produced. Analysis of this spectrum therefore allows deductions to be made as to the chemical structure of the molecule.

1.3.1.1 Nuclear Magnetisation

The magnetic moment of a nucleus, μ, is also a vector quantity and is directly proportional to **I** with a proportionality constant γ, known as the magnetogyric ratio: $\mu = \gamma \mathbf{I}$, where μ may be parallel (γ +ve) or antiparallel (γ -ve) to the spin angular momentum **I**.

1.3.1.2 The effect of a Magnetic Field

In the absence of a magnetic field, all $2I + 1$ states of a spin-I nucleus have the same energy. When a magnetic field is applied, this degeneracy is removed such that the energy E in the magnetic field $\mathbf{B}_0$ is equal to $E = -\mu \cdot \mathbf{B}_0$.

In a strong field the quantisation axis z coincides with the field direction such that $E = -\mu_z B_0$ and thus overall $E = -m \hbar \gamma \mathbf{B}_0$. This means that the energy of the nucleus is shifted by an amount proportional to the magnetic field strength, magnetogyric ratio,

and the z component of the angular momentum. The energy states are spaced equally, with energy gap $\hbar\gamma B_0$ (see ***Figure 1***).

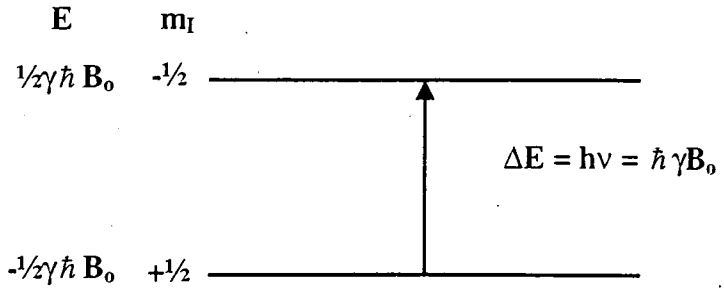

Figure 1 I= ½ nuclear spin energy levels for the case of +ve γ.

The NMR selection rule is $\Delta m = \pm 1$, only allowing transitions between adjacent energy levels. Thus the resonance condition is given by the equation $\Delta E = h\nu = \hbar\gamma B$, or $\nu = \gamma B/2\pi$.

When placed in a magnetic field, the collection of magnetic nuclei distribute themselves among the 2I+1 energy levels according to the Boltzmann Distribution, which may be expressed as $\frac{n_{upper} - n_{lower}}{n_{lower} + n_{upper}} = \frac{\Delta E}{2kT}$. As in any form of spectroscopy, an electromagnetic field excites the matter involved from the lower energy state to the upper one with the same probability as it induces the reverse transition, from excited to ground state. The net absorption of energy and hence the intensity of the spectroscopic transition is dependent upon the difference in populations of the two levels. In NMR spectroscopy, the upward transitions outnumber the downward ones by only one in 10^4-10^6, and therefore the signals are fairly weak. It is therefore of crucial importance to maximise ΔE by using strong magnetic fields to optimise signal strengths.

Since the magnetic field experienced by a nucleus in a molecule differs slightly from the external field, the exact resonance frequency is characteristic of the chemical environment of the nucleus.

1.3.2 Differences between solid- and solution-state NMR

The universal abundance of solution-state NMR spectrometers in chemistry laboratories reflects the high regard in which modern chemists hold this technique. However, dedicated solid-state spectrometers tend still to exist as 'stand-alone' pieces of equipment, housed in dedicated solid-state NMR groups and are not generally available to non-specialists. Possibly this will change with the time-related development of technology and education, but the current situation indicates the perception of the technique and data obtainable as possessing a higher common denominator of complexity when compared to solution-state NMR. However, this is the very aspect that makes solid-state NMR so very useful and intriguing and solid-state NMR is still in its infancy as applied to pharmaceutical problem solving.
The basic principles of NMR spectroscopy remain the same for both solids and liquids. However, whereas the molecules in liquids rotate rapidly, with frequent changes in the axis and speed of rotation as a result of collisions with other molecules, in solids the molecules are held fairly rigidly in fixed positions. Consequently, in solution the dipolar coupling interactions are rapidly modulated, causing linewidths of less than 1 Hz to result.

In the solid state, the dipolar interactions that remain facilitate the determination of intermolecular interactions and structural characteristics of the molecule in question by analysis of the solid-state NMR spectra.

It has been already established that the NMR signal is brought about by transitions between the nuclear spin energy levels. Thus, due to the dependence of NMR spectroscopy upon the property of nuclear spin, the exact energies of the transitions observed involve the nuclear spin Hamiltonian. This Hamiltonian contains terms that account for all the internal and external interactions of the spin system under study and can be expressed by the summation of the external and internal factors detailed below.

The external interactions are controlled by the experimentalist and are represented by the Zeeman term, $\hat{H}_Z$ (due to B_o, the static magnetic field of the spectrometer) and the effect of the rf magnetic field, $\hat{H}_{RF}$.

The internal interactions include $\hat{H}_{CS}$, $\hat{H}_Q$, $\hat{H}_{SR}$, $\hat{H}_D$, and $\hat{H}_J$, which represent the internal interactions of the nuclear spins with induced magnetic fields due to orbital electronic motions ($\hat{H}_{CS}$, chemical shift); electric field gradients ($\hat{H}_Q$, quadrupolar coupling); molecular moments associated with molecular angular momentum ($\hat{H}_{SR}$, spin rotation); mutually and directly, via magnetic dipole moments ($\hat{H}_D$, dipolar coupling); mutually but indirectly, through electrons ($\hat{H}_J$, scalar coupling).

In a liquid the isotropic averages of all but the shielding and the indirect spin-spin coupling tensors are zero due to the averaging brought about by rapid tumbling of the molecules. This is true due to the fact that each Hamiltonian (apart from the two that are named) possess isotropic averages of zero. This is caused by the orientational dependence factors of these Hamiltonians being $(3\cos^2\theta - 1)$ where θ can be taken to equal the angle between the static magnetic field, B_o and a local molecule-fixed direction.

Therefore, in solid-state NMR, the lines are much broader than those in liquid NMR mainly due to the dipole-dipole interactions. However, although the spectra are of much lower resolution, they contain much more valuable information. The question is how to extract it!

1.3.3 Problems and their solutions in solid-state NMR

Conventional utilisation of solution-state NMR data acquisition techniques on solid samples yields broad, featureless spectra. The following section outlines the three techniques that are used to overcome the problems posed by the solid state to yield highly-resolved 'solution-like' spectra of solids, which, though more complicated than solution spectra, contain much more information.

1.3.3.1 Problem: Chemical Shift Anisotropy (CSA)[20,21]

In a solid powder all the values of θ exist at random and the resulting spectrum forms a broad *powder pattern.* This appears as a broad envelope, the shape of which is dependent upon the symmetry of the molecule involved. If the molecule is axially symmetric then there will be two turning points arising from the parallel and perpendicular shielding tensor components, whereas for other, non-axially symmetric systems there will be three turning points in the envelope.

1.3.3.2 Solution: Magic Angle Spinning (MAS)[22,23,24,25]

By spinning the sample in the rotor at the 'magic angle' of 54.7 ° to B_o the term $(3\cos^2\theta\text{-}1)$ in the Dipolar Hamiltonian which causes line broadening for solids collapses to zero. Provided that the spinning frequency exceeds the maximum width of the chemical shift anisotropy of the compound this leaves a single isotropic peak for each type of nucleus. If the spinning speed is lower than the spectral width of the CSA then sidebands[35] will appear, equally spaced about the isotropic peak by multiples of the spinning speed. In some cases these are usefully analysed.

1.3.3.3 Problem: ^{13}C nuclei possess very long T_1 values[26,27,28,29]

Due to the rare nature of the ^{13}C nucleus, at only 1.108% natural abundance, the number of acquisitions required to achieve a good signal-to-noise ratio for a particular experiment is very great. This problem is compounded by the fact that the spin-lattice relaxation time (T_1) of ^{13}C in solids is often very long, sometimes of the order of hours! It should be noted that ^{13}C is used here as an example, but other nuclei (e.g. ^{15}N) can be treated similarly.

1.3.3.4 Solution 2: Cross Polarisation[30,31,32,33,34,35,36,37] *from abundant proton nuclei*

This method involves using the 'Cross Polarisation' technique whereby a 90 ° pulse is first applied to the proton channel and to spin-lock the ^1H magnetisation in the y direction of the rotating frame of reference. At this point, the ^{13}C radiofrequency is switched on under Hartmann-Hahn ($\gamma_H B_{1H} = \gamma_C B_{1C}$) matching conditions in order to allow good transfer of magnetisation by ensuring that the protons and the carbons are precessing at equal rates in their respective rotating frames of reference.

This sequence relies on the shorter T_1 of the abundant proton nuclei and therefore allows a much greater number of acquisitions in a given time, hence improving the signal to noise ratio.

1.3.3.5 Problem: large dipolar interactions give rise to broad spectra[38,39]

In the solid state, dipolar interactions are not averaged out as in the liquid. The magnitude of dipolar coupling is almost 1000 times greater than indirect (scalar) coupling and acts through space with a distance dependence proportional to $1/r^3$ i.e. not through bonding electrons as in scalar coupling. Dipolar interactions cause broadening of the spectral lines and thus should be removed in order to observe the chemical shift and indirect coupling information which is so useful in structure elucidation.

1.3.3.6 Solution: High Power Proton Decoupling (HPPD)

Whereas in the liquid state heteronuclear dipolar decoupling is effected by double irradiation techniques often requiring powers of only 1-2 Watts, in the solid state, due to the greater magnitude of the dominant dipolar broadening interaction, powers of 100-150 Watts are commonly required.

Homonuclear dipolar decoupling is not so straightforward to treat in the solid state as in solution since it is not feasible to decouple a proton signal whilst simultaneously decoupling at the same frequency. Thus, complex multiple-pulse techniques have been devised to overcome this problem. In these techniques, such as CRAMPS[54-57], the multiple-pulse scheme causes an 'averaging in spin space' by consecutively altering the phase of the radiation such that at specific points in the pulse sequence (detection points) the effects of the dipolar Hamiltonian on the magnetisation is zero and therefore homonuclear dipolar interactions are suppressed.

Overall therefore, with increased optimisation of experimental conditions and implementation of the above three fundamental techniques of MAS, CP and HPPD, modern solid-state spectra can provide the expermentalist with a plethora of results, with the high-resolution spectra now obtainable in many situations.

1.4 So why use solid-state NMR for pharmaceuticals research?

The efficiency and aptitude of solid-state NMR for the discovery of polymorphic characteristics is exemplified by the work of Byrn *et al.*[40], who used solid-state NMR to analyse prednisolone tablets that were on the market in 1993. This research immediately uncovered the existence of two different polymorphic forms within the commercially available brands. This led to further investigations which yielded a total of five stable polymorphic forms possessing variations in hydrogen-bonding characteristics! So why was NMR able to distinguish this information from drugs which had already passed stringent regulatory guidelines in order to reach the dispensaries?

Steroids seem to be particularly prone to give rise to polymorphic forms. Cortisone acetate[7,8] is a typical example. A substantial number of polymorphs and pseudopolymorphs are known, and seven have been studied[7,8] by solid state NMR. MAS NMR readily distinguishes the three anhydrous forms from the five hydrates and other solvates, and it also informs us that form III possesses three molecules in the crystallographic asymmetric unit. Conclusions can also be drawn about variations in the hydrogen bonding of the forms. What aspects of solid-state NMR allow this information to be retrieved so conveniently?

Since the electronic environments of corresponding atoms in different polymorphs differ, the NMR shifts will be distinguishable. Therefore, if more than one molecule exists in the asymmetric unit, unrelated by symmetry, then NMR signals will exhibit 'crystallographic splitting'. The differences in chemical shifts can arise from intra-molecular effects, including variation in geometry or conformation, or inter-molecular effects such as packing, hydrogen bonding, or the influence of neighbouring molecules.

It has been found that in some cases the final manufacture and work-up procedure required to produce drugs on a large scale may alter their polymorphic make up. Therefore, the fact that solid-state NMR is performed with minimal sample handling is in itself useful. It is possible to examine the final dosage form[41,42] using solid-state

NMR, whereas other techniques would require degradation of the sample in some way. Examining any differences that would be evident from the solid-state NMR spectra, can therefore assess the influence of excipients and different processing techniques[43] on the active molecules in the final dosage form. The potential for the application of solid-state NMR in this capacity is exemplified by studies performed on Aspirin in a complex mixture[44].

Powder X-ray diffraction is often the preferred technique for differentiating polymorphs. However this technique is not sensitive to poorly crystalline or amorphous forms. In industry IR is the technique that is looked to in the first instance[45]. Nujol mulls are used as the high pressures involved in alternative KBr disc methods may alter the polymorphic form. Single-crystal X-Ray Diffraction[2] is the definitive technique in some cases, but very often a suitable single crystal can not be grown, rendering this technique unavailable.

An advantage of solid-state NMR over diffuse reflectance IR and X-ray powder diffraction techniques is that it is a bulk technique that does not have to consider particle size effects upon the intensity of the measured signal. Differential Scanning Calorimetry may be used but this is very crude since it gives little or no chemical information. Infrared spectroscopy often suffers from lack of resolution and from difficulties in resolving intensities. NMR does not suffer from either of these problems.

Solid-state NMR generally requires a fairly small amount of powdered or crystalline sample that is not altered or destroyed in any way by the technique and thus is recyclable. By careful choice of experiments and manipulation of pulse sequences it is possible to obtain detailed information regarding crystal-packing arrangements[3], numbers of molecules in the unit cell[46], and both inter- and intra-molecular interactions. It is also possible, under the correct experimental conditions, to acquire quantitative[47] data, such that the intensity of the signal is directly proportional to the number of nuclei producing it.

The study of mobility in solids may also be usefully approached using solid-state NMR. The rate of relaxation of the ^{13}C spins towards equilibrium is characterised by

the spin-lattice relaxation time, T_1, whereby excess energy from the spin system is transferred to the lattice. Mobility studies can give valuable information about fast motions in the MHz range such as methyl group rotations. In polymer science the relaxation characteristics may be used to study main-chain and side-group motion[48]. In addition, studies have been made of the relationship between polymer crystallinity and relaxation parameters including T_1, $T_{1\rho}$, and T_2. These parameters may access a large range of timescales, from seconds (T_1), to milliseconds ($T_{1\rho}$) and μs (T_2). Measurements of T_1 and $T_{1\rho}$ have proved extremely useful in the work presented in this thesis.

The mobility of functional groups in solids is of great interest since this may lead to insight into the forces responsible for conformational interconversions, and the factors responsible for solid-state reactions. It has been suggested that solid-state degradations of pharmaceuticals are related to molecular mobility. This is exemplified by work carried out on the order/disorder transitions in potassium penicillin-V[49].

The detailed knowledge of all the polymorphic characteristics leads to the production of well-understood, accurately reproducible, stable and uniform batches of drugs for use in clinical trials.

Solid-state NMR is rapidly becoming a vital technique for use in intellectual property cases and patent law. The ability of the technique to 'fingerprint' the polymorph, whether in the bulk or dosage form, often provides the only source of proof of the presence of a particular polymorphic form.

1.5 Novel techniques – Fluorine

Ironically, all the problems in obtaining high-quality ^{19}F and relevant ^{13}C spectra are accentuated by the very properties that make fluorine such a favourable nucleus for NMR, namely high magnetic moment and 100 % natural abundance.

Magic-angle spinning (MAS) ^{19}F NMR spectra of partially fluorinated solid organic compounds are difficult to obtain with high resolution for two main reasons. Firstly, strong dipolar (^{1}H, ^{19}F) interactions are likely to exist, which cannot be simply overcome by MAS because of complications resulting from strong homogeneous (^{1}H, ^{1}H) dipolar coupling. High-power proton decoupling is therefore necessary, but work in this area has been inhibited by the fact that ^{1}H and ^{19}F resonance frequencies differ by only ca. 6%, so that highly efficient frequency isolation is required. However, ^{19}F-{^{1}H} spectra for organic solids with isolated fluorine nuclei have recently been obtained successfully[50,51]. The second problem arises when the solid system contains fluorine atoms in close spatial proximity, thus giving rise to strong (^{19}F, ^{19}F) dipolar interactions. Since these are homogeneous in nature, MAS is not as efficient an averaging technique as it is for heteronuclear dipolar interactions and for shielding anisotropy. Either very fast MAS or combined rotation and multiple pulse spectroscopy (CRAMPS) is required[52,53,54]. One aim of the work reported here was to see to what extent a combination of modest MAS rates (ca. 10 kHz) combined with high-power proton decoupling would suffice to give ^{19}F spectra capable of distinguishing between polymorphs containing perfluoroethyl groups. Obviously, ^{19}F spectra can be obtained much more rapidly than natural-abundance ^{13}C spectra and so in principle may be preferred for polymorph identification and quantitative analysis.

However, in most polymorphic systems of pharmaceutical interest, the number of fluorine atoms in the molecule is likely to be relatively small, so that more detailed information should be available from ^{13}C CP/MAS spectroscopy. Here, too, the existence of fluorines constitutes a drawback to obtaining high-resolution spectra with conventional techniques, i.e. with two-channel spectrometers using proton decoupling. In the first place ^{19}F, ^{13}C isotropic indirect coupling can complicate spectra. Secondly, the effects of homogeneous ^{19}F, ^{19}F dipolar interactions result in broadened ^{13}C lines at modest MAS rates. Of course, high-power continuous-wave or multiple-pulse ^{19}F decoupling can overcome both problems, but clearly when protons are also present in the molecule this requires triple-channel ^{13}C-{^{1}H, ^{19}F} operation. Suitable spectrometers and probes have only recently become available, but few applications to systems of pharmaceutical interest have yet been reported.

1.6 Compounds studied

The work contained in this thesis concentrates upon two compounds of pharmaceutical interest, which each exist in a number of polymorphic forms. In all cases, the polymorphism has arisen as a result of recrystallisation of the sample in different solvents. The difference between the compounds' structural characteristics encouraged concentration on different aspects of NMR for the two systems.

The first system (named BRL55834), is a fluorinated benzopyran derivative. The work on this compound has concentrated upon resolution enhancement and assignment of the ^{13}C NMR spectra of the two polymorphic forms. The presence of a perfluoroethyl group has also provided an excellent opportunity for the application of novel fluorine and triple-channel NMR techniques. This compound also demonstrates the effectiveness of the NMR technique for identifying the number of inequivalent molecules in the asymmetric unit of the unit cell since this characteristic varies between the two forms.

The second system (BRL61063) provides a good example of Mitscherlich's theory (1822 AD): 'the number of polymorphs in existence is directly proportional to the amount of time spent looking for them'! It is the comparative mobility characteristics of these polymorphs that make this system particularly interesting and experiments have been carried out at variable temperatures to compare the relative mobility characteristics of the polymorphs. The knowledge of crystallographic data for the forms previously identified by SmithKline Beecham allows important structural comparisons to be drawn based on the solid-state NMR results for the newer polymorphs.

The presence of five nitrogen sites in the molecules of the second polymorphic system encourages the study of this system to be approached using the ^{15}N sites to probe the molecular characteristics. The ^{15}N nucleus, of lower natural abundance than its counterpart ^{14}N, has sharper NMR signals that are capable of yielding nuclear shielding, spin-spin coupling, and relaxation data. The less efficient nuclear relaxation processes, such as those arising from dipole-dipole or chemical shielding anisotropy,

normally control ^{15}N relaxation. It is the large extent of the ^{15}N NMR chemical shift range that causes ^{15}N NMR to be so useful as a structure determination technique. The nitrogen lone-pair electrons appear to be responsible for providing the shielding sensitivity to subtle molecular interactions. (A similar shielding sensitivity does not always appear to be experienced by a number of commonly studied NMR nuclei such as ^{1}H and ^{13}C.)

The temperature-related properties of these polymorphs are of particular relevance for their stability for pharmaceutical applications.

1.7 References

1 T. L. Threlfall, Analyst, **120**, 1995.

2 J. A. Davies, S. G. Dutremez, A. A. Pinkerton, *Magn. Reson. Chem.*, **31**, 435, 1993.

3 D. Casarini, R. K. Harris, A. M. Kenwright, *Magn. Reson. Chem.*, **31**, 540, 1993.

4 R. K. Harris *'Polymorphism and related phenomena' Encyclopedia of NMR,* Eds. D. M. Grant and R. K. Harris, Wiley, **6**, 3734, 1996.

5 S. R. Byrn, R. Pfeifer, G. Stephenson, D. W. Grant, W. B.Gleason, *Chem. Mater.*, **6**, 1148, 1994.

6 S. R. Byrn, G. Gray, R. R. Pfeiffer, J. Frye, *J. Pharm. Sci.*, **74**, 5, 565, 1985.

7 G. A. Stephenson, T. B. Borchardt, S. R. Byrn, J. Bowyer, C. A. Bowyer, C. A. Bunnell, S. V. Snorek, L. Yu, *J. Pharm. Sci.*, **11**, 1385, 1995.

8 R. K.Harris, A. M. Kenwright, B. J. Say, R. R. Yeung, R. A. Fletton, R. W.Lancaster, G. A. Hardgrove, *Spectromchimica Acta.*, **46A**, 6, 927, 1990.

9 E. A. Christopher, R. K.Harris, R. A. Fletton, *Solid State Nucl. Magn. Reson.*, **1**, 93, 1992.

10 L. Lamartina, D. Spinelli, F. Guerrera, M. C. Sarvá, *Mag. Reson. Chem.*, **33**, 883, 1995.

11 R. A. Fletton, R. W. Lancaster, R. K .Harris, A. M. Kenwright, K. J. Packer, D. N. Waters, A. Yeadon., *J. Chem. Soc. Perkin Trans.* 2, 1705, 1986.

12 S. Sudo, K. Sato, K. Harano, *Y. J. Chem. Eng. Jpn.*, **24**, 628, 1991.

13 B. Y. Shekunor, M. E. Aulton, R. W. Adamah-Acquah, D. J. W. Grant, *J. Chem. Soc. Faraday Trans.*, **92**, 3, 439, 1996.

14 P.York, *Conference proceedings 'Polymorphism and solvates-dosage form design and processing', British Pharmaceutical Conferemce,* Scarborough, 18th September, 1997.

15 Financial Times Survey on Pharmaceuticals Monday, March 25th, 1996.

16 J. Bernstein, 'Disappearing polymorphs', conference proceedings, RSC National Congress, Durham, 1998.

17 S. R. Byrn, R. Pfeiffer, M. Ganey, C. Hoiberg, G. Poochikan, *Pharm. Res.* **12**, 7, 1993.

18 ICH web site www.pharmweb.net/pwmirror/pw9/ifpma/ich1.htm

19 M. J. Hardy, personal communication, 1998.

20 M. J. Duer, C. Stourton *Bull. Magn. Reson.*, **17,** 1-4. 27, 1995.

21 R. J. Iuliucci, D. M. Grant *Solid State NMR,* **6,** 55, 1996.

22 E. O. Stejskal, J. Schaefer, J. S. Waugh, *J. Magn. Reson.*, **28,** 105, 1977.

23 M. Goldman, V. Fleury, M. Gueron, *J. Magn. Reson. A.*, **118,** 11, 1996.

24 T. J. Bonagamba, H. Panepucci, E. A. Vidoto, E. L. G. Vidoto, *Bull. Magn. Reson.*, **17,** 1-4, 286, 1992.

25 T. Mildner, H. Ernst, D. Freude, *Solid State NMR,* **5,** 269, 1995.

26 R. K. Harris, *'Nuclear Magnetic Resonance - A Physicochemical View' Longman Scientific and Technical,* Ch. 6.

27 C. L. Khetrapal, B. S. A. Kumar, K. V. Ramanthan, N. Suryaprkash, *J. Magn. Reson.* **73,** 516, 1987.

28 M. H. Maricq, J. S. Waugh, *J. Chem. Phys.*, **70,** 7, 1979.

29 A. Pines, M. G. Gibby, J. S. Waugh, *J. Chem. Phys.*, **59,** 2, 1973.

30 P. Tekely, V. Gerardy, P. Palmas, D. Canet, A. Retourard, *Solid State NMR,* **4,** 361, 1995.

31 J. Zhou, C. Ye, *Solid State NMR,* **5,** 213, 1995.

32 F. Engelke, *'Cross Polarisation in rotating solids: Spin ½ nuclei' Encyclopedia of NMR*, Eds. D. M. Grant and R. K. Harris, Wiley, **2**, 1529, 1996.

33 A. C. Kolbert, A. Bielecki, *J. Magn. Reson. A,* **116,** 29, 1995.

34 R. Pratima, K. V. Ramanthan, *J. Magn. Reson. A.*, **118,** 7, 1996.

35 S. Hediger, B. H. Meier, R. R. Ernst, *J. Chem. Phys.*, **102,** 10, 1995.

36 D. P. Burum *'Cross Polarisation in Solids' Encyclopedia of NMR,* Eds. D. M. Grant and R. K. Harris, Wiley, **3**, 1535, 1995.

37 A. Bax, N. M. Svzerenyi, G. E. Maciel, *J. Magn. Reson.*, **50,** 227, 1982.

38 R. E. Wasylishen, *'Dipolar and indirect Coupling Tensors in Solids' Encyclopedia of NMR,* Eds. D. M. Grant and R. K. Harris, Wiley, **2**, 1685, 1996.

39 M. H. Levitt, D. P. Raleigh, F. Creuzet, R. G. Griffin, *J. Chem. Phys.*, **92,** 11, 1992.

40 S. R. Byrn, R. R. Pfeiffer, G. Stephenson, D. W. Grant, W. B. Gleason, *Chem. Mater.*, **6**, 1148, 1994.

41 P. J. Saindon, N. S. Cauchon, P. A. Sutton, C. J. Chang, G. E. Peck, S. R. Byrn, *Pharm. Res.*, **10**, 12, 1993.

42 G. A. Stephenson, J. G. Stowell, P. H. Toma, D. E. Dorman, J. R. Greene, S. R. Byrn, *J. Am. Chem. Soc.*, **116**, 13, 5776, 1994.

43 D. E. Bugay, *Pharm. Res.*, **10**, 3, 317, 1993.

44 C. Chang, L .E. Diaz, F. Morin, D. M. Grant, *Magn. Reson. Chem.*, **27**, 768, 1986.

45 M. J. Hardy, SmithKline Beecham Pharmaceuticals, personal communication.

46 S. C. Campbell, R. K. Harris, M. J. Hardy, D. C. Lee, D. J. Busby, *J. Chem. Soc. Perkin Trans. 2,* 1913, 1997.

47 R. K. Harris, *Analyst,* **110**, 649, 1985.

48 S. Doyle, R. A. Pethrick, R. K. Harris, J. M. Lane, K. J. Packer, F. Heatley, *Polymer*, **27**, 19, 1986.

49 J. Fattah, J. M. Twyman, S. J. Heyes, D. J. Watkins, A. J. Edwards, K. Prout, C. M. Dobson, *J. Am. Chem. Soc.*, **115**, 5636, 1993.

50 S.A.Carss, PhD. Thesis, Durham University, 1995.

51 R.K.Harris, P.Jackson, *Chem. Rev.*, **91,** 1427, 1991.

52 J.M.Miller, *Progr. NMR. Spectrosc.*, **28** 255, 1996.

53 K.Kimuru, A.Naito, H.Saito, N.Satoh, *Bull. Magn. Reson.*, **17,** 1-4, 1993.

54 B.C.Gerstein 'CRAMPS' *Encyclopedia of NMR,* Eds. D.M.Grant and R.K.Harris, Wiley, **3**, 1501, 1996.

Chapter 2

Experimental

2.1 Solid-state NMR spectrometers

The majority of solid-state NMR experiments were performed using a Chemagnetics CMX 200 spectrometer, operating at 200.13 MHz for protons. This spectrometer is controlled by a Sun workstation running the Chemagnetics 'Spinsight' software. There are four amplifiers that are accessible to this spectrometer. These include: a middle frequency broad-band AMT (6-220 MHz); a low frequency broad-band AMT (30-122 MHz); a narrow-band CE amplifier (188-200.13 MHz), plus a narrow-band Bruker amplifier which usually operates in the 188-200.13 MHz frequency range, but can be altered to cover other narrow frequency bands by swapping the final-stage amplifier box. The low-frequency AMT requires blanking when used in pulse sequences due to the way in which it calculates its duty cycle. Altering relevant amplitude parameters on the software control panel may control all amplifiers except the Bruker. The output power of the amplifiers may be measured by connecting the output to an oscilloscope, measuring the peak-to-peak voltage and then converting this to Watts by reading values off a conversion chart.

Some higher-field solid-state NMR experiments have also been carried out in order to improve resolution at Durham Industrial Research Laboratories (I.R.L) using a Varian Unity Plus spectrometer operating at 300 MHz for protons.

2.1.2 Probes

Four Chemagnetics MAS probes were used during the course of this Ph.D. research, comprising two double and two triple channel probes. Each probe possesses a spinning module that can be oriented at the magic angle, and accepts a zirconia rotor. Although the

dimensions of the rotor may alter between the different probes, the basic sample set up is similar in all cases.

With drive tip and spacer firmly in place, the powder sample is packed into the rotor and compressed gently with the packing tool. An end cap is then also pushed into the top of the rotor. A continuous black line is then drawn around a portion of the outside top of the rotor to enable the tachometer to read the MAS rate of the rotor.

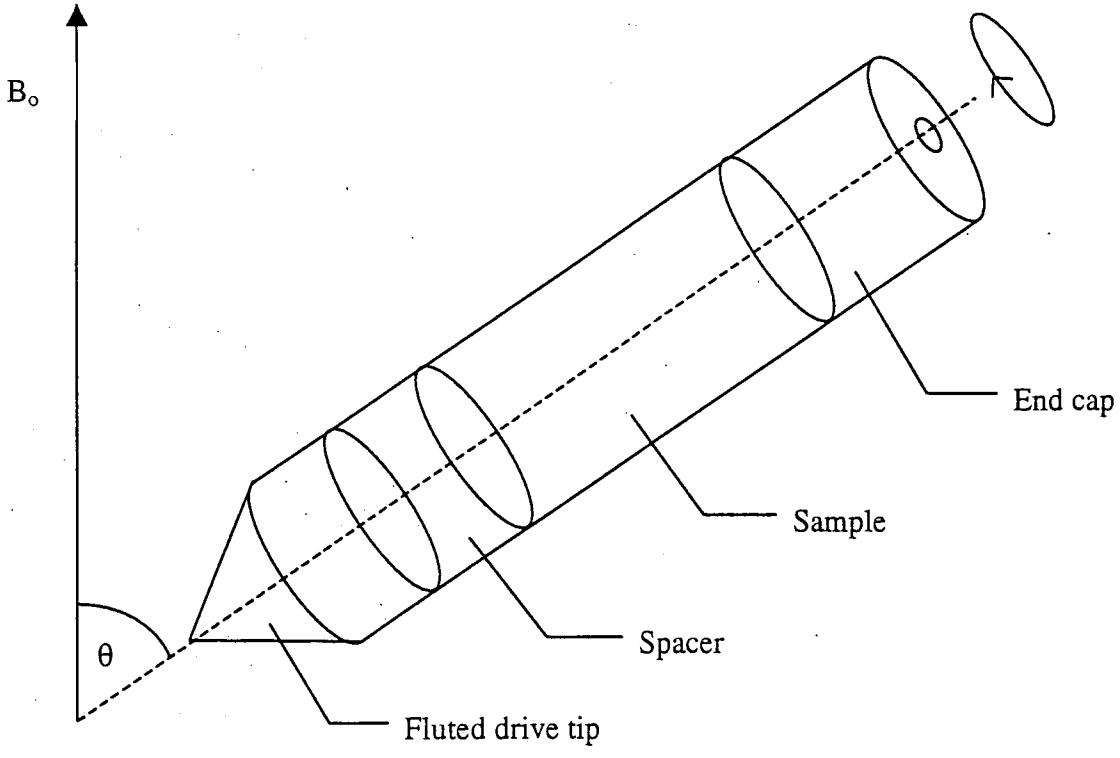

Figure 1 Schematic of a standard rotor as placed inside a CMX probe (θ is the magic angle and B_0 is the static magnetic field).

2.1.2.1 The HX probe

This double-channel probe operates for the proton channel at 200.13 MHz while the X channel may be altered through adding 'plug-in' top and bottom capacitors within the frequency range of 19.2 MHz to 82.6 MHz. The spinning module accepts 7.5 mm

zirconia rotors, for which the drive tip is made from Kel-F, with Teflon for the end cap and spacers leaving a sample length of 1.5 cm. The MAS rate can range up to 6.5 kHz.

A proton decoupling power of ~60 kHz is generally used. Filters suitable for the nuclei being observed, for example a 200 MHz band-pass filter and a 100 MHz low-pass filter for the proton and carbon channels respectively are required for standard cross polarisation and single pulse excitation experiments.

2.1.2.2 The HF probe

This probe was purpose-built by Chemagnetics to facilitate proton or fluorine observation with simultaneous decoupling of the other nucleus and was the first of its type in the UK due to the previously insurmountable challenge provided by the close proximity of the proton and fluorine Larmor frequencies.

Minimum radiofrequency breakthrough between the two channels is ensured by tuning and setting the traps on each channel by viewing the output of each channel on an oscilloscope whilst tuning the other channel. The trap is then adjusted until a node (minimum) is observed in the centre of the oscilloscope signal, at which point breakthrough is minimised and experiments may proceed.

Proton and fluorine high-power band-pass filters are used, with a proton decoupling power of approximately 100 kHz being standard.

The probe's spinning module accepts zirconia rotors of 4 mm outer diameter. The drive tip is made of Vespel whereas the end cap and spacers used depend upon the nucleus of observation. Teflon end caps and spacers are employed during experiments where proton spectra are acquired, and Vespel is used during fluorine observation experiments. It is sensible to restrict the sample in the centre of the rotor (to 3.5 mm) in order to minimise the effects of inhomogeneity in B_1.

The module is capable of spinning rotors up to ~18 kHz, and for experiments requiring slow spinning, such as CRAMP spectroscopy, a smooth drive tip is used.

2.1.2.3 The HFX probe

This triple-channel probe allows the nucleus X to range from 19.7 MHz to 102.2 MHz, with simultaneous or individual proton and fluorine decoupling. One other advantage is its ability to facilitate cross polarisation from fluorine to the other nuclei, as well as the more usually accepted proton-to-X CP.

Isolation between the proton and fluorine radiofrequency channels is optimised via an adjustable fluorine trap and a fixed proton trap. Only the standard 200 MHz filters are required for the proton and fluorine channels of this probe (as opposed to the high power band-pass filters required for the HF probe) since we are not observing one of these high-frequency, close nuclei whilst decoupling the other.

The HFX probe accepts 7.5 mm zirconia rotors which can be spun up to ~6.5 kHz. The choice of the material of the drive tip and end cap that are used in carbon CP experiments depends on whether CP is from proton or fluorine. Therefore, Kel-F is used for proton-to-carbon CP, whereas Vespel is used for CP from fluorine. Boron nitride spacers are used at the top and bottom of each rotor to restrict the sample.

Proton and fluorine decoupling powers typically of ~56 kHz are used.

Two new top capacitors were purchased, to enable observation of ^{15}N spectra with proton and fluorine decoupling.

2.1.2.4 The HXY probe

This triple-channel probe may also be referred to as the HML probe (High, Medium and Low probe) and has been used during the course of this Ph.D. for the ^{1}H, ^{13}C and ^{15}N nuclei. Considerable time has also been taken during the course of this research project, to modify the available set up in order to facilitate ^{14}N capabilities on the low channel. Before any experiment may take place the probe must be partially dismantled and a new capacitor arrangement may be added in. This involves carefully fixing in the following: a front capacitor, which isolates the low frequency from the middle frequency; a back capacitor that is necessary in order to tune the low-frequency side of the probe in the lower part of its range; plus a trap, which is a coil and capacitor arrangement serving the function of isolating the middle frequency from the lower frequency.

The spinning module in the HXY probe accepts rotors of 5 mm outer diameter and can spin up to a maximum of 12 kHz.

2.2 Magic Angle Spinning

The spectrometer allows automatic or manual control of the spinning speed by altering the bearing and drive air pressures entering the spinning module. The spinning speed can be controlled to ± 1 Hz.

2.2.1 Background

In solids, molecules are held rather rigidly such that dipolar interactions are not averaged to zero as they are in liquids. If scalar coupling and shielding are ignored the nuclear spin Hamiltonian becomes the sum of the Zeeman and dipolar terms. For a two-spin heteronuclear AX spin system this may be written as:

$$h^{-1}\hat{H}_{NS} = (-\nu_A \hat{I}_{AZ} + \nu_X \hat{I}_{XZ}) + h^{-1}\hat{H}_{dd}$$

where ν represents the Larmor frequency and $\hat{H}_{dd}$ is the dipole-dipole Hamiltonian. Only term A of the alphabetical expansion of the dipolar Hamiltonian (see chapter 6) is effective, since Zeeman energies are much larger than dipole energies. Thus the truncated Hamiltonian becomes:

$$h^{-1}\hat{H}_{NS} = -(\nu_A \hat{I}_{AZ} + \nu_X \hat{I}_{XZ}) + R\hat{I}_{AZ}\hat{I}_{XZ}(3\cos^2\theta - 1).$$

The energies of the spin states are:

$$h^{-1}U = -(\nu_A m_A + \nu_X m_X) - Rm_A m_X(3\cos^2\theta - 1).$$

The usual selection rules apply, so that for a single crystal with only one orientation for r_{AX} there are two *A* transitions at:

$$\nu = \nu_A \pm \tfrac{1}{2}R(3\cos^2\theta - 1)$$

and corresponding X lines with doublet splitting $R(3\cos^2\theta\text{-}1)$.

For a homonuclear pair of nuclei, the Zeeman energies of the αβ and βα states are equal. Thus, term B of the dipolar Hamiltonian must be included and the expression becomes:

$$h^{-1}\hat{H}_{NS} = -\nu_O(\hat{I}_{AZ} + \hat{I}_{BZ}) - R(3\cos^2\theta - 1)\left[\hat{I}_{AZ}\hat{I}_{BZ} - \tfrac{1}{4}\left(\hat{I}_{A+}\hat{I}_{B-} + \hat{I}_{A-}\hat{I}_{B+}\right)\right]$$

The flip-flop term mixes the αβ and βα states. The eigenvalues are the symmetric and antisymmetric combinations $(\alpha\beta \pm \beta\alpha)/\sqrt{2}$. Only a pair of lines is observed for a single crystal with one orientation of r_{AB} at:

$$\nu = \nu_A \pm \tfrac{3}{4}R(3\cos^2\theta - 1)$$

and a doublet of spacing $\frac{3}{2}R(3\cos^2\theta - 1)$ is seen.

Thus, since all terms in the dipolar Hamiltonian which cause NMR line broadening involve the factor $(3\cos^2\theta\text{-}1)$, by spinning at the angle, β, for which $\cos\beta = 1/\sqrt{3}$ (i.e. 54.7°), these contributions will be scaled to zero[1,2].

However, in a solid, all microcrystallites exist in random orientations. Thus, one nuclear magnetic dipole is coupled to a number of neighbours. Whatever the sample orientation,

if one pair is at the magic angle, the others will usually not be. Therefore MAS provides a clever manipulation whereby the dipolar interaction between all pairs is removed at once.

Therefore: $\langle 3\cos^2\theta - 1\rangle = \frac{1}{2}(3\cos^2\beta - 1)(3\cos^2\chi - 1)$ where χ is fixed for a rigid solid and takes all possible values in a powder; β may be set by the experimentalist and θ is the value of each specific angle between B_o and r.

By rotation of the rotor at 54.7 °, every average internuclear vector in the sample will now coincide with the rotation axis. Thus, the rotation in effect makes all the internuclear vectors parallel to each other and to the rotation axis. When this axis is chosen to be at 54.7 °, all interactions with the factor ($3\cos^2\theta$-1) will vanish.

To be completely successful the MAS rate must be greater than the static bandwidth in frequency terms. If the rate is less than this then spinning sidebands[3] spaced about the isotropic peak at multiples of the rotor period will result.

2.2.2 Setting the magic angle.

The rotor may be set at the magic angle (54.7 °) by twisting a rod at the base of the probe whilst continually observing the spectrum of a sample, specifically chosen for its sensitivity to its orientation within the magnetic field. The set up of the CMX probes only allows this angle to be altered through a few degrees on either side of the magic angle.

Before measuring ^{13}C spectra the ^{79}Br (50.143 MHz) spectrum of KBr is used to set the magic angle by observation of the FID and maximising the number of rotational echoes observed at a MAS rate of 2-3 kHz, at which point the magic angle is taken to be set ($\pm$ 0.1 °). These rotational echoes arise from the effect of MAS on the quadrupolar interaction that is only non-zero due to imperfections in the KBr (cubic) crystal lattice. This method is chosen since it is particularly convenient due to the close proximity of the bromine and carbon resonance frequencies that therefore require minimal experimental (capacitor and filter) alterations.

Prior to acquisition of some ^{15}N spectra it is always important to set the magic angle accurately due to the large shielding anisotropy of ^{15}N nuclei. In this case, ammonium nitrate is used by observing the nitrate peak, and optimising the lineshape such that it is narrow, and not a powder pattern. This sample is also used to set the referencing for the ^{15}N spectrum.

The magic angle on the HF probe may be set by observation of the proton spectrum of $KHSO_4$ and optimising the proton line shape. However, this technique is not simple since the sample is hygroscopic, and complex CRAMPS experiments are required. A new, alternative method involving observation of the fluorine signal (with CP and decoupling of protons) has also recently been proposed by *Brouwer and Harris*[4] in which a host: guest inclusion compound p-*tert*-butylcalix[4]arene: α, α, α-trifluorotoluene is used. A deviation from the magic angle of only 0.1 degrees causes significant broadening and then splitting of the ^{19}F resonance.

2.3 Experimental set up

The following section details the setup procedure necessary to acquire signals using a basic, two-channel, proton-to-carbon CP sequence.

2.3.1 Setting proton 90 pulse duration and power (PDMSO)

It is first necessary to use PDMSO to set the power of the proton 90° pulse. This is carried out by repetitively/continuously acquiring proton spectra whilst manually incrementing the amplifier power such that a null signal may be observed at chosen proton pulse duration. At this point (where no signal is observed) it is assumed that the proton magnetisation has precessed through 180° and thus has no observable component along the axis of observation. Thus the power will be set for a proton 90° pulse if the pulse duration is divided by two and may be checked by arraying the pulse duration around this value to look for a maximum in the proton signal.

Since the probes' power tolerances vary considerably, the standard 90 ° proton pulse durations vary accordingly. Whilst the HF probe may take a 3 μs proton 90 °, the other probes are usually set with 4-5 μs proton 90° pulse durations.

2.3.2 Shimming (PDMSO)

It is important to alter the current in the shim coils within the magnet in order to compensate for inhomogeneities in B_o. This is carried out by optimising the PDMSO lineshape whilst using the software to alter the shimming components. Obviously, the shim sets are different in each probe and thus standard sets may be developed and updated for re-use.

2.3.3 Set the magic angle

Please see section **2.2.2 Setting the magic angle.**

2.3.4 Setting the X-channel power

For efficient magnetisation transfer to occur during the contact time it is necessary to set the Hartman-Hahn matching condition between the relevant nuclei. This requires use of a suitable compound, the spectrum of which is continuously acquired whilst manually arraying the X power.

Advantages of using CP and the HH condition are that the experiment then relies upon the much shorter T_1 of the protons, and there is also a gain in signal intensity of γ_H/γ_C. Adamantane is the sample of choice when setting the proton-to-carbon CP conditions since it has a short proton T_1 and two, sharp ^{13}C resonances. However, adamantane also has a narrow matching profile therefore must be spun at low rates (*ca.* 1.0-1.5 kHz) since above this, its matching profile splits into sidebands.

The samples used for the various nuclei are summarised in ***Table 1***, below.

CP conditions	Standard
^{1}H-to-^{13}C	Adamantane
^{1}H-to-^{15}N	Isotopically enriched $^{15}NH_4{}^{15}NO_3$
^{1}H-to-^{19}F	Hexafluorobenzene
^{1}H-to-^{15}N-to-^{13}C	Doubly-labelled glycine

Table 1 Standards used for setting the HH match.

At the Hartmann-Hahn match, maximum signal intensity is observed since at this point, efficient magnetisation transfer occurs between the protons.

It should be noted that for experiments that require CP to ^{15}N, or other nuclei with low Larmor frequency, the proton CP power must be set at a lower value during the contact time so that the ^{15}N power entering the probe does not exceed the probe's power specifications.

2.3.5 Referencing

In order to ensure comparability of results it is necessary to reference the spectrum to a 'universally' recognised standard. The standards that have been used are summarised in ***Table 2***.

Nucleus	Frequency/ MHz	Reference standard	Chemical shift/ ppm
^{1}H	200.13	PDMSO	0 w.r.t. TMS
^{19}F*	188.288	C_6F_6	-166.4 w.r.t. $CFCl_3$
^{13}C	50.329	Adamantane	38.4 (high ν peak) w.r.t. TMS
^{15}N	20.284	$^{15}NH_4{}^{15}NO_3$	-5.1 (high ν peak) w.r.t. CH_3NO_2

Table 2 Referencing standards

*The Bloch-Siegert effect must be taken into account for ^{19}F spectra and thus spectra referenced accordingly. The magnitude of this shift may be used to calibrate the proton decoupling power (see section 2.6).

2.3.5.1 ^{15}N chemical shift scale referencing

It is important to establish a chemical referencing system for ^{15}N spectra that allows accurate comparison between results achieved from the solid and solution state. In solution-state spectroscopy, spectra are referenced to liquid ammonia at 0 ppm via DMF at 114 ppm. Solid state spectra are referenced to the nitrate peak of ammonium nitrate at – 5.1 ppm relative to $CH_3{}^{15}NO_2$. In solution, a saturated aqueous solution of $CH_3{}^{15}NO_2$.gives a ^{15}N resonance at 380.2 ppm[5] relative to a saturated aqueous solution of NH_4NO_3 with the $^{15}NO_3$ resonance 3.9 ppm away, at 376.3 ppm relative to $NH_{3(l)}$ at 0 ppm. This is summarised in the schematic below!

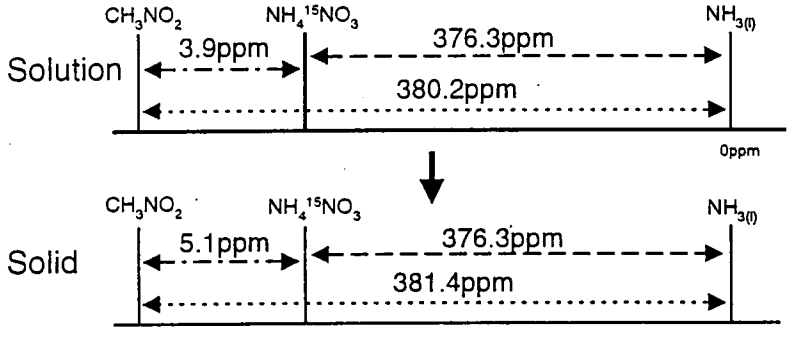

Figure 2 Summary of shift comparison between solid and solution NMR

Therefore, overall, the two shift referencing scales may be compared by addition of -381.4 ppm to the solution-state resonances. Results quoted in this thesis are relative to nitromethane.

2.4 Variable temperature operation

All the CMX probes are able to carry out VT operation in the temperature range 123-523 K. Most experiments within this Ph.D. work involved low-temperature operation due to the instability of the compounds at higher temperatures. Variable-temperature work often gives interesting information on mobility characteristics and phase transformations of compounds.

Passing nitrogen gas over the rotor lowers the temperature of the sample. This gas is cooled by passage through a copper coil that may be immersed in a small dewar of liquid nitrogen and then heated, if necessary, inside the VT stack which is in the magnet.

A thermocouple measures the temperature of the outlet gases and this may be read off on a display on the VT controller stack. Therefore it is necessary to calibrate the actual sample temperature with respect to the thermocouple's reading.

In solution-state NMR it is possible to monitor temperature by changes in the chemical shift[6], or by phase transition temperatures. However, in solid-state NMR, heating and pressure effects induced by the magic-angle spinning complicate the measurement of temperature. Also, a temperature gradient may exist along the long axis of the pencil rotor since the drive and bearing temperatures are at room temperature.

2.4.1 VT Calibration

Together with a group of other postgraduate students at the Durham SSNMR group we calibrated the three probes that were used for VT experiments. The method used was that of Aliev *et. al.*[6] whereby the chemical shift difference between the methyl and hydroxyl protons may be measured as a function of the temperature.

Some absolute ethanol was absorbed onto TTMSS (Tetrakistrimethylsilylsilane) in a glove box, under an atmosphere of N_2. The sample was then sealed in a glass insert to ensure that the moisture form the air could not affect the –OH chemical shift. The glass insert was wrapped in PTFE tape to assist stable spinning. Inserts were made to fit the HX, HF and HFX probes.

Experiments were run between 173-313 K, and at various MAS rates to investigate the effects of varying spinning speeds. Ample time was allowed between temperature changes to allow the temperature of the sample to equilibrate.

2.4.2 Calibration results

HX probe: 7.5mm outer diameter rotor – at 1 kHz spinning speed the actual temperature is 25% higher than the reading on the display. At 5 kHz, the temperature will be 40-50% higher than on the VT display panel.

HF probe: 4 mm outer diameter – the actual temperature will be 10% higher. Even at 10 kHz, the sample temperature will only be 15-20% higher. For complete detail, see the thesis of Nordon[7].

2.5 Combined Rotation and Multiple Pulse Spectroscopy (CRAMPS[8]) set up

The relatively high abundance and large magnetic moment of the proton make it particularly valuable in solution-state spectroscopy, but in solids the situation is more complex. In a static field the proton produces a magnetic field with symmetry rather like the traditional arrangement of iron filings around a bar magnet. However, in solids each proton dipole will be exposed not only to the static field but also to the sum of the dipolar fields of all other protons in the sample. The effect of these dipolar fields will be to homogeneously broaden the lines.

CRAMP spectroscopy was developed in order to attenuate the two major sources of line broadening, with multiple-pulses to remove the homonuclear dipolar coupling, and MAS to remove the shielding anisotropy, such that liquid-like spectra may be obtained in favourable cases. This is carried out by manipulating the system such that the interactions appear static over time.

These homonuclear dipolar decoupling experiments are carried out on the HF probe. Since the spinning module in this probe is designed to spin to high speeds such as 18 kHz, it is necessary to fit the rotors with a smooth, rather than a fluted drive tip to facilitate the necessary stable, slow spinning.

Accurate pulse durations are essential for these multi-pulse experiments[9,10]. There are three pulse sequences for setting these precisely: 'x', for setting the 90° pulse, 'xx' for setting an accurate 180°, and 'tx' which is used to make two 90° pulses as close as possible to a single 180° pulse. These conditions are set for proton and fluorine using PDMSO and C_6F_6, respectively. Good shimming is vital for the accurate and effective observation of these results.

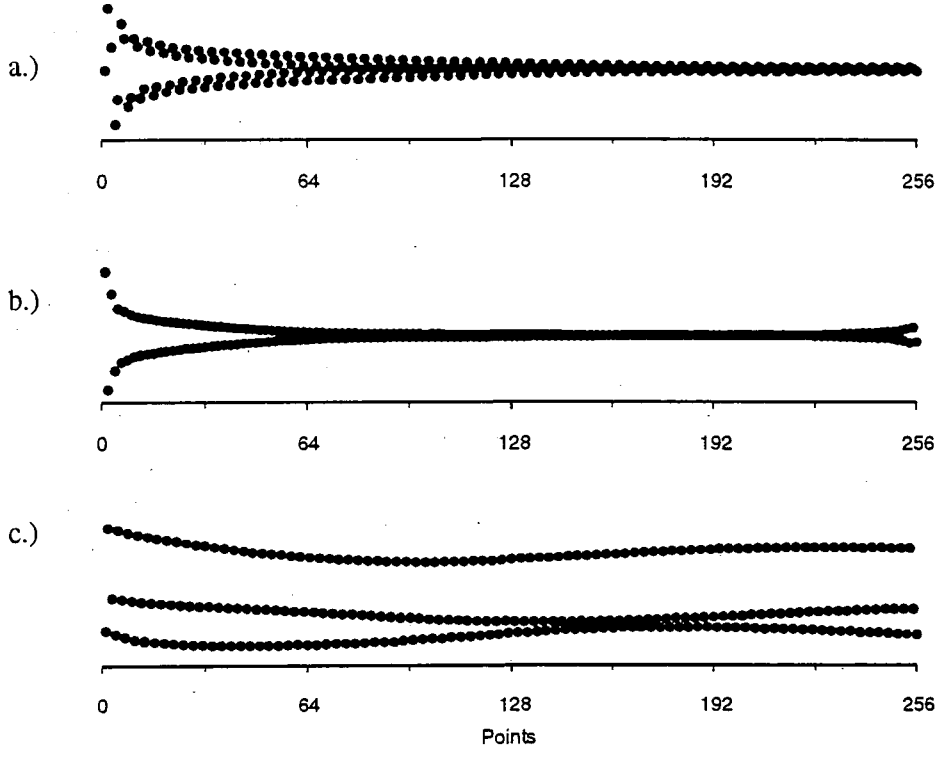

Figure 3 Diagrams showing the FIDs (marked point-wise) for the x, xx, and tx pulse sequences, when the necessary conditions are met

The standard order of set up is as follows. Firstly, the approximate pulse duration is set with the transmitter on resonance. Whilst displaying both the real and the imaginary part of the FID, the receiver phase is then altered using the software control panel such that all the signal is in the real dimension.

The next step is to cycle through the three pulse sequences in the order x, xx, tx, optimising them using a combination of the CRAMPS diode box, software control panel and the amplifier output tuning dial. The CRAMPS diode box is able to alter the sharpness of the pulse edges.

Usually, the narrow-band Bruker amplifier is used, and when heteronuclear decoupling is applied, the CE amplifier is used in class C mode, on the channel that is not being observed. The CMX spectrometer is equipped with digital phase shifters that have a settling time of 270 ns. Due to the multiple-pulse nature of the pulse sequences used, all spectra then possess scaled chemical shift axes. This is then corrected and set using adipic acid, noting the peak separation and altering the dwell parameters in the software control panel during processing. It is also usually necessary when processing CRAMPS data to left-shift the data by one point. It should be noted that filters are only required if rf is to be applied on the decoupling channel whilst the FID is being observed simultaneously.

Normally, the transmitter is placed to one side of the spectrum so that only one half of the spectral width is accessed. Techniques[11] are now available with quadrature detection, whereby signals on the other side of the transmitter are averaged out allowing the whole spectral width to be sued. This is particularly useful for ^{19}F, which exhibits a greater chemical shift range than proton.

2.6 Bloch-Siegert Shift

The Bloch-Siegert shift is the name given to the amount by which the resonance frequency of an observed nucleus, ν_o, shifts when a second, off-resonance rf field is applied. This shift effect is produced by a contribution to B_o that arises due to the off-resonance component of the oscillating rf irradiation field, B_1.

Due to the direct dependence of the BS shift upon the square of the decoupling field, and its inverse dependence upon the difference between the squared Larmor frequencies of the observed and decoupled nuclei, the BS effect is notably pronounced for proton-decoupled, fluorine NMR experiments.

For the case in which the difference between the Larmor frequencies of the decoupled and observed nuclei is much larger than the frequency-equivalent of the decoupling field, $|\omega - \omega_o| >> |\gamma B_1|$.

$$\Delta_{BS} = \frac{(\gamma_{obs} B_1)^2}{\omega_o^2 - \omega^2}$$

Thus the BS shift expresses the interaction between the B_1 field and the field of the observed nucleus. Since $\omega = 2\pi\nu$, the above equation becomes:

$$\Delta_{BS} = \frac{((\gamma_{obs})B_1)^2}{(2\pi\nu_o)^2 - (2\pi\nu)^2} = \frac{\left(\frac{\gamma_{obs}}{2\pi} B_1\right)^2}{\nu_o^2 - \nu^2}$$

Whereas in solution-state NMR, where decoupling serves to remove scalar couplings (^{13}C {^1H} ~ 10 kHz), in solid-state ^{13}C CP/MAS NMR, proton decoupling fields are much larger, typically 50-70 kHz. These powers are necessary to remove the proton-carbon dipolar interactions that are averaged out by rapid tumbling in solution. However, the BS shift in these instances, remains unobservable, with magnitude of the order of 6-7 $x10^{-2}$ ppm (1.7 Hz).

For the proton-decoupled fluorine case in MAS NMR spectroscopy, there is only a 6 % chemical shift difference between the observed and decoupled nuclei. This factor, when combined with typical decoupling fields of 50 kHz, leads to a BS shift of the order of ppm (1.9 ppm for 50 kHz and 7.7 ppm for 100 kHz (at B_o of 4.7 T, with proton at 200 MHz))! For a lower field spectrometer (e.g. 1.4 T and 60 MHz for proton) this effect is exacerbated further giving much larger BS shifts of approximately 21 ppm. Therefore it is critical for comparison of ^{19}F {^1H} results, that the BS is corrected for. This is usually carried out by running a reference spectrum of C_6F_6 both with and without proton decoupling, before experiments are carried out, and measuring the shift difference of the peak for the given proton decoupling power applied.

The Bloch-Siegert shift may also be used to calibrate the effective proton decoupling power, by plotting the chemical shift versus the B_1 amplitude. When calibrating power it

is important to remember the effect of the cross-diodes, which are capable of reducing the power on the observed channel by up to 75 % when they are in place.

It is also important and useful to note that due to inhomogeneities in B_1 across the sample when in the coil, there will be a spread of the effective B_1 and thus a spread of BS shifts displayed by the nuclei involved. This will cause a broadening of the lineshape – a phenomenon that may be avoided by restricting the sample size to as small a volume as is convenient.

2.7 Equipment used for techniques other than NMR (i.e. IR, DSC etc.)

2.7.1 Infra red Spectroscopy

Initial IR spectra were run at SB. These spectra were obtained as Nujol Mulls, using a Perkin-Elmer 1750 FTIR spectrometer. The spectrometer was run with 2 scans, in interleaved mode, with a resolution of 4 cm^{-1}.

IR spectra that were run at Durham were carried out on a Perkin-Elmer Paragon 1000 FT-IR spectrometer, controlled by GRAMS software. This instrument is fitted with a Graseby Specac Golden Gate containing a 45 ° single reflection-type IIa diamond. This technique uses ATR[12] (attenuated total reflectance) and requires only a small amount of the solid, which may be recycled. Resolution is 4 cm^{-1}.

2.7.2 Differential Scanning Calorimetry

Traces were obtained at SB for the heating and cooling of BR55834 using a Perkin-Elmer DSC-2C instrument at a heating rate of 10 °C min^{-1} over a temperature range from 30 °C and upwards in an atmosphere of nitrogen flowing at 5 ml min^{-1}.

Traces obtained in Durham for BRL55834 were run by Dr. S. Peace, with the permission of Professor R. Richards at Durham Interdisciplinary Research Centre for Polymer Science and Technology. The heating rate was 10 °C min^{-1}.

2.7.3 Powder X-Ray Diffraction

This work was carried out in Durham using a software-controlled Philips PW1050 powder diffractometer. The software was called 'Traces' and was produced by Diffraction Technology, 38 Essington Street, P.O. Box 444, Mitchell, ACT, 2911, Australia.

2.7.4 Raman Spectroscopy

This work was carried out during visits to SB at 'The Frythe', Welwyn Garden City and all measurements were taken using a Perkin-Elmer 2000R spectrometer. This was fitted with a 3 mm sample cup. However, samples were housed in glass vials. The apparatus ustilised a Nd:YAG CW laser and a quartz beam splitter. Spectra were corrected for instrument response to give resolution of 4 cm^{-1}. The laser power used was 1 Watt.

The chemometric analysis program that was used on these Raman spectra was entitled 'QUANT+' version V3.0, produced by Perkin-Elmer Ltd., Post-Office Lane, Beaconsfield, Buckinghamshire, HP71QA.

2.7.5 Single crystal X-ray diffraction

Single crystal X-ray diffraction data were acquired for polymorphic forms 1, 2 and 4 of BRL61063. The structure determinations were carried out by Dr. D. Eggleston at SmithKline Beecham, during the period 1991-92, but the detailed results have been evaluated for the first time in this thesis. Experimental details are provided (from this work) below for completeness[13].

Lattice parameters were determined from the setting of angles of 25 reflections well distributed in reciprocal space measured on an Enraf Nonius CAD-4 diffractometer. A full sphere of intensity data was also collected on the diffractometer using graphite monochromated copper radiation from a rotating anode source and an ω-2θ variable-speed scan technique. Intensities of three monitor reflections measured at the beginning, end and every two hours of exposure time changed by at most $\pm$ 0.1 %. Three orientation controls also were monitored to assess any crystal movement during the experiment. Data were corrected for Lorentz and polarisation effects and, using the DIFABS algorithm, for the effects of absorption. Redundant observations were averaged to obtain the final data set.

The structures were solved by direct methods, using the SHELXS program series for forms 1 and 4, and the MULTAN80 program series for form 2. Atomic positions were initially refined with isotropic temperature factors and subsequently with isotropic displacement factors. The function minimised was $\sum w(|F_o|-|F_c|)^2$. Weights, w, were eventually assigned to the data set as $w = 1/\sigma^2(F_o) = [\sigma^2(I_C) + (0.04I)^2]$. Positions for the hydrogen atoms attached to the nitrogen atoms were discovered in subsequent difference Fourier maps. Positions for hydrogen atoms attached to carbons were calculated based upon geometrical considerations and held fixed in the final refinement stages along with isotropic temperature factors assigned 1.3(Beq) of the attached atom. Hydrogen atoms on the cyclopropyl groups in form 1 were omitted from the refinement of this structure. All other refinements were carried out using isotropic temperature factors. The full matrix least-squares refinement converged (max $\Delta/\sigma = 0.5$) to values of the conventional crystallographic residuals R = 0.056, 0.044, 0.049, wR = 0.092, 0.054, 0.071, for forms 1, 2 and 4, respectively. A final difference Fourier map was featureless, with maximum density of $\pm$ 0.285, $\pm$0.196, and $\pm$0.515 e Å^{-3}, again for forms 1, 2 and 4, respectively. Values of the neutral atom scattering factors were taken from the International Tables for X-ray Crystallography.

2.8 Solution-state NMR

A Varian VXR400 spectrometer operating at 9.4 T was used (^{13}C at 100.58, and ^{1}H at 399.96 MHz).

2.8.1 Solution-state NMR pulse sequences

2.8.1.1 DEPT[14,15]

Distortionless enhancement of NMR signals by polarisation transfer was developed by NMR spectroscopists as an improvement to the previously used INEPT pulse sequence, which incorporated multiplicity selection capability. Whereas the INEPT sequence displayed proton-coupled spectra in which the multiplets did not show the normal intensity distribution, the DEPT pulse sequence does not depend upon J and only depends upon the flip angle, θ, since the two 180° pulses serve only to refocus the chemical shift.

The DEPT-135 sequence shows CH and CH_3 as positive and the CH_2 signals as negative with respect to the baseline. There are no signals for the quaternary carbons.

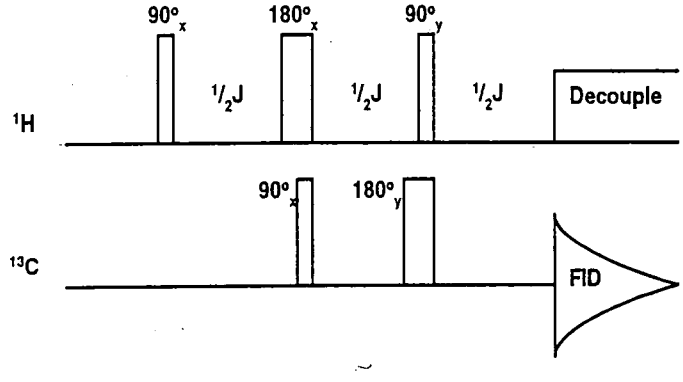

Figure 4 DEPT Pulse sequence

2.8.1.2 DQF-COSY[16]

Double quantum filtered correlation spectroscopy is a two-dimensional technique that may be used to correlate heteronuclear (^{1}H, ^{13}C), or in this case homonuclear (^{1}H, ^{1}H)

interactions within the compound. The homonuclear case allows identification of the coupling between individual nuclei in the molecule by showing the proton spectrum along the leading diagonal of the 2D plot, together with cross peaks (off-diagonal peaks) corresponding to scalar coupling between the specific protons. In the DQF case, the proton spectrum shown along the leading diagonal only shows peaks for protons that are coupled to other protons.

2.8.1.3 HMQC[17] and HMBC[18,19,20]

The Heteronuclear Multiple Quantum Correlation pulse sequence is shown in ***Figure 5***. This technique was initially a very popular method of performing indirect detection experiments in the solution state. The resulting 2D spectrum correlates protons and carbons that are directly coupled via ^{1}J couplings, suppressing proton signals that are not coupled to a ^{13}C nucleus by phase cycling of the first ^{13}C pulse through x, y,-x, -y.

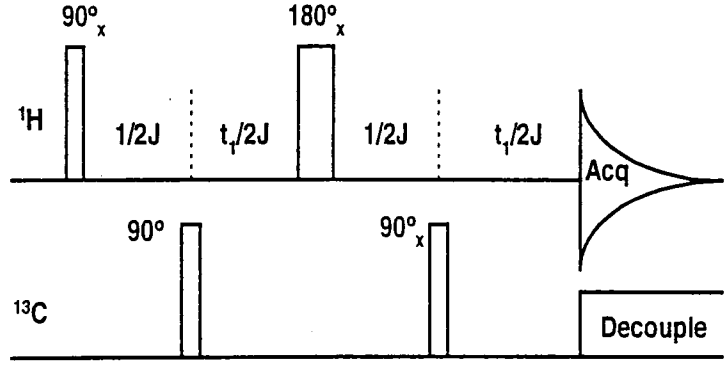

Figure 5 HMQC pulse sequence for ^{1}H-detected heteronuclear chemical shift correlation with heteronuclear multiple quantum coherence during the evolution period.

The HMBC experiment is used to correlate long-range (two and three bond) signals. Often a low pass J filter is used to suppress the direct one-bond correlations. This is seen in ***Figure 6***, where the first ^{13}C 90° serves as a low-pass J-filter.

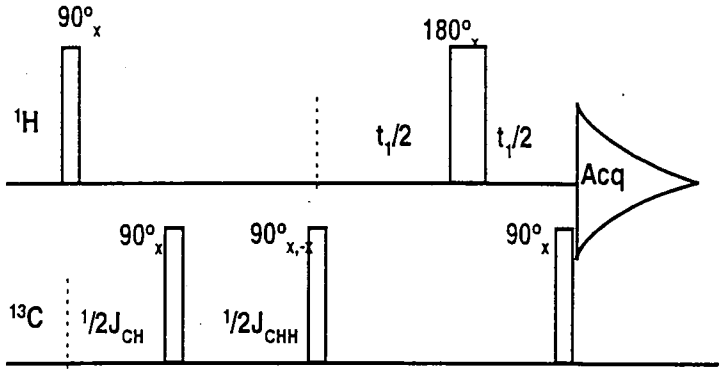

Figure 6 HMBC pulse sequence for proton-detected HMBC using heteronuclear multiple quantum coherence during the evolution period.

These techniques have been used on systems containing ^{15}N, such as proteins[17,18]. However, they are also used for ^{13}C-^{1}H correlation in BRL55834 to aid assignment of the spectra (see chapter 4).

2.9 Solid-state NMR experiments

2.9.1 Basic acquisition pulse sequences (SPE and CP)

In cases of abundant nuclei with short spin-lattice relaxation times (T_1), such as ^{19}F and ^{1}H, it is feasible to use a single-pulse experiment, with a recycle delay greater than five times the T_1 of the nucleus involved. The standard pulse programs used in this Ph.D. are '1pulse', '1pncyc', which are single pulse experiments with and without phase cycling, respectively, or '1pda', which incorporates CW decoupling during the acquisition time and has phase cycling. When using 1pda to observe ^{19}F with proton decoupling, it is necessary to allow for the Bloch-Siegert shift (see section 2.6). To observed high-resolution proton spectra of solids it is necessary to use CRAMPS techniques (see section 2.9.2.2).

In solid-state NMR the study of rare spin nuclei (e.g. ^{13}C, ^{15}N) by direct excitation of the nucleus involved is hampered by low sensitivity and a requirement for long recycle delays due to their long T_1 values. A combination of cross polarisation and MAS, with

high-power proton decoupling, if protons are abundant, has made acquisition of spectra more viable.

In the CP technique, the recycle delay is governed by the T_1 of the protons, which is generally much shorter than those of the rare spins. The repetition rate therefore increases and the rare-spin signal is also enhanced by a factor of γ_H / γ_C.

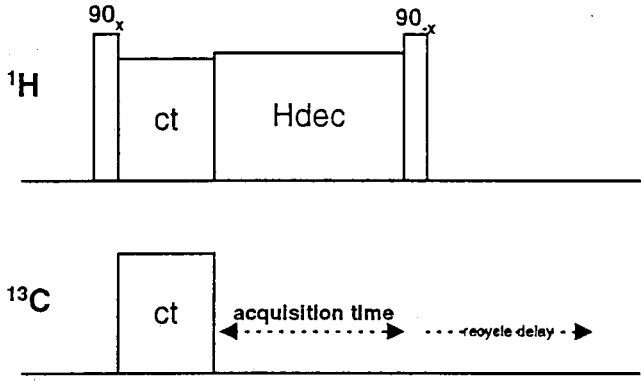

Figure 7 Pulse program for cross polarisation with flip-back (CPFlip)

Cross polarisation[21] involves transfer of proton magnetisation to the rare-spin nucleus using the pulse sequence[22] shown in ***Figure 7***. The 90 ° pulse (phase ±x) applied to the protons places the magnetisation along the y axis. During the contact time, irradiation of ^1H is continued with phase y (thus spin-locking the protons) whilst the ^{13}C spins are also irradiated. The transfer of irradiation from ^1H to ^{13}C is enabled by matching the radiofrequency magnetic fields according to the **Hartmann-Hahn**[23] condition:

$$\gamma_C B_{1C} = \gamma_H B_{1H}$$

where γ_x is the magnetogyric ratio of nucleus x, and B_{1x} is the applied rf magnetic field.

At the HH match polarisation transfer can occur between the I and S spins by mutual spin flips. This is because when $\omega_{1I} = \omega_{1S}$ the Zeeman energy levels of the I and S spins are 'matched' and therefore efficient energy transfer can occur between the two types of spins. It is still possible for CP to occur if $\omega_{1I} \neq \omega_{1S}$ because spin flips amongst the I spins broaden the Zeeman energy level of the I spins such that a range of matching conditions exists. MAS may separate the matching profile into sidebands[24,25] that are spaced by the spinning rate, with lowest efficiency in the centre band.

Magnetisation thus develops along the axis of irradiation for the ^{13}C nucleus, resulting in a ^{13}C magnetisation value that is enhanced over its Boltzmann value by a factor of $\gamma_H / \gamma_C \approx 4$. Finally, the ^{13}C magnetisation is observed under high-power proton decoupling conditions.

Ramped[26,27,28,29,30] CP, where the irradiation power for one or both of the 'contacting' nuclei is arrayed during the contact time, may be used where the matching profile will have split into sidebands due to MAS. Experiments that were carried our on BRL55834 on the 600 MHz CMX infinity spectrometer used ramped CP on the proton channel, since spinning speeds of ~13 kHz rendered normal CP inefficient.

2.9.2 Decoupling techniques

2.9.2.1 Heteronuclear decoupling

In solid-state NMR experiments of dilute spins such as ^{13}C and ^{15}N, broad band[31,32,33,34] high-power proton decoupling (typically, rf of 50-100 kHz) is applied to the proton channel during the acquisition time to decouple the protons. The decoupling results from the fast nutation of the proton spin states about an on-resonance radiofrequency field, which averages the dipolar interactions between the observed spins and the protons.

However, because of the presence of chemical shift dispersion and chemical shift anisotropy it is impossible to set the rf on resonance for all the proton spins. With a rf offset[35], the nutation about a tilted effective field causes incomplete proton decoupling, which has been one of the major sources of line broadening in MAS spectra[36]. In order to be effective, the decoupling power must be at least equal to the rate of flip-flop fluctuations of the I spins.

Often insufficient proton decoupling power causes residual linewidths of CH_2 groups in the ^{13}C CP/MAS spectrum to remain quite large. This gives rise to problems, especially in

the spectra of organic molecules where the large number of peaks means that high resolution is vital.

A new, multiple-pulse heteronuclear decoupling scheme, TPPM (two pulse phase modulation) has been proposed by Bennet *et. al.*[37]. This technique has been proved to be more efficient than CW decoupling. Initial studies claimed that there is an optimum combination of pulse duration and modulation angle for a given MAS rate and sample. The paper also claimed an enhancement in resolution and in sensitivity on incorporation of this decoupling scheme.

The TPPM pulse sequence is shown in ***Figure 8***. A small region of the decoupling period is expanded in order to illustrate the rapid alternation of the phase of excitation of the rf excitation between the two values, $\pm \phi/2$, with the overall period $2\,\tau_p$ which is carried out throughout the acquisition of the FID.

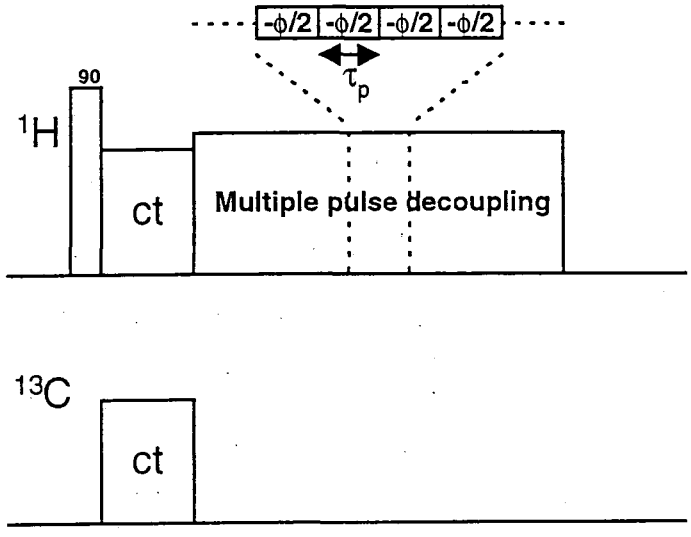

Figure 8 Pulse sequence for the CP/MAS experiment with the addition of phase-modulated TPPM decoupling on the ^1H channel

2.9.2.1.1 Experimental investigation into TPPM

A significant amount of time has been spent carrying out an investigation of the efficiency of TPPM decoupling when applied to a variety of organic, pharmaceutical compounds whilst altering spinning speed, decoupling power, and modulation angle, ϕ. Pulse sequences for the triple-channel HFX probe were also modified, and TPPM was applied for proton and fluorine decoupling (also on the HF probe).

The TPPM decoupling scheme was applied to the ^{13}C CP/MAS spectra of the two systems concentrated upon during this Ph.D. (BRL55834 and BRL61063) as well as the steroid 'minaxalone'[38], and a polymorph of cortisone acetate, plus a trifluorinated steroid. Efficiency appeared to vary between compounds.

2.9.2.1.2 Summary and discussion of results of TPPM investigation

A modulation angle of $\pm 7^{\circ}$ was found to be optimum for most spinning speeds, decoupling powers and samples. An obvious improvement in spectral resolution could be observed in the ^{13}C CP/MAS spectra of BRL55834 (see chapter 4) and BRL61063, especially form 2 (see chapter 5). A sample of cortisone acetate was also tested, but this showed negligible resolution enhancement in the ^{13}C CP/MAS spectra.

A sample of 'Minaxalone' was analysed 'blind', i.e. without knowledge of its molecular structure. On comparison of the ^{13}C CP/MAS spectra with CW decoupling and with TPPM decoupling, it was easy to assign the four CH_2 carbon resonances, since only these showed significant narrowing, with a general decrease in linewidth of 43 ($\pm$ 3) %.

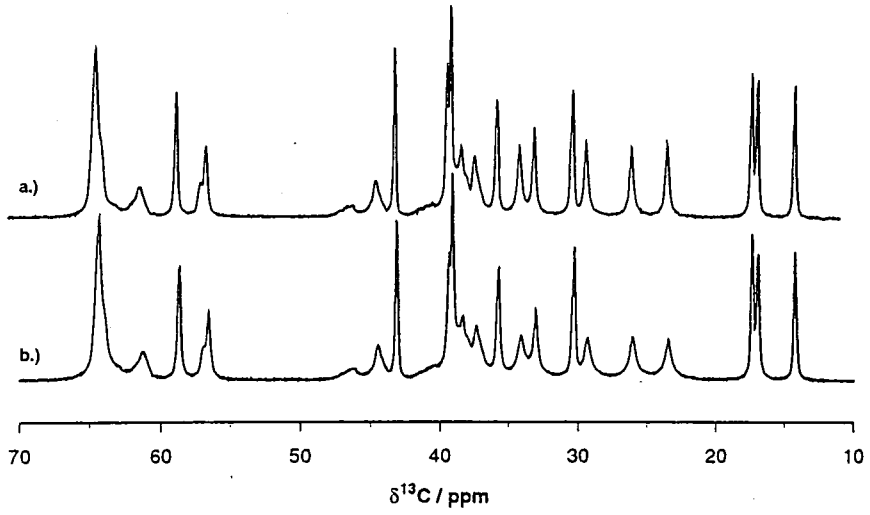

Figure 9 Low-frequency region of the ^{13}C CP/MAS spectra of Minaxalone comparing a.) TPPM with b.) CW decoupling on the proton channel (MAS rate 5 kHz, ct 10 ms, 860 transients, acqtm 200 ms)

Frequency / ppm	Linewidth (fwhh / ± 0.5 Hz)	
	CW decoupling	TPPM
34.1	32.0	17.1
29.3	26.4	14.8
26.1	27.8	15.8
23.4	25.0	15.8

Table 3 Comparison of linewidths of CH_2 resonances with CW and TPPM decoupling

Application of TPPM for proton decoupling whilst observing ^{19}F for BRL55834 showed variable results in that whilst ^{19}F CP/MAS spectra of form I showed a linewidth reduction of 5 (± 0.4) %, similar experiments on form II showed no observable improvement.

The variation of the efficiency of TPPM decoupling in comparison to CW may be influenced by the proton broadband lineshape as the MAS rate is altered. The TPPM sequence reduces the degradation of CW decoupling by perturbations that are present in the system, including the ^{1}H shielding anisotropy as well as other fields that resemble the Zeeman term in the spin Hamiltonian, such as magnetic susceptibility fields and heteronuclear couplings to additional nuclei, for example ^{14}N.

For rigid organic solids, MAS has little effect upon the proton spectrum due to the nature of the homonuclear dipolar interactions. Sometimes it is possible to attain MAS rates of the order of the average homonuclear dipolar coupling. This is usually brought about by motional averaging or by use of a high-speed MAS probe. In these cases, the homonuclear dipolar interactions may be partially suppressed. Hence, communication between protons, which proceeds via the flip-flop term of the homonuclear dipolar Hamiltonian is reduced and the proton spectrum may start to break into sidebands. Therefore the effect of MAS on the proton spectrum may have a dramatic effect upon decoupling[39].

A recent paper by Gan *et. al.*[40] proves that TPPM reduces line broadening which is attributed to MAS causing a second-order recoupling[41] of the heteronuclear dipolar coupling tensor of the irradiated spin, giving terms that are not averaged out by the MAS. This paper suggested the use of a new technique, 'TPFM', in which the pulse sequence is frequency- instead of phase-modulated. By application of so-called left- and right-handed versions of these experiments the authors are able to prove that the efficient decoupling brought about by TPPM is caused by a secondary resonance effect. This secondary resonance occurs when the average strength matches the modulation frequency of the pulse sequence.

2.9.2.2 Homonuclear decoupling[42] and CRAMPS[43]

The broadening of the NMR absorption spectrum due to homonuclear dipolar interactions in powders can be reduced by introducing a periodic Hamiltonian under which the spin system evolves. Multiple-pulse sequences, MAS, and a combination of both (CRAMPS)[44] (see section 2.5) are commonly applied for this purpose.

In CRAMP spectroscopy, efficient homonuclear decoupling can be obtained using suitable multiple-pulse[45] sequences, provided that their cycle time (t_c) is short compared

with the rotor period (t_r). Then, the spatial part of the dipolar interaction is quasi-static during the coherent averaging process by the pulses.

To observe ^{1}H or ^{19}F in the solid state, when these are present in high abundance, it is necessary to use multiple-pulse programs such as WAHUHA[46], MREV-8[47,48,49], or BR24[50] to decouple the abundant spins from each other. It should be noted that when both ^{1}H and ^{19}F are present, it is necessary to also apply heteronuclear decoupling. Typically, heteronuclear decoupling is achieved in solid-state NMR by irradiating the appropriate spins at their Larmor frequencies. However, this would require powers too high[51,52] for modern probes since in order to remove the heteronuclear dipolar interaction it is necessary to rotate the S spins through multiples of 2π during the 'large windows' of the homonuclear multiple-pulse averaging sequence. These windows are typically of 6 μs duration, thus requiring S decoupling powers of ~167 kHz.

CRAMPS pulse sequences are basically coherent averaging techniques for which the undesirable terms in the Hamiltonian (usually the homonuclear dipolar Hamiltonian) vanish to as high an order as is possible, while the desirable terms are largely retained. The desired interaction, (the chemical shift) is usually scaled to something slightly less than half of its original value. (Scaling factors: WAHUHA = $1/\sqrt{3}$ =0.577; MREV-8 = $\frac{\sqrt{2}}{3}$ = 0.471).

2.9.3 Determination of physical parameters and quantitative results

2.9.3.1 Variable contact time experiments

It is possible to acquire a significant amount of information through arraying the contact time between the rare (^{13}C, ^{15}N) and abundant (^{1}H, ^{19}F) nuclei. Since CP is mediated by the dipolar interactions between the I and S spins, it is dependent upon r_{IS}^{-3}, where r_{IS} is measured through space, so that the characteristic CP time, T_{IS} is dependent upon both the number of I spins and their distances from the S nucleus.

Processes compete within CP kinetics. Whilst magnetisation may be transferred to the dilute nuclei at a rate T_{IS}^{-1}, the polarisation of the proton spins may also be dissipated to the lattice by relaxation under spin-locked conditions at a rate $T_{1\rho}^{-1}$.

Therefore, when contact times are very long, the CP process is reversed and polarisation is lost from the dilute spins to the abundant spins and thence to the lattice. There is therefore an optimum contact time, which maximises the signal of the dilute spins. This is shown by the expression below:

$$S_{(t)} / S^{o} = \left(\frac{1}{1-\lambda}\right)\left[1-\exp\left\{\frac{-(1-\lambda)t}{T_{CP}}\right\}\right]\exp\left(-\frac{t}{T_{1\rho}}\right)$$

where S^{o} is the total, hypothetical signal for the total CP transfer given by extrapolation of the linear decay to zero; $\lambda = {}^{T_{CP}}/_{T_{1\rho}}$; and S_t is the signal at time t.

Therefore in principle, the proton-to-carbon CP rate decreases in the order $CH_3 > CH_2 > CH > C$. This is very useful in the assignment of the spectra of organic molecules. However, if the CH_3 group is mobile, the efficiency of proton-to-carbon CP is reduced for the methyl carbon. An example is in the assignment of the ^{13}C spectra of 6-aminopenicillanic acid[53].

Within the scope of this Ph.D. research CP has been carried out for $^{1}H \rightarrow {}^{13}C$, $^{1}H \rightarrow {}^{19}F$, $^{1}H \rightarrow {}^{15}N$, $^{19}F \rightarrow {}^{13}C$[54], $^{15}N \rightarrow {}^{13}C$[55] and $^{13}C \rightarrow {}^{15}N$ (C-N examples used labelled samples).

Oscillations in the signal intensity are often observed in the rise of the signal during a variable contact time experiment. The first reported observation of these oscillations was for a single crystal of ferrocene[56] [$(C_5H_5)_2Fe$]. Theoretical explanations[57] have been proposed as to the cause of these oscillations, which view them as coherence effects produced by the dipolar coupling of the ^{13}C to the directly bound proton. In the case of the osmium complex, $[H_2Os_3(CO)_{10}]$[58], the authors suggest that the oscillations are caused by the slow proton spin diffusion rate. Stoll[59] suggests that these dipolar oscillations are due to the effect of the I_zS_z Hamiltonian. The I spins 'see' a small magnetic field along

the z axis due to the S spin. The I spin will precess about this magnetic field, but since at room temperature almost as many S spins are 'up' as are 'down', then half the I spins precess clockwise and half precess counter-clockwise. This leads to a net oscillation of the I spins due to both the rotating and the contra-rotating components.

Some research groups have also attempted to use these transient oscillations to determine the dipolar coupling[60] between the proton and adjacent carbon, and thus determine the internuclear distance.

2.9.3.2 Quantitative single-pulse methods: the Ernst angle[61,62,63]

Unlike solution-state NMR spectroscopy, it is difficult to obtain quantitative results from solid-state NMR experiments. One technique using CP is to back-extrapolate to S°, the ^{13}C intensity from a proton-to-carbon variable contact time experiment, to achieve an accurate comparison of the relative numbers of carbons in each location.

In single-pulse experiments it is desirable to use a fast repetition rate in order to increase the s/n ratio. In order to do this, one assumes that transverse magnetisation decays irreversibly during the recycle time, t. However, the recovery of the longitudinal relaxation magnetisation towards its equilibrium value M_o in the pulse intervals is normally not complete.

After a small number of pulses a dynamic equilibrium may be established. This can be easily computed by equating the z magnetisation before a pulse ($M_{Z(0-)}$) and the z magnetisation at the end of the recycle time ($M_{Z(t)}$).

$$M_Z(0_+) = M_Z(0_-)\cos\beta$$

$$M_Z(t) = M_Z(0_+)E_i + M_0(1-E_i)$$

$$with E_i = \exp\left(\frac{-t}{T_1}\right)$$

where t is the inter-pulse spacing and T_1 is the longitudinal relaxation time.

From $M_Z(t) = M_Z(0\_)$ we immediately find that $M_Z(0\_) = M_0 \frac{1-E_i}{1-E_i \cos\beta}$

The initial amplitude of the FID $M_x(0_+)$ is $M_X(0_+) = M_0 \frac{1-E_i}{1-E_i \cos\beta} \sin\beta$

The maximum signal is therefore no longer obtained for $\beta = \pi/2$ and we have the equation:

$$\cos\beta_{opt} = E_i = \exp\left(\frac{-t}{T_1}\right).$$

Therefore, for shorter values of T_1, the optimum pulse angle is smaller. When t used is much greater than T_1 there is little interference and greater than 95 % of the equilibrium magnetisation can be brought into the transverse plane for observation.

This technique has been used during this Ph.D. research in attempts to achieve quantitative results for ^{13}C spectra.

2.9.3.3 T_1 measurements (I and S nucleus)

When a 180° pulse is applied to a nucleus, this inverts the magnetisation and the spin-lattice relaxation time, T_1[64,65,66,67,68,69] may be determined. The decay of this longitudinal magnetisation may be described by the equation: $M_{Z(t)} - M_o = [M_{Z(0)} - M_0]\exp(-t/T_1)$.

At any point in time the magnetisation is in the z or -z direction and therefore no signal is observable. A 90 ° 'read pulse' applied at any time after the 180 ° pulse allows the state of magnetisation to be monitored.

The inversion-recovery method of measuring T_1 uses the pulse sequence:

$$[180°\text{-}\tau\text{-}90°(\text{FID})\text{-}T_d]_n$$

The recycle delay (T_d) must be significantly greater than the longest T_1 to be measured so that the Boltzmann equilibrium is re-established between 180 ° pulses.

The evolution period, τ, is varied and hence T_1 may be found by plotting a graph using the equation: $\ln[S_\infty - S_t] = \ln 2 + \ln S_\infty(-\tau/T_1)$. When τ is short the signal is negative since in effect a 270 ° pulse has been applied. When τ is maximum, $S_o = S_\infty$. At an intermediate time the signal passes through a null point at which $T_1 = \tau_{null}/\ln 2$.

Carbon nuclei in different environments differ in their value of T_1, with more mobile groups, such as methyl groups, possessing a much shorter T_1.

The T_1HCP pulse sequence (see ***Figure 10***) has been used to find the average T_1 of the protons. This is a cross polarisation version of the Freeman-Hill method, which decreases errors brought about by spectrometer drift.

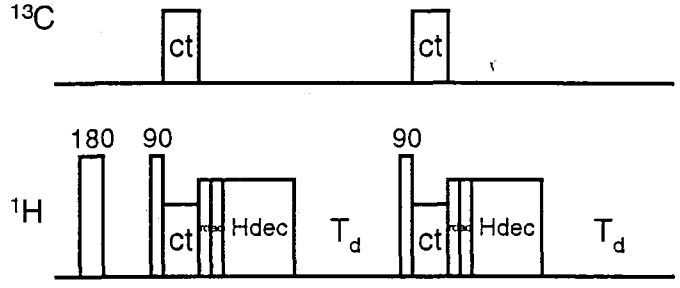

Figure 10 The T_1HCP experiment for measuring proton T_1.

The difference between the first and second acquisition in the loop is the presence of a H180° pulse and τ period in the first. The pulse sequence involves subtraction of the first FID from the second *before* Fourier transformation. The result is a series of spectra with only positive peaks of intensity ranging from $2S_o(\tau=0)$ to zero as τ approaches infinity.

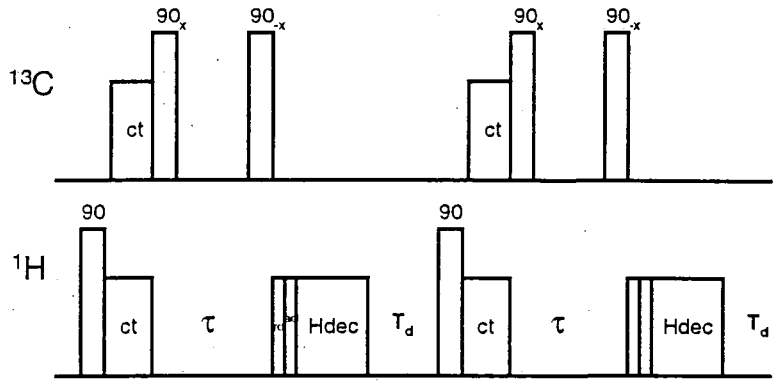

Figure 11 The T_1XCP experiment for measuring T_1 of the X nucleus

The T_1XCP sequence shown in ***Figure 11*** is used for measuring the individual T_1 values of the rare nuclei (^{13}C). When carrying out this experiment it is important to leave a delay time greater or equal to 5 times the T_1 of the abundant nuclei.

2.9.3.4 Measurement of $T_{1\rho}$

The proton $T_{1\rho}$[70] may be estimated from analysis of the gradient of the decay curve of variable contact time experiments. Results acquired in this way are extracted using the 'Spinsight xy data analysis panel'.

The direct measurement of the spin-locked longitudinal relaxation time for ^{19}F was carried out using the 'ant1rhohdec' pulse sequence. This experiment is a single-pulse variable spin-lock experiment in which proton decoupling is applied during acquisition of the FID.

2.9.4 Spectral editing[71] techniques

Spectral editing techniques are methods that aid the spectroscopist in assigning or simplifying complex spectra. In the case of liquid-state NMR, these editing techniques rely upon the narrow range of ^1J couplings between protons and carbons giving rise to

techniques such as DEPT[14,15] (see section 2.8.1.1), INEPT, and the attached proton test (APT).

Throughout the course of this Ph.D. research, it has been necessary to apply several spectral editing techniques in order to assign the ^{13}C (and ^{15}N) solid-state spectra. Many of these techniques to solids rely on dipolar interactions with attached protons[72,73,74,75], or on mobility effects[76]. Often the conditions for these techniques have to be adapted for individual samples based on the knowledge of the (often discriminatory) relaxation parameters for the nuclei as determined by methods outlined in the section above. Improved selectivity may also be achieved by incorporation of homonuclear[77] (^1H,^1H) decoupling techniques within some of these pulse sequences.

The four main editing techniques for solids that have been used are the interrupted decoupling pulse sequence, wideline separation (WISE), separated local field spectroscopy, and cross polarisation inversion recovery techniques. Techniques also exist where subspectra[78,79,80] for each type of carbon (CH_n) may be produced by addition and subtraction of sequential FIDs.

2.9.4.1 Interrupted decoupling[81]

This technique has also been referred to as the 'dipolar dephasing experiment[82,83,84] and the 'non-quaternary suppression' (NQS) experiment. It provides one of the simplest ways to discriminate between different types of carbons in the solid state. It involves placing a window or delay of duration τ after CP and before decoupling is applied to the abundant spins.

The general pulse sequence is shown in ***Figure 12,*** in which contact time (ct) and acquisition time are ~ms, dephasing time (τ) and recycle delay (pd) and are ~s, receiver delay (rd) and acquisition delay (ad) are ~μs.

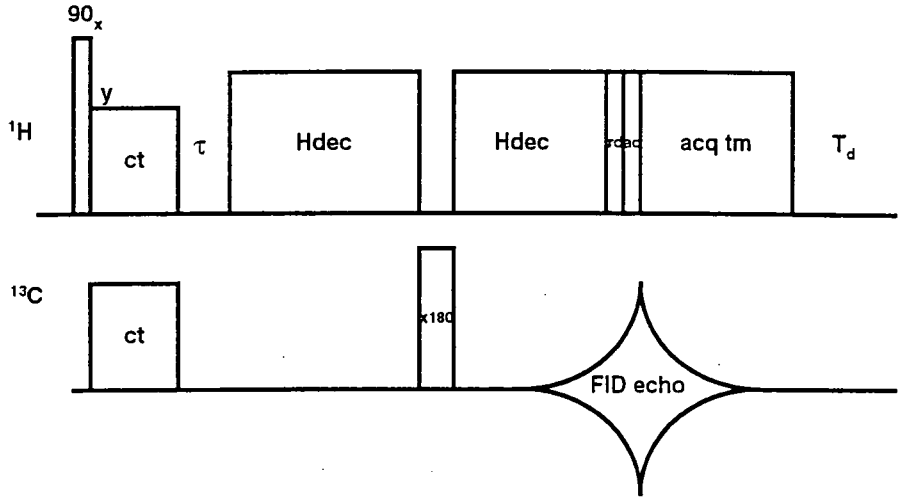

Figure 12 The dipolar dephasing experiment with rotational echo

During the dephasing time, τ, magnetisation decays most rapidly from the ^{13}C nuclei that are strongly dipolar coupled to protons. Since the ^{13}C-^{1}H dipolar interaction is proportional to r_{CH}^{-3}, where r is the distance between the ^{13}C and ^{1}H through space, τ may be adjusted such that protonated carbons are completely suppressed relative to unprotonated ones.

However, it should be noted that methyl groups frequently undergo rapid internal motion (of the order of 10^4 Hz)[85] in the solid-state, the motion of which significantly reduces the local dipolar field. Thus, methyl resonances also appear in NQS spectra.

The technique is rotor synchronised in that the FID is collected from the 'top' of an echo, at a multiple of the rotor period in order to avoid first-order phasing problems in the spectrum.

This technique has also been used for ^{19}F[86] instead of ^{1}H (see chapter 4).

2.9.4.2 Wideline separation (WISE[87,88])

The width of proton lines can give information on the mobility and molecular dynamics of a system. While broad lines arise from rigid conformations due to the static dipolar couplings present, mobility causes the averaging of these couplings and therefore reduces the linewidth. The extreme narrowing limit is exemplified in solution-state NMR where rapid molecular tumbling gives rise to lines of the order of 0.1 Hz.

The WISE experiment is particularly useful in its application to polymeric systems, where there may exist domains of varying morphology. The pulse program at its simplest is shown in ***Figure 13***. An incremental delay, t_1, is placed after the initial ^1H 90 ° pulse. This allows detection of the proton magnetisation through the amplitude modulation of the ^{13}C signal generated by cross polarisation.

The resulting data are then Fourier transformed over the two dimensions (t_1 and t_2) to give a 2D spectrum in which the proton wideline spectra are separated by the corresponding ^{13}C isotropic chemical shifts.

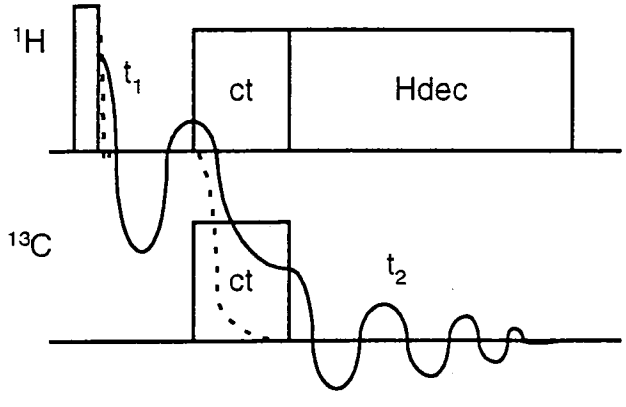

Figure 13 Pulse program for WISE. (The thick line represents the magnetisation of a mobile group, the dashed line a rigid group)

It should be noted that it is not only the ^1H-^1H, but also the ^1H-^{13}C dipolar interactions that affect the magnetisation decay of the protons that are close enough to the ^{13}C nuclei

to cross polarise to them. In reality, a ^{13}C that is bonded to a proton structurally isolated from the other protons can exhibit sharp spinning sidebands with a Pake-like envelope, since the ^{13}C-^{1}H pair interaction dominates the evolution of the single proton cross polarising to the carbon.

Since ^{1}H-^{1}H and ^{1}H-^{13}C dipolar interactions are affected by motional averaging in a similar way, the information on the dynamical state of these segments is not impaired by these couplings.

Since proton spin-diffusion in WISE is undesirable, both during CP and during the mixing time, a very short contact time should be used.

2.9.4.3 Separated local field (SLF[89,90]) experiments – including sccslf3

Complications are produced by proton-proton and proton-carbon through-space magnetic dipolar interactions. In a few cases where molecular motion has attenuated dipolar couplings, solution analogues of J spectroscopy have been successful. The dipolar dephasing technique effectively discriminates between rigid protonated and methyl (and quaternary) carbons but fails to distinguish between methine and methylene carbons.

^{13}C MAS spectra obtained with homonuclear proton decoupling (MPPD) detail the dipolar coupling information from directly-bonded protons by giving splittings from J_{CH} and offer the most elegant solution to the assignment problem.

Furthermore, C-H dipolar coupling patterns obtained with MPPD can be analysed to establish the identity of a particular carbon line as methyl, methylene, or methine. Analysis of dipolar coupling patterns can reveal important information about molecular motion, bond lengths, bond angle and relative orientation of the shielding anisotropy tensor and the internuclear vector. These techniques are called SLF techniques[91,92,93], and may also be referred to as 'Dipshift'[94,95,96,97,98] experiments.

2D SLF experiments are used to disentangle CH dipolar coupling information from individual lines. The experiment typically requires an evolution period with MPPD during which the spin magnetisation evolves in time under the influence of the chemical shift and the heteronuclear dipolar (and scalar) coupling from the attached protons. A 180° pulse followed by evolution under HPPD is then used to refocus the chemical shifts. The evolution period is incremented discretely to obtain a 2D data set.

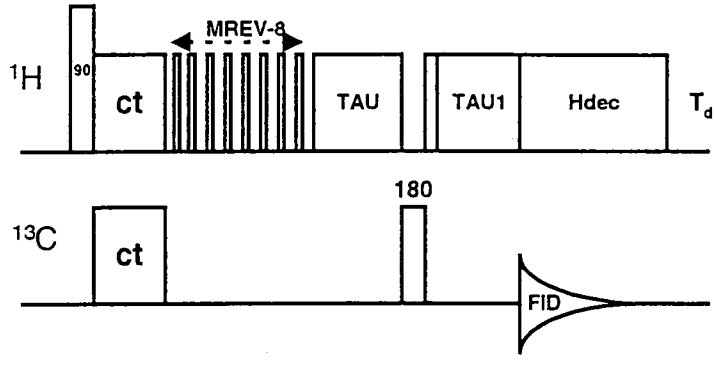

Figure 14 Pulse sequence for sccslf3, SLF experiment with MREV-8.

The sccslf3 and sccslfw (with WAHUHA) pulse sequences were written and implemented during the Ph.D. research (see Chapter 5). The experiment was acquired using the acquisition macro sccvlc, which allows 200 separate FIDs to be acquired in t_1.
A one-dimensional ~SLF technique has been proposed[99] whereby the evolution time may be selected according to the specific relaxation properties of carbons of specific multiplicities.

2.9.4.4 Inversion recovery Cross Polarisation

The IRCP technique is a solids version of the APT in solution and is also very useful, showing, by the rate of inversion of a ^{13}C signal, the possible CH_n multiplicity of the specific site to be determined (see chapter 5).

2.9.5 Triple-channel experiments

2.9.5.1 Normal pulse sequences on HFX and HXY probes

All the usual dual-channel pulse programs may be modified for triple-channel operation, taking care to use the suitable amplifier set ups which will be necessitated by the use of three amplifiers. The triple-channel set up is more complex and much more time consuming, but if carried out accurately, there are far more experimental variables that may be altered. Examples include the double-decoupling experiments ('uscp2dec'), where simultaneous proton and fluorine decoupling is applied whilst observing carbon. CP may be forced from proton to fluorine, or vice versa[54], giving a completely different set of information.

The REDOR[100,101,102] technique, to determine dipolar couplings between spin pairs, is a variant on the dipolar dephasing technique. Although this method was applied to labelled BRL55834, results were inconclusive as labelling would have required isotopic enrichment of both the ^{13}C and ^{15}N sites. (SB is still working on this possibility for the future as I feel that it would provide valuable information as to the rotational orientation of the piperidinone ring).

2.9.5.2 Other experiments

2.9.5.2.1 Double CP (DCP[103,104]) and Drain experiments

The double cross polarisation experiment involves the sequential transfer of polarisation among three spin-½ systems (e.g. ^{13}C, ^{15}N, ^{1}H). The technique has been used particularly for labelled, solid proteins[105] to detect the occurrence of ^{13}C-^{15}N bonds.

The usual method (***Figure 15***) begins with abundant ^{1}H magnetisation which is then transferred to either of the rare nuclei, then the ^{1}H radiation is turned off and a second contact is made between the ^{15}N and ^{13}C. Following this, the FID of either of the rare nuclei is acquired. If the FID observed is that of channel 2, the experiment is called a

DRAIN experiment as, when the second contact is optimised, the magnetisation will drain to the nucleus on channel 3 such that no observable magnetisation will remain for the rare nucleus on channel 2.

The initial transfer from ^{1}H is carried out to improve sensitivity to get around awkward rare-spin problems. The second transfer is used to detect ^{13}C-^{15}N dipolar coupling. Since the signal is detected under high-resolution conditions, it is possible to differentiate between different C-N bonds. This technique has also been used on the HFX probe for the HFC case[7].

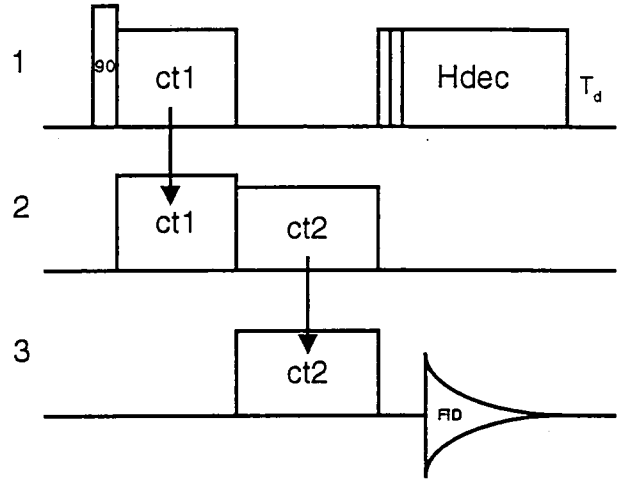

Figure 15 Pulse sequence for DCP experiment

2.9.5.2.2 ^{15}N-^{13}C correlation

This experiment requires DCP and correlates adjacent carbon and nitrogen sites. The pulse sequence was written by the incorporation of a delay (t_1) after the ^{1}H 90 ° pulse and before CP. The aim was to produce an experiment that could be applied to the spectra of labelled form II of BRL55834 in order to separate the three isotopic ^{13}C chemical shift spectra for each molecule in the asymmetric unit (see chapter 4).

Although the sequence was deemed to be successful by its application to doubly-labelled glycine, a lack of enriched compounds meant that any meaningful results could only be collected for this sample, and not BRL55834. However, when the doubly-enriched samples are finally produced by SB this experiment should be usefully applied within future research, maybe within another Ph.D.!

2.10 References

1 E. R. Andrew, R.G. Eades, *Proc. Roy. Soc. A.*, **218**, 537, 1953.

2 A. Pines, M. G. Gibby, J. S. Waugh, *J. Chem. Phys.*, **59**,569, 1973.

3 J. Herzfeld, X. Chen, *'Sideband analysis in MAS NMR of solids'*, *'Encyclopedia of NMR'*, Eds. D. M. Grant, R. K.Harris, Wiley, **7**, 4362, 1996.

4 E.B. Brouwer, R.K. Harris, *J. Magn. Reson.* in press, accepted May 1998.

5 S. Berger, S. Braun, H. O. Kalinowski, *'NMR spectroscopy of the non-metallic elements'*, Wiley, 113, 1997.

6 A. E. Aliev, K. D. M. Harris, *Magn. Reson. Chem.*, **32**, 366, 1994.

7 A. Nordon, *Ph.D. Thesis*, Solid state NMR of inclusion compounds, Durham, 1997.

8 B. C. Gerstein, *Phil. Trans. R. Soc. Lond. A.*, **299**, 521, 1981.

9 D.P.Burum, M. Linder, R. R. Ernst, *J. Magn. Reson.*, **43**, 463, 1981.

10 P. Jackson, R. K. Harris, *Magn. Reson. Chem.*, **26,** 1003, 1988.

11 D. P. Burum, D. G. Cory, K. K. Gleason, D. Levy, A. Bielecki, *J. Magn. Reson. A.*, **104**, 347, 1993.

12 J. Fahrenfort, *Spectrochimica Acta,* **17**, 698, 1961.

13 A. F. Barnes, D. Egglestone, SB internal memos dated 3/04/92, 1/10/91, 15/11/91.

14 D. M. Doddrell, D.T. Pegg, M. R. Bendall, *J. Magn. Reson.*, 48, 323, 1982.

15 L .Fielding, N. Hamilton, R. Mcguire, M. Maridauf, A. C. Campbell, *Magn. Reson. Chem.*, **34**, 59, 1996.

16 H. Friebolin, 'Basic one and two-dimensional spectroscopy', VCH, 238, 1993.

17 A. Bax, R. H Griffey, B. L. Hawkins, *J. Am. Chem. Soc.*, **105**, 7188, 1983

18 J. E. Heritage, N. Soffe, I. O. Campbell, T. J. Norwood, J. Boyd, *J. Magn. Reson.*, **87**, 488, 1990.

19 A. Bax, M. Ikra, L. E. Kay, D. A. Torchia, R. Tschudin, *J. Magn. Reson.*, 86, 304, 1990.

20 C. J. Turner, *'Heteronuclear assignment techniqes'*, Encyclopedia of NMR, Eds. D. M. Grant and R. K. Harris, Wiley, Chichester/ New York, **4**, 2335, 1996.

21 D. P. Burum, *'Cross polarisation in solids', Encyclopedia of NMR,* Eds. D. M. Grant and R. K. Harris, Wiley, **3**, 1535, 1996.

22 R. K. Harris, *'Multinuclear magnetic resonance in liquids and solids – chemical applications'* , Eds. P. Granger and R. K. Harris, NATO ASI, Maratea, 1988.

23 S. R. Hartmann, E. L. Hahn, *Phys. Rev.* **128**, 2042, 1992.

24 M. Sardashati, G. e. Maciel, *J. Magn. Reson.*, **72**, 467, 1987.

25 F. Engelke, *'Cross polarisation in rotating solids: spin-1/2 nuclei', Encyclopedia of NMR,* Eds. D. M. Grant, R. K. Harris, Wiley, **2**, 1529, 1996

26 S. Hediger, B. H. Meier, R. R. Ernst, *J.Chem. Phys.*, **102**, 10, 4000, 1995.

27 G. Metz, X. Wu, S. O. Smith, *J. Magn. Reson. A.*, **110**, 219, 1994.

28 O. B. Peersen, X. Wu, I. Kustanovich, S. O. Smith, *J. Magn. Reson. A.*, **104**, 334, 1993.

29 G. Metz, M. Ziliox, S. O. Smith, *Solid state Nucl. Magn. Reson.*, **7**, 155, 1996.

30 B. J. Van Rossum, H. Forster, H. J. M. de Groot, *J. Magn. Reson.*, **124**, 516, 1997.

31 R. Freeman, *Handbook of NMR,* Longman Scientific, 17, 1991.

32 M. H. Levitt, R. Freeman, T. Frenkiel, *J. Magn. Reson.*, **50**, 157, 1987.

33 J. S. Waugh, *J. Magn. Reson.*, **50**, 30, 1982.

34 J. S. Waugh, *J. Magn. Reson.*, **49**, 517, 1982.

35 U. Haeberlen, J. Eliot, J. S. Waugh, *J. Chem. Phys.*, **55**, 1, 1971.

36 R. L. Vanderhart, W. L. Earl. A. N. Garroway, *J. Magn. Reson.*, **44**, 361, 1981.

37 A. E. Bennet, C. M. Rientstra, M. Auger, K. V. Lakshmi, R. G. Griffin, *J. Chem. Phys.*, **103**, 6951, 1996.

38 R. K. Harris, A. M. Kenwright, R. A. Fletton, R. W. Lancaster, unpublished work.

39 P. Tekely, P. Palmas, D. Canet, *J. Magn. Reson. A.*, **107**, 129, 1994.

40 Z. Gan, R. R. Ernst, *Solid state Nucl. Magn. Reson.*, **8**, 153, 1997.

41 M. Ernst, S. Bush, A. C. Kolbert, A. Pines, *J. Chem. Phys.*, **105**, 9, 1988.

42 D. P. Burum, *Concepts Magn. Reson.*, **2**, 213, 1990.

43 B. C. Gerstein, *'CRAMPS', Encyclopedia of NMR,* Eds. D. M. Grant and R. K. Harris, Wiley, **3**, 1501, 1996.

44 B. C. Gerstein, R. G. Pembleton, R. G. Wilson, L. M. Ryan, *J. Chem. Phys.*, **66**, 361, 1977.

45 I. Chang, G. Diezemann, G. Hinze, R. Bohmer, H. Sillescu, *J. Magn. Reson.*, **124**, 165, 1997.

46 J. S. Waugh, L. M. Huber, U. Haeberlen, *Phys. Rev. Lett.*, **20**, 180, 1968

47 P.Mansfield, *Phil. Trans. R. Soc. Lond. A.*, **299**, 479, 1981.

48 P. Mansfield, *J. Phys. C; Solid State Phys.*, **4**, 1444, 1971.

49 W. K. Rhim, D. D. Elleman, R. W. Vaughan, *J. Chem. Phys.*, **59**, 3740, 1973.

50 D. P. Burum, W. K. Rhim, *J. Chem. Phys.*, **71**, 944, 1979.

51 S. F. Dec, C. E. Bronnimann, R. A.Wind, G. E. Maciel, *J. Magn. Reson.* **82**, 454, 1989.

52 S. Hafner, H. W. Speiss, *J. Magn. Reson. A,* **121**, 160, 1996.

53 M. R. M. P. Aguiar, S. M. C. Menezes, A. L. Gernal, R. A. S. San Gil, *Solid State Nucl. Magn. Reson.*, **4**, 179, 1995.

54 S. C. Campbell, R. K. Harris, M. J. Hardy, D. C. Lee, D. J. Busby, *J. Chem. Soc. Perkin Trans. 2.*, 1913, 1997.

55 M. Baldus, D. G. Guerts, S. Hediger, B. H. Meier, *J. Magn. Reson. A.*, **118**, 140, 1996.

56 L. Muller, A. Kumar, T. Baumann, R. R. Ernst, *Phys. Rev. Lett.*, **32,** 25, 1402, 1974.

57 S. Ding, C. A. McDowell, C. Ye., *J. Magn. Reson. A.*, **109**, 1, 1994

58 G. E. Hawkes, M. D. Mantle, K. D. Scales, S. Aime, R. Gobetto, C. J. Groombridge, *J. Magn. Reson. A.*, **116**, 251, 1995.

59 M. E. Stoll, *Phil. Trans. R. Soc. Lond. A.*, **299**, 565, 1981.

60 R. Pratima, K. V. Ramanathan, *J. Magn. Reson. A.*, **118,** 7, 1996.

61 E. Fukushima, S. B. W. Roeder, *'Experimental Pulse NMR – a nuts and bolts approach'* Addison Wesley, 446. 1981.

62 R. R. Ernst, G. Bodenhausen, A. Wokaun, *'Principles of NMR in one and two dimensions'*, p124; Oxford Science Publications, 1987.

63 R. R. Ernst, *Adv. Magn. Reson.*, **2**, 1, 1996.

64 A. Roscher, L. Emsley, C. Roby, *J. Magn. Reson. A.*, **118**, 112, 1996.

65 J. S. Frye, *Concepts Magn. Reson.*, **1**, 27, 1989.

66 J. Seliger, *J. Magn. Reson. A.*, **116**, 67, 1996.

67 N. Bloembergen, *Concepts Magn. Reson.*, **6**, 185, 1994.

68 M. A. K. Williams, R. D. Keenan, T. K. Halstead, *Solid-state Nucl. Magn. Reson.*, **6**, 47, 1996.

69 F. Laupetre, *NMR Basic Principles and Progress,* **30**, 63, 1994.

70 J. Seliger, *J. Magn. Reson. A.*, **116**, 67, 1995.

71 K. W. Zilm, *Encyclopedia of NMR 'Spectral editing techniques'*, (Eds. D. M. Grant and R. K. Harris), Wiley, **7**, 4498, 1996.

72 J. Z. Hu, X. Wu, N. Yang, L. Li, C. Ye, R. J. Pugmire, D. M. Grant, K. Qin, *Bulletin. Magn. Reson.*, **17**, 1, 2581, 1995

73 W. Xialong, Z. Shanmin, W. Xuewen, *Phys. Rev. B,* **37,** 16, 9827, 1988.

74 X. Wu, K. Zilm, *J. Magn. Reson. A.*, **104,** 119, 1993.

75 L. B. Alemany, D. M. Grant, T. D. Alger, R. J. Pugmire, *J. Am. Chem. Soc.*, **105,** 669, 1983.

76 H. Pan, *J. Magn. Reson.*, **124**, 1, 1997.

77 M. Munowitz, W. P. Aue, R. G. Griffin, *J. Chem. Phys.*, **77**, 4, 1992.

78 R. Sangill, N, Rastrup-Anderson, H. Bildsoe, H. J. Jakobsen, N. C. Nielsen, *J. Magn. Reson. A.*, **107**, 67, 1994.

79 X. Wu, K. Zilm, *J. Magn. Reson. A.*, **102**, 205, 1993.

80 E. F. Rybaczewski, B. L. Neff, J. S. Waugh, J. S. Sherfinski, *J. Chem. Phys.*, **67,** 1977.

81 S. J. Opella, M. H. Frey, *J. Am. Chem. Soc.*, **101**, 19, 1979.

82 R. H. Newman, *J. Magn. Reson.*, **86**,176, 1990.

83 R. H. Newman, *J. Magn. Reson.*, **96**, 370, 1992.

84 G. S. Harbison, P. P. J. Mulder, H. Pardoen, J. Lugtenburg, J. Herfield, R. Griffin, *J. Am. Chem. Soc.*, **107**, 17, 1985.

85 J. Kummerlein, A. Sebald, *Encyclopedia of NMR, 'Reorientation in crystalline solids: Propellor-like R3M species'*, **7**, 4127, Eds. D. M. Grant and R. K. Harris, Wiley, 1996.

86 E. W. Hagaman, *J. Magn. Reson. A.*, **104**, 125-131, 1993.

87 K. Schmidt-Rohr, J. Clauss, H. W. Speiss, *Macromlecules,* **25**, 5273, 1992.

88 D. P. Burum, A. Bielecki, *J. Magn. Reson.*, **95**, 184, 1991.

89 N. K. Sethi, *J. Magn. Reson.*, **94**, 352, 1991.

90 J. Schaefer, R. A. Mckay, E. O. Stejskal, W. T. Dixon, *J. Magn. Reson.*, **32**, 125, 1985.

91 R. G. Griffin, G. Bodenhausen, R. A. Haberkorn, T. H. Huang, M. Munowitz, R. Osredcar, D. J. Ruben, R. E. Stark, H. Van Willigen, *Phil. Trans. R. Soc. Lond. A.*, **299**, 547, 1981.

92 J. Schefer, E. O. Stejskal, R. A. McKay, W. T. Dixon, *Macromolecules*, **17**, 1479, 1984

93 H. Pan, *J. Magn. Reson.*, **124**, 1, 1997.

94 M. G. Munowitz, R. G. Griffin, *J. Chem. Phys.*, **78**, 2, 1983.

95 M. G. Munowitz, R. G. Griffin, *J. Chem. Phys.*, **76**, 6, 1982.

96 P.Palmas, P. Tekely, D. Canet, *Solid State Nucl. Magn. Reson.*, **4**, 105, 1995.

97 M. G. Munowitz, T. H. Huang, C. M. Dobson, R. G. Griffin, *J. Magn. Reson.*, **57**, 56, 1984.

98 A. C. Kolbert, D. P. Raleigh, M. H. Levitt, R. G. Griffin, *J. Chem. Phys.*, **90**, 2, 1989.

99 N. K. Sethi, *J. Magn. Reson.* **94**, 352, 1991.

100 Y. Pan, *Solid State Nucl. Magn. Reson.*, **5**, 263, 1995.

101 E. R. H. van Eck, W. S. Veeman, *Solid State Nucl. Magn. Reson.*, **2**, 307 1993.

102 T. G. Oas, R. G. Griffin, M. H. Levitt, *J. Chem. Phys.*, **89**, 2, 1988.

103 J. Schaefer, R. A. McKay, E. O. Stejskal, *J. Magn. Reson.* **34**, 443, 1979.

104 M. Baldus, D. J. Guerts, S. J. Hediger, B. H. Meier, *J. Magn. Reson. A.*, **118**, 140, 1996.

105 E. O. Stejskal, J. Schaefer, R. A. McKay, *J. Magn. Reson.*, **57**, 471, 1984.

Chapter 3

Multidisciplinary approach to the study of polymorphism

3.1 Introduction

It is the primary aim of this chapter to provide the background to the polymorphic systems studied during this Ph.D. research. This will be carried out by presentation of the results of analytical and structural techniques that allude to the existence of polymorphism and on which basis solid-state NMR experiments were initiated.

The importance of the application of a number of analytical techniques to a new pharmaceutical compound is highlighted in a recent paper by Byrn[1], which is entitled: 'Pharmaceutical solids: A strategic approach to regulatory considerations'. The flow charts that are presented in this article stress the importance of fully resolving solid-state issues before the critical stages of drug development are reached. This concept is supported throughout this chapter by the varying degree of sensitivity towards polymorphic differences in the output (spectra/ thermograms) of the various analytical techniques when applied to different polymorphic systems.

The combination of several spectroscopic techniques is particularly valuable when it is considered that the various arbitrary regions of the electromagnetic spectrum may probe effects occurring on widely varying timescales and levels of energy requirement. In the radiofrequency region (NMR) this energy (~0.001-10 J mol^{-1}) is required to change the orientation of a nuclear spin, which is influenced by its electronic environment. Infrared spectroscopy is sensitive to vibrations, indicating a change in the molecular configuration caused by the bending or stretching of atom-to-atom bonds (~10^4 J mol^{-1}). Raman spectroscopy is complementary to IR, also indicating a change in the molecular configuration, but this technique is only sensitive to a change that alters the polarisability.

Finally, X-radiation is able to probe a change in the inner electron distribution within the molecular structure. These energy changes may be of the order of 10^4 kJ mol^{-1}.

The types of data that are presented in this chapter vary between the two polymorphic systems studied. Whilst initial indications of the polymorphic characteristics of BRL55834 arose from the IR spectra and DSC thermograms, the microcrystalline nature of this compound has meant that no structurally-definitive X-ray data had been acquired.

The polymorphism of BRL61063 is less obvious from a combination of IR and DSC data. However, single-crystal data of three of these polymorphs have developed a significant amount of understanding of the structural differences between the polymorphs. A large amount of original analysis has been carried out on the original X-ray data for three polymorphs of Brl61063 and this is presented towards the end of this chapter. The results of this work did not come to light until a late stage of the Ph.D., after the majority of NMR research had been carried out.

Finally, an investigation into the detection limits of Raman spectroscopy for mixtures of the two forms of BRL55834 is presented. Work like this is important for three reasons. Firstly, to probe at what level of contamination a certain analytical technique will identify a small amount of form X in form Y. Secondly to develop techniques to quantify the amount of 'contaminant' present in a sample. Finally it is the aim in the pharmaceutical industry to assess the biological implications of the detection limit upon the patient.

3.2 BRL55834

3.2.1 Chemical name

The chemical name of BRL55834 is (3S-trans)-1-[3,4-dihydro-3-hydroxy-2, 2-dimethyl-6-(pentafluoroethyl)-2H-1-benzopyran-4-yl]-2-piperidinone. The molecular formula of BRL55834 is $C_{18}H_{20}NO_3F_5$, and the molecular weight is 393.36 g mol^{-1}.

3.2.2 Molecular structure

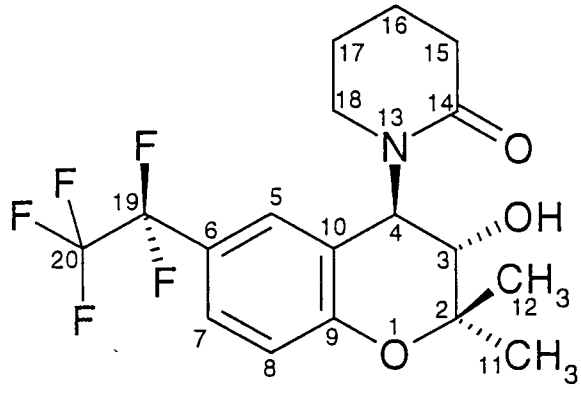

Figure 1 Structure and atomic numbering system for BRL55834

3.2.3 Appearance, storage, solubility and colour

Colour / form	White powder
Storage conditions	Cool, dry place
Solubility details	Ethanol, DMSO, DMF
Toxicity hazards	Unknown

Table 1 Appearance, storage, solubility and colour of BRL55834.

3.2.4 Compound background

The compound BRL55834 used to be of particular interest to SmithKline Beecham due to its pharmaceutical properties. The drug is a calcium channel activator for smooth muscle and was being developed to treat asthma. A combination of commercial reasons and the dubious efficacy of this molecule have led to cessation of the development of BRL55834.

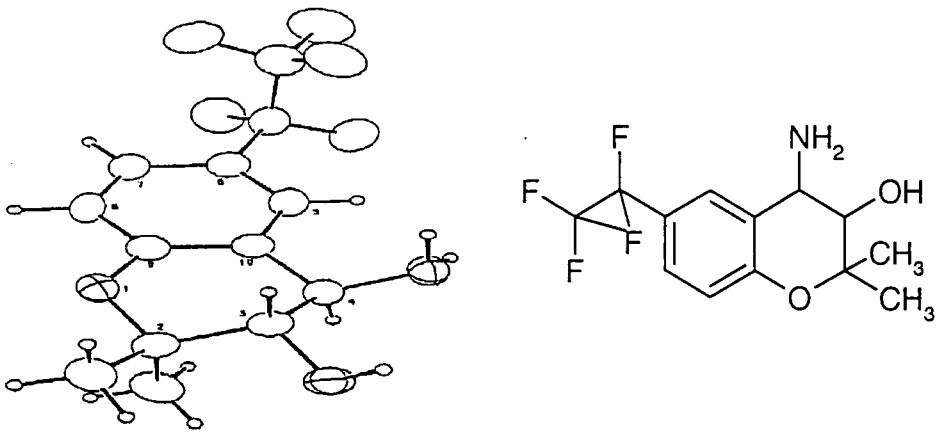

Figure 2 ORTEP diagram and molecular structure of precursor to BRL55834 (SB20137)

Initial structure determination carried out by SB gave several results[2,3,4] that indicated polymorphism may be present in this system. Added to these facts, it has proved extremely difficult to obtain a suitable single crystal of this material and therefore the unit cell conformation is unable to be determined by single-crystal X-ray diffraction. The only relevant X-ray data that have been collected is that of the precursor to BRL55834 (see ***Figure 2***). This confirmed the core structure of BRL55834.

3.2.5 Preparation of the polymorphic forms I and II

During the SB synthetic route development to BRL55834, two different methods were used for the final purification and isolation procedures. These resulted in the preparation and identification of two distinct crystalline forms of BRL55834, which have been designated as forms I and II. Form I is obtained by recrystallisation of BRL55834 from di-isopropyl ether followed by drying under a vacuum. Form II is prepared by dissolution in ethyl acetate, followed by evaporation to dryness in a vacuum. The resulting solid is triturated with hexane, filtered off, washed again with hexane and dried under a vacuum. Attempts to form single crystals were made, but without success due to the microcrystalline nature of both forms.

DSC and IR measurements, which had provided the initial demonstration of the existence of the two polymorphic forms were obtained at SmithKline Beecham Pharmaceuticals

Harlow. These were used for identification purposes. The conversion of form I into form II can be induced thermally (the reverse transformation has not been observed).

3.2.6 Differential Scanning Calorimetry

DSC traces of forms I and II are shown in ***Figure 3***. Both show relatively sharp melting endotherms with onsets of 150 and 147 ^{0}C respectively. The heating rate was 10 °C per minute. These onset temperatures are fairly typical of the two forms, although for some batches of form I the onset of melting has been observed around 151 °C. No thermal events are observed on cooling the melt, which solidifies to form a glass. ***Figure 3*** also shows the DSC trace of the glass obtained from form I (as expected, the glass derived from form II gives essentially the same trace (data not shown)). The small endothermic drift around 50 °C is believed to be a glass transition. The broad exotherm over the range 90-120 °C corresponds to crystallisation, which is followed by melting (onset 147 °C). This is consistent with the formation and melting of form II (which was subsequently confirmed by variable temperature IR studies). To summarise, melting, cooling and reheating either form produces form II.

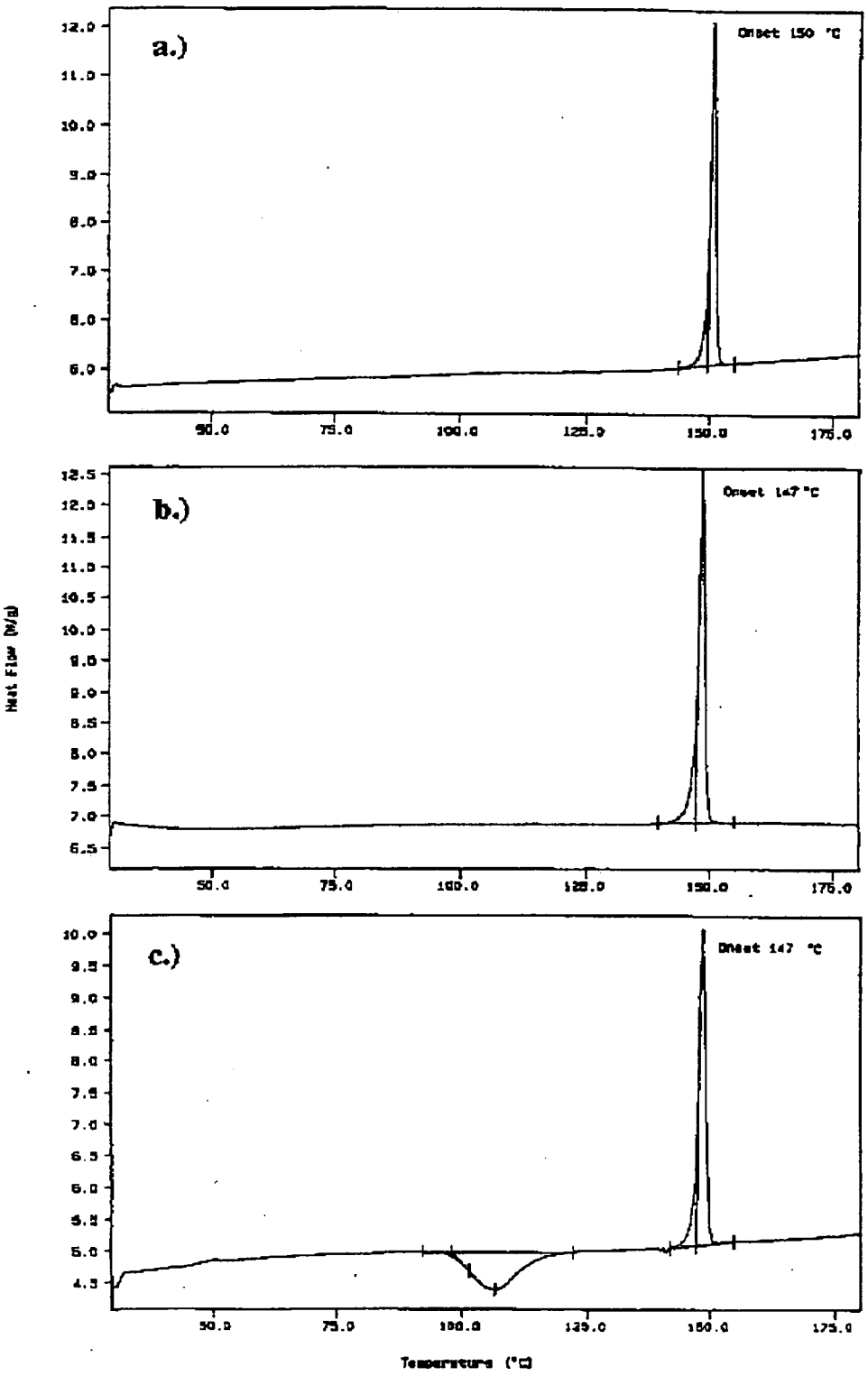

Figure 3 DSC traces of (a) form I and (b) form II and (c) the glass obtained from cooling the melt of form I

3.2.7 Infra Red Spectroscopy

The IR spectra of the two forms show extensive differences (see ***Figure 4***). Form I has a single O-H stretching band at 3436 cm^{-1}, whereas form II shows a complex envelope between 3600 and 3100 cm^{-1} (principal bands at 3428 and 3209 cm^{-1}). The carbonyl stretching region reflects the hydroxyl stretching region to some extent, with form I displaying a single band at 1619 cm^{-1} and form II displaying principally two bands at 1643 and 1607 cm^{-1}. Clearly the hydrogen bonding is significantly different in the two forms, with greater complexity in form II. Significant differences also occur around 1200 cm^{-1} (asymmetric C-O-C stretching in the chroman ring); form I displays a single intense band at 1206 cm^{-1} and form II shows two intense bands at 1214 and 1201 cm^{-1}. C-F stretching is expected to give rise to several strong bands between 1400 and 1100 cm^{-1}, but vibrational coupling with the aromatic ring makes unambiguous assignment difficult. The coupled out-of-plane deformation of the two adjacent aromatic hydrogens gives absorption near 830 cm^{-1}, which is again split into two components in the case of form II. Below 800 cm^{-1} the spectra of both forms are relatively similar.

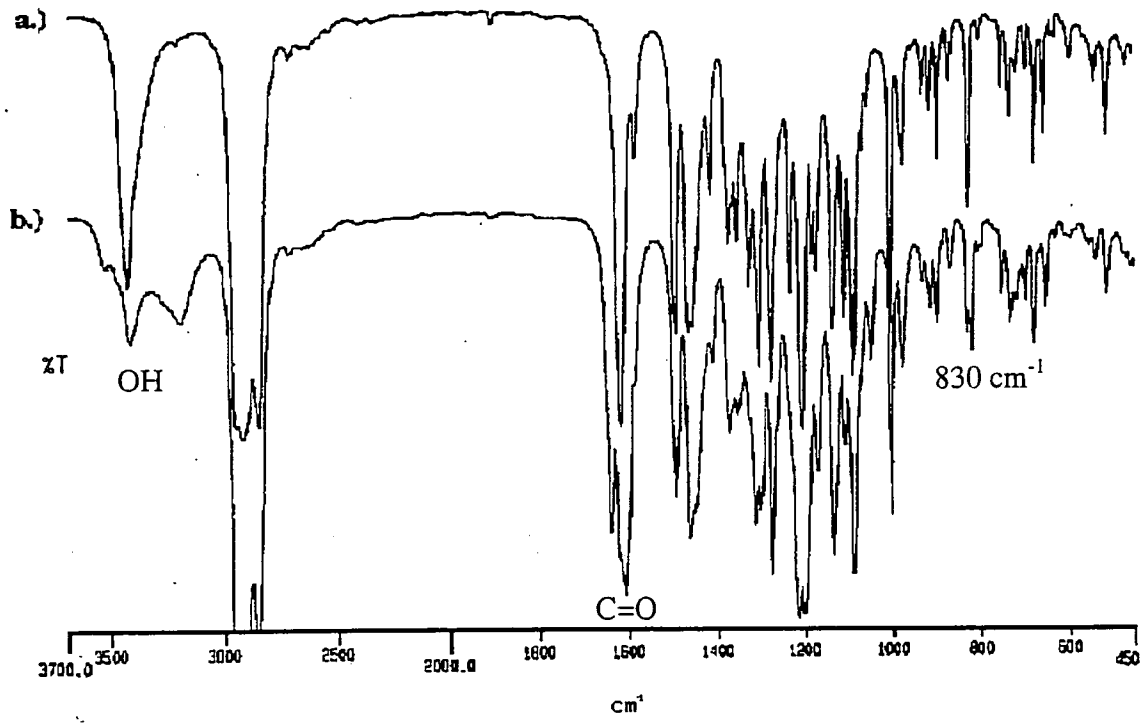

Figure 4 Infrared Spectra of nujol mulls of (a) form I and (b) form II (SB).

3.2.8 Powder X-ray diffraction

Powder X-ray diffractograms confirmed that the two polymorphs are, indeed, crystallographically very different (see ***Figure 5***). Form II shows more peaks. A detailed analysis has been initiated involving acquisition of the PXRD data with synchotron radiation, with the long-term aim of finding a structure solution using genetic algorithm techniques for this system.

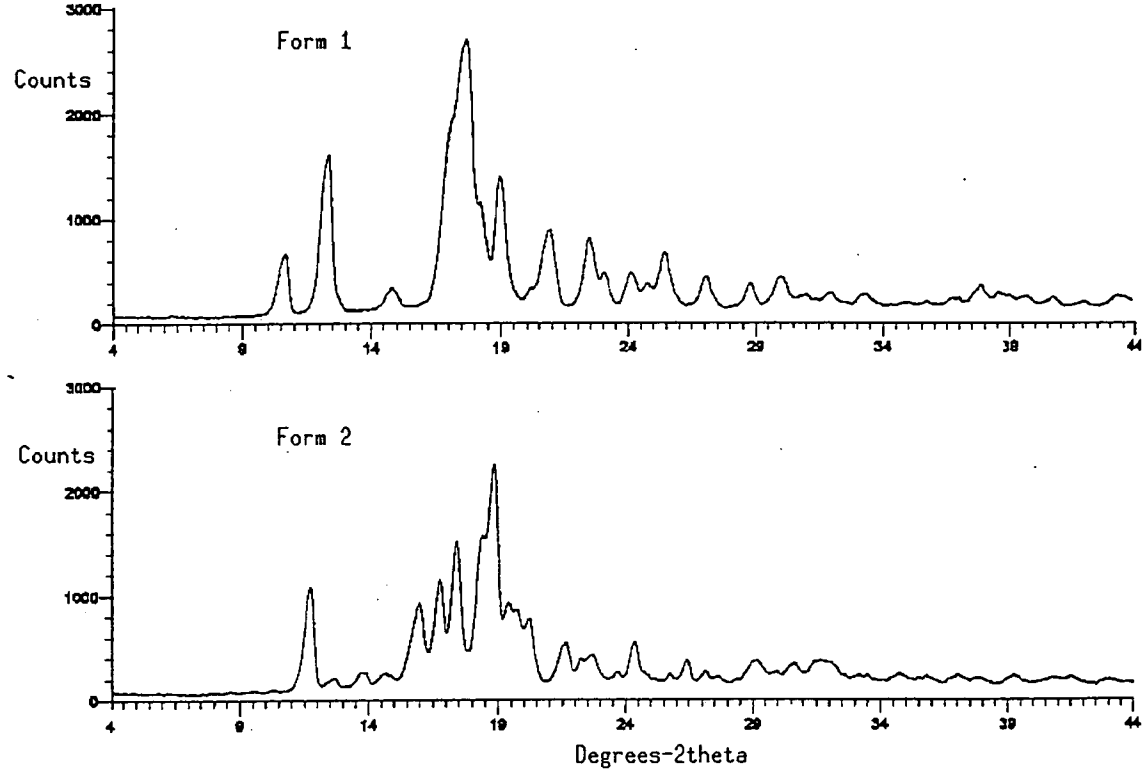

Figure 5 Powder X-ray diffraction traces of (a) form I and (b) form II (Durham)

3.2.9 Structural Background of BRL55834

Although single-crystal X-ray diffraction of this compound has not been carried out due to the difficulty in forming good-quality, single crystals, there are several references in the literature[5,6] that point to a possible preferred conformational orientation of the molecule in the solid state.

A crystal structure determination carried out on an analogue of BRL55834, which has an -OC(O)NHCH(CH_3)(Ph) group in place of the hydroxy group on the C(3) position, confirmed the absolute configuration to be 3S, 4R. This has also been proved to be the case for BRL55834 by solution-state proton NMR spectra and the Karplus relationship. Results also show that the C(4) amine moiety takes up a position orthogonal to the benzopyran nucleus. However, the position of the carbonyl group is under some debate because work carried out on similar compounds has reported cases in which this may be aligned either away from or towards the C(4) proton. As yet, no reason for this orientational difference is known but it may reflect conformational differences between the piperidinone ring in BRL55834, and the pyrrolidinone or planar six-membered ring systems of other compounds.

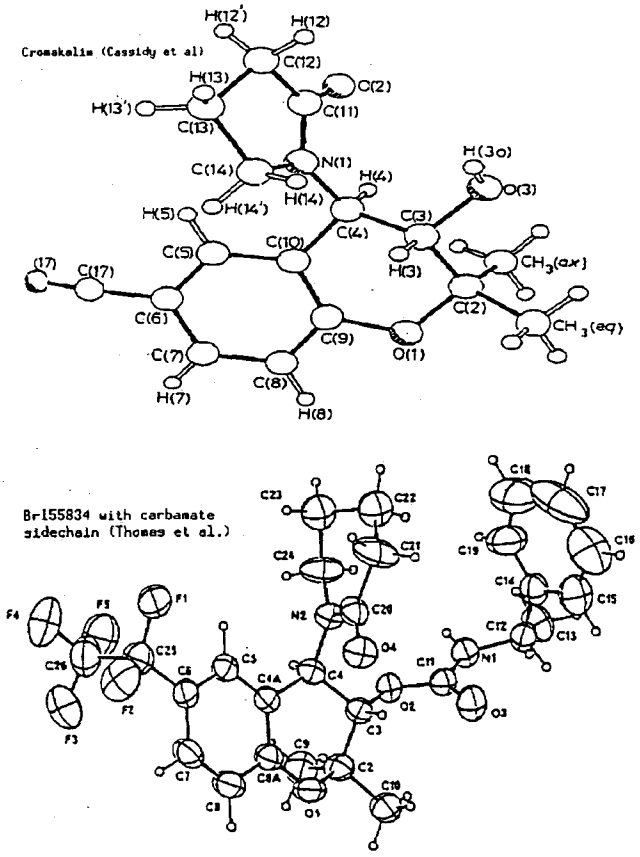

Figure 6 Crystal structure of two compounds that are structurally-related to BRL55834

Initial work performed by Cassidy *et al.*[6] (Beecham Pharmaceuticals) on BRL34915, a similar compound to BRL55834 which has a five-membered ring at the C(4) position,

suggested that there is no rotation of the pyrrolidone ring about the C(4)-N(1) bond. This assumption was based on the results of variable temperature work and ^{13}C T_1 measurements that provided no indication of the pyrrolidone carbons having any more mobility than those carbons in the fused benzopyran system.

However, later work carried out by Thomas *et al*[7]. (Roche Pharmaceuticals) disputed this on the basis of results previously reported for similar compounds[8], suggesting that extremely rapid rotation about this CN bond does take place, but that one rotational conformation is overwhelmingly predominant in the solvent used. They calculated an energy barrier to rotation of 48.1-56.4 $kJmol^{-1}$ (11.5-13.5 kcal mol^{-1}), which would allow rapid rotation at ambient temperatures. The possibility of these compounds forming varying proportions of rotamers was also investigated in different solvents, paying special attention to those most similar to physiological conditions.

It was also shown[7] that even when the steric hindrance to rotation of these molecules was increased by placing a methyl group on the pyrrolidone ring, the motion was still quite rapid at ambient temperatures.

3.3 BRL61063

3.3.1 Compound Background

The compound BRL61063 is of particular interest to SmithKline Beecham Pharmaceuticals due to its pharmaceutical properties. The existence of polymorphism was first discovered when development batches of BRL61063 showed differences in their IR mull spectra. As the same route was used to prepare all batches, with ethanol as the final recrystallisation solvent, therefore it appeared possible that the speed of crystallisation may affect crystal form.

Initial structure determination carried out by SB gave several results that indicated the existence of polymorphism in this system. Recrystallisation work in various solvents seems to confirm that there are several polymorphic forms. It has been possible to grow good-quality single crystals of three of these polymorphs, forms 1, 2 and 4, allowing the crystal structure of these forms to be found using X-ray diffraction.

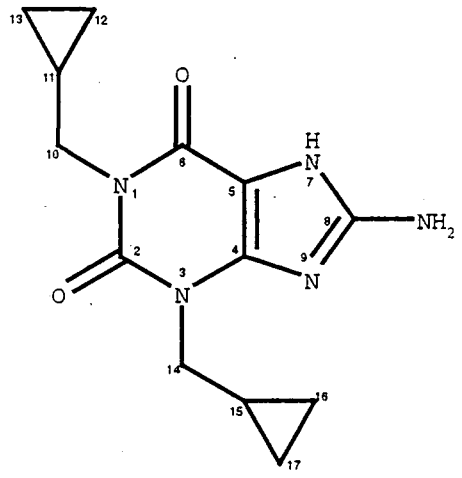

Figure 7 Molecular structure and numbering of BRL61063 (1,3-di-(cyclopropylmethyl)-8-aminoxanthine)

3.3.2 Preparation of the polymorphic forms

The preparation routes for the various forms are summarised in ***Table 2***, below. However, it should be noted at this stage that the 'form three' that is described here was produced in a very limited amount and was not properly characterised. Further attempts to produce this have been totally unsuccessful and extra efforts only produced form 2. There is no longer any access to this 'form 3' sample.

The majority of the work described in this thesis has been carried out on forms 1 and 2, the two forms that have been supplied by SB pharmaceuticals. However, a significant amount of effort has also been put into recrystallisation studies in attempts to form new polymorphs or the so-called forms 1, 2, 3 and 4. This work was carried out using the standard batch (H96/61063-HP3 batch 2 of 2 14/10/92) provided by SB.

Polymorph	Recrystallisation solvent
Form 1	Ethanol (s/f), propanol (s/f), butanol (s/f), isopropanol (s/f), ethyl acetate (s/f), water*, toluene*, tetrohydrofuran (s/f), acetone (s).
Form 2	Methanol (s/f), tetrahydrofuran (s), chloroform*, pyridine, acetone (f)
Form 3	Tetrahydrofuran (s/f)
Form 4	50:50 ethanol: propan-2-ol
(s) = slow, ambient recrystallisation (f) = fast, crash cool recrystallisation in ice * = Particularly low solubility of BRL61603 in these solvents, therefore modified procedure, i.e. solution was filtered to remove undissolved material and filtrate allowed to stand and crystallise out BRL61063.	

Table 2 Summary of polymorphic forms produced from various solvents (SB)

Using Total Internal Reflection Infra-red spectroscopy (the golden gate technique, to conserve the solids), it was extremely difficult to ascertain exactly which polymorph had been recrystallised, or, indeed to identify any new polymorph. Recrystallisation results were analysed using solid-state NMR, IR, and DSC (see later chapters 4 and 5).

Polymorph expected	Solvent	Cooling rate		Form produced
		Slow	Fast	
Form 1	Abs. EtOH	√	√	**A**
Form 2	MeOH	√	√	**B**
Form 2 /4	50:50 Abs. EtOH: IPA	√ Tried 20 mins, overnight & 4 days – yellow!!	√	**Yellow**
Form 3	THF	√	√	**D**
!! This was repeated, and crystals with a yellow tinge were still produced.				

Table 3 Recrystallisations successful in forming the different forms (Durham).

From this point onwards, the polymorphs of BRL61063 that have been worked upon will be referred to as form 1 and form 2 (each of these provided by SB), form D (recrystallised from THF in Durham) and 'yellow' (recrystallised from EtOH/IPA as above, in Durham).

3.3.3 DSC and thermal analysis

DSC (SB) could not differentiate the three forms of BRL61063. In each case, thermograms showed melting only, with similar onset and peak temperatures, typically $T_o = 312$, and $T_p = 314$ °C. However, when the heating rate was reduced sufficiently the melting endotherm appeared as a fused melt i.e. two components melting at once. This behaviour was common to all three forms.

Thermomicroscopic observations showed that all three forms sublime. The onset of sublimation was different for each form and continued over a wide temperature range (130-290 °C). This is not evident on the DSC thermograms. Melting occurred over the range (310-323 °C) for all three forms. The possibility of two components melting consecutively could not be distinguished. The sublimate was collected for all three forms and analysed by IR and NMR. This showed that form 1 had been produced.

Forms 1, 2, and 3 were annealed and were found to have converted to form 1 by IR. The annealing procedure consisted of heating at 10 °C min^{-1} from ambient to ca. 250 °C and holding at this point for 30-60 minutes, then allowing the sample to cool slowly to room temperature. This thermal information indicates that form 1 is the most stable form, which is also consistent with grinding studies.

3.3.4 Infra red Spectroscopy

The nujol mull IR spectrum was the initial technique by which the individual polymorphs were identified and distinguished at SB. The significant absorptions, and corresponding assignments are tabulated below. These IR bands confirm the basic structural moieties within BRL61603.

Frequency /cm^{-1}	Assignments
3455	NH_2 asymmetric stretch
3301	NH_2 symmetric stretch
3145	NH stretch
1689	C=O asymmetric stretch
1636	C=O symmetric stretch
1534	Heterocyclic ring stretch
1263	Primary aryl amine C-N stretch
1018	Cyclopropyl C-C stretch
756	Cyclopropyl band
830-670	NH_2 skeletal mode (wag)
1380, 1458, 2800-3000	Nujol absorptions

Table 4 Summary of IR absorptions generally observed for BRL61063 (SB)

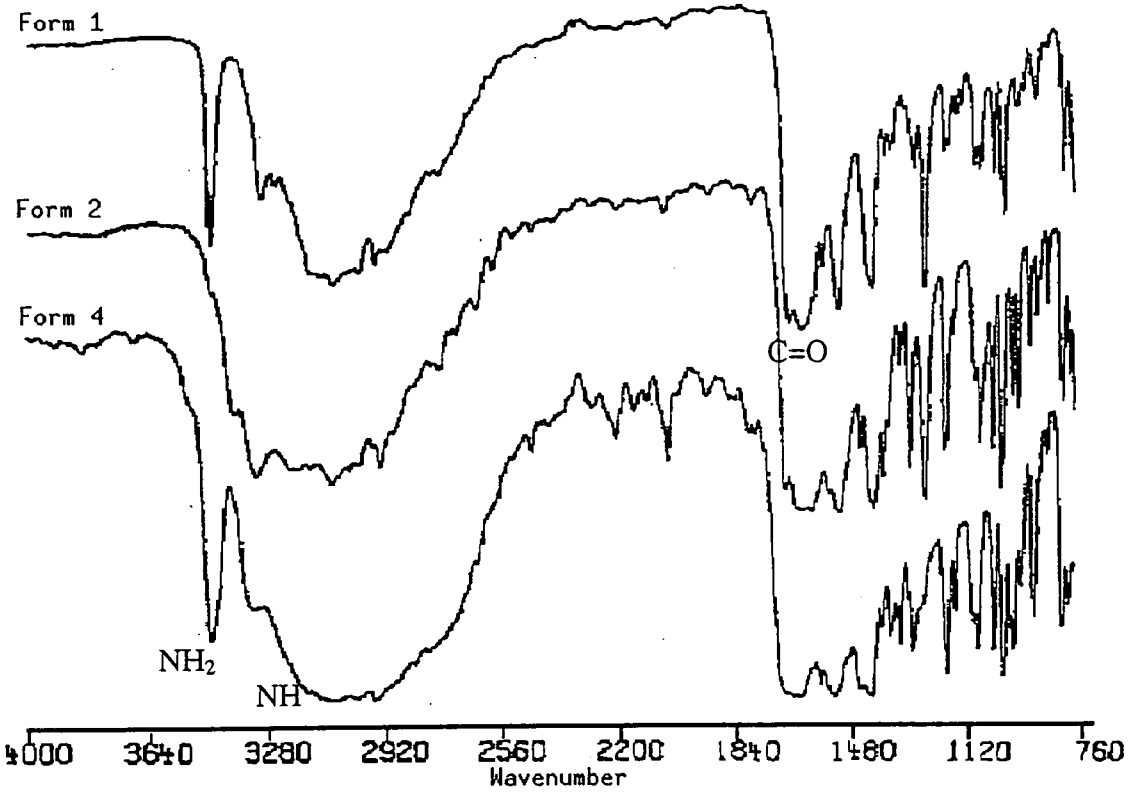

Figure 8 IR spectra of BRL61063, forms 1, 2, and 4 (Nujol Mull, SB)

The individual polymorphs of BRL61603 show interesting variations and contrasts in their IR spectra (see ***Figure 8***). The comparison of the IR spectra of forms 1 and 4 show some notable differences. The prominent band (1263 cm^{-1}) in the C-N stretching region for form 1 is absent or shifted in the spectra of form 4. Also, the prominent band with a shoulder at 1189 cm^{-1} in the spectrum of form 4 is weak in the form 1 spectrum and is accompanied by a nearly equal intensity band at 1202 cm^{-1}. Also, weak features in the spectrum of form 4 around 2000-2300 cm^{-1} are absent in form 1.

3.3.5 Powder X-ray Diffraction

X-ray powder diffraction spectra of BRL61603, polymorphic forms 1, 2, D, and 'yellow' have been obtained. These are each different and are consistent with being of different polymorphic forms. Whilst traces for forms 1, 2 and 'yellow' are very different, the trace for form D shows reflections in similar positions to those of form 1 although the intensities are very different. This infers that both forms 1 and D exist in the same cell type, but with different motifs.

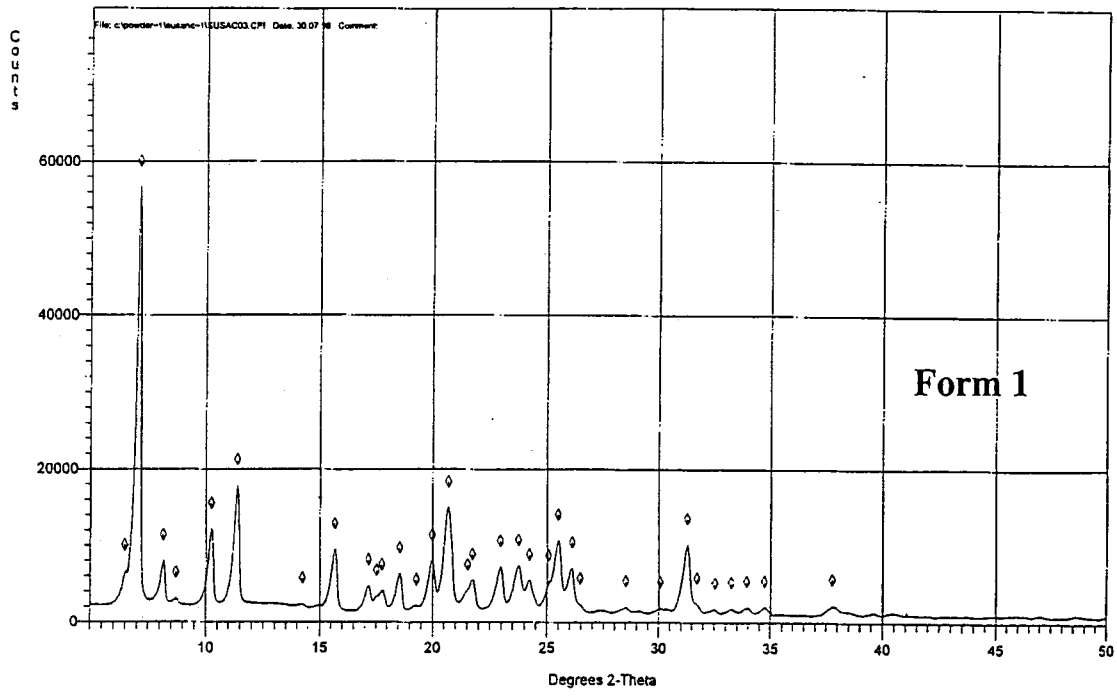

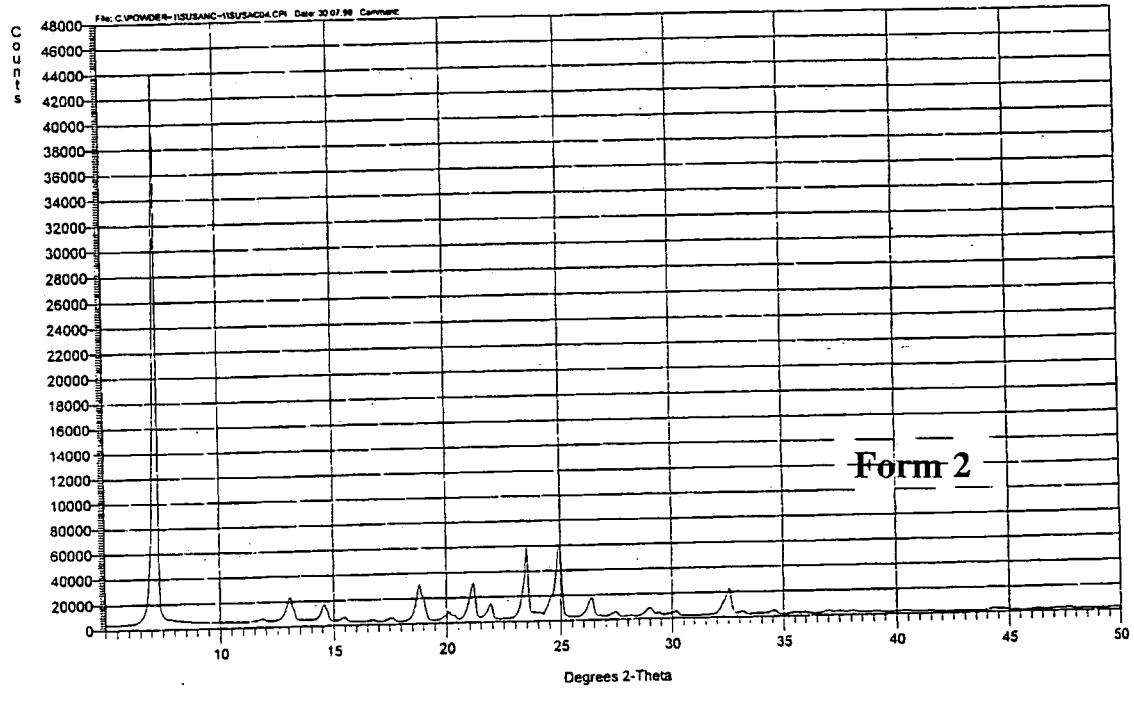

Figure 9a Powder X-ray diffraction traces of the samples of BRL61063 (Durham)

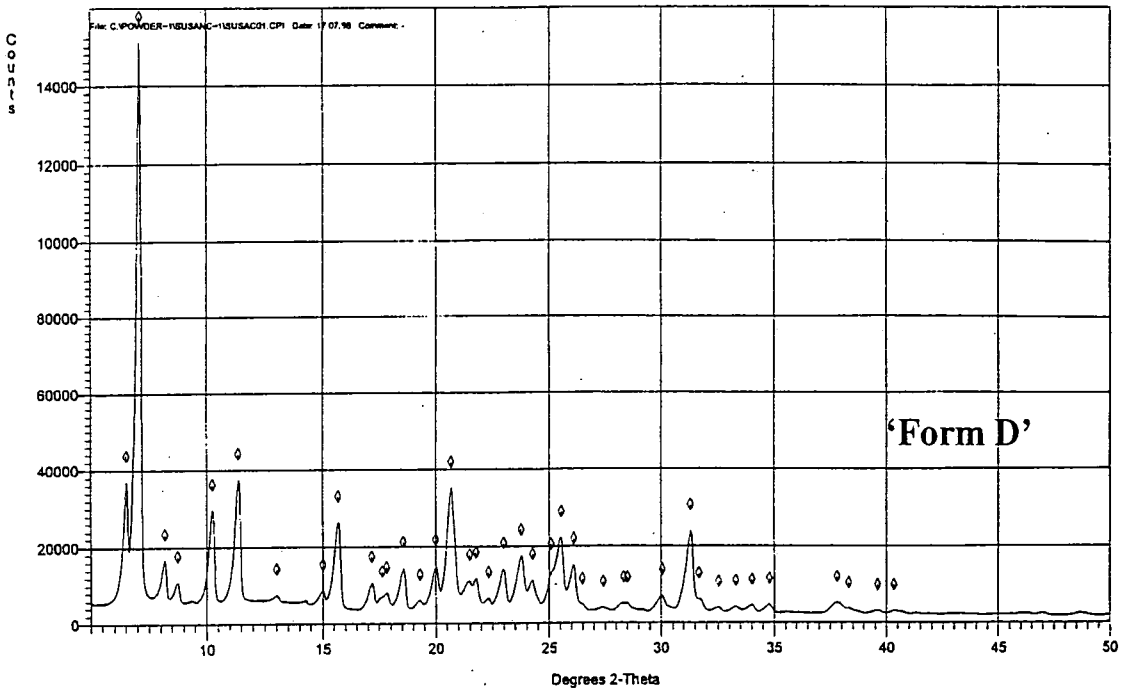

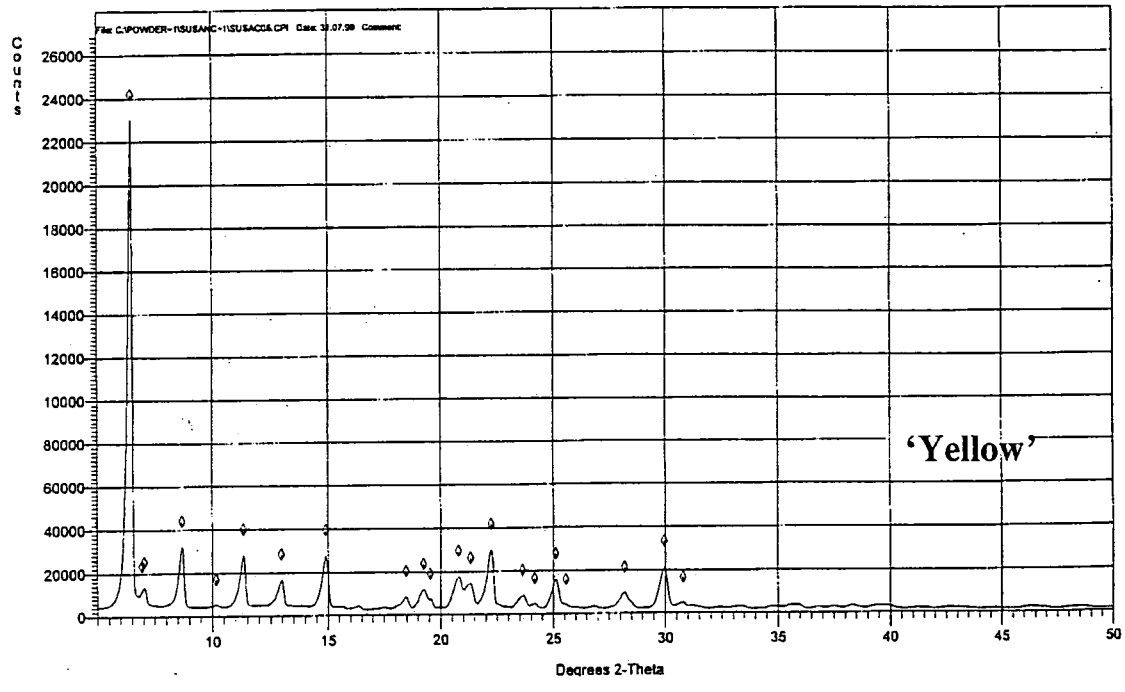

Figure 9b Powder X-ray diffraction traces of the samples of BRL61063 (Durham)

3.3.6 Single Crystal X-ray diffraction

Three-dimensional X-ray data have been used to determine the crystal and molecular structure of polymorphs 1, 2 and 4 of BRL61063[9]. Measurements were carried out at ambient temperature at SB. The results associated with each form are summarised in *Table 5*, below.

Parameter	Form 1	Form 2	Form 4
Crystal Shape	Flat needles	Rectangular blocks	Flat needles
Space group	$P\bar{1}$ triclinic #2	$P2_1/c$ monoclinic #14	$P\bar{1}$ triclinic #2
Cell constants	a = 10.829(2) Å b = 12.636(2) Å c = 5.105(3) Å α = 99.48(4) ° β = 91.53(4) ° γ = 83.84(3) °	a = 12.227(4) Å b = 7.448(2) Å c = 14.946(8) Å α = 90(4) ° β = 97.95(4) ° γ = 90(4) °	a = 10.210(3) Å b = 13.753(2) Å c = 4.942(1) Å α = 97.94(2) ° β = 97.95(4) ° γ = 83.33(2) °
Volume	685.0(8) $Å^3$	1348.1(9) $Å^3$	677.1(5) $Å^3$
Z	2	4	2
Density	1.335 g cm^{-3}	1.356 g cm^{-3}	1.350 g cm^{-3}

Table 5 Summary of the crystal measurements of polymorphic forms 1, 2 and 4 of BRL61063 (SB)

3.3.6.1 BRL61063 form 1

Single crystals of form 1 were crystallised slowly, from a mixture of ethyl acetate and butanol.

The distinguishing feature of the molecular conformation of form 1 is the clear disorder in the cyclopropyl groups. X-ray data pertaining to the group containing carbons numbered (12) and (13) show two possible positions of equal occupancy. Data for the other pendant

cyclopropyl group C(16) and (17) indicate the presence of a high degree of thermal motion, suggesting that this group may be undergoing conformational flexing.

The unit cell diagram shows the packing arrangement of form 1. These results are in keeping with the presence of disorder in the channel which the cyclopropyl groups occupy as the volume for form 1's unit cell is 8 $Å^3$ larger (with a corresponding density reduced by 0.15 g cm^{-3}) than that of form 4. Since the molecular conformation and unit cell of form 4 is similar to form 1 (see later section on form 4) (minus the disorder present in form 1) these results are in keeping with the observations.

Hydrogen bonding in form 1 is completely intermolecular in nature. In terms of the specific interactions this is also similar to those observed in form 4. This is summarised in **Table 6**, below.

H-bonding atoms	Atom-atom distance	Angle
N(2)----------N(1)	3.067(3) Å	
H(1)N(2)----------N(1)	2.16(3) Å	173(3) °
N(3)----------O(5)	2.793(3) Å	
HN(3)----------O(5)	2.02(3) Å	165(4) °

Table 6 Summary of hydrogen-bonding for BRL61063 form 1

It should be noted that the possibility of a weak interaction between N(2) and O(5) should not be overlooked, since the distance of only 3.993(3) Å between these two atoms may suggest that this is present. (This interaction *is* present in form 2). However, when a position for H(2)N(2) was calculated which would satisfy a hydrogen-bonding interaction and attempts were made to refine this, the thermal value became unreasonable large, suggesting that the data do not support this alternate position.

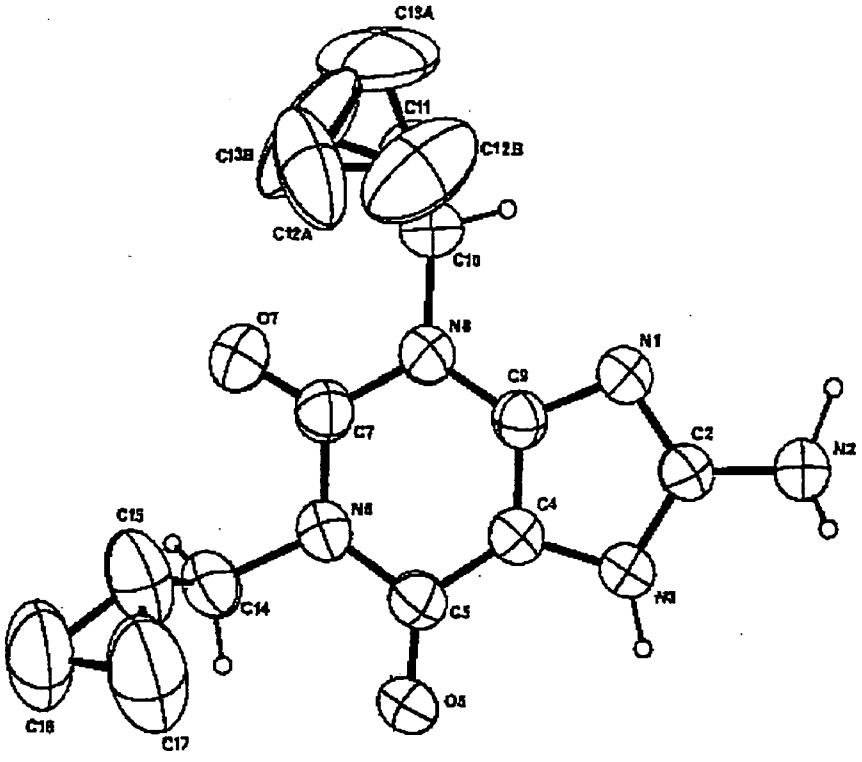

Figure 10 Crystal structure of BRL61063, form 1

3.3.6.2 BRL61603 form 2

The single crystal of polymorph 2 was formed from slow evaporation of a solution prepared in methanol and 2-butanone.

H-bonding atoms	Atom-atom distance	Angle
N(2)----------N(1)	3.071(3) Å	
H(2)N(2)----------N(1)	2.41(3) Å	137(3) °
N(3)----------O(5)	2.741(3) Å	
HN(3)----------O(5)	1.90(3) Å	168(4) °
N(2)----------O(5)	3.049(3) Å	
HN(2)----------O(5)	2.26(3) Å	168(2) °

Table 7 Summary of the hydrogen bonding in form 2

Data for form 2 support the existence of three hydrogen bonds, all intermolecular in nature. These results are summarised in ***Table 7***, and show that in this form *both* protons on the NH_2 (amine) group are involved in hydrogen bonds.

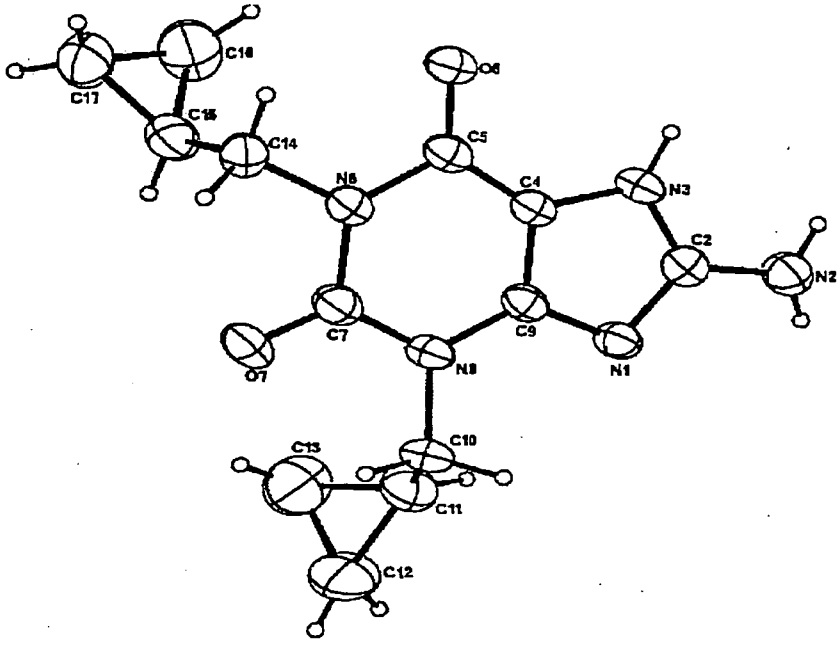

Figure 11 Crystal structure of BRL61063, form 2

3.3.6.3 BRL61063 form 4

The flat crystals of form 4 were crystallised by slow evaporation from a 50:50 solution of ethanol and isopropanol. Crystals of form 2 were also produced from this solution, appearing to nucleate first, with needles of form 4 forming after the solution had evaporated for several days. Transmittance microscopy was also used to prove the fact that form 4 is not the same as forms 1 and 2.

The molecular conformation of form 4 is overall very similar to form 2. The principal difference is in the rotational orientation of the cyclopropyl groups, which display a nearly enantiomorphous relationship to their counterparts in the form 2 structure. This may be summarised in the torsion angles tabulated in ***Table 8***.

Atoms	Torsion angle / (3)°	
	Form 2	Form 4
C7-N8-C10-C11	101.8	74.6
C9-N8-C10-C11	-84.6	-99.5
C5-N6-C14-C15	98.7	91.7
C7-N6-C14-C15	-80.2	-85.1
N8-C10-C11-C12	-77.5	80.4
N8-C10-C11-C13	-146.6	149.8
C10-C11-C12-C13	-104.9	-107.5
N6-C14-C15-C16	-88.5	89.4
N6-C14-C15-C17	-158.3	158.8
C14-C15-C16-C17	-108.1	-111.4

Table 8 Comparison of the torsion angles for the cyclopropyl groups of BRL61063, form 2 and form 4.

The hydrogen-bonding present in form 4 is very similar to that in form 1. However, a major difference involves one of the two hydrogen atoms on the NH_2 group. There is a clear indication of the position for H(1)N(2) (in form 4) in difference Fourier electron maps. This position is *not* consistent with the participation of that hydrogen in a hydrogen-bonding interaction.

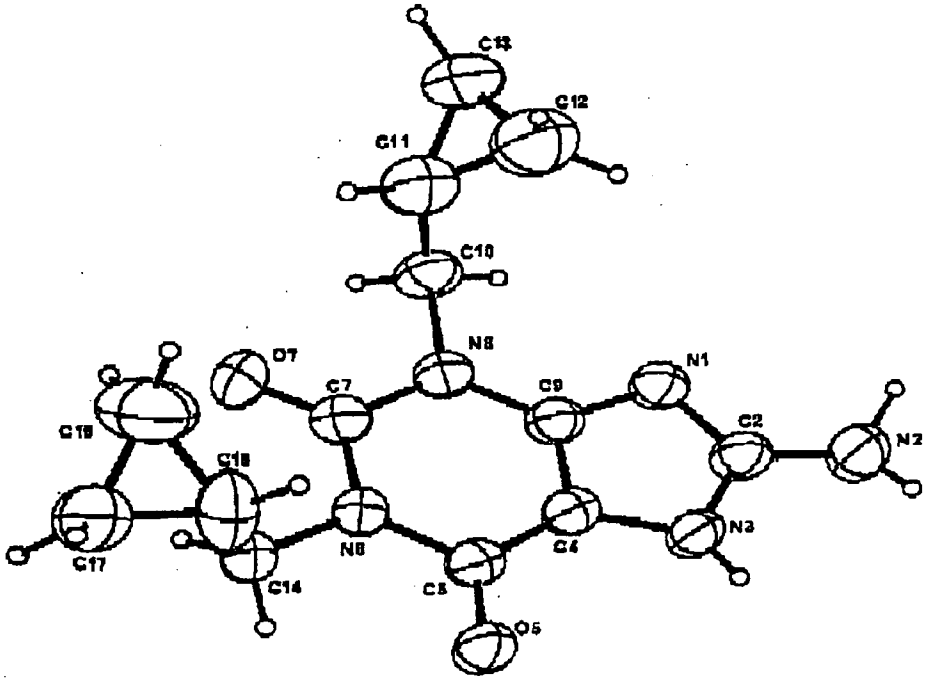

Figure 12 Crystal structure of BRL61063, form 4.

H-bonding atoms	Atom-atom distance	Angle
N(2)----------N(1)	3.042(3) Å	
H(1)N(2)----------N(1)	2.10(3) Å	173(2) °
N(3)----------O(5)	2.731(3) Å	
HN(3)----------O(5)	1.91(3) Å	160(2) °

Table 9 Summary of the hydrogen bonding in form 4

However, a distance of 3.273(3) Å between N(2) and O(5) in form 4 suggests the possibility of an hydrogen-bonding interaction analogous to that observed in the form 2 structure (although this distance is longer by 0.2 Å in form 4). When a position was calculated which would satisfy this hydrogen bonding interaction, and attempts were made to refine it, the thermal value became unreasonably large, suggesting that the data do not support this alternate position. (A similar situation has previously been described for form 1). The refinement was therefore completed with the H(1)N(2) in its original position as indicated by difference Fourier synthesis.

3.3.6.4 Summary and comparison of the known structures of BRL61063.

We now possess structural knowledge upon which to base the solid-state NMR investigation of the polymorphism of BRL61063. A summary of the distinguishing properties of each form is shown on the following page.

Forms 1, 2, and 4 of BRL61603 are all crystallographically different. The hydrogen bonding in all the forms is intermolecular in nature, and all three possess hydrogen bonding between HN(2)-----N(1) and HN(3)-----O(5).

The tentative prediction of the existence of a third hydrogen bond for forms 1 and 4, may be explored by using solid-state NMR. Variable temperature studies will also be applied to explore the disorder in form 1 (see chapter 5).

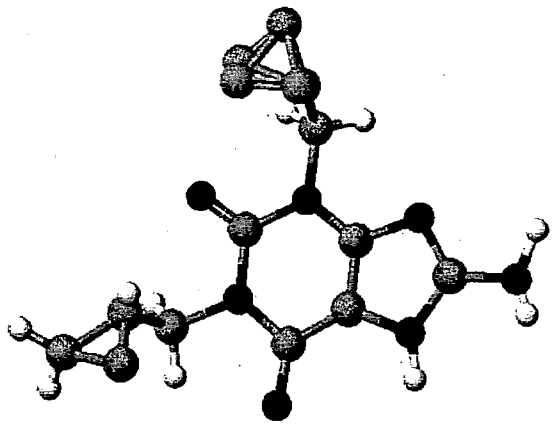

Form 1

There is clear disorder exists in the pendant cyclopropyl groups, with C(12)(13) existing in two positions of equal occupancy, and C(16)(17) showing disorder indicative of conformational flexing.

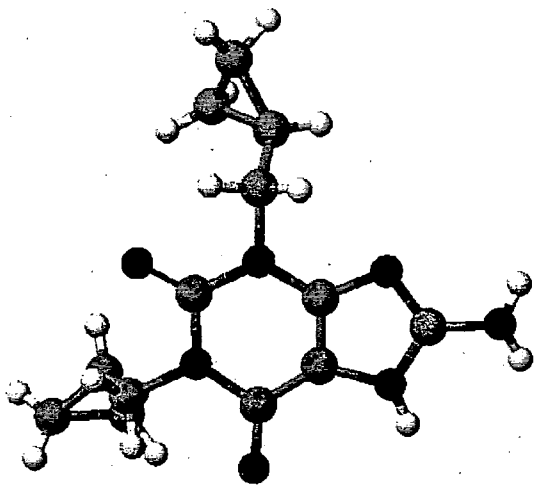

Form 2

This possesses one extra hydrogen bond (to O(5)), suggesting that both NH_2 protons are involved in hydrogen bonding.

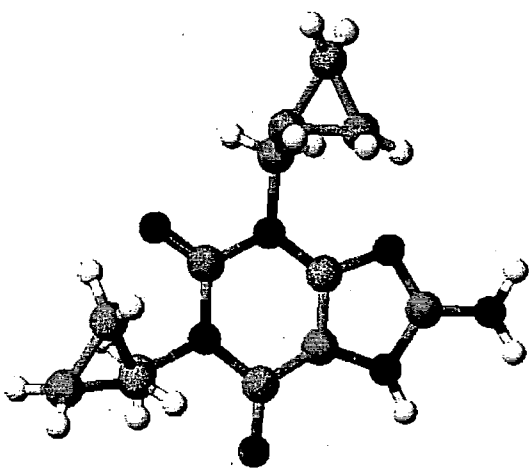

Form 4

This structure is very similar to that of form 2, though the cyclopropyl groups are enantiomorphous to those in form 2. The hydrogen bonding is characteristic of form 1.

3.4 Single-crystal X-ray Diffraction data analysis for forms 1, 2, and 4 of BRL61063

Crystallographic data derived from SB data for forms 1, 2, and 4 have been briefly described in section 3.3. However, until now no evaluation fo the long-range order and intermolecular interactions has been carried out. The work that is described in this section is all original research carried out with the assistance of Dr. Andrei Batsanov, of Durham crystallography group. It should be noted that the results and conclusions that are drawn from this work were brought to light at a relatively late stage of the Ph.D., after the majority of solid-state NMR experiments had been carried out.

All data shown are for forms 1, 2 and 4 of BRL61063. The X-ray data acquisition parameters and refinement techniques are fully and accurately summarised in the chapter 2. It should be noted that there is always a large systematic error in the hydrogen atom position located by XRD, causing the N-H distances to be underestimated by up to 0.2 Å. Therefore, to make relevant comparisons, hydrogen positions were idealised to fit the N-H covalent bond distances of 1.03 Å as found by neutron diffraction. There is also considerable random error, which is normally an order of magnitude higher than for carbon, nitrogen and oxygen atoms. This results in values that may be quoted to 0.003 Å for the heavy atom positions and 0.03 Å for the hydrogen atoms. The visualisation software that was used was the XP, version 5.04 interactive molecular graphics package, running on a silicon graphics workstation.

3.4.1 Comparison of the short- and long-range order of the polymorphs

The individual molecular structures of the three forms are shown in ***Figure 13***, viewed along the carbonyl functional group that is located between the two pendant cyclopropyl groups. This comparison shows that the core of the molecule is identical for the three forms, forming an essentially planar fused-ring system.

The major differences lie in the pendant cyclopropyl groups. Form 1 exhibits disorder in one cyclopropyl group (only), namely that which contains C(12) and C(13). The data indicate an occupancy ratio of 50:50 for these positions at ambient temperatures.

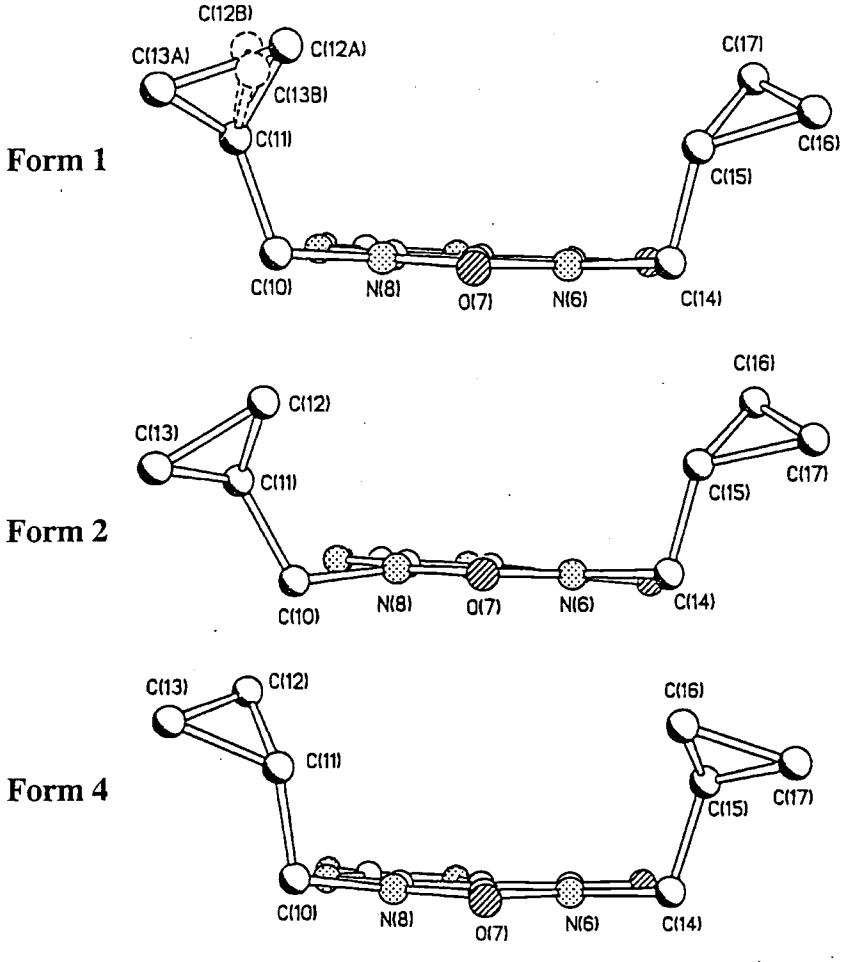

Figure 13 Comparison of the molecular structures of forms 1, 2 and 4 of BRL61063, viewed along the carbonyl group between the two pendant groups.

The orientation of the cyclopropyl groups in form 2 is very similar to that observed in form 1, but without the disorder characteristics, one group adopting positions similar to the A positions for C(12) and (13).

The orientations of the two pendant cyclopropyl groups in form 4 appear to be different from those in form 2.

A comparison of the density data for the three polymorphs shows that the density increases from form 1 (1.335 gcm^{-3}), to form 4 (1.350 gcm^{-3}) to a maximum of 1.356 gcm^{-3} for form 2. This supports the theory that due to the lower density of the structure of form 1, mobility in this form is enabled because the presence of a greater amount of 'free space' available for fragment movement.

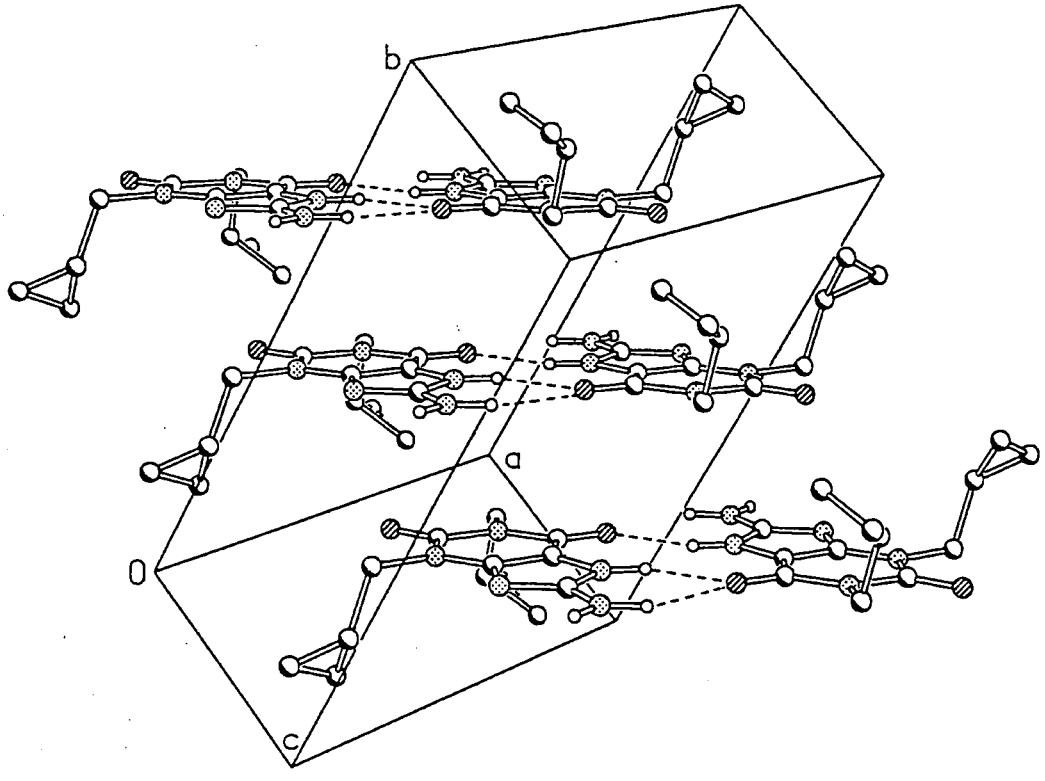

Figure 14 BRL60163 form 1. Unit cell arrangement, showing hydrogen bonding of the dimers in a stair-like fashion, edge-to-edge.

The unit cell diagram (***Figure 14***) usefully shows the existence of form 1 in dimers that are hydrogen bonded in an edge-to-edge fashion in a step-wise formation. Hydrogen bonds between the N(7)H group and the CO(5) carbonyl group hold the molecules together.

The carbonyl group between the two pendant cyclopropyl groups is not involved in any hydrogen bonding interactions.

The question as to the existence and cause of the disorder in the C(12)(13) cyclopropyl group must now be addressed. Introduction of the disorder information from the XRD data is shown for one dimer in ***Figure 15*** and for longer-range interactions in ***Figure 16.***

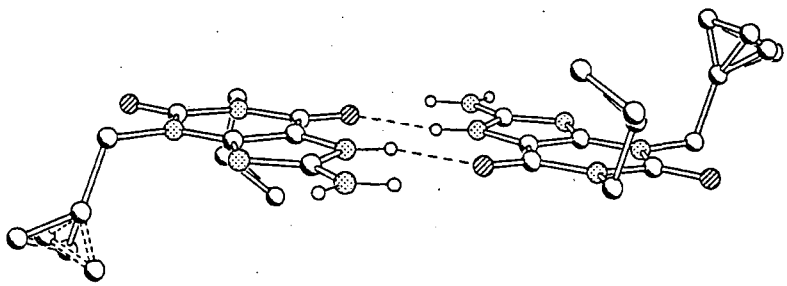

Figure 15 BRL61063 form 1. Dimer, showing mobility in the 'outer' pendant cyclopropyl groups.

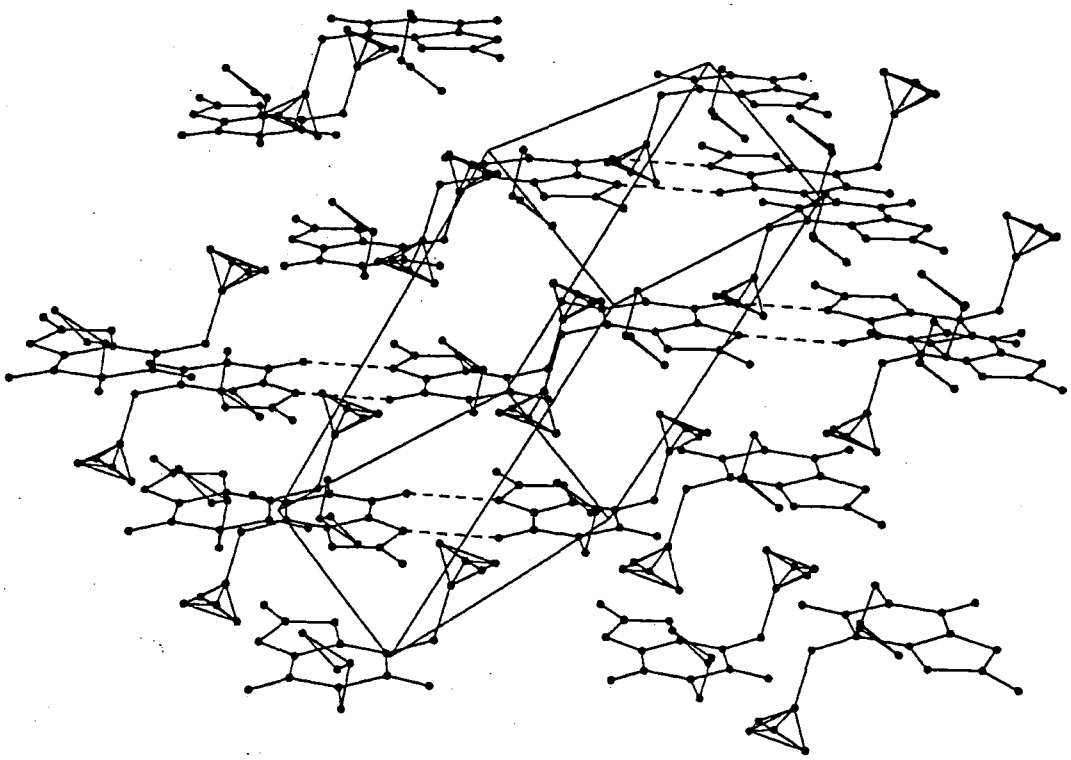

Figure 16 BRL61063 form 1. Long-range packing diagram.

The disordered C(12)(13) groups are clearly located on the 'outer-edges' of the dimers of form 1. This is shown in ***Figure 15*** and is expanded upon in ***Figure 16***, in which it is apparent that these disordered groups exist in channels between the step-wise, diagonally-offset dimers.

In ***Figure 17*** the overhead view of layers of molecules in the structure of form 1 are shown. This illustrates the manner in which these molecules are offset and arranged with cyclopropyl groups on the same 'end' of the molecule. An inter-planar spacing of 3.30 Å exists between the fused cores of the molecules.

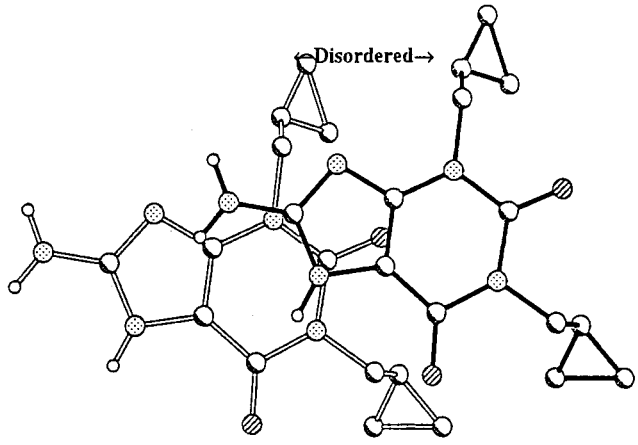

Figure 17 BRL61063 form 1. Diagram showing the face-to-face orientation. The inter-planar distance is 3.30 Å.

The disordered cyclopropyl groups in form 1 exist on the equivalent side of both molecules, away from the edges of the molecules that are involved in the inter-molecular hydrogen-bonding interactions.

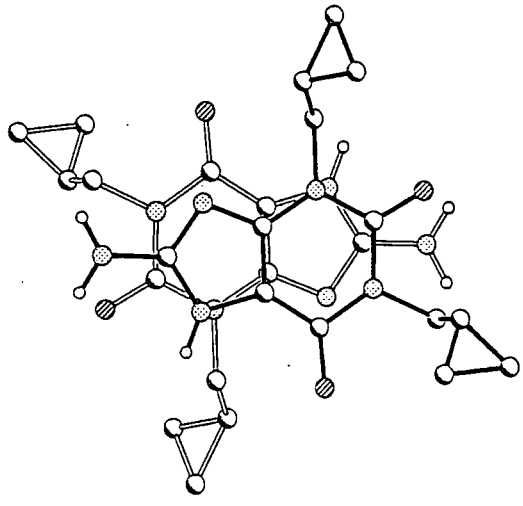

Figure 18 BRL60163 form 2. Diagram showing face-to-face orientation. The inter-planar distance is 3.38 Å.

The equivalent diagram for form 2 is shown in ***Figure 18*** and appears quite different to the situation for form 1. The cyclopropyl groups exist on opposing sides of molecules in adjacent planes, the molecules in which seem to be overlaid more directly than in form 1, where they are offset from each other. The inter-planar spacing is 0.38 Å greater than for form 1.

The long-range order in form 2 is further explored and illustrated in the unit-cell diagram (***Figure 19***) below.

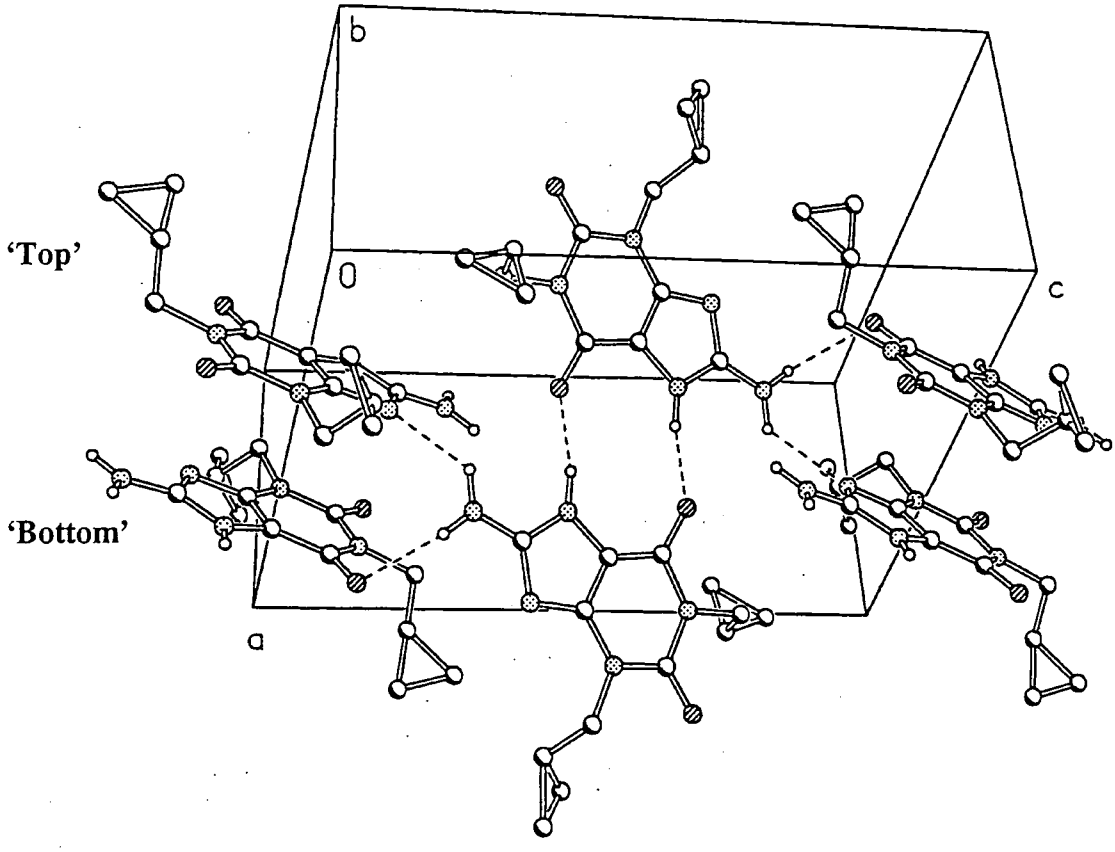

Figure 19 BRL61063 form 2: unit cell and hydrogen bonding.

The long-range order of form 2 is dramatically different to that present in form 1. No disorder is present in this structure, and instead of forming dimers that are hydrogen bonded edge-to-edge by the CO(5) position and the N(7)H position, this structure is better described as forming dimers that exist in a 'face-to-face' conformation, with the pendant cyclopropyl groups directed away from the centre of the dimer.

Each dimer is held in place by hydrogen-bonding interactions involving both of the hydrogen atoms in the NH_2 group of an adjacent molecule. However, the nature of the hydrogen bond to the relevant NH_2 proton for each molecule in the dimer is different. The 'top' molecule (described for ease as is shown in ***Figure 18***) forms a hydrogen-bond from the non-protonated N(9) position to NH(1) and the 'bottom' molecule forms a hydrogen bond effectively to the opposite end of the bottom molecule, from the NH(2) to the CO(5) carbonyl oxygen. This contrasts with the structure of form 1, where there are no hydrogen-bonding interactions with the N(9) position.

Hydrogen bonds also occur within the planes from the CO(5) position on the 'top' molecule and from the N7(H) position (on the 'bottom').

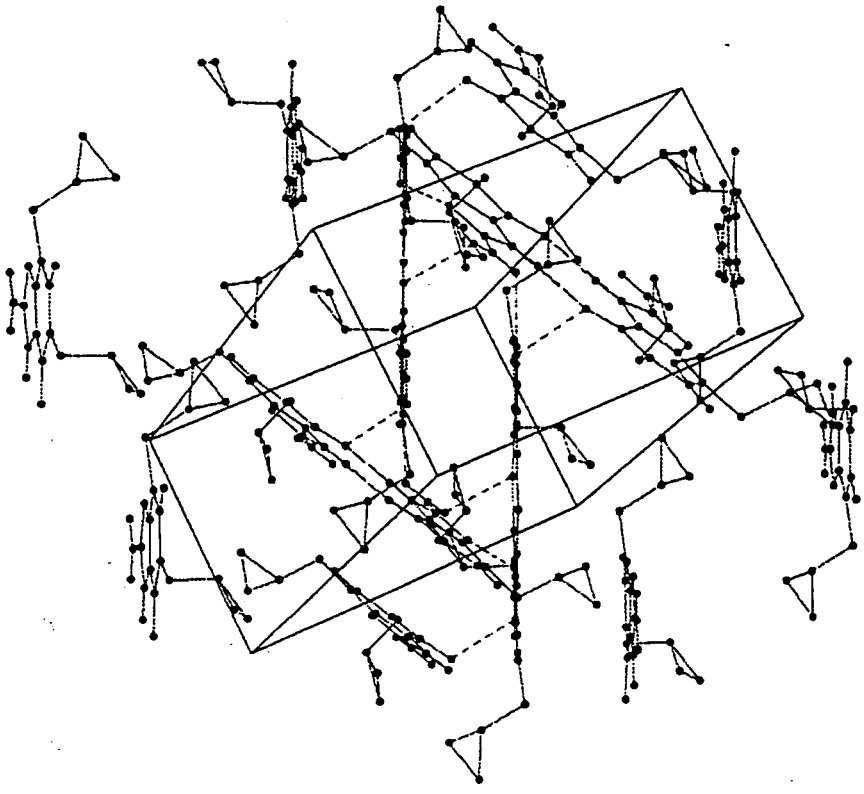

Figure 20 BRL61063 form 2 long-range packing diagram.

Figure 20 demonstrates clearly the way in which the long-range structure of form 2 consists of planes of dimers, which are hydrogen-bonded by adjacent molecules existing in diagonal planes that intersect these planes at an angle of 54 °.

The structure of form 4 exhibits no disorder, and although the core of the individual molecules appear to exist in a similar conformation to those in form 2, the main difference on the molecular scale is the different orientation of the cyclopropyl group between these two forms.

The long-range order of form 4 is more similar to form 1 in terms of its hydrogen-bonding characteristics and formation of edge-to-edge dimers (see ***Figure 21***).

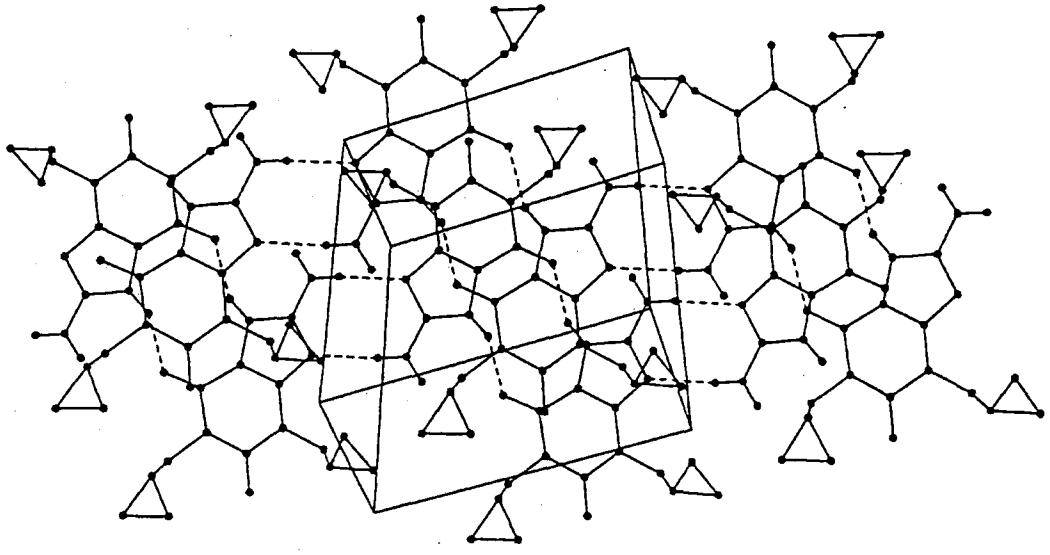

Figure 21 BRL61063 form 4. Long-range packing diagram (viewed along a different axis than that for form 1 in Figure 14).

3.4.3 Comparison of the geometries of the amine groups

Comparisons may be made of the C-NH_2 groups in each of the polymorphs. The intra-molecular distances were measured by importing the crystallographic data (in .pdb format) into the CAChe molecular-modelling package. It is valid to make the following comparison since the amine hydrogen atoms were directly located from electron-density maps, rather than input during the latter stages of analysis in idealised positions.

The amino groups in each form differ in their planarity, with form 2 existing in the most tetrahedral conformation. This is also suggested by the C-N bond length, which is much

shorter than in forms 1 and 4. The X-ray data show that the amine hydrogen atoms are directed towards the side of the molecule on which the pendant cyclopropyl groups reside.

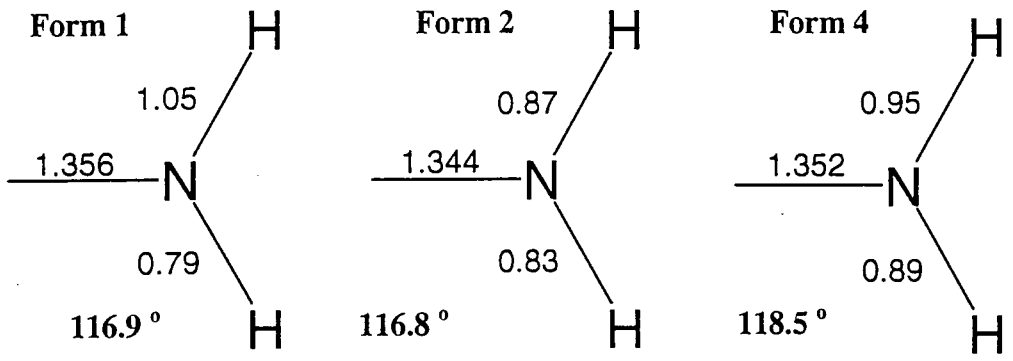

Figure 22 Comparison of C-NH$_2$ distances for the polymorphs of BRL61063 (N-H distances ±0.003 Å, ±0.03 Å for C-N) Average CNH angles are shown as indicators of planarity: 120 ° infers the group is planar, 109.5 ° indicates tetrahedral).

The length of the amine N-H bonds in each form may be compared. In form 2, where both atoms are involved in inter-molecular hydrogen bonds, the N-H bond lengths are both of similar magnitude and very short. This may be consistent with both sites being involved in interactions of similar character and strength.

Form 1 shows a large variation between the NH distances. This is consistent with only one of the amine hydrogen sites being involved in a hydrogen-bonding interaction. The measured CN bond length in this form is the greatest of the three forms. Possibly the strongest hydrogen bonding involves the NH group of length 1.05 Å (see page 102).

3.4.4 Comparison of the carbonyl groups

A comparison of the carbonyl bond lengths in each of the three forms has yielded interesting results, which are summarised in ***Figure 23***.

It is interesting to note that in each form the carbonyl group that is located between the two pendant cyclopropyl groups is not involved in a hydrogen-bonding interaction. These carbonyl bonds are thus of similar length between the forms and shorter than the other carbonyl group in the molecules, since the latter are involved in inter-molecular hydrogen bonding. The decrease in bond length from form 2 (1.250 Å) to 4 (1.243 Å) to 1 (1.237 Å) is symptomatic of the relative strengths of the hydrogen bonds that exist in the three structures, with the strongest and thus shortest hydrogen-bonding length involving a carbonyl group existing in form 2.

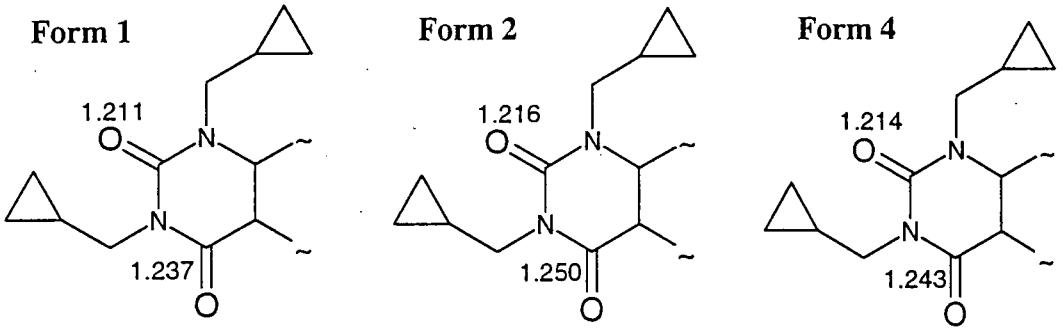

Figure 23 Comparison of carbonyl bond lengths in BRL61063 polymorphs (bond lengths shown in Å).

Figure 24 compares more directly the hydrogen bonding characteristics of form 1 and form 4. The longer contacts are shown with dotted (rather than dashed) lines.

3.4.6 Analysis of the hydrogen-bonding characteristics

Further analysis of the hydrogen-bonding characteristics of each of the polymorphs has been carried out in Durham. These results agreed largely with those that were acquired by SB pharmaceuticals and are shown earlier in the chapter. However, these newer results will be shown here due to the extra data on hydrogen positions that have been generated.

It is well established that a stronger hydrogen bond will possess a shorter distance between the heavy atoms involved, an angle at the hydrogen that is as close as possible to 180 °, and with the hydrogen atom located as close as possible towards the centre of the bond.

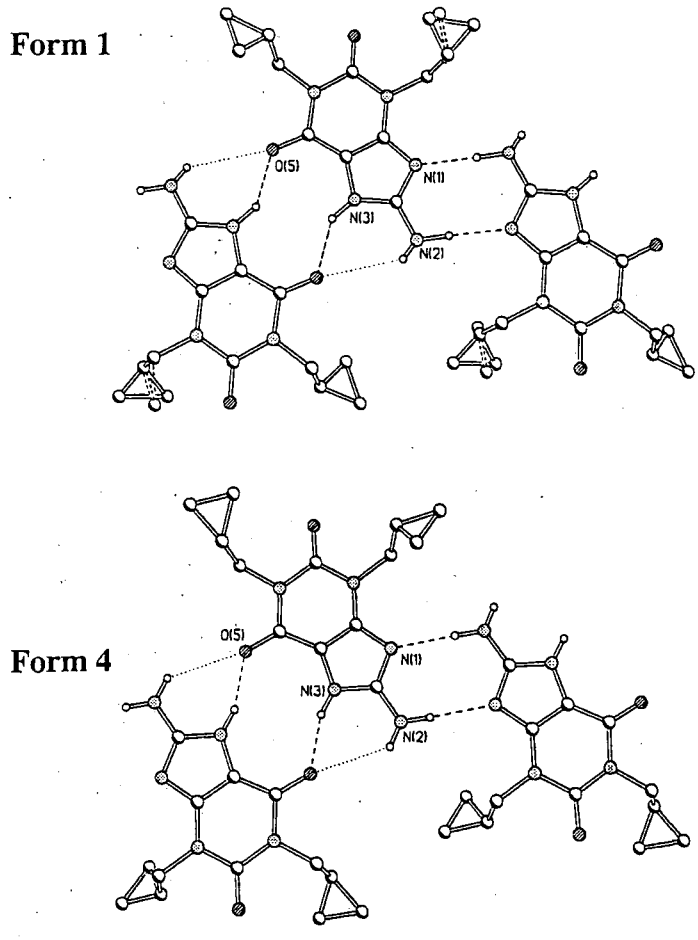

Figure 24 Comparison of the hydrogen-bonding geometry of BRL61063 forms 1 and 4 showing the similarity of these forms (Dotted lines represent longer NH-O contacts).

The similarities in hydrogen-bonding characteristics of forms 1 and 4 are shown in ***Figure 24*** and the comparison of the hydrogen-bonding geometries for forms 1, 2 and 4 is shown in ***Figure 25***. From analysis of these sets of data it is possible to conclude that the equivalent dotted contacts (between N(2)H and (O5)) shown in the structures of form 1 and 4 are stronger in form 4 than in form 1, though both will still be very weak in comparison to the other hydrogen bonds present in each form.

The strongest hydrogen bond in form 1 appears to exist between N(2)-H-N(1) as this bond angle appears to be very close to 180 °. The equivalent bond exists with a similar degree of linearity in the structure of form 4, but in form 4 the N(3)-H-O(5) hydrogen

bond appears to be even stronger as this shows a shorter bond length as well as a bond angle of 162 °. The N(3)-H-O(5) bond in form 1 may be weaker than the hydrogen bond existing between the equivalent sites in form 4, due to the lower bond angle (146 °) and despite the shorter distance between the heavy atoms.

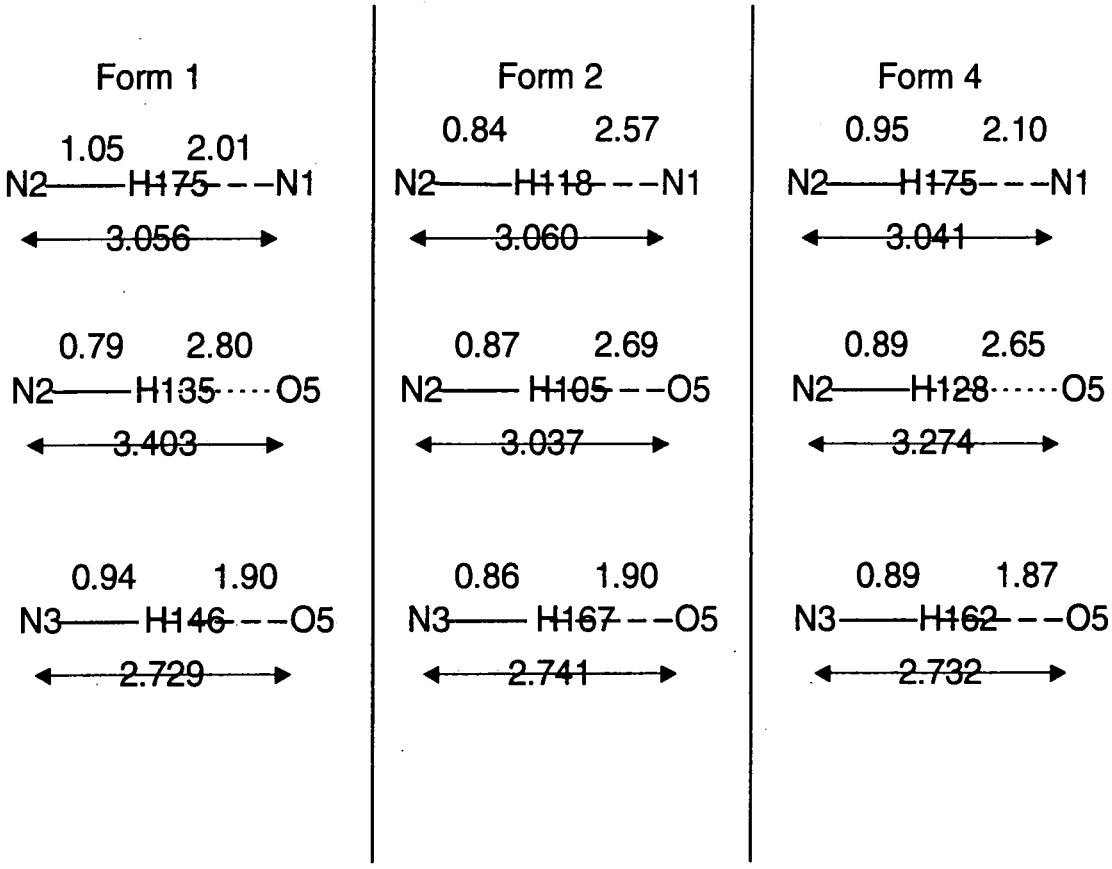

Figure 25 Summary of the hydrogen-bonding geometries of the three forms of BRL61063. (All bond lengths in Å, bond angles in red, heavy atom distances in blue).

In general, the shortest hydrogen bond for each form exists between N(3)-H-O(5)., It appears that this is the strongest interaction in the structure of form 2 by virtue of the high bond angle, short heavy atom separation and the position of the hydrogen closer towards the centre of the bond, although the heavy atom separation is, in fact, the greatest of the three forms.

In a survey[10] of 1509 bonds in 889 crystallographic structures existing in the form N-H...O=C the average H...O bond distance has been measured to be 1.92 Å (with a standard deviation, σ, of 0.14 Å). The average N...O bond length that was found was 2.878 Å ($\sigma = 0.12$). It was also noted that the intramolecular N...O distances (2.755 Å) in these hydrogen bonds are shorter than the intermolecular N...O distances (2.892 Å), but the average measured H...O distances are longer for intramolecular (1.988 Å) than intermolecular (1.913 Å) hydrogen bonds. The σ value for the intramolecular O...H hydrogen bonding value is greater, which is probably due to non-linearity of molecular conformations.

From comparison of the results of this literature survey with those reported here, it appears that the average H...O distance measured from this work is greater than the average quoted in the literature, although the N(3) hydrogen bonding interaction in form 4 approaches the same magnitude. The average N...O bond distances quoted in this work also appear longer than the literature average, although again the N(3) hydrogen bonds in each form show shorter values.

3.4.7 Analysis of the cyclopropyl groups

The question as to what exactly drives the disorder in one of the cyclopropyl groups in form 1 remains to be answered at this stage of the discussion. The lower crystal density of form 1 has been mentioned previously as a factor that may allow disorder to exist. The investigation is now extended to include the space between the cyclopropyl groups.

In the crystal structures of each of the forms 1, 2 and 4, it appears that the cyclopropyl groups exist in channels. It is possible to assess the closest contacts between the cyclopropyl groups within these channels and to determine the way in which these groups are positioned with respect to each other within each form. The results of these investigations are summarised in ***Table 10***.

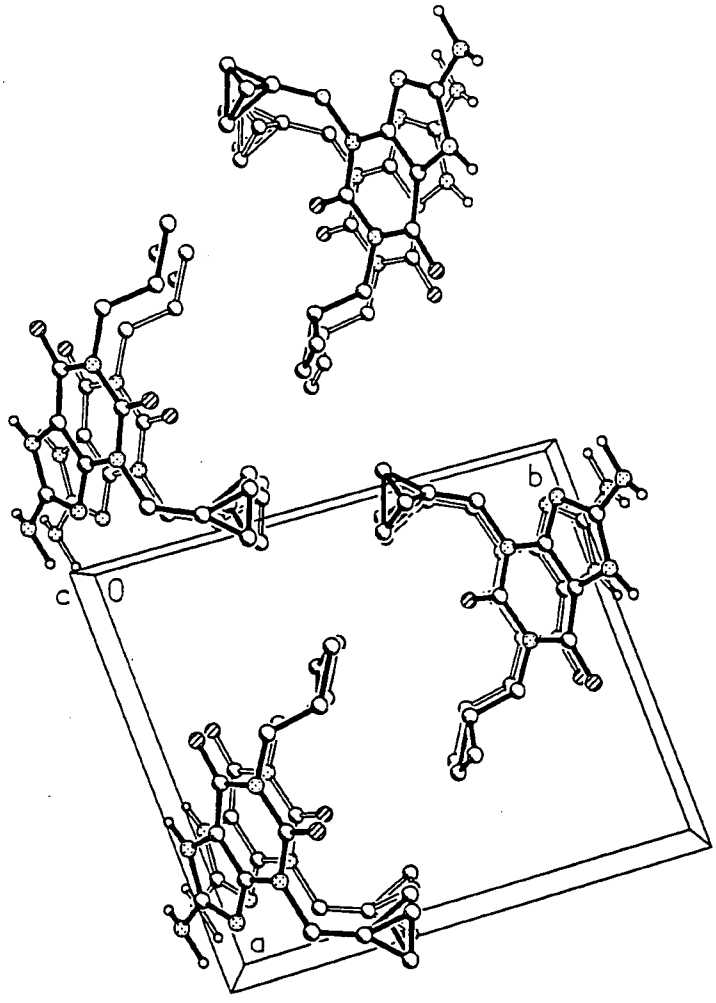

Figure 26 View along the cyclopropyl 'channel' in the structure of BRL61063, form 1.

From the data presented in ***Table 10*** it is possible to draw the conclusion that form 1 possesses the largest values of 'shortest contact distances' between the cyclopropyl groups, and this may explain the disorder that is present in these groups since there exists more space for the flexing to occur. The packing diagram that is shown in ***Figure 26*** shows clearly that the inter-cyclopropyl group contact that is the shortest is that which exists between disordered groups, which are on opposite sides of the channel. However, this contact is still 3.94 Å, which is greater than twice the known rotation radius of a methyl group, which is 2 Å, indicating that no flexing should be forced by the cyclopropyl groups existing this distance apart.

Form	Shortest cyclopropyl contacts (± 0.03 Å)	Description of the contacts between cyclopropyl groups.
1*	3.94, 4.11, 4.17	Across the channel, between disordered groups. Edge-to-non-parallel-edge.
2	3.70, 3.80, 3.84, 3.74, 3.75	Across the channel. Close cyclopropyl groups exist in alternate pairs, pointing towards each other in one pair, which is pressed on both sides by cyclopropyl groups that exist in the opposite conformation. Edge to edge.
4	3.77, 3.67, 3.70, 3.91, 3.86	Not across the channel, but between translationally-related molecules along the channel axis. Face-to-edge. The cyclopropyl groups are rotated away from each other (inter-molecularly) in contrast to forms 1 & 2.
* Distances quoted for form 1 are measured between the different conformations of the disordered cyclopropyl groups only, since these are the shortest contacts.		

Table 10 Comparison of inter-molecular cyclopropyl group distances for the three polymorphs of BL61063

Possibly the most interesting result of this investigation was the comparison of the relative orientation of the cyclopropyl groups which exist within a short distance of each other.

In form 1 there exists disorder, with the largest distance (4.19 Å) existing between the cyclopropyl groups when an edge-to-non-parallel-edge conformation exists. The other two distances exist for the two other possibilities on either side of this, i.e. edge-to-parallel edge.

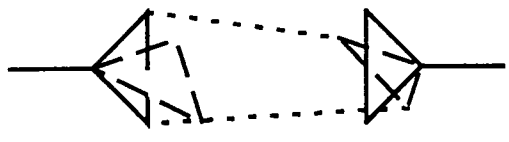

Figure 27 Schematic of the cyclopropyl groups in form 1, with dashed lines indicating alternative cyclopropyl positions and dotted line indicating the 'edge-to-non-parallel-edge' conformation, which shows the longest short contact!

The cyclopropyl groups in form 2 actually point towards each other in space. However, these types of directed interactions exist in layers, with the cyclopropyl groups oriented roughly perpendicular in successive layers, such that it appears that the layer above and below any specific layer 'press' the cyclopropyl groups in the central layer into the perpendicular orientation to their own.

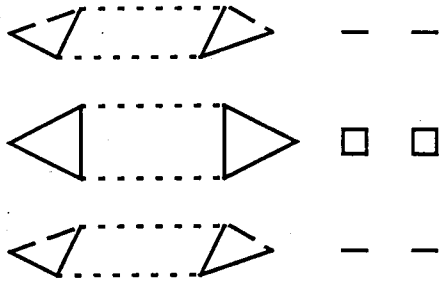

Figure 28 Schematic diagram of the way in which the cyclopropyl groups are directed towards each other in 'sandwich-type' layers of BRL61063 form 2.

In form 4, the cyclopropyl groups exhibit a different conformation again, with the cyclopropyl groups pointing face-to-edge rather than the edge-to-edge that is preferred in forms 1 and 2. The groups on adjacent molecules are also rotated away from each other.

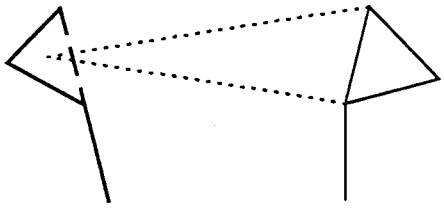

Figure 29 Schematic drawing of the face-to-edge cyclopropyl contact in form 4, with the cyclopropyl groups exhibiting this close contact oriented away from each other and related translationally along, rather than across the channel.

Another way in which the closest contacts of the cyclopropyl groups in form 4 differ from those in forms 1 and 2 is due to the relationship of the molecules that forms the closest contacts. Rather than these existing across the channel, the molecules involved are translationally-related along the channel. Also, only one of the cyclopropyl groups in each molecule forms short contacts.

3.4.8 Conclusions on the structures of forms 1, 2, and 4 of BRL61063.

The structural differences between forms 1, 2 and 4 of BRL61063 have been described. These include differences in crystal space group, density, bond lengths and angles plus different arrangements and strengths of hydrogen bonding.

The driving force for the disorder in form 1 may be caused by the ability of the pendant cyclopropyl groups to move due to their existence in a channel of greater diameter than for the other two forms. It is not clear at this stage whether the disorder that has been observed at ambient temperatures is temporal or spatial, but an interesting conclusion can be drawn now that more information is known about the cyclopropyl group orientations and relative distances. The largest inter-cyclopropyl distance (4.17 Å) has been measured for the 'edge-to-non-parallel-edge' arrangement of the cyclopropyl groups. Of course, in each unit cell it is quite possible that this may exist as the energetically-favourable conformation, but either way around i.e. from left to right, 'edge-to-non-parallel-edge', or 'non-parallel-edge to-edge', giving the disorder as indicated by X-ray work. (This is hard to describe in words but is easily visualised by observing ***Figure 27*** and then imaging what it would look like after rotating it by 180 ° in any direction!) Therefore, X-ray crystallography would not be able to differentiate between this 'variation' in conformation between adjacent unit cells, or truly random orientations of the relevant cyclopropyl groups (which would result in a statistical distribution of the three mutual orientations indicated in ***Figure 27***), or temporal disorder in which the cyclopropyl group in form 1 is flipping between two positions of equal occupancy.

Overall, this work on the structure of the three crystal forms of BRL61063 has proved to be extremely interesting and a base on which to discuss the results of solid-state NMR experiments on form 1 and 2, plus the two new samples that have been created, 'yellow' and form 'D'.

3.5 Pharmaceutical legislation – the detection limit!

Due to current FDA regulatory legislation requiring good levels of detection of impurities in drug substances, it is desirable to develop reliable techniques that can predict polymorphic composition and thus optimise the level of detection of polymorphic impurity in a given sample. This is of particular importance in the pharmaceuticals industry due to the possibility of a large difference existing between the bioavailability of many polymorphs. It is necessary to be able to detect and quantify the amount of a polymorph in a large percentage of another one. Although a small amount of the wrong polymorph may be without effect if the bioavailability of the impurity is very low, the opposing situation, in which a polymorph with a very large bioavailability is introduced into the body, may cause the dose to reach toxic levels.

3.5.1 Detectability limits in polymorphic mixtures of BRL55834

Previously, the techniques of IR and DSC have been used to analyse mixtures of polymorphs of BRL55834. DSC proved to be more accurate for the analysis of mixtures of Form II in Form I with a detection limit of 2 %. Whilst visual detection limits for the polymorphs of BRL55834 have been ascertained at ca. 5 % for form I in form II by both Raman and IR spectroscopy, the detection limit for form II in form I is much less efficient, at *ca.* 15 % for Raman and 10% for IR.

In the case of BRL55834 polymorphs, the differences in the IR spectra themselves are much greater than for the Raman case. However, it is possible that this situation may become reversed for other polymorphic systems and hence the experiment discussed herein was aimed at developing good detection techniques, which may then be made widely available for other polymorphic systems.

This section describes the work carried out during two visits to the Frythe site of SmithKline Beecham Pharmaceuticals Research and Development in Welwyn, in 1996.

During this time a method of approach was developed, followed through and then its efficiency was rated against a standard evaluation technique using chemometric analysis.

3.5.2 Method development and process

Fourier transform solid-state Raman spectroscopy[11] was used to analyse mixtures of the two polymorphs of BRL55834.

A series of 25 standard mixtures of form I (H92/4774) and form II (H92/0431) of BRL55834 were prepared. Raman spectra were obtained by placing the mixtures in turn into the Perkin Elmer 3 mm sampling cup for solids. This was fitted with a quartz window through which the laser beam can pass. Once the sample cup was full it was attached to the base plate, inverted, and twisted several times such that the powder made good contact with the quartz window. The compressor rod designed to fit the sampling cup was never used to compress the sample.

3.5.2.1 Normalisation - a problem with using Raman Spectroscopy

Raman[12,13,14] spectroscopy is a scattering method, and unlike many other spectroscopic techniques it does not allow quantitative results to be easily obtained.

In this experiment the sampling position was kept constant in order to ensure the reproducibility of results by controlling the laser intensity on the sample, and Perkin-Elmer's 'Auto-align' procedure was used to minimise instrument drift.

The amount of scattering undergone by the laser beam depends on the quantity of sample 'seen' by the laser beam. This is in turn related to the degree of sample compactness as it is thought that the laser beam is able to penetrate the sample to a maximum sample depth of 2 mm with an area of 1 mm^2. It is for this reason that the sample homogeneity is very important and all samples had been thoroughly mixed on preparation.

Consideration must also be given to the fact that the two polymorphs may scatter Raman radiation to different extents i.e. have different scattering intensities, and any technique which may be developed must take this factor into account.

Sample no.	Sample letter	Form I %	Form II %	Sample no.	Sample letter	Form I %	Form II %
1	A	100	0	14	N	45.05	54.95
2	B	98.90	1.10	15	O	40.02	59.98
3	C	97.76	2.24	16	P	34.97	65.03
4	D	94.96	5.04	17	Q	30.05	69.95
5	E	90.21	9.79	18	R	25.03	74.97
6	F	84.11	15.89	19	S	20.37	79.63
7	G	79.65	20.35	20	T	15.00	85.00
8	H	74.58	25.42	21	U	9.99	90.01
9	I	70.30	29.70	22	V	4.99	95.01
10	J	64.48	35.52	23	W	1.97	98.03
11	K	59.74	40.26	24	X	1.02	98.98
12	L	55.03	44.97	25	Y	0.00	100
13	M	49.15	50.85	-	-	-	-

Table 11 Composition of the Standard Mixtures

Having established the extreme difficulty of regulating sample compactness it was decided to try an alternative technique. Spectra of all 25 mixtures were recorded without trying to control the sample compactness. The results were then corrected by dividing the spectra by the background spectrum, saved onto disc (IR204I) and named 55834A-Y. A background spectrum of the quartz glass signal was also recorded under the filename 55834Z. The spectra were corrected for instrument response to give 4 cm^{-1} resolution

Next, samples of pure form I and form II were each made up to contain 10 wt % of dopant. These mixtures were then ground for an equal amount of time to try to ensure sample homogeneity and adequate mixing. The dopant was chosen to produce a very sharp, distinct peak in a region which did not overlap with the sample spectrum. For this reason the initial choice of NaN_3 was discarded and it was found that KCN was the preferable dopant.

The samples were spaced at approximately 5 % intervals, except at the extremes of composition where additional samples are inserted. This helps overcome inherent weakness at the extremes of composition.

	Pure Polymorph	**KCN Dopant**
Form I	91.28 mg	9.12 mg
Form II	93.04 mg	9.31 mg

Table 12 Composition of the doped mixtures of BRL55834.

Spectra were then recorded of each of these two doped forms and scaled such that the dopant peak was of equal intensity. It was hence supposed that the spectra were comparable i.e. the spectra had thus been normalised by an internal standard.

This technique assumes adequate mixing of the dopant/ pure polymorphic mixture and accurate reproducibility of results.

The doped spectra R10457N and R10458 were then overlaid in order to identify a peak that has a very similar intensity, shape and frequency for the two polymorphs. A difference spectrum was also produced in order to identify a suitable peak/ region.

The best peak identified for this purpose was at approximately 756 cm^{-1}, which *may* be attributed to a C-C stretching mode of the piperidinone ring. The normalisation of the 25 spectra was then carried out by scaling the area under the peak between 770 and 745 cm^{-1} to a constant value, also taking into account the baseline between the same limits in the calculation.

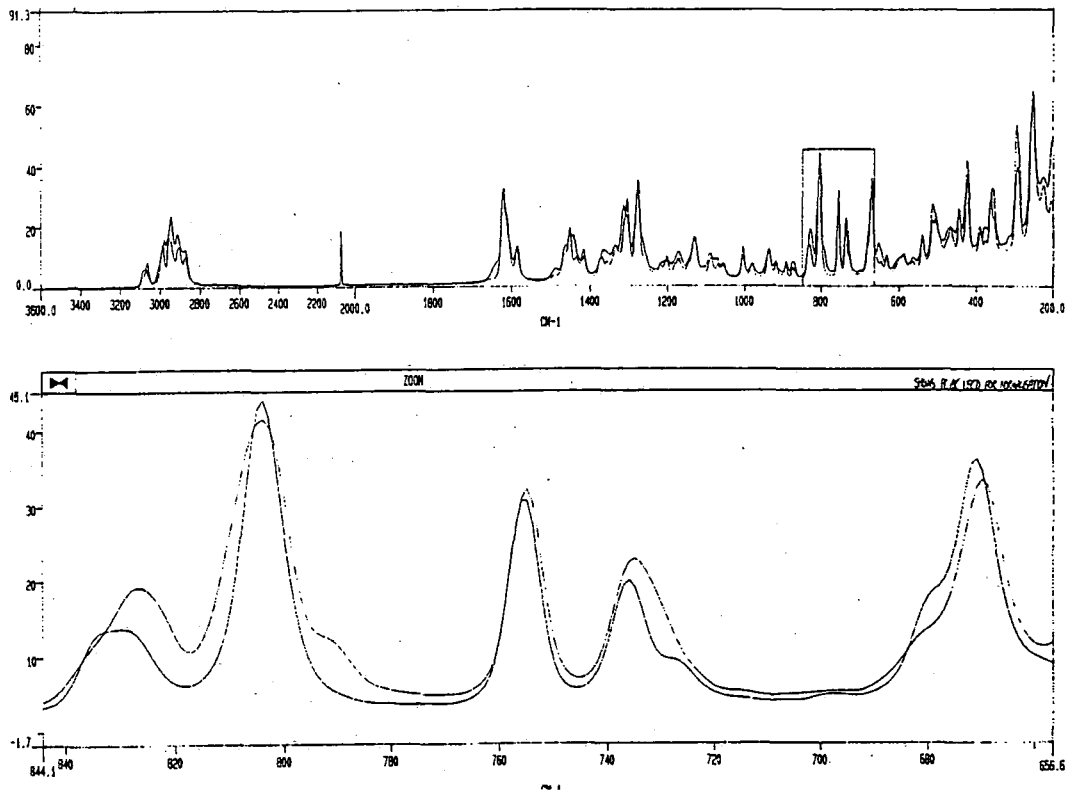

Figure 30 Raman scattering spectra of BRL55834 polymorphs doped with KCN, plus zoom box showing the calibration peak at 756 cm^{-1} (glass vial)

Once all the spectra had been normalised in this way they were saved under their initial filenames with the suffix 'N'. It was these spectra which were then used for the QUANT+ chemometric analysis technique.

3.5.2.2 Chemometric analysis – An overview of the QUANT+ package

This chemometric quantitative analysis technique allows quantification of components in complex mixtures and is thus ideal for multi-component spectroscopic analysis. Thus the technique will allow the determination of any characteristics of a sample which are reflected in its spectrum, however small.

Within the QUANT+ package there is a choice of three multivariate calibration algorithms: PCR+ (principal components regression analysis) plus PLS1 and PLS2, which are single and multicomponent forms of partial least squares analyses[15].

QUANT+ applies these techniques between the spectra of a set of calibration standards (in this case the 25 mixtures) and the corresponding values determined by independent means. The aim is to find relationships that may be used subsequently for prediction of the polymorphic composition of samples of unknown polymorphic make up.

Atypical samples may be identified by the user and excluded from the calibration set, or the user may alternatively choose the QUANT+ 'Expert Assist' facility which will perform the calibration several times, modifying the initial method by identifying outliers and eliminating the corresponding standards until an optimised model has been achieved.

The five main steps in the process are: 'Method build', 'Calibration', 'Validation', 'Review', and 'Prediction'.

Twenty four individual methods were developed in which I varied the conditions used to set up the calibration model. This included varying factors such as: the spectral region; the number of standards; normalised data; non-normalised data; with/ without baseline offset; and with/ without the 'Expert Assist' facility.

Each method could also have been repeated three times, to use each of the three possible algorithms. However, due to the time-consuming nature of this process PCR+ was favoured as a preliminary indicator of a particular method's validity.

3.5.2.3 Treatment of results

The degree of success of a particular method could be measured by the final standard error of prediction (SEP) % value obtained at the end of the calibration. The lower the

value, the more accurate the calibration technique. The equation to calculate the SEP is shown below.

$$SEP = \frac{\sqrt{\left(\sum_{j}^{n}(P_{pj} - P_{aj}\right)^2}}{n}$$

where P_{pj} = the PLS-predicted percentage of polymorph in sample j; P_{aj} = Actual percentage of polymorph in sample j, and n is the number of samples.

3.5.2.4 Results

Early on in the development of an accurate method, one particular outlier was identified as spectrum S. Interestingly, this anomaly, also found in spectrum Q, seemed to correspond with an unusually high baseline for the corresponding Raman spectra. These standards were discarded at an early stage in the calibration process.

After experimenting with a large number of spectral regions, the optimum result was obtained by using the 1400-1200 cm^{-1} region. This gave a SEP of 6.401 % using the PCR+ algorithm and also after eliminating standards Q and S. When the 'Expert Assist' facility was applied to this method it succeeded in bringing the SEP down to 6.314 %, but it also discarded 9 of the reference standards, and the acceptability of a model derived from only 16 standards must be questioned.

Thus, method R17 seems to give the best SEP value and would be the calibration technique of choice for a mixture of polymorphic forms I and II. All the methods and corresponding results are summarised in ***Table 13***.

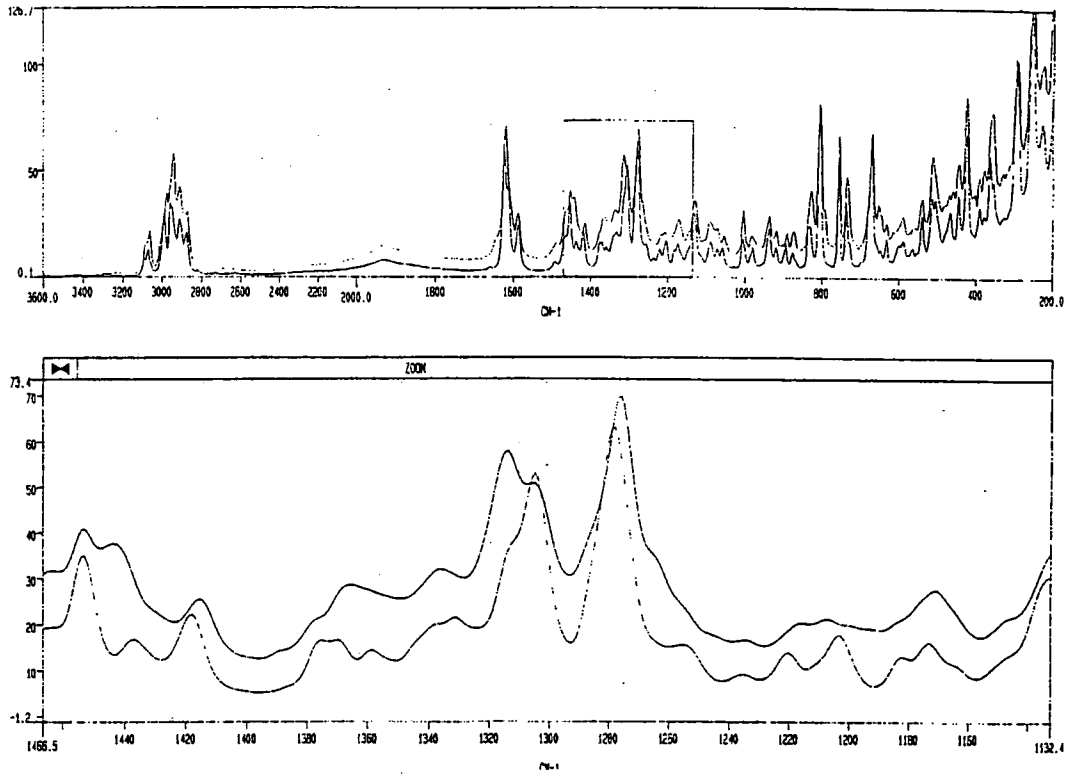

Figure 31 Raman spectra (normalised) of pure form I and II of BRL55834, showing the region selected for the calibration of the mixtures (1400-1200 cm^{-1})

All spectra were only analysed as far down as 600 cm^{-1} after which point the noise level is considered to be too great for accurate comparisons to be drawn. All spectra were previously normalised and run under the same conditions, for 64 scans.

3.5.2.5 Discussion

Analysis of the Raman spectra of mixtures of form I and II of BRL55834 has been optimised by using the region 1400-1200 cm^{-1}, which gives a SEP value of 6.401 %. This region has been identified to be the region that exhibits the greatest difference between the spectra of the two pure polymorphs.

Despite this value (6.4 %) being a significant improvement on the visual detection limit for the Raman spectra of the mixtures which was previously estimated at 15 %, the

improvement is possibly not quite as great as was first expected for the implementation of this technique.

Method code	Calibration Region (cm^{-1})	Spectra cut out	Standards used	Standard Error of Prediction (SEP) %		
				PCR+	**PLS1**	**PLS2**
55834R1	All	-	25	9.437	10.63	10.21
55834R2	C-H stretch	-	25	9.213	9.228	9.214
55834R3	All	SN	23	8.46	-	-
55834R4	C-H stretch	SN + QN	23	7.456	7.457	7.456
55834R5	All	SN + QN	23	7.467	-	-
55834R6	All + no baseline correction	SN + QN	23	7.562	-	-
55834R7	All to 800	SN + QN	23	7.095	-	
55834R8	All to 1000	SN + QN	23	7.495	-	-
55834R9	Non normalised data (to 800)	S + Q	23	7.252	7.052	-
55834R10	1700-1400	SN + QN	23	6.603	-	-
55834R11	1700-1400	-	25	7.615	-	-
55834R12	1700-1500	SN + QN	23	6.635	-	-
55834R13	1400-1000	SN + QN	23	7.252	-	-
55834R14	1700-1250	SN + QN	23	6.640	-	-
55834R15	1500-1400	SN + QN	23	6.460	-	-
55834R16	3030-2820	SN + QN	23	7.474	-	-
55834R17	1400-1200	SN + QN	23	6.401	7.215	-
55834R18	1400-1200	SN + QN	16*	6.314	6.306	-
55834R19	1400-1200	SN + QN	18*	-	-	-
55834R20	1400-1200	SN + QN	16*	6.314	-	-
55834R21	900-650	SN + QN	23	-	-	-
55834R22	900-650	SN + QN	17*	7.133	-	-
55834R23	C-H Stretch	SN + QN	16*	7.456	-	-
55834R24	All	SN + QN	16*	-	-	-

* QUANT+ Expert Assist facility used – this may give erroneous results due to the harsh elimination of many reference standards. PCR+ = Principle Components Regression Analysis. PLS1, PLS2 Principal Least Squares Analysis. 'All' implies that the regions containing no signal are blanked - this includes 3600-3150 cm^{-1} and 2800-1700 cm^{-1}. C-H stretch = 3150-2800 cm^{-1}

Table 13 Summary Table Detailing the 24 Methods and the Resultant SEPs.

As may be observed in the overlaid spectra there is a large variation in the baseline height between the samples. This characteristic does not vary gradually with increase in concentration of form II in the mixtures or with any other immediately obvious experimental factor.

An offset baseline correction was used in the QUANT+ analysis in an attempt to remove any discrepancies brought about by the baseline variation. This option mean centres each spectrum i.e. the mean intensity over all wavelengths is subtracted at each wavelength. However, this modification seemed to make only a small contribution to the resultant accuracy of the methods (~1 % for the whole spectrum - compare methods R5 and R6).

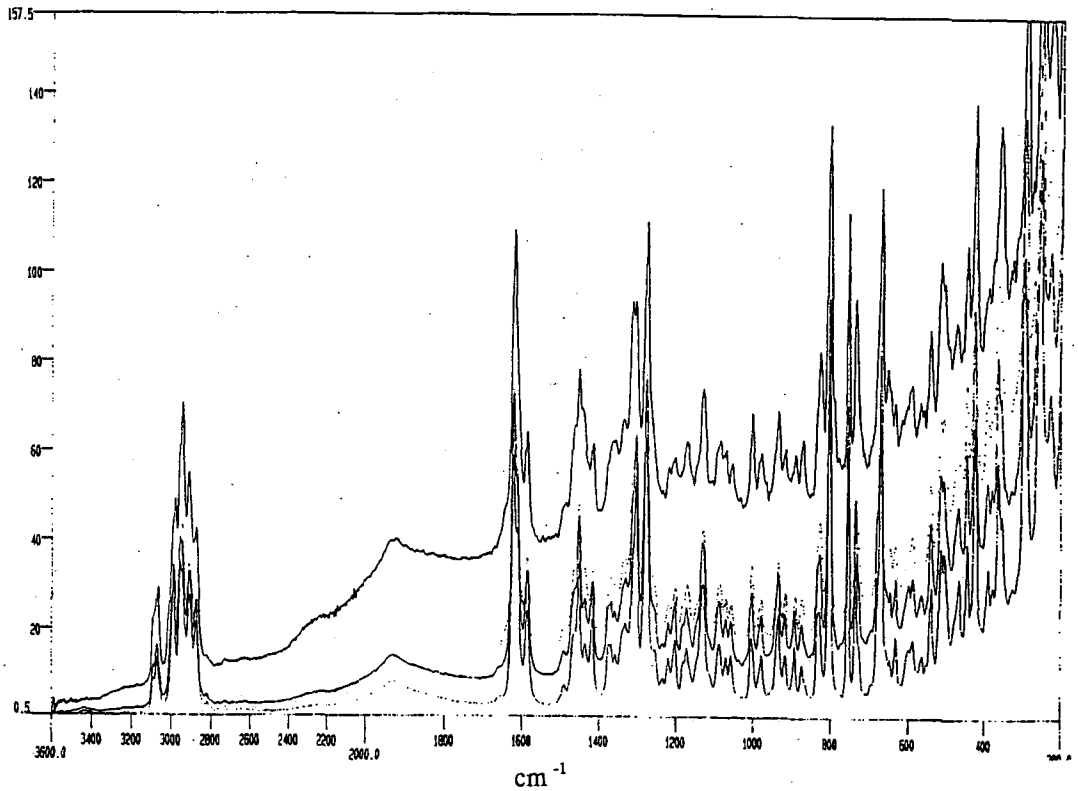

Figure 32 Overlaid Raman spectra of mixtures of form I and II, showing baseline variation observed for different mixtures (quartz window)

It may also be noted that the signal-to-noise ratio for the spectra exhibiting higher baselines seems to be much poorer and the question of machine reliability is thus also brought into the argument.

Finally, the normalisation method that formed the major part of this technique must be examined for possible sources of error. The reproducibility of the results relies on the homogeneity of mixing and particle size of the doped standards. The discrepancy in area of the peak at 756 cm^{-1}, which was used for normalisation, was found to be 2 % in the scaled, doped standards' spectra.

3.5.2.5 Potential for development of this approach

It could possibly be useful to extend this work in an attempt to try to increase the accuracy of prediction of this technique. An area that seems to possess potential for improvement is that of the baseline variation between samples.

In this initial work, all spectra were acquired under similar conditions, divided by the reference background spectrum, and then normalised. The offset baseline correction was then applied as a pre-calibration condition in the QUANT+ analysis package. Therefore, it would possibly prove useful to apply a more complex polynomial baseline correction instead of the simple offset correction. However, it is important to determine the cause of the baseline variation and whether this in turn is the major contributor in increasing the optimum SEP value. Thus, by probing factors such as particle size, the reproducibility of results could possibly be improved.

It is also interesting to note that the region which has been identified as providing the most accurate calibration, must therefore be the region in which the Raman scattering is the most markedly different between the two polymorphic forms of BRL55834. Could this possibly allude to the major structural difference between the two polymorphs?

3.6 Conclusions

This chapter has summarised the structural and molecular background of each of the two polymorphic systems studied during this Ph.D. research. A detailed analysis of the original XRD data for three polymorphs of BRL61063 has also developed a significant amount of understanding of the structure of the polymorphs. Also, the problem of detection limits has been investigated using mixtures of BRL55834.

The importance of the use of a wide variety of analytical techniques in the analysis and identification of polymorphism has been underlined by the sensitivity of the different techniques when applied to the two systems. The following chapters, which concentrate on the solid-state NMR technique and its application to the analysis of solid, organic pharmaceutical polymorphs will support, underline, and develop the themes developed in this chapter.

3.7 References

1 S. R. Byrn, R. Pfeiffer, M. Ganey, C. Hoiberg, G. Poochikan, *Pharm. Res.*, **12**, 7, 1993.

2 SB Report HW/0098 A.F.Barnes Polymorphism of BRL55834.

3 SB Report HW 0103 Proof of structure and analysis of BRL55834

4 SB Memo DSC and IR Micro-spectrometry of polymorphism of BRL55834

5 D. R. Buckle, D. S. Eggleston, I. L. Pinto, D. G. Smith, J. M. Tedder, *Bioorg. Med. Chem. Lett.*, **2**, 9, 1161-1164, 1992.

6 F. Cassidy, J. M. Evans, D. M. Smith, G. Stemp, C. Edge, D. J. Williams, *J. Chem. Soc. Chem. Commun.*, 377, 1989.

7 W. A. Thomas, I. W. A. Whitcombe, *J. Chem. Soc. Chem. Commun.*, 528, 1990.

8 J. Roscheter, U. Berg, M. Pierrot, J. Sandstrom, *J. Am. Chem. Soc.*, **109**, 492, 1987.

9 SB Internal memo, A. F. Barnes, D. Eggleston, 29/9/1992

10 R. Taylor, V. Kennard, W. Versichel, *Acta Cryst.*, **3**, 280, 1984.

11 T. L. Threlfall, *Analyst*, **120**, 1995.

12 A. Naito, S. Ganapathy, C. A. McDowell, *J. Magn. Reson.*, **48**, 367, 1982

13 C. N. Banwell, '*Fundamentals of Molecular Spectroscopy*', 3rd edition, Ch. 4, McGraw-Hill, 1983.

14 J. M. Hollas, '*Modern Spectrsocopy*', 2nd edition, J. Wiley and Sons.

15 D. M. Haaland, E. V. Thomas, *Anal. Chem.*, **60**,1193, 1988.

Chapter 4

BRL55834 – A fluorinated organic compound

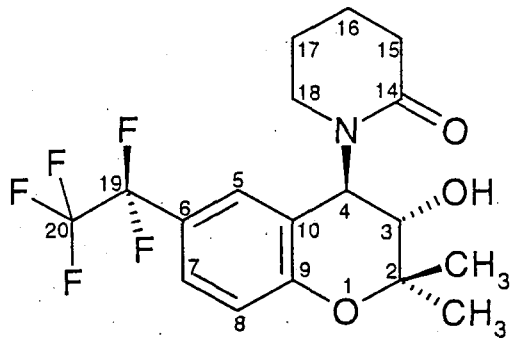

4.1 Introduction

The molecular structure of BRL55834 was confirmed initially by SmithKline Beecham, using a variety of techniques. The salient points are summarised in ***Table 1***. This chapter aims to outline the results of solid-state NMR studies on BRL55834.

Feature	Confirmation technique
Molecular formula	**Elemental analysis** **Mass spectrometry** – loss of 114amu (piperidinone and methyl group) from the molecular ion.
Relative and absolute **stereochemistry** at C_3 & C_4.	Single-crystal **X-ray diffraction** on the precursor.
Position of **pentafluoroethyl** group on C_6.	Single-crystal **X-ray diffraction** on the precursor. **NMR**: ^{19}F, ^{1}H, and ^{13}C.
Position and relative **stereochemistry** of **lactam**.	**NMR**: DQF-COSY – shows protons H_5 and H_4 are coupled very weakly. **NMR**: C_{14} $\delta^{13}C$ = 174.04 ppm (characteristic of C=O) **IR**: $\nu_{C=O}$ = 1650-1600cm^{-1}. **NMR**: ^{3}J = 10.2 Hz indicates trans relationship between H_3 and H_4. (Karplus relationship)
Existence of a 1,2,4 **trisubstituted aromatic ring**	**NMR**: ^{1}H resonances.
Attachment of **piperidinone** to C_4	**NMR**: C_3 $\delta^{13}C$ = 71.20 ppm therefore the methine C is adjacent to an oxygen. **NMR**: HMQC correlates C_3 and H_3.

Table 1 Summary of the structure determination of BRL55834

4.2 Solution-state NMR studies

Initial solution-state NMR measurements were carried out during a visit to the NMR group of the analytical sciences department, Harlow. These experiments repeated earlier results of SB and verified the structure of BRL55834 and provided a basis for the assignment of the solid-state ^{13}C CP/MAS spectra.

4.2.1 ^{1}H NMR

Proton spectra show a resonance corresponding to each proton in the molecule, although the coupling is complicated by both the presence of fluorine atoms and also complex second-order effects around the piperidinone ring.

^{1}H Chemical shift	Assignment	Coupling (± 0.1) Hz
7.40, 7.40, 7.38, 7.38	7 q	$^{4}J_{5,7} = 1.94$ $^{3}J_{7,8} = 8.59$
7.26	H impurity in $CDCl_3$	
7.17	5	Broad, poorly resolved doublet
6.92	8 d	$^{3}J_{7,8} = 8.59$
5.96	4 d	$^{3}J_{3,4} = 10.16$
3.78	3 d	$^{3}J_{3,4} = 10.16$
3.67	OH	
3.11, 2.88	18 & 18'	Complex second order coupling
*2.62, 2.60, 2.59, 2.57	15 & 15'	
*1.90, 1.88, 1.88, 1.87, 1.86, 1.86	17', 16 & 16'	
1.7	17	
1.52	CH_3 (eq)	
1.28	CH_3 (ax)	
* : complex splittings, peak positions only		

Table 2 ^{1}H chemical shifts, assignments and coupling constants (solvent $CDCl_3$)

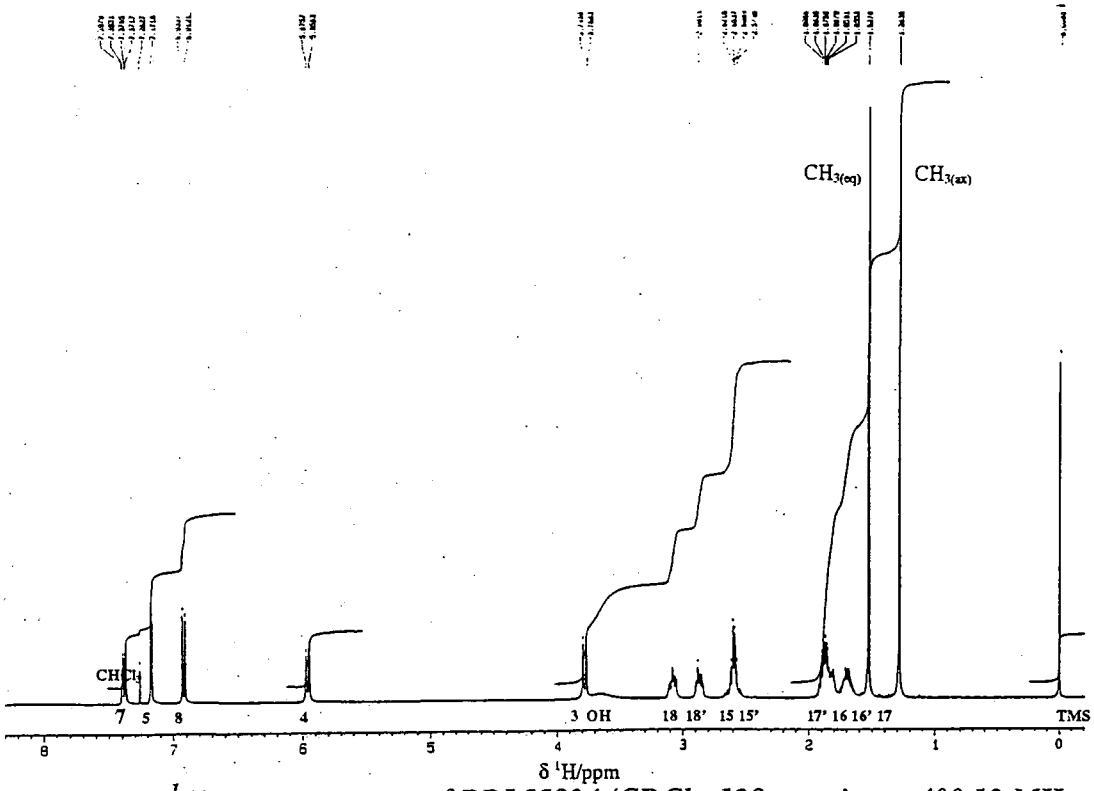

Figure 1 ^{1}H NMR spectrum of BRL55834 ($CDCl_3$, 128 transients, 400.13 MHz, 2.4 s acqtm, 2 s rd)

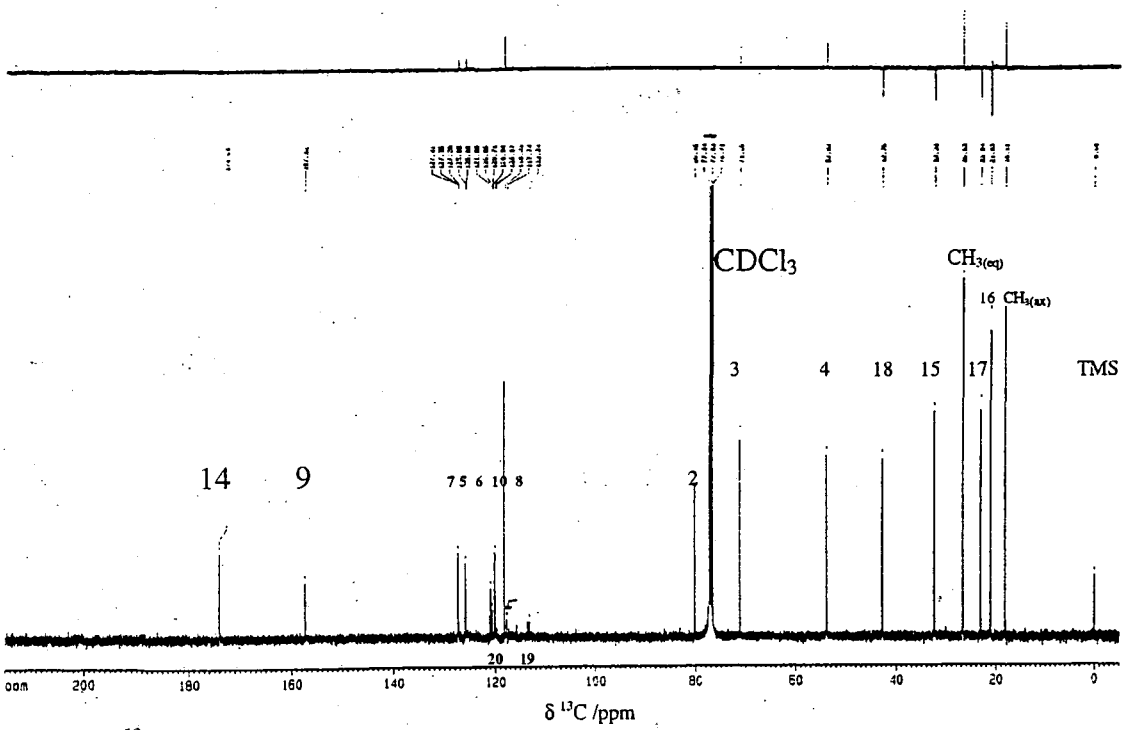

Figure 2 ^{13}C solution-state spectrum ($CDCl_3$, 4096 transients, 100.6 MHz, 1.31 s acqtm, 1.5 s rd)

4.2.2 ^{13}C NMR

Form I batch HP5 (non-micronised) was dissolved in $CDCl_3$ to acquire the ^{13}C spectrum. Assignment of the resonances was assisted by running a DEPT[1] experiment, which shows CH and CH_3 signals as positive and CH_2 as negative with respect to the baseline. No signals appear for quaternary carbon atoms.

Chemical shift / ppm	DEPT phase	Assignment and coupling
174.04	0	14
157.32	0	9
127.41, 127.35, 127.29	+ve CH	7
125.95, 126.98	0	5
120.88	0	6
120.31	0	10
Centred around ~ 119.3	+ve	20 CF_3 Quartet of triplets
~118.23	+ve	8
Centred around ~113.5	0	19 CF_2 Triplet of quartets
80.16	0	2
77.34, 77.03, 76.01	0	$CDCl_3$
71.20	+ve CH	3
53.82	+ve CH	4
42.76	-ve CH_2	18
32.38	-ve CH_2	15
26.63	+ve CH	eq CH_3
23.04	-ve CH_2	17
21.03	-ve CH_2	16
18.11	+ve CH	ax CH_3

Table 3 ^{13}C chemical shift, DEPT phase, assignment and coupling information($CDCl_3$).

4.2.3 ^{19}F NMR

Solution-state spectra show two peaks of intensity ratio 3:2 corresponding to the CF_3 and CF_2 groups respectively. However, the resonance corresponding to the two fluorine atoms on C(19) displays second order coupling characteristics. This effect, sometimes known as the 'roofing' effect, is due to the similarity in the shifts of the two fluorine atoms, due to their diastereotopic relationship to each other, which thus gives rise to an AB-type coupling. The isotropic shift may be calculated from AB calculations using the formula:

$|\nu_A - \nu_B| = \{(\nu_1 - \nu_4)(\nu_2 - \nu_3)\}^{1/2}$, where $\nu_{1\text{-}4}$ are the peak positions in the coupling pattern and $\nu_1<\nu_2<\nu_3<\nu_4$.

The CF_3 group acts similarly to a methyl group, displaying very rapid rotation and thus resulting in a narrow resonance of intensity three.

^{19}F Chemical shift /ppm	Assignment and coupling
-85.4	20
ν_A = -113.51 ν_B = -115.49	19 and 19' Quartet displays $^2J_{F19\text{-}19'}$ =329 Hz

Table 4 ^{19}F Chemical shift, assignment and coupling information

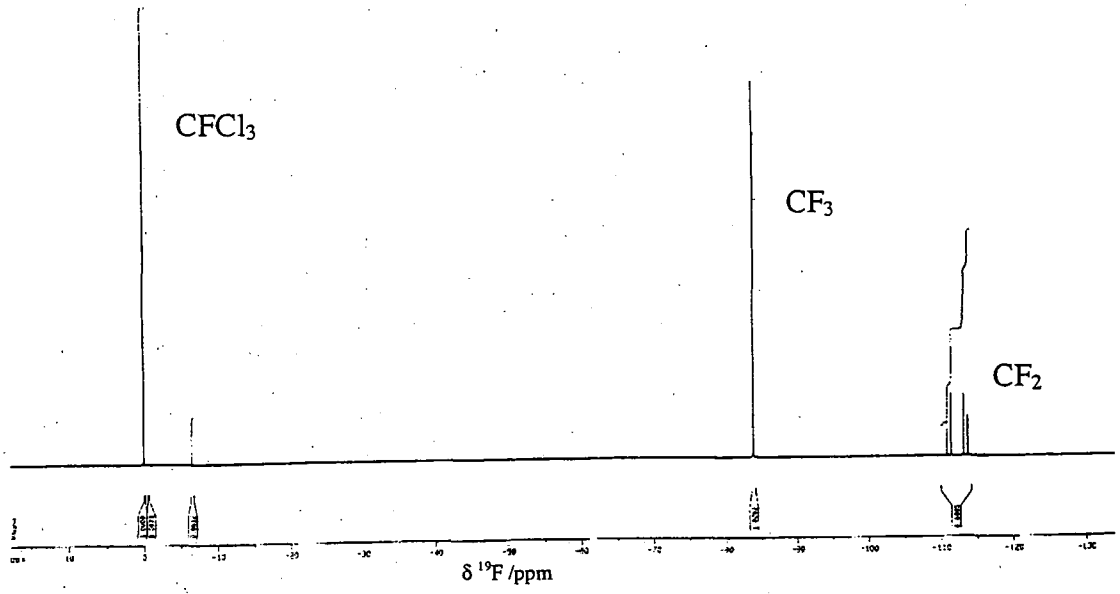

Figure 3 ^{19}F Solution-state NMR spectrum of BRL55834 ($CDCl_3$, referenced to $CFCl_3$ 0 ppm, 470 MHz)

4.2.4 Two-dimensional correlation techniques

Several heteronuclear assignment techniques[2] were used to help to interpret the NMR spectra of BRL55834. All techniques used involved multiplicity selection or 'spectral editing'.

Proton correlation Double Quantum Filtered COrrelation SpectroscopY[3] was used and the resultant 2-Dimensional spectrum is shown in ***Figure 4***. This technique allows connectivity information to be extracted and displays the proton dimension along the t_1 and t_2 axes, and the leading diagonal only showing peaks for protons that are coupled to other protons.

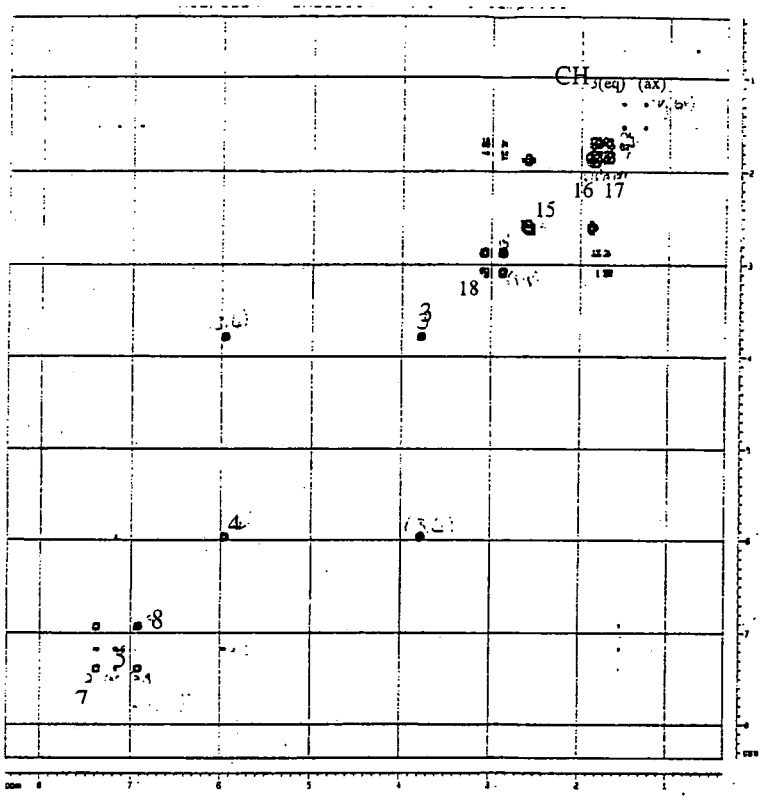

Figure 4 ^1H DQF COSY of Brl55834 in $CDCl_3$ (^1H @ 400 MHz, 2 s rd, 0.32 s acqtm).

The following two techniques were also applied to help the assignment of the spectra. Proton multiple Quantum Correlation (HMQC)[4], in which the spectrum correlates proton and carbon chemical shifts which are directly coupled to each other via ^1J coupling. Proton Multiple Bond Correlation (HMBC)[5,6] was also used to correlate protons and carbons with couplings through more than one bond.

4.3 Solid-state NMR assignment

4.3.1 ^{13}C CP/MAS spectral acquisition

Standard conditions of a MAS rate between 4.5 and 6 kHz, a recycle delay of 3 s (set after proton T_1 measurements), acquisition time 100 ms (2048 data points). CP from protons with a contact time of 10 ms gives the optimum signal.

The room temperature $^{1}H \rightarrow ^{13}C$ CP/MAS spectra for polymorphic forms I and II are shown in ***Figure 4***. These spectra show marked differences. That of form II contains extensive splitting of many signals, indicating the existence of more than one molecule in the asymmetric unit. Splittings into two peaks are particularly clear for the resonances of C(2) at ~80 ppm, C(15) at ~33 ppm and CH_3(eq) at ~27 ppm with approximate 1:2 or 2:1 relative intensities, though the band assigned to C(3) is split into three distinct peaks (70.6, 69.0, 67.2 ppm) which may indicate, along with the complex shape of the resonances for C(14), the presence of three chemically distinct molecules in the asymmetric unit.

(^{13}C, ^{14}N) dipolar coupling interactions, which are not averaged out by the rapid MAS, manifest themselves in the form of asymmetric doublets of intensity ratio 1:2 or 2:1. This residual dipolar splitting exists for resonances assigned to carbons (14), (18) and (4), which are directly bound to the nitrogen atom. In the spectra of form II the splitting is very pronounced, and is especially evident in the case of C(14), which shows asymmetric bands at 178 and 173 ppm. However, in the spectra of form I this effect only contributes to the broadening of the C(14), C(4) and C(18) resonances.

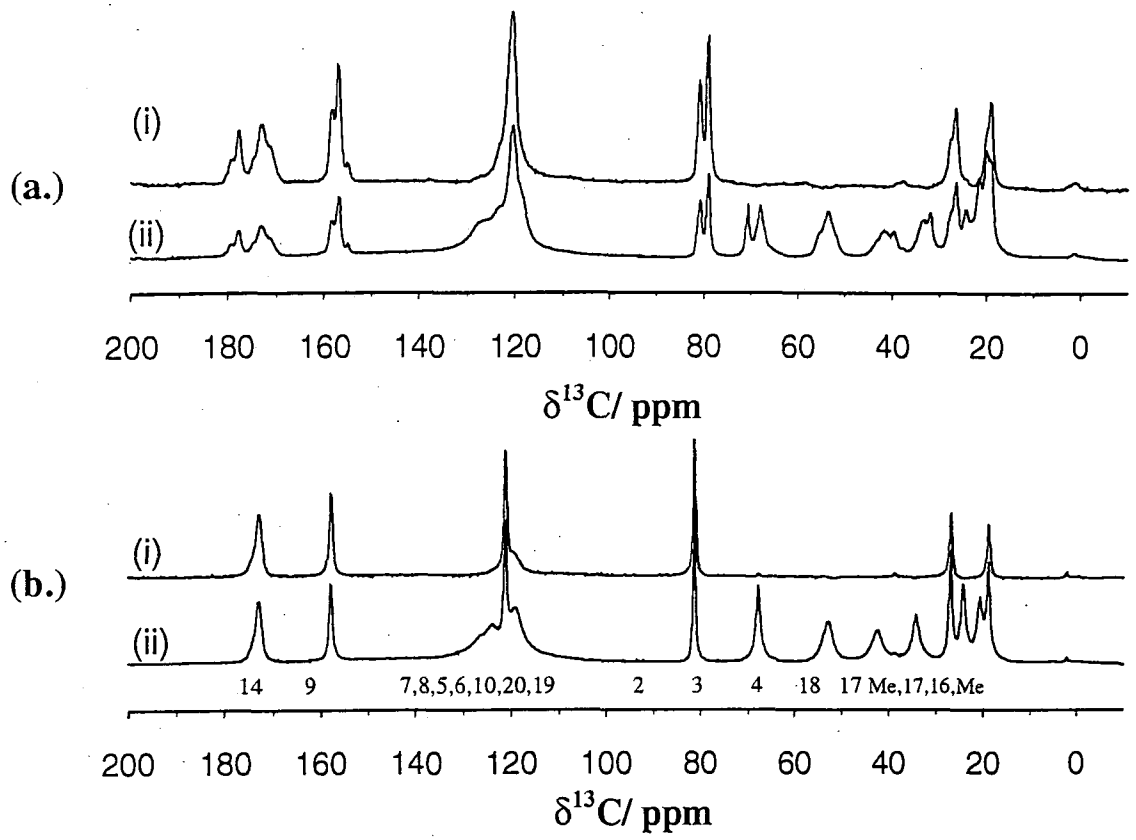

Figure 5 Solid-state ^{13}C CP/MAS NMR spectra of (a) form II, and (b) form I. Comparison of (i) nqs and (ii) Cpflip (6 kHz MAS, 10016 transients, 10.0 ms ct, 3.0 s rd).

The splittings and/ or broadenings for resonances of C-N carbons were confirmed as arising from residual dipolar interactions by observation of spectra obtained at higher magnetic field (Varian Unity Plus 300 spectrometer), which showed reduced splittings and/or narrower peaks (see chapter 6) .

4.3.2 Comparison of solid- and solution-state ^{13}C NMR spectra.

In order to assist with the assignment of the solid-state NMR spectra, the resonances were compared to those observed in the solution-state ^{13}C NMR spectra, which had been previously assigned with the aid of 2D correlation techniques. Although it is appreciated that the presence of solvent[7], and variations in inter- and intra-molecular interactions

between the solid and solution may alter the chemical environment of individual ^{13}C nuclei, this provided a useful guide for the initial assignment of the resonances.

	Solution state		Solid state /ppm	
Assignment	ppm	Scalar couplings (J / Hz)	Form I	Form II
14	174.04		172.9	178.0, 173.4, 171.2 (6) RDC
9	157.32		157.8	158.4, 156.9, 155.0 (3)
7	127.35	$^3J_{CF} = 6.0$	126.7	127.7
8	118.23		124.0	126.3
5	126.47	$^3J_{CF} = 6.3$	121.3	123.6
6	120.88	$^2J_{CF} = 24.8$	121.0	121.0
10	120.31		119.3	120.1
20	119.30	$^1J_{CF} = 285.9$ $^2J_{CF} = 40.3$	118.7	119.3
19	113.51	$^1J_{CF} = 253.6$ $^2J_{CF} = 38.1$	114.3	113.6
2	80.16		81.1	80.8, 79.0 (2)
3	71.20		67.7	70.6, 68.0, 67.2
4	53.82		52.7	55.4-51.8 RDC
18	42.76		42.3	43.5-39.3 RDC (4)
15	32.38		34.1	33.5-32.0 (2)
CH_3 (eq)	26.63		26.7	27.8-26.6 (2)
17	23.04		24.0	24.5-23.1 (2)
16	21.03		20.5	21.7
CH_3 (ax)	18.11		18.6	20.2-19.1 (2)
RDC = Residual Dipolar Coupling - weighted mean isotropic shift given; (3) = 3 peaks All RDC signals (form II) are split into 1:2 asymmetric doublets, with the high intensity peak at low frequency.				

Table 5 Comparison of ^{13}C solution-state NMR assignments with CP/MAS experiments of both polymorphs of BRL55834

The largest variations in the chemical shifts of individual ^{13}C nuclei seem to occur for atoms which may be involved in inter- or intra- molecular hydrogen bonding. This includes carbon atoms (14) and (3). Both signals show large inter-form variations between form I and II (a maximum of 3 ppm for site C(3) and –1.7 ppm to 5.1 ppm) as well as large individual deviations from the isotropic, solution-state values. These results appear to suggest strong intra-molecular hydrogen bonding, or a different conformation about the C(14)-N bond, for one of the independent molecules of form II only, giving a high frequency shift of *ca.* 5ppm from the other C(14) peaks.

4.3.3 Assignment of the solid-state ^{13}C CP/MAS NMR spectra

A broad area of indistinguishable peaks that is very difficult to resolve can be observed around 120 ppm. On the basis of solution-state assignments this may be attributed to the fact that there are possibly seven individual resonances occurring for form I in this region. These include the signals for quaternary carbons (6) and (10); fluorinated carbons (19) and (20); plus the protonated aromatic carbon resonances (5), (7) and (8).

The resonances of carbon atoms that are close in space to the fluorine atoms will be greatly broadened by strong (^{13}C, ^{19}F) dipolar interactions, not fully averaged by MAS. They will also be split by (^{13}C, ^{19}F) isotropic electron-mediated ('scalar') coupling. This obviously does not help the assignment problem and it is desirable to remove these interactions by decoupling. These sites would also be expected to possess lower proton-to carbon CP efficiency

4.3.3.1 Spectral editing techniques

Dipolar dephasing experiments were carried out in order to identify the quaternary and methyl carbons (see ***Figure 5***). A dephasing window of 50 μs was used. WISE experiments showed that on the timescale of between 0.1 and 40 μs groups appear to be mobile.

4.3.3.2 Triple-channel, HFX experiments

Triple-channel HFX experiments were carried out with high-power continuous wave ^{19}F and ^{1}H decoupling. This increased the resolution of the 120 ppm region although seven peaks were still not discernible for form I (see next figure).

Fluorine-to-carbon CP was then implemented, with interesting results. Both forms I and II now displayed broad peaks at approximately 114 ppm, which may be attributed to the CF_2 group, C(19), and which were not evident in previous proton-to-carbon CP spectra. A background spectrum of an empty rotor was run and subtracted from the spectra in order

to verify that this peak was not arising from fluorinated components in the rotor or the probe (see ***Figure 6***). Greater resolution than for $^{1}H \rightarrow ^{13}C$ CP was also achieved, most noticeably for form II, where five more peaks are now easily recognised in the 120 ppm region. Variable contact time CP/MAS experiments were used to elucidate the signals for protonated carbons (5), (7) and (8), whose lower T_{CH} values cause these resonances to appear after a shorter cross polarisation time within the poorly resolved region around 120 ppm.

The final assignments of the ^{13}C CPMAS spectra, which were made using the combination of non-quaternary suppression, variable contact time, and triple-channel experiments, are displayed in ***Table 5***.

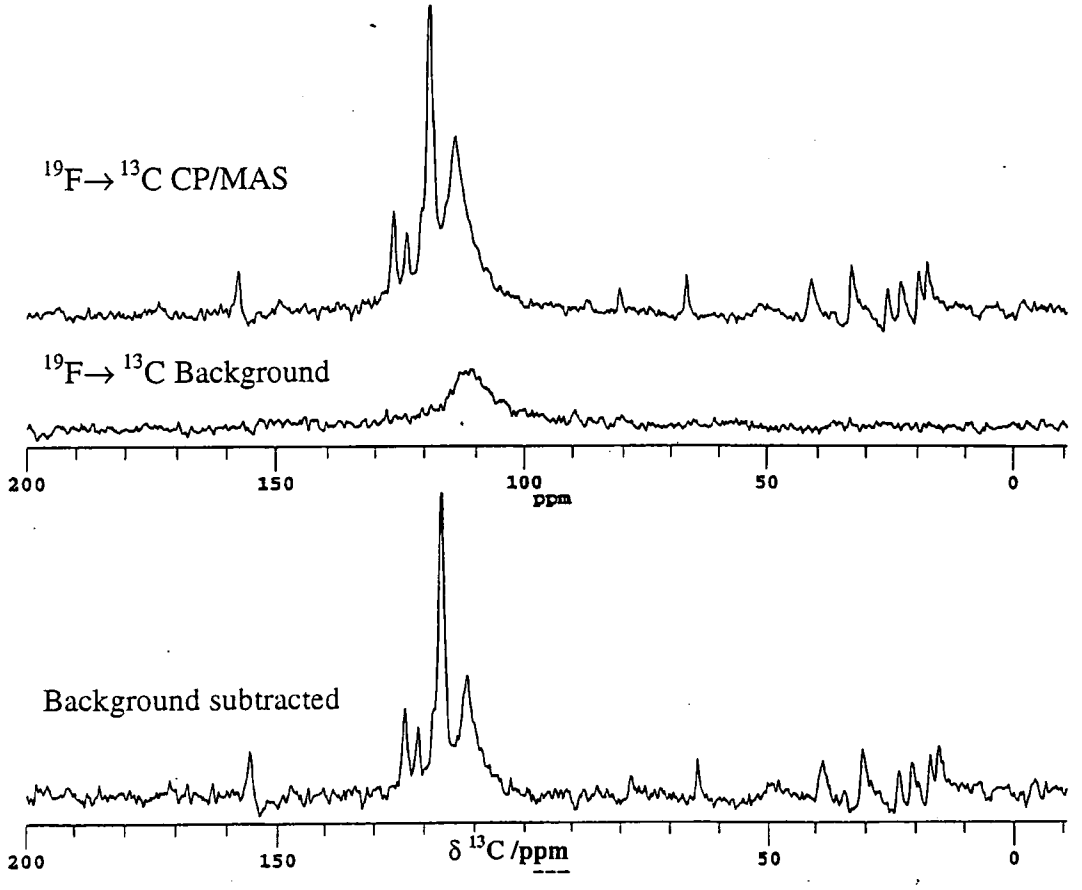

Figure 6 ^{13}C CP/MAS spectra showing background subtraction for $^{19}F \rightarrow ^{13}C$ CP. BRL55834, form I (Cpflip, MAS 6 kHz, ct=10.0 ms, acqtm 50 ms).

The spectra in ***Figure 7*** show the improvement in resolution of the ^{13}C CP/MAS spectra on application of dual channel decoupling and with CP from $^{19}F \rightarrow ^{13}C$.

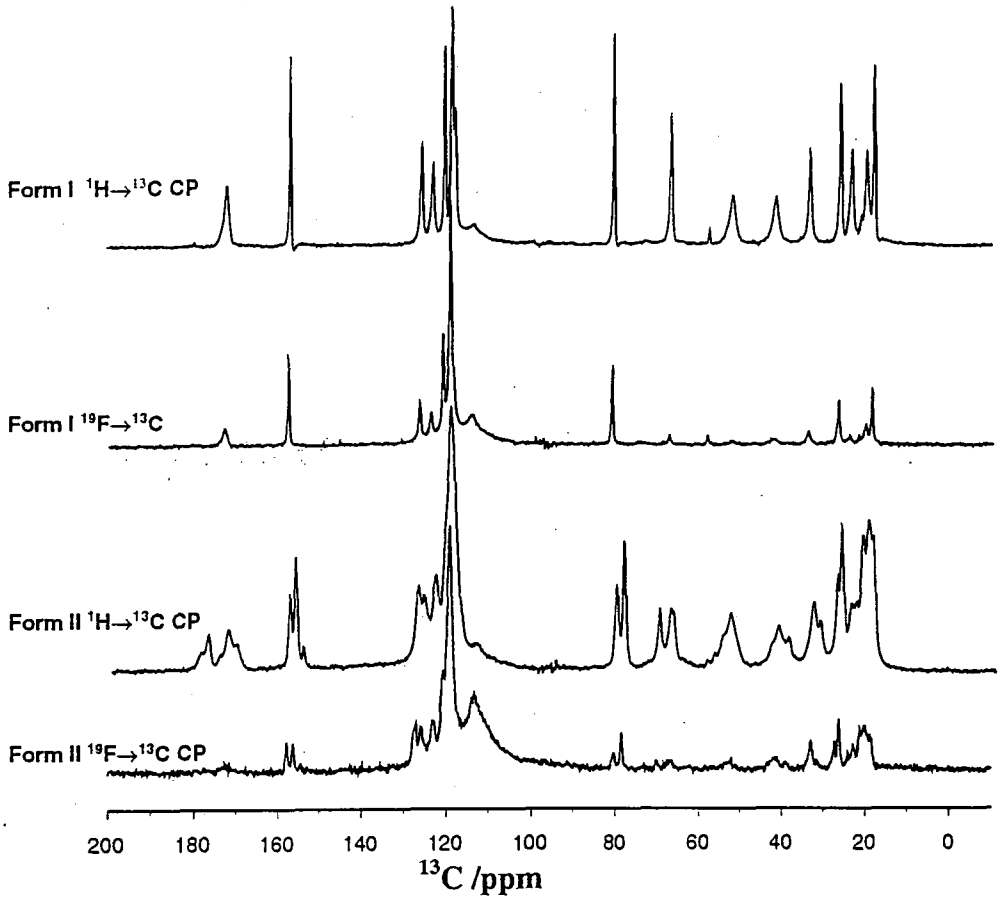

Figure 7 Comparison of spectra with simultaneous {^{1}H}{^{19}F} decoupling. (uscp2dec, acqtm 75 ms, 2884 transients, ct 10.0 ms, rd 3.0 ms, MAS rate 5 kHz).

In the ^{19}F spectra of BRL55834 there is a 5 kHz separation between the CF_3 and CF_2 peaks. The ^{19}F decoupling frequency at 188.288 MHz falls directly on resonance with the broader, CF_2 resonance. In an experiment where the ^{19}F decoupling frequency was arrayed between the two peak positions, it was shown that a significant resolution enhancement occurred for decoupling with the ^{19}F decoupling on resonance with either ^{19}F peak. However, poor resolution was observed with an average value of the decoupling frequency (see ***Figure 8***). Modulating the decoupling frequency using TPPM on the proton and fluorine channels was attempted with no significant resolution improvement.

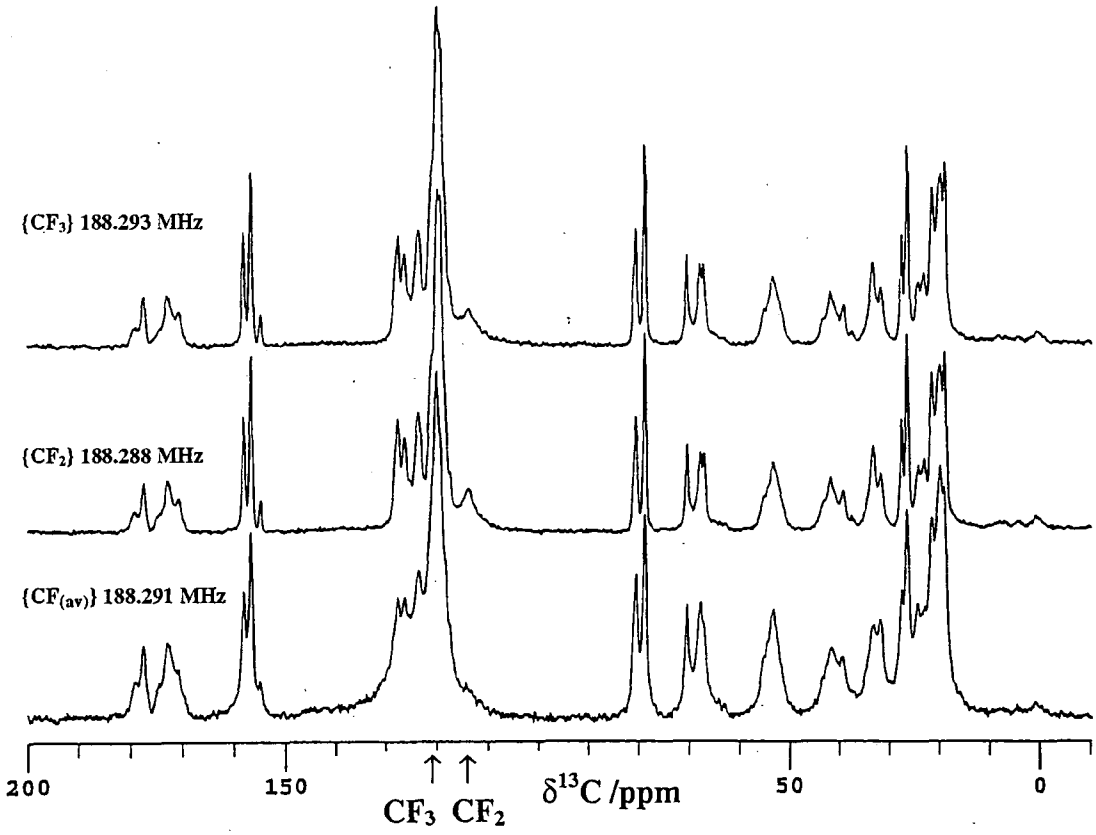

Figure 8 Comparison of applying simultaneous ^{1}H and ^{19}F CW decoupling, with ^{19}F frequency on resonance with the CF_3, CF_2, and at an average position between the resonances. (uscp2dec, 1800 transients, MAS 6 kHz, 10 ms ct, 51 ms acqtm)

4.4 Resolution enhancement – TPPM on the proton channel

The two-pulse phase modulation decoupling sequence (TPPM) aided resolution of the ^{13}C spectra greatly, showing the greatest improvement over Cpflip for the CH_2 signals in the spectrum. However, the greater improvement in resolution comes from the double decoupling of fluorine and proton simultaneously. The tppm (cp4_pm) sequence is therefore more useful on the HX probe, where only proton decoupling may be applied.

4.5 Fluorine

One aim of the work reported here was to see to what extent a combination of modest MAS rates (*ca.* 10 kHz) combined with high-power proton decoupling would suffice to give ^{19}F spectra capable of distinguishing between polymorphs containing perfluoroethyl groups. Obviously, ^{19}F spectra can be obtained much more rapidly than natural-abundance ^{13}C spectra and so in principle may be preferred for polymorphic identification and quantitative analysis.

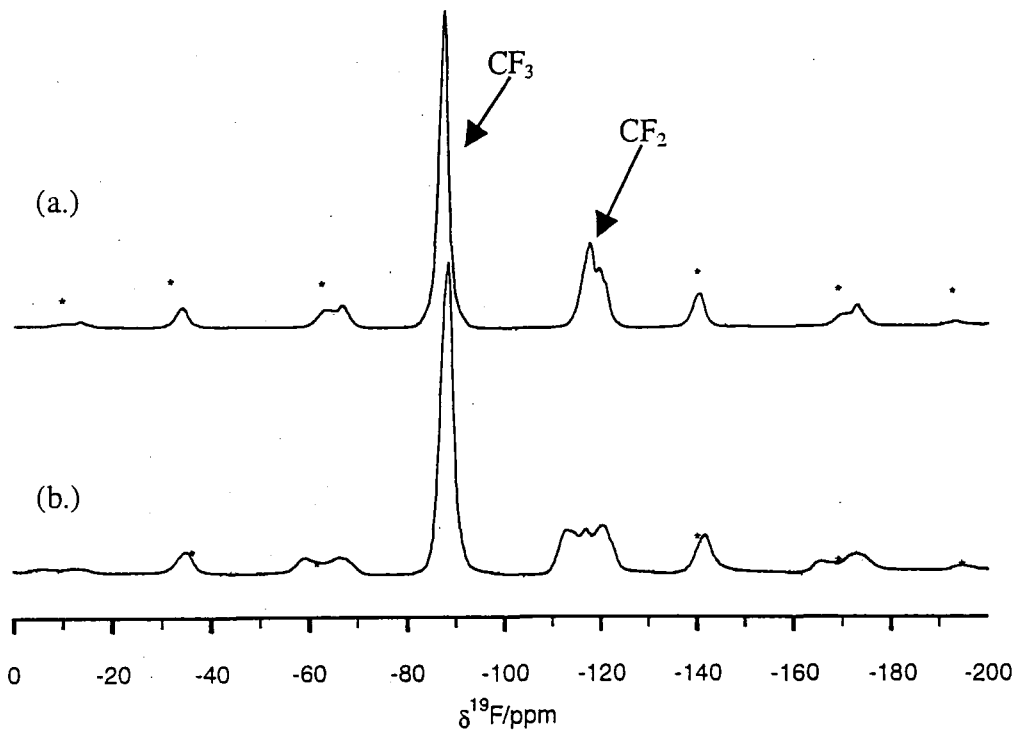

Figure 9 Comparison $^{19}F\{^{1}H\}$ spectra of (a.) form I and (b.) form II of BRL55834 using CPflip (* = ssb, 128 transients, acqtm 10 ms, 10.0 ms ct, 3s rd, 10 kHz MAS).

The two polymorphic forms of BRL55834 show subtle differences in their solid state spectra. The AB coupling evident in the solution-state NMR of BRL55834 is replicated by the broadness of the signal for C(19) for the solid (***Figure 9***). Differences between the spectra of the two polymorphs occur both for the CF_2 resonances (for which form I shows three maxima) and for the CF_3 resonances (***Table 6***).

Assignment	δ $^{19}F^{a}$	
	Form I	Form II
CF_3	-85.0	-86.2
CF_2	-115.8 -117.1[b]	-110.6 -115.0 -118.3

[a] Corrected for the Bloch-Siegert shift which is measured to be –2 ppm. [b] Shoulder (see Figure 9)

Table 6 Comparison of ^{19}F chemical shifts of the two polymorphs.

Although these differences are not great, they are definitive, and they allow distinctions to be made between the samples in much shorter times than is the case for ^{13}C NMR. It is evident that improvements in resolution are necessary if ^{19}F NMR is to become fully useful for BRL55834, *e.g.* to examine polymorphic mixtures. However, high power proton decoupling has clearly been successful and the resulting bandwidths for the CF_3 signals are commensurate with those that have been obtained[8] for systems with well-separated fluorine atoms. Bandwidths typically observed for the proton-decoupled CF_3 resonances are *ca.* 420 and 580 Hz for forms I and II respectively.

4.5.1 ^{19}F relaxation parameters

Fluorine-19 T_1 inversion-recovery experiments with proton decoupling have been carried out by observation of the CF_3 peak giving values of 0.62 (form I) and 0.47 s (form II). Variable spin-lock experiments (with proton decoupling during the acquisition time) have also been applied to this system, resulting in the observation of $T_{1\rho}$ values of 85-105 ms for the fluorine resonances of form I and 170-185 ms for the fluorine resonances of form II. These results are of the order of magnitude expected and were valuable in establishing the optimum conditions for proton-to-fluorine cross polarisation experiments.

The variation in ^{19}F $T_{1\rho}$ values for the two polymorphs alludes to mobility differences between the perfluoroethyl groups in the two different polymorphic forms, with the lower value for form I indicating a greater degree of mobility than for the CF_3 in form II.

4.6 Relaxation and quantitative parameters

Proton T_1 values were measured using the T1hcp experiment (i.e. via the ^{13}C signals) and found to be 1.24 s (±0.2 s) for both form I and form II.

^{13}C T_1 values for individual sites were measured using T1xcp experiments. Resolution of individual signals was a problem and so results are not complete despite repeating the experiments several times. On the whole, the T_1 values of carbon sites in form II are much greater than those in form I. This may infer a greater degree of rigidity in this form.

	Form I		Form II	
Assignment	**$\delta^{13}C$/ppm**	**^{13}C T_1 /s**	**$\delta^{13}C$/ppm**	**^{13}C T_1 /s**
14	174.9	51	178.0, 173.4, 171.2 (6) RDC	107, -, 153
9	157.8	68	158.4, 156.9, 155.0 (3)	-, 107, -
7	126.7	-	127.7	-
8	124.0	68	126.3	-
5	121.3	26	123.6	-
6	121.0	-	121.0	-
10	119.3	-	120.1	60
20	118.7	-	119.3	-
19	114.3	-	113.6	-
2	81.1	21	80.8, 79.0 (2)	34, 40
3	67.7	19	70.6, 68.0, 67.2	57, 61, -
4	52.7	14	55.4-51.8 RDC	96
18	42.3	-	43.5-39.3 RDC (4)	21, 117
15	34.1	5	33.5-32.0 (2)	44
CH_3 (eq)	26.7	2	27.8-26.6 (2)	2.0, 2.0
17	24.0	3	24.5-23.1 (2)	5.0
16	20.5	3	21.7	12
CH_3 (ax)	18.6	2	20.2-19.1 (2)	7.0
RDC = Residual Dipolar Coupling; (3) = 3 peaks; (Hz); - = irresolvable				

Table 7 Comparison of known carbon T_1 values (from T1xcp experiments)

Carbon T_1 data were collected over 20 data points for both forms (with tau values of 0, 1, 2, 3, 4, 5, 8, 10, 12, 16, 20, 24, 28, 32, 36, 40, 60, and 120 s) with 600 transients per slice. This resulted in values of ^{13}C T_1 accurate to ± 2.5 s.

Figure 10 and ***Figure 11*** present the results of variable contact time experiments, which helped the assignment, especially of the spectrum of form II, due to dependence upon the

proton-carbon distance. The large difference between the rates of CP to the fluorinated carbons (19) and (20) compared to the other resonances may be observed immediately.

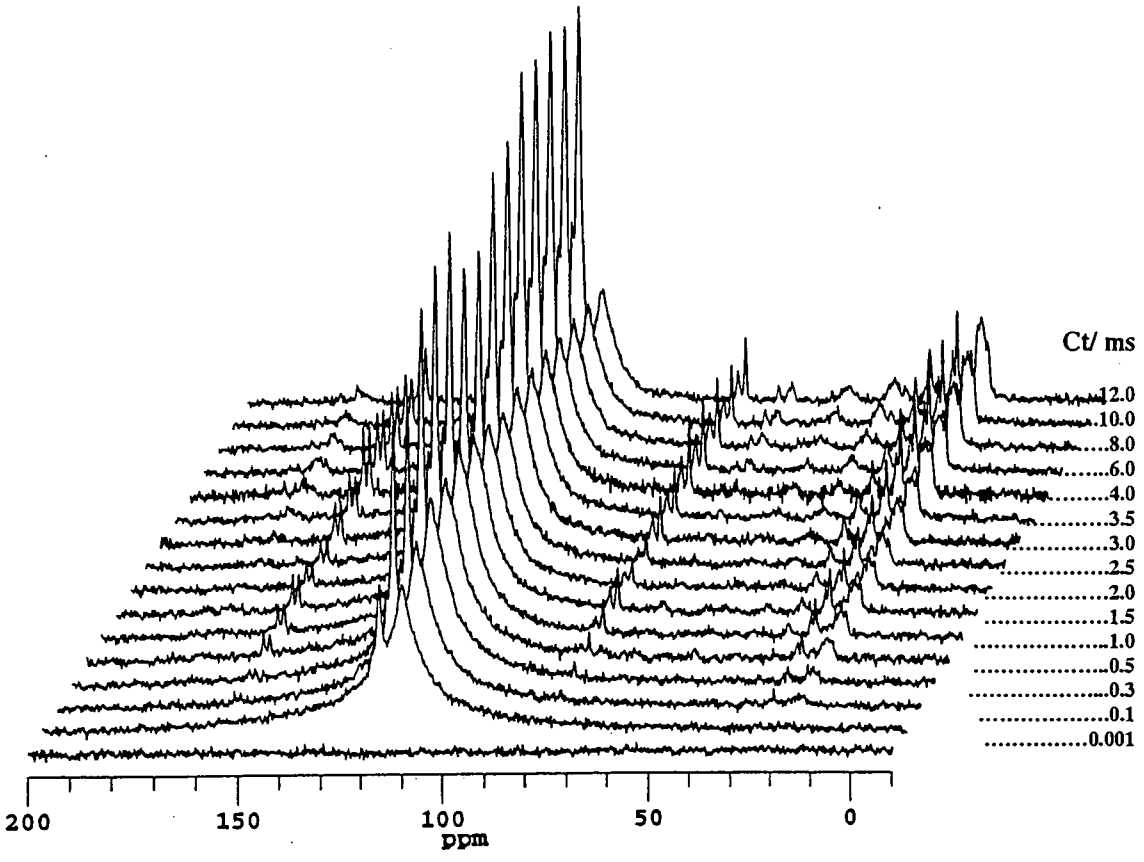

Figure 10 BRL55834 form II $^{19}F \rightarrow {}^{13}C\{^1H\}\{^{19}F\}$ variable contact time experiment showing short T_{FC} of fluorinated carbons, C(19) and (20) sites (uscp2dec, MAS 6 kHz, rd 3 s, acqtm 102 ms, 50.329 MHz, 2200 transients).

The high CP efficiency to the fluorinated sites, C(19) and (20) is shown by their high intensity after a contact time of only 0.1ms. The signals for C(5), (6), (7), (8), and the two methyl groups appear next (after a contact time of 0.3 ms), along with C(9) and C(2). After a contact time of 12.0 ms all the carbon peaks are present in the spectrum, but with the greatest intensity for the positions directly bound to the ^{19}F sites.

The same technique applied to form I showed much more inefficient CP to other carbons, with signals observed only for C atoms in close bonding proximity to the perfluoroethyl

group. After 4 ms there still remained no resonances from carbons other than (19), (20), (6), (5), (7), and possibly (8).

		T_{FC} /(± 0.1 ms)	
Peak assignment	$\delta^{13}C$/ ppm*	Form I	Form II
14	172	-	3.30
9	156 154	-	1.85 0.04
7	127	-	0.27
20	119	0.19	0.17
19	114	0.17	0.06
2	80	-	2.17
* approximate, for the sake of comparison only, - value not obtainable			

Table 8 A comparison of T_{FC} values for the BRL55834 polymorphs.

The T_{FC} data that can be extracted from these experiments are summarised in ***Table 8*** and this information reinforces the assignment analysis given above. It is also interesting to note that in form II only one of the two C(14) resonances is observable within the time constraints of the experiment (contact times arrayed from 0.001 ms to 12 ms). This peak shows the greatest T_{FC}, indicating that the r_{CF} is greatest for this site. However, as the other C(14) is not apparent one can assume that the fluorinated groups are in closer proximity to some molecules in the unit cell than others. This argument may be extended to the resonance of C(9) for form II, which also show contrasting, yet resolvable T_{FC} values. The large T_{FC} value for C(2) could be explained by the fact that the two methyl groups bonded to this site provide steric hindrance causing $r_{FC(2)}$ to be great. The possible greater rate of rotation of the CF_3 group in form I (as suggested from ^{19}F $T_1\rho$ experiments) may explain the greater T_{FC} times for C(19) and (20) compared to form II.

The $^1H \rightarrow ^{13}C$ variable contact experiment (see ***Figure 11***), shows the decreased CP efficiency of the fluorinated carbons in comparison with the $^{19}F \rightarrow ^{13}C$ variable contact time experiment. In fact, the signals (at 114 ppm and 119 ppm) are not even observable in the $^1H \rightarrow ^{13}C$ CP experiment.

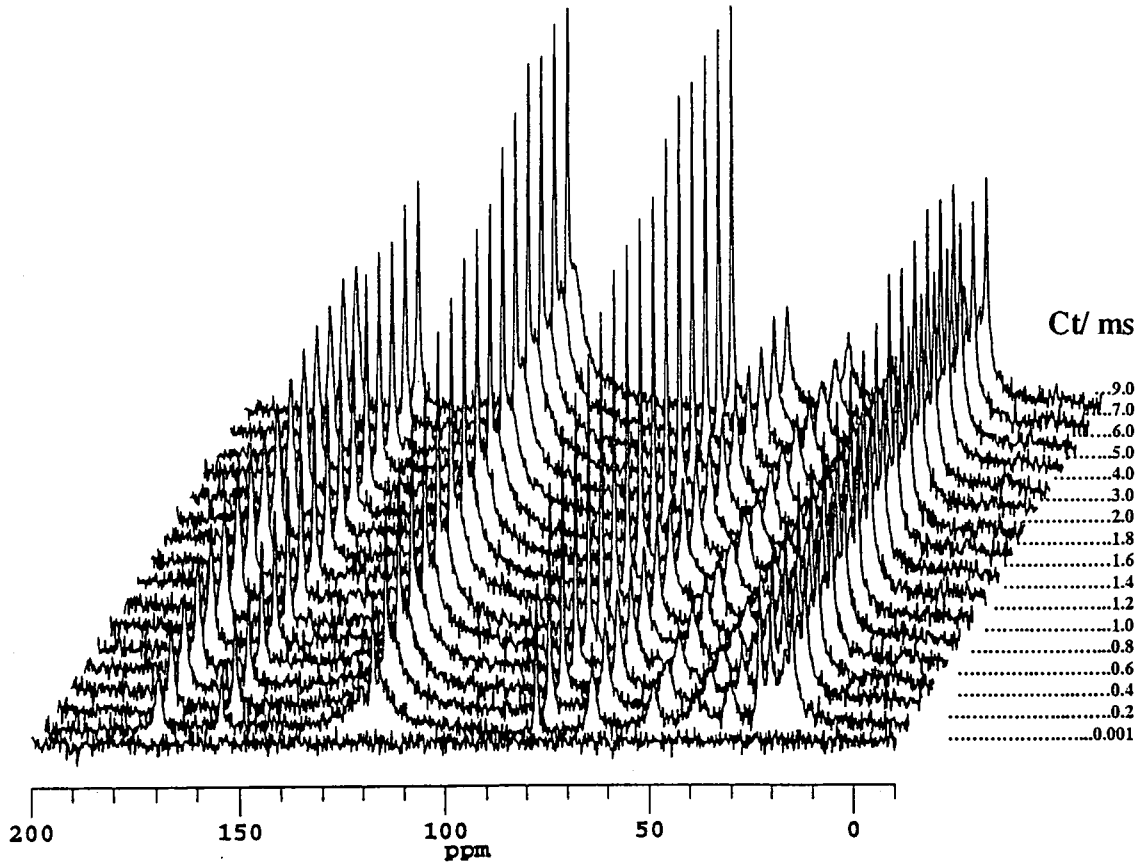

Figure 11 BRL55834 form 1 $^{1}H \rightarrow {}^{13}C\{^{1}H\}\{^{19}F\}$ variable contact time experiment showing short T_{HC} of most ^{13}C sites (Cpflip, MAS 6 kHz, rd 3 s, acqtm 102 ms, 50.329 MHz).

These variable proton-to-carbon contact-time experiments aided assignment, showing the quaternary carbon sites to possess longer T_{HC} values (C(14) 0.6 ms, C(9) 1 ms), and the protonated carbons, have shorter T_{HC} times of the order of 0.1 ms (e.g. CH(3) 0.13 ms, CH_2(18) 0.069 ms, and CH_2(15) 0.090 ms). The fluorinated carbon sites have much longer T_{HC} times than their corresponding T_{FC} values, not actually becoming observable until contact times greater than 9 ms. These values were calculated by plotting the intensity data of the ^{13}C data in the spinsight 3.0 xy fitting panel.

4.8 Proton CRAMPS

Proton CRAMP spectra of both polymorphs of BRL55834 were quite inconclusive although differences are visible between the forms and on addition of ^{19}F decoupling. The spectra of form II appears broader than that of form I, possibly due to the existence of more molecules in the asymmetric unit of form II.

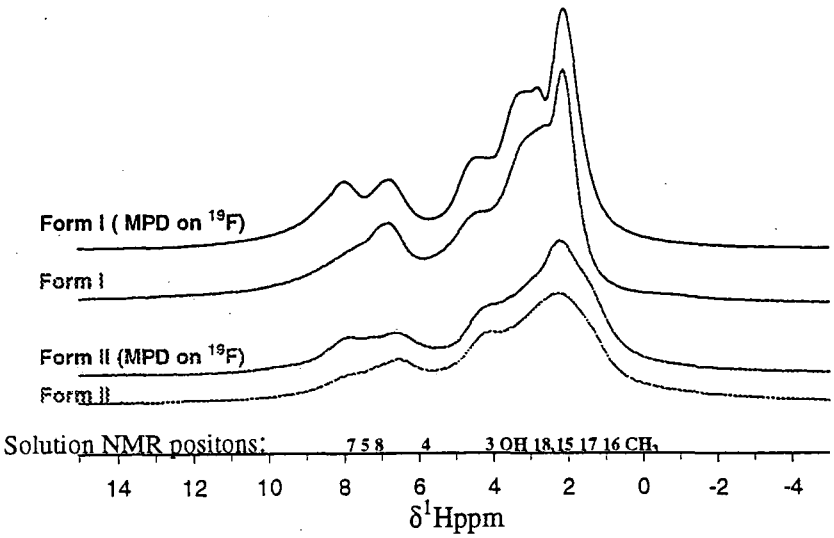

Figure 12 ^{1}H CRAMP (BR-24) spectra of BRL55834, forms I and II with and without 180° pulses on the ^{19}F channel to decouple fluorine (MAS 957 Hz, 200.127 MHz, 128 transients, acqtm 27 ms, rd 10 s).

The CRAMPS results are consistent with those of solution-state proton NMR although a lack of peaks above 10 ppm indicates that no significant hydrogen bonding is present in the solid.

The large number of fluorine atoms in BRL55834 causes strong heteronuclear dipolar interactions to exist with the proton nuclei. A MAS rate of 957 Hz is not sufficient to average these interactions out. On application of 180° pulses in the large windows of the BR-24 pulse sequence on the fluorine channel, the proton CRAMP spectra alter since these interactions are decoupled. It may be expected that resonances of protons 7, 5 and 8 will be the most strongly coupled due to their proximity to the perfluoroethyl group.

Indeed, upon decoupling the area of the spectrum assigned to these resonances shows the greatest change.

4.8 Variable temperature experiments

Variable temperature work on both polymorphs shows no significant changes in the ^{13}C spectra. (It must be noted that due to the use of different contact times, the spectra below 198 K are not directly comparable with those at 198 K and above.)

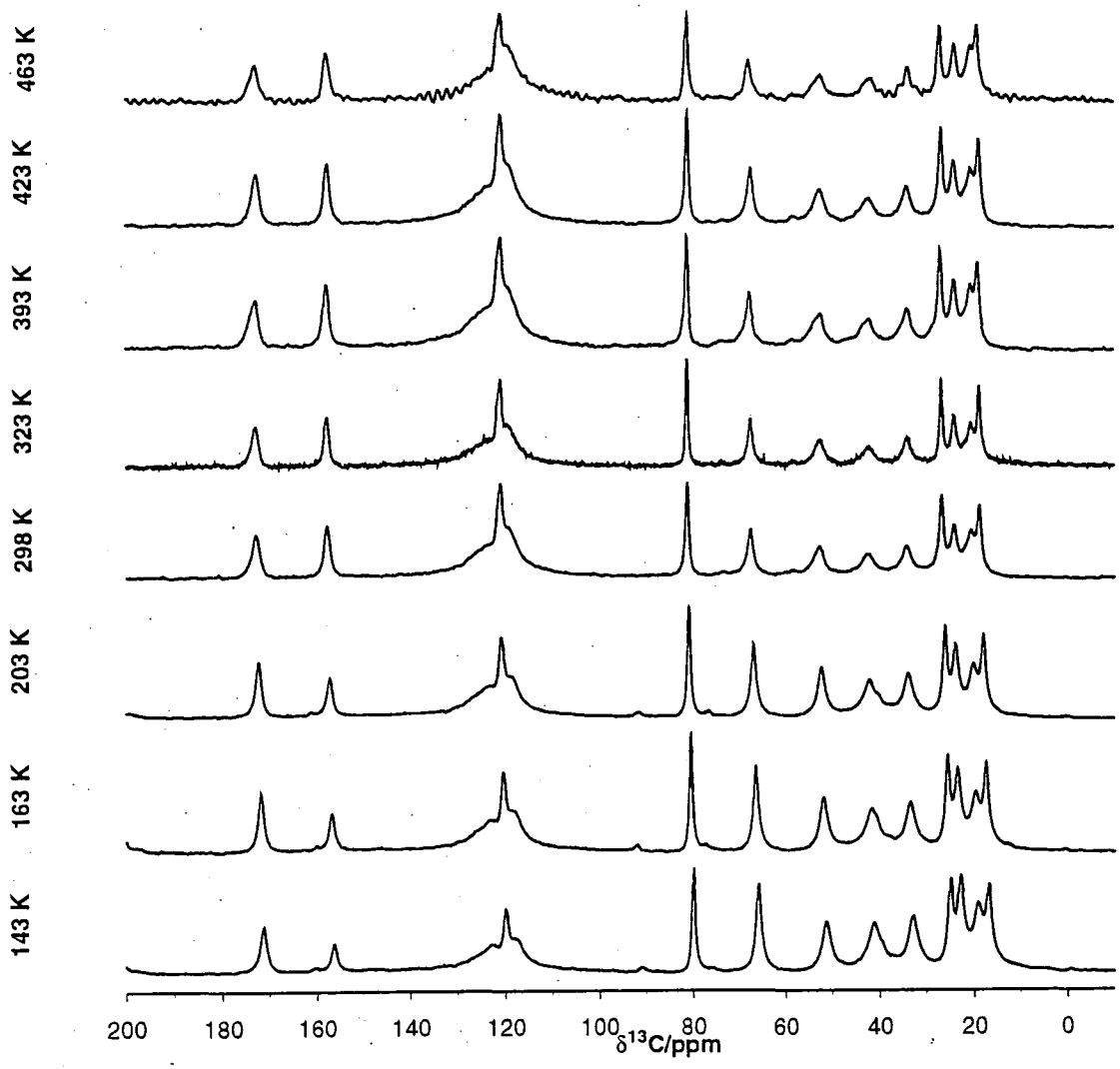

Figure 13 $^{1}H \rightarrow ^{13}C$ CP/MAS variable temperature study of form I (Cpflip, MAS 5kHz 100ms acqtm, 10ms ct for 298 K and above, 2 ms below 298 K).

The main difference is in the relative intensity of specific signals. On going to low temperature this could indicate improved CP efficiency, e.g. for C(2), attached to mobile methyl groups, the rate of rotation of which should decrease. No significant changes in chemical shift are apparent. No difference exists in variable temperature NQS spectra.

4.9 ^{15}N natural abundance

The natural abundance $^{1}H \rightarrow ^{15}N$ CP spectra showed a significant difference between the forms. Form I shows a single, sharp ($\Delta\nu_{1/2}$ = 11 Hz), resonance at –255.5 ppm relative to the nitrate peak of ammonium nitrate. However, form II shows a complex superposition of peaks centred around -247 ppm (these are shown in ***Figure 14***).

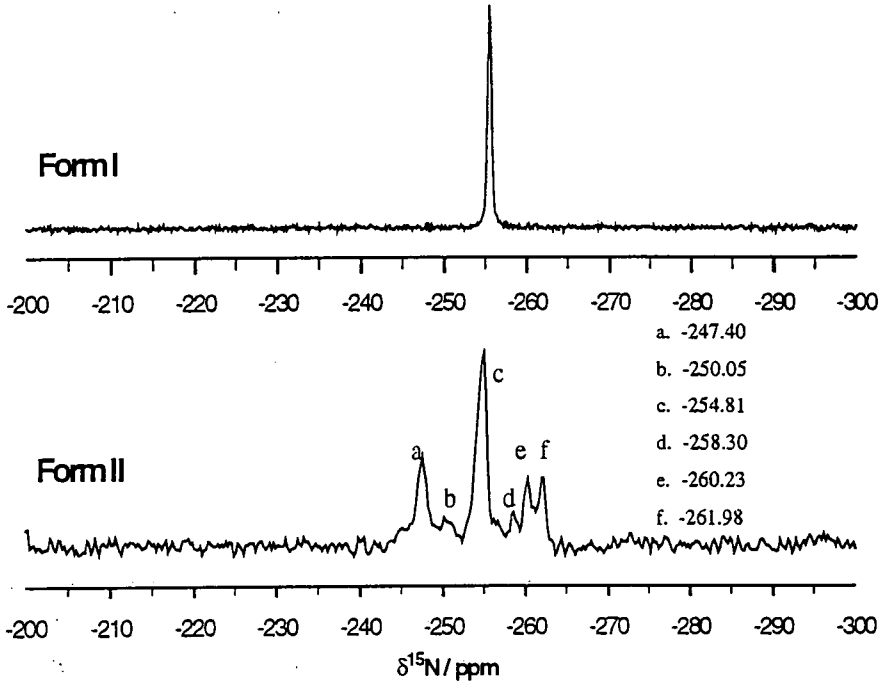

Figure 14 ^{15}N natural abundance spectra of BRL55834 (Cpflip, MAS rate 5 kHz, 21632 transients, 3 s rd, 10 ms ct, 200 ms acqtm).

The cause of the multiple peaks for form II is unclear, but supports the theory that there is more than one molecule in the asymmetric unit for this polymorph. Similar, unexpected multiplicities for natural abundance ^{15}N sites in pharmaceutical solids that display polymorphism have been noted[9] but as yet with no structural explanation.

4.10 ^{15}N labelled studies

A ^{15}N-labelled sample of BRL55834 was created with several specific aims. These included removal of residual dipolar coupling effects (see chapter 6), along with the potential for direct study of the ^{15}N site. The pathway was developed (from parallel methods used by SB) on non-labelled chemicals, during a one-week visit to SB. The final sample was synthesised by Dr. Badman of the radioisotope chemistry group at SmithKline Beecham, Harlow.

4.10.1 The labelled synthesis and analysis: DSC, IR.

The route was scaled to 1/60th from the 'working directions for stage three of route B to SB 204269'.

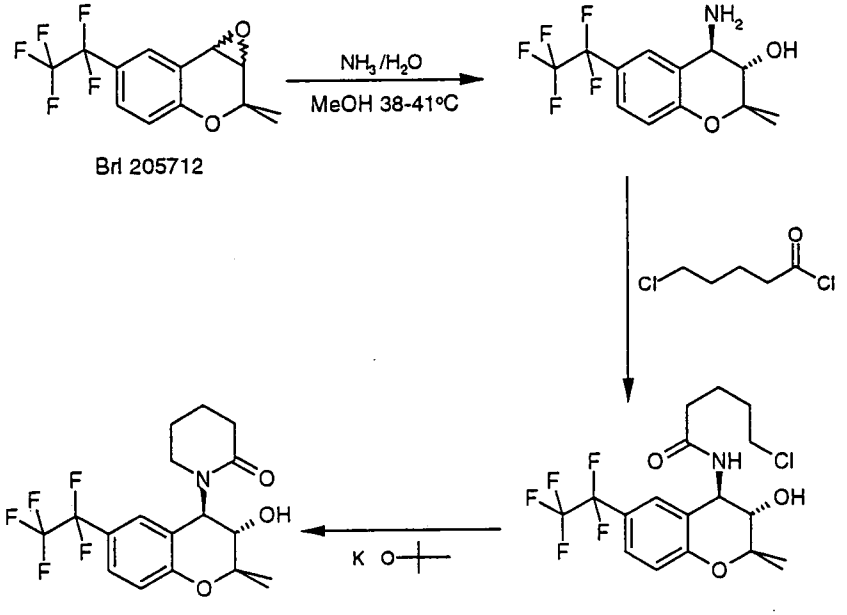

BRL 205712 (0.7984 g) was placed in methanol (2 ml) with water and ammonia [s.g. 0.880 ~15N],.(5 ml). On addition of the $NH_{3(l)}$ a white suspension formed. The liquid was left stirring at 40°C. Some effervescence was visible. After $5^1/_2$ hours heating, the mixture was removed from the heat and the solvent was then removed by rotary-evaporation to near-dryness. Next, whilst there was still some water left in the sample, some

cyclohexane was added and then evaporated off using a rotary evaporator to give a drier product.

The dried sample was placed in a silicone oil bath at 70 °C. A 1:1 solution of methanol (205) and water was made and added gradually, by pipette. MeOH was added, gradually, by pipette. All but 20 mg of the sample had dissolved, therefore all but this was then transferred to a centrifuge tube. Upon centrifuging, immediately, fine needle-like crystals crashed out. The sample was then warmed a little in an oil bath in order to let it crystallise out more slowly and then cooled slowly to room temperature with stirring. The solution was left in a refrigerator at 4 °C over night.

The crystals were filtered off making use of a vacuum pump. The filtrate then crystallised out at the bottom of the round-bottomed flask to give clean, white crystals (~570 mg), these were then left to dry in the air.

TLC using hexane:ethyl acetate (3:1 v/v) as the solvent showed that the starting material had merely been recrystallised and the amino-alcohol actually existed in the mother liquor. This was confirmed by running two solution-state proton NMR spectra in $CDCl_3$.

After the formation of the [N15]BRL55834 from the cyclisation reaction, the crude reaction mixture was purified by column chromatography on silica. The product after columning (ca. 1.05 g of yellow oil/gum, foaming on continued rotary evaporation) was then re-dissolved in methanol (ca. 6 ml) and stirred at 50 °C. Water (ca. 4 ml) was added drop-wise, with a temperature of 50 °C being maintained. The mixture was then allowed to cool to room temperature and then to ca. 4 °C, with stirring. A white precipitate formed and the mixture was stored at 4 °C in the refrigerator over the weekend. The white solid product was then filtered off and washed on the filter with ice cold water/methanol (1:1 v/v) (ca. 15 ml), dried on the filter and then dried over night under vacuum at room temperature. Mass after drying = 810 mg (74 % recovered from recrystallisation).

4.10.2 Carbon, proton and fluorine spectra of [^{15}N]BRL55834

The sample of [^{15}N]BRL55834 has provided opportunities for other types of studies including spinning sideband analysis of the ^{15}N spectrum, variable temperature work, drain, REDOR, and (^{13}C, ^{15}N) correlation studies. Sensitivity problems hindered the latter three techniques and double labelling of the compound is necessary for future work.

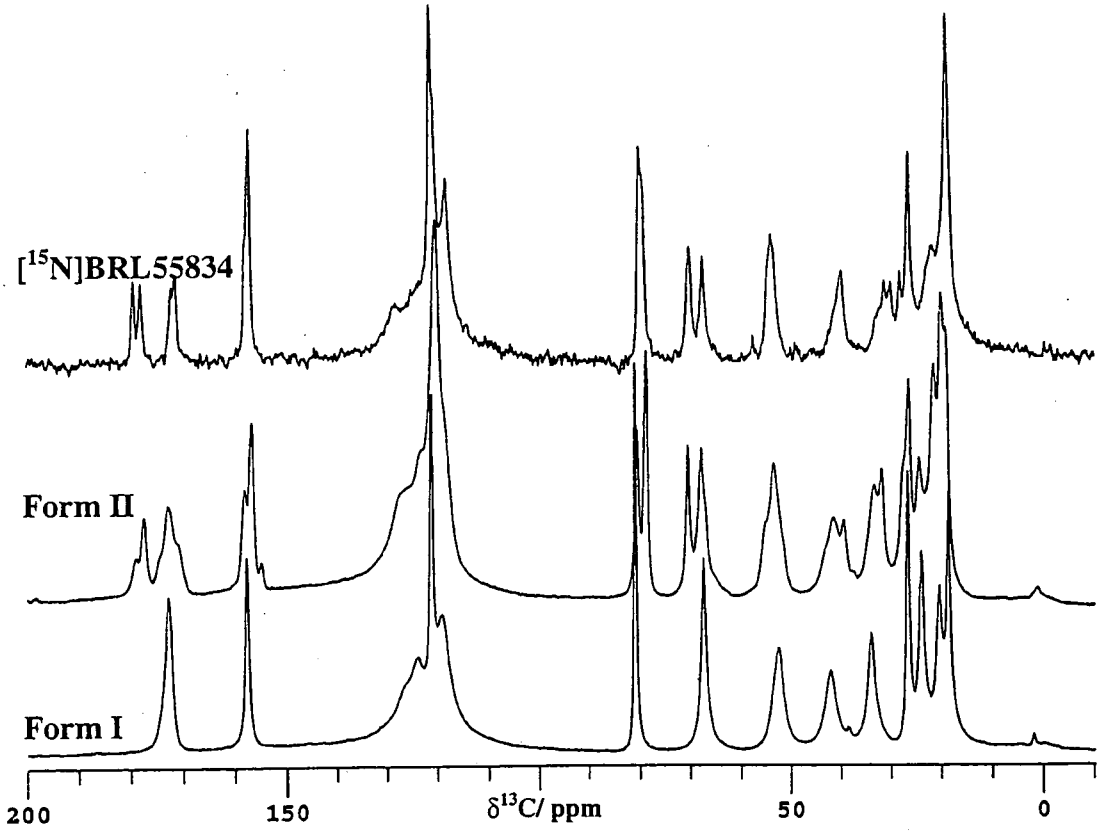

Figure 15 Comparison of $^{1}H \rightarrow ^{13}C$ CP of [^{15}N]BRL55834 and forms I and II (50.329 MHz, Cpflip MAS 4.5 kHz, cpflip, rd 3 s, 51 ms acqtm, transients: 20000(^{15}N), 10016(I & II)).

However, as may be observed from the ^{13}C CP/MAS spectra above, rather than simplifying the work, the subject has become further complicated, since it appears that a new polymorph may have been produced!

The ^{13}C CP/MAS spectrum of [^{15}N]BRL55834 displays some characteristics of form II (such as peak splitting for resonances attributed to C(14), (2) and (3)), as well as some characteristics of the spectra of form I.

However, there also exist some characteristics that are not observed in either of the non-labelled samples, such as the splitting of the C(14) peak at 171-172 ppm, and the small splittings of the peaks at 157.2, 121.3, and 80.4 ppm.

The 600 MHz proton spectra of the three compounds indicate that the labelled sample shows more similarities to form I than to form II.

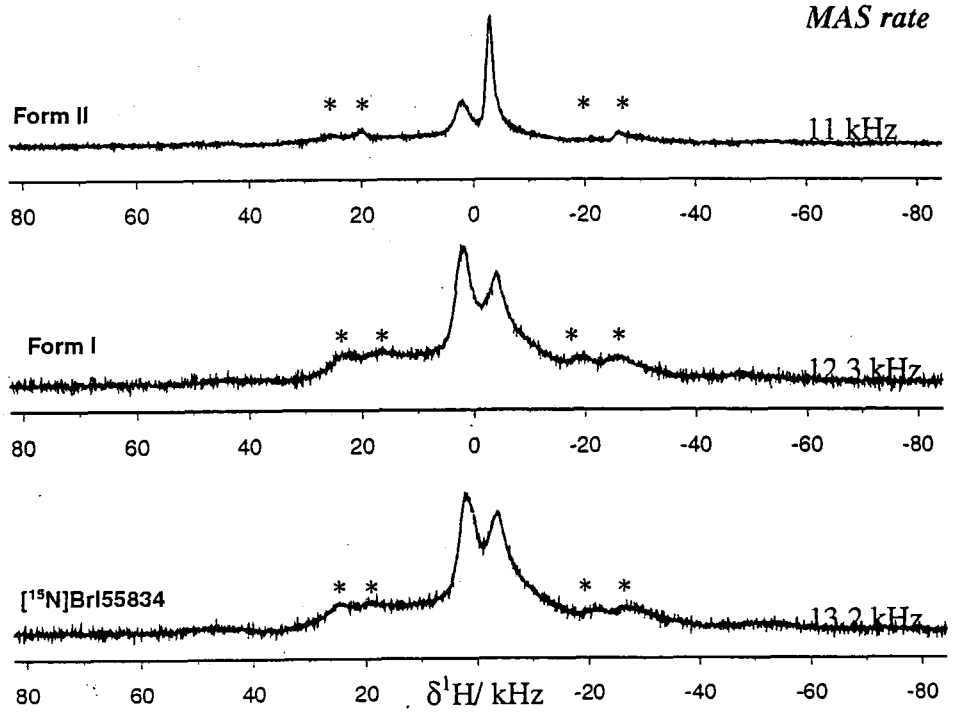

Figure 16 600.13 MHz ^{1}H spectra at high MAS rates. (*=ssb, 32 transients, 10.24 ms acqtm, rd 6 s, 1pulse).

Proton spectra were referenced to water at 0 ppm and were acquired by Lindsey Crowe and Eric Hughes during a visit to the Department of Physics, Warwick University.

The ^{19}F spectrum of the labelled sample also appears more similar to that of form I than form II (see ***Figure 17***).

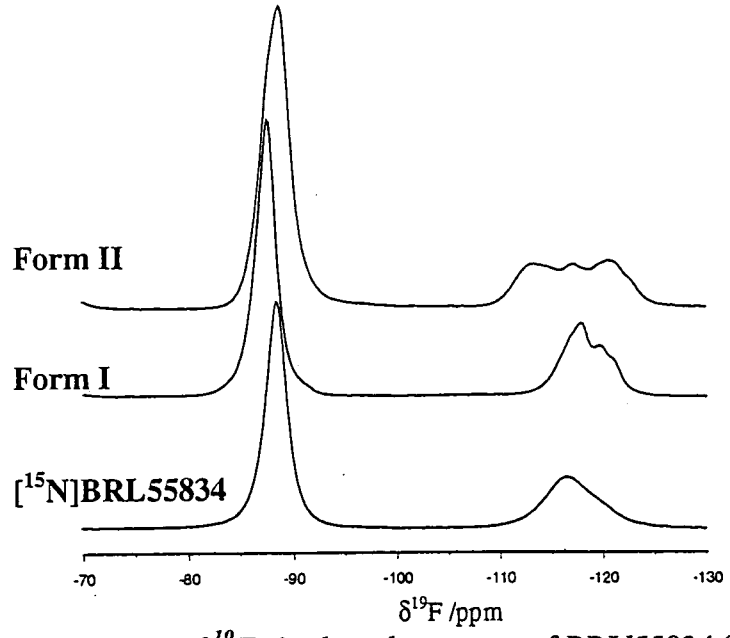

Figure 17 Comparison of ^{19}F single-pulse spectra of BRL55834 (188.288 MHz, 10 kHz MAS, 3s rd, 10 ms acqtm, 32 transients, 1pulse, no Hdec).

Cooling each of the three samples and acquiring the ^{19}F spectra and $T_{1\rho}$ values provides interesting results from which it is possible to draw the conclusion that the fluorinated group is undergoing some motion at ambient temperatures. This causes the ^{19}F spectra to show relatively narrow linewidths, since the rotation of these groups is at least partially averaging out the homonuclear dipolar interactions. As the temperature is lowered, the motion slows in each form, such that a broad, homogeneous lineshape is observed, and CRAMP spectroscopy would be required to resolve the individual peaks. These results are illustrated for form II in ***Figure 18***, below. The $^{1}H \rightarrow ^{19}F$ CP spectra of form I exhibit similar behaviour, giving a broad, homogeneous lineshape at 143 K.

The ^{19}F $T_{1\rho}$ value for the [^{15}N]BRL55834 sample at ambient temperatures is 62-77 ms with the larger value (as for the other forms) measured for the CF_2 resonance. This value is comparable to that measured for form I.

Corresponding with a decrease in temperature, the $T_{1\rho}$ values for each form decrease to a minimum value, supporting the theory that there is a decrease in the mobility of these groups on going to lower temperatures.

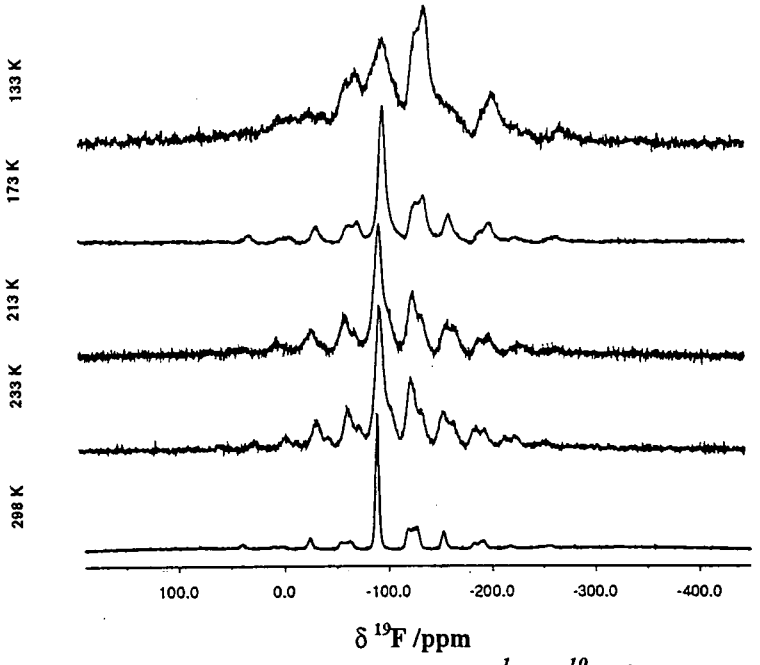

Figure 18 BRL55834 form II: variable temperature $^{1}H \rightarrow ^{19}F$ CP experiments. (MAS 10 kHz, Cpflip, 10 ms acqtm, 16 transients, 5 ms ct, 3 s rd).

The influences of a decrease in temperature are illustrated in ***Figure 18*** and ***Figure 19***. It should be noted that, for form I, a change in the ^{19}F CP spectra similar to that presented for form II is observed. The difference between the forms is the rate of change of $T_{1\rho}$ with temperature from the varying values at ambient temperature.

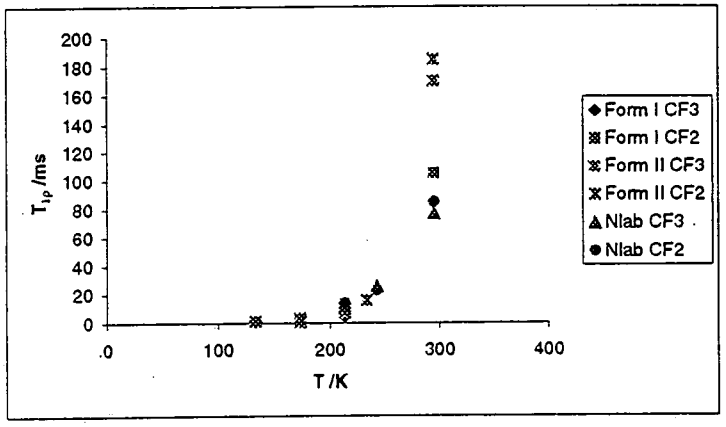

Figure 19 Plot of variation of ^{19}F $T_{1\rho}$ with temperature for the forms of BRL55834.

From the results described it may be concluded that the rate and degree of rotation of the CF_3 groups varies between the forms. This may be ascribed to the different amounts of free space in the crystal structure of each form, with form I having the greatest amount of free space (possibly due to only one molecule existing in the asymmetric unit) and thus the lowest $T_{1\rho}$ and form II being at the other end of the scale (possibly arising from the presence of 3 molecules in the crystallographic asymmetric unit).

4.10.3 Powder XRD of the labelled sample

Powder X-ray data were collected for [^{15}N]BRL55834 and compared with those for forms I and II. (Andres Goeta, Durham PXRD group). The traces for the three samples certainly seem to be different indicating that a new polymorph has been produced.

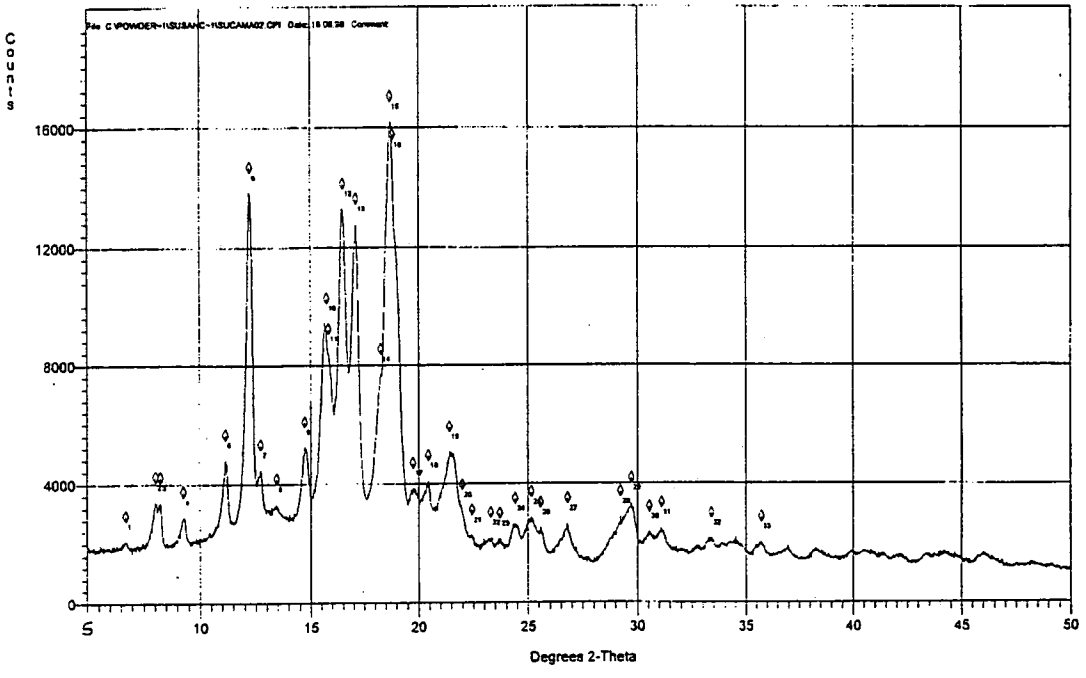

Figure 20 Powder XRD trace for [^{15}N]BRL55834.

4.10.4 Nitrogen-15 NMR studies of the labelled sample

The ^{15}N spectrum exhibits two peaks at room temperature. Due to the large chemical shift anisotropy of the ^{15}N nucleus, it is also possible to observe a spinning sideband manifold

at moderate spinning speeds (see below). The following experiments were carried out in order to try to decipher any differences between the two sites.

A new experimental setup was implemented to facilitate simultaneous ^{1}H and ^{19}F decoupling whilst observing ^{15}N. Double decoupling caused the linewidths to decrease by 21 % (from 14.99 to 11.8 Hz) and 8 %, (from 17.23 to 15.8 Hz) for the less and more intense peak, respectively. This may indicate the closer spatial proximity of the fluorines to one of the ^{15}N sites than to the other.

4.10.4.2 Relaxation and cross polarisation dynamics of the ^{15}N sites.

Variable contact time experiments were carried out with proton-to-nitrogen cross polarisation times incremented from 0.01 ms to 16 ms. The results were fitted in the xy panel of spinsight, and therefore the two nitrogen sites were compared and analysed.

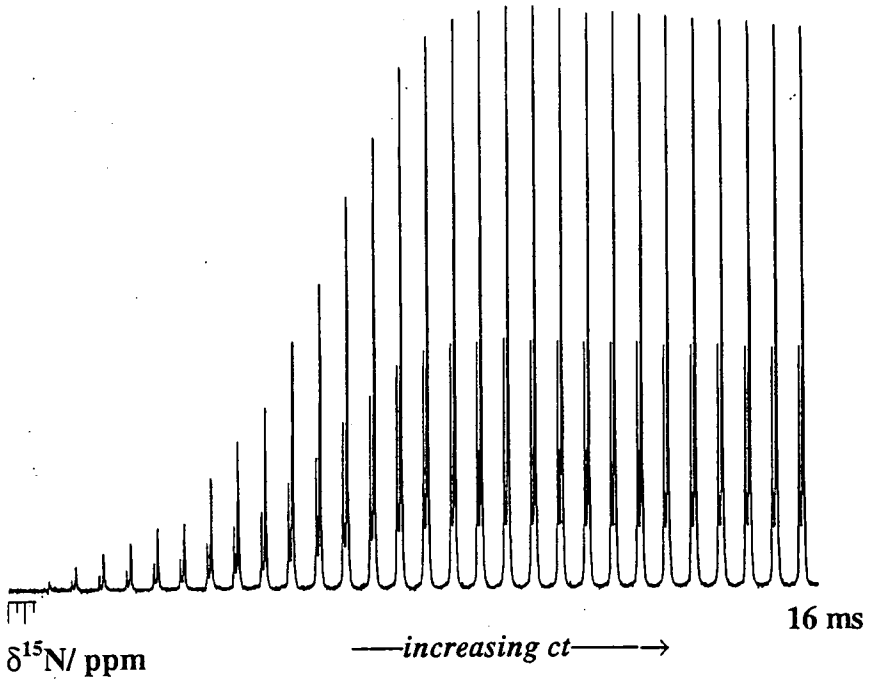

Figure 21 Stacked plot of the variable $^{1}H \rightarrow ^{15}N$ contact time experiment. [^{15}N]BRL55834. (Cpflip, 3 kHz MAS, 12 s rd, 153 ms acqtm, ^{15}N @ 20.283 MHz)

The T_1 relaxation time of the N-15 sites was also determined using the T1xcp pulse sequence. Both sites possess a T_1 of approximately 30 minutes (± 2 minutes) and over all results show that both sites appear to have similar properties.

$\delta_{N\text{-}15}$/ ppm	T_{HN}/ ± 0.1 ms	$T_{1\rho}^{H}$/ ± 3 ms	T_1/ ± 120 s
-254.99	1.4	217	1850
-257.24	1.4	226	1600

Table 9 Summary of CP and relaxation properties of ^{15}N[BRL55834]

A variable dipolar dephasing experiment also showed no difference between the two ^{15}N locations. Extrapolation of the linear decay of the variable contact time experiment to zero, and deconvolution shows an intensity ratio of 1:2 for the high and low frequency peak, respectively.

4.10.4.3 Variable temperature studies of the ^{15}N sites.

On decreasing the temperature (***Figure 21***), spectra infer that the sample undergoes an irreversible transition of some description. This seems to cause the most intense peak to split, and the whole spectrum to become narrower and shifted to lower frequency. Experiments were carried out on the sample, observing a spectrum every 20 minutes during the warm-up period for 24 hours and the sample did not appear to reconvert to its initial state.

A powder XRD trace of the sample that had been subjected to these very low temperature studies showed no obvious changes in the number, position, and intensity of reflections. The ^{13}C CP/MAS spectrum of this same sample was acquired after the low temperature experiments had been carried out and some of the finer splittings previously observed were no longer resolved. For example, the splitting of 0.8 ppm (40 Hz) of the C(14) peak at ~172 ppm is not evident after the low temperature experiments whilst the splitting of the other C(14) peak remains the same, although the relative intensities alter. This may infer that there was previously some sort of disorder in the labelled sample, which had 'fallen out' on going to low temperature.

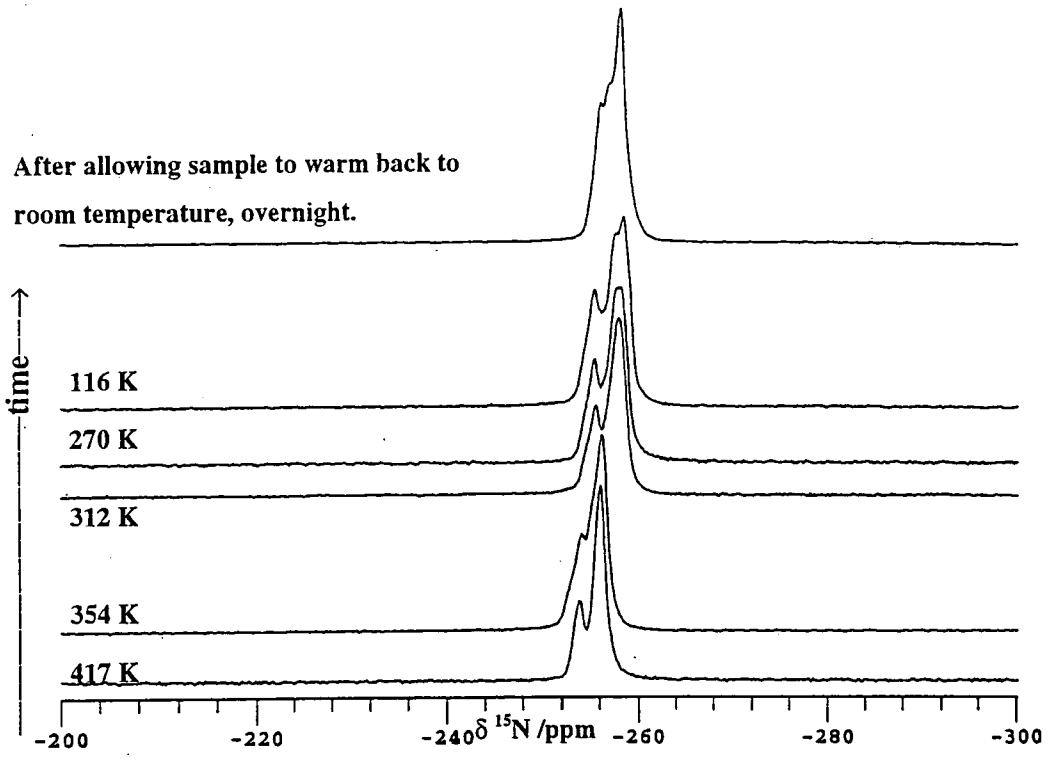

Figure 22 [^{15}N]BRL55834 variable temperature spectra. (MAS 4kHz, Cpflip, 64 transients, 153 ms acqtm, 10.0 ms ct)

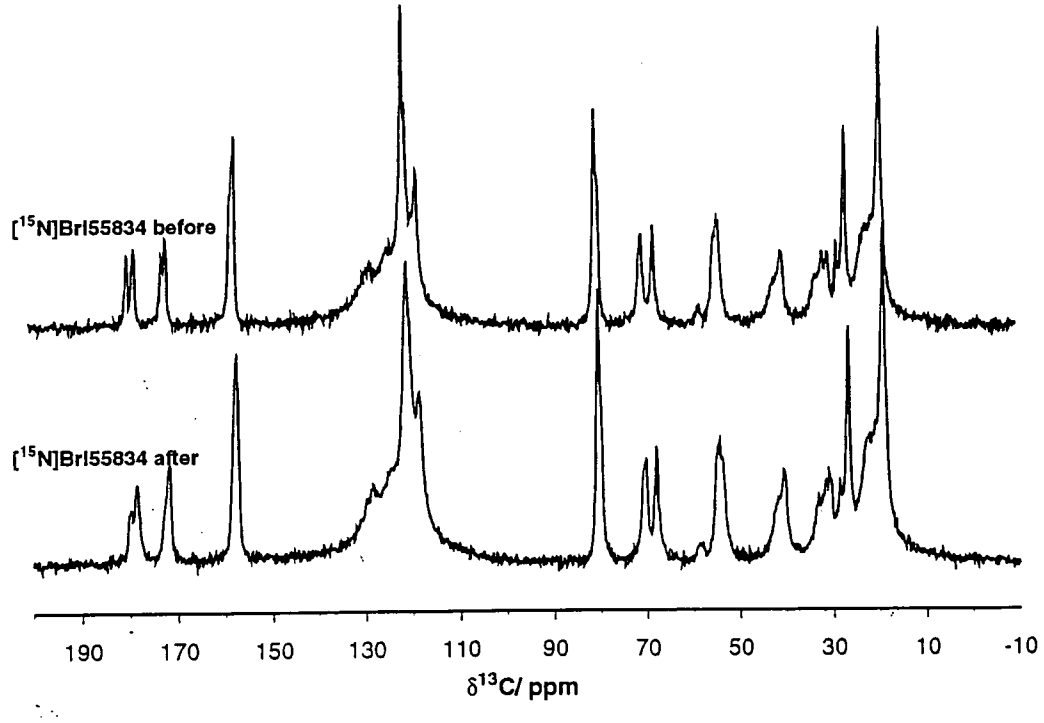

Figure 23 Comparison of $^{1}H \rightarrow ^{13}C$ CP/MAS spectra before and after low temperature was applied (MAS 4.5 kHz, Cpflip, 10 ms ct, 100 ms acqtm, room temp, 3s rd).

4.10.4.4 Variable temperature spinning sideband analysis

Analysis of the spinning sideband manifold gives information about the chemical shift tensor of the ^{15}N nucleus such as the anisotropy and the asymmetry. By calculation and comparison of these factors at various temperatures, subtle alterations in the molecular geometry about the ^{15}N centre may be alluded to. This may assist in the understanding of the precise geometry about the ^{15}N centre, and support RDC modelling work.

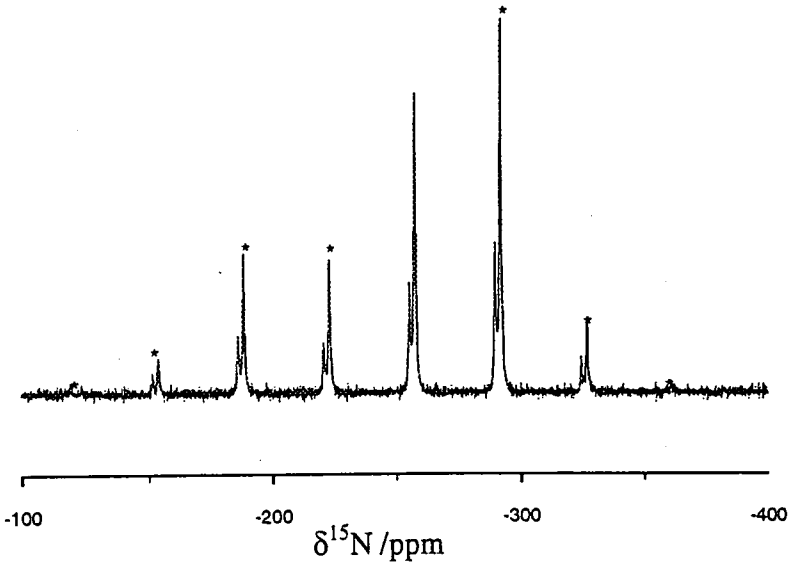

Figure 24 $^{1}H \rightarrow ^{15}N$ CP Spinning sideband manifold of [^{15}N]BRL55834 at room temperature. (700 Hz MAS, Cpflip, 153 ms acqtm, 12 s rd, 128 transients, * = ssb.)

Results of spinning sideband analysis using Durham's ssb97 program showed no definite changes on going to low temperature conditions. Anisotropy values of ζ (where $\zeta=\sigma_{33}-\sigma_{iso}$) –105(±2) and -110(±10) are observed for the peaks at –257.7 and –255.3 ppm, respectively. The asymmetry values for both sites are between 0 and 0.1 i.e. within experimental error the sites have axial symmetry. Whilst this cannot be precisely true, the nitrogen in question is a tertiary amine so all the nearest neighbours are carbon.

4.11 Conclusions

The work that is contained within this chapter has shown the use of solid-state NMR as an effective technique for discerning polymorphs of BRL55834 by their ^{13}C, ^{19}F, ^{15}N and ^{1}H spectra. Carbon-13 spectra have allowed original conclusions to be drawn as to the existence of one and three molecules in the crystallographic asymmetric unit of forms I and II, respectively. This knowledge was not previously available due to the microcrystalline nature of the forms causing there to be no molecular information derived from single-crystal X-ray diffraction data.

Second-order effects transferred from the single ^{14}N site to the resonances of adjacent ^{13}C atoms infer differences in the molecular conformation between the forms. This topic is discussed further in chapter 6.

The sheer number of resonances in the ^{13}C CP/MAS spectra of BRL55834, especially that of form II, due to the crystallographic splittings, has required the development of precise experimental setup procedures, and has provided the driving force for the application and development of resolution enhancement techniques. TPPM decoupling on the proton channel and operation at a higher magnetic field have improved the resolution of the ^{13}C CP/MAS spectra. Novel triple-channel work allowing simultaneous ^{1}H and ^{19}F decoupling has also improved the resolution, not least by the ability to cross polarise from the abundant ^{19}F nuclei, which has been valuable in establishing assignments of the ^{13}C CP/MAS spectra in the complex region around 120 ppm. Spectral editing techniques have also been usefully applied to aid the assignment of the ^{13}C CP/MAS spectra.

The solid-state NMR results have reinforced data obtained by other techniques. The crystallographic splitting of peaks in the fingerprint region of the IR spectra of form II (see chapter 3) suggested the existence of more than one molecule in the asymmetric unit. Of course, solid-state NMR results quantify this number as three, and initial attempts at deriving crystal structure information using Genetic Algorithm techniques appear to confirm this theory.

During the method development for the chemometric analysis of mixtures of BRL55834 polymorphs using Raman spectroscopy (described in chapter 3), the region of the Raman spectra that shows the greatest difference between the forms was identified. This was assigned to C-F stretching (1400-1200 cm^{-1}). Although the ^{19}F solid-state NMR spectra of the two polymorphs appear relatively similar, values of $T_{1\rho}{}^{F}$ and variable-temperature experiments allude to varying rates of mobility of the CF_3 groups between the forms, with the rate of motion in form I predicted to be greater than that in form II. This observation is consistent with the expected variation of the amount of free space within the structure of each form corresponding with the different number of molecules in the crystallographic asymmetric units.

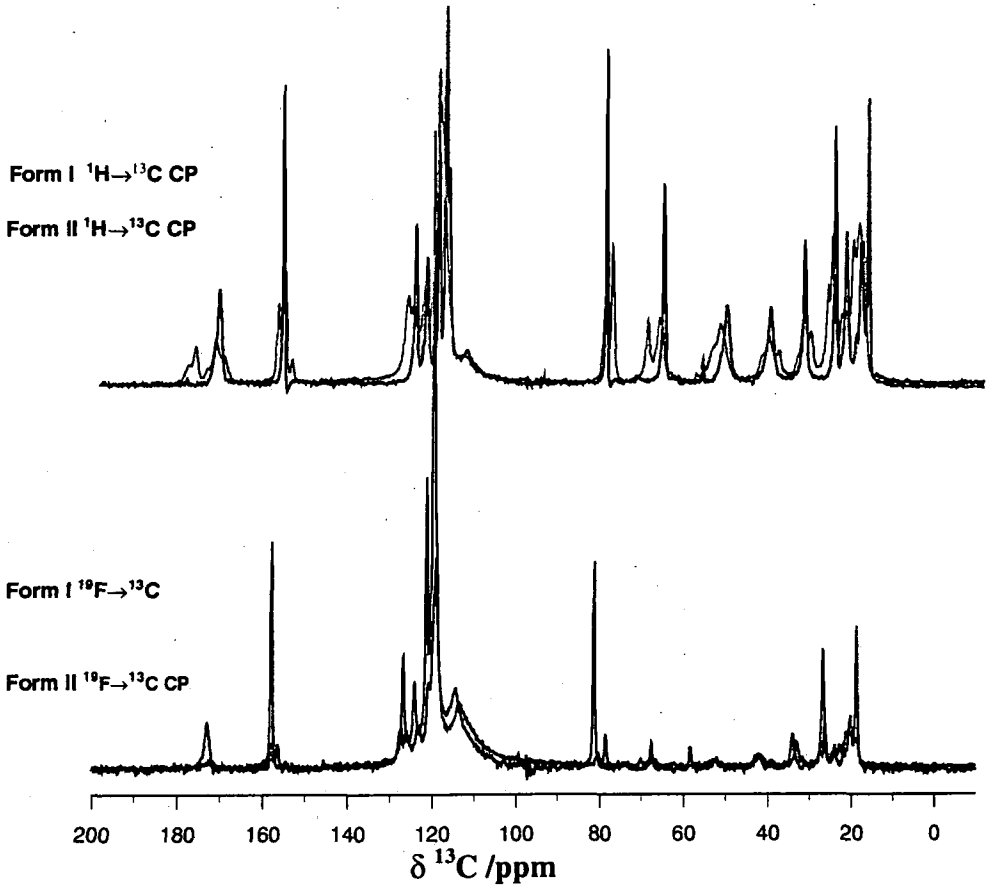

Figure 25 Overlapped ^{13}C spectra of forms I and II with {^{1}H} and {^{19}F}. (MAS 5 kHz, uscp2dec, 2884 transients, 10 ms ct, acqtm 75 ms, 3 s rd).

Overlaying the high-resolution, triple-channel spectra may raise the question as to whether in fact form II contains molecules of the conformation of form I as one of its

three inequivalent components (see ***Figure 25***). However, this is unlikely, since no asymmetric doublets are visible in the form I spectra and each of the three components of form II (see C(14) peaks around 174 ppm) show this characteristic, indicating that the molecular conformation of the inequivalent molecules in form II all are of different conformation to that in form I. By performing a subtraction of the spectra, it is also possible to observe that the chemical shifts in the ^{13}C spectra of form I do not directly relate to those of form II.

Comparison of the ^{15}N CP/MAS NMR spectra of the nitrogen site in forms I and II gives results that are still difficult to explain structurally. A novel $^{1}H \rightarrow ^{15}N$ triple-channel experiment with simultaneous ^{19}F and ^{1}H decoupling has not suggested interactions between the nitrogen and fluorine sites. Rather than shedding light on the matter, the enrichment of the ^{15}N site has complicated the issue by producing a sample that appears to be a new polymorph of BRL55834! This conclusion has been based upon PXRD data, combined with the ^{13}C, ^{15}N and ^{19}F NMR spectra, which show extra splittings, irreversible variable-temperature behaviour and differing ^{19}F relaxation times.

Areas that I would like to see developed in the future include the double labelling of form II of BRL55834 at the nitrogen location and ^{13}C sites on the fused benzopyran core. This would enable measurement of internuclear distances, leading to an understanding of the relative conformation of the piperidinone ring with respect to the benzopyran system. Double enrichment would also allow application of the ^{13}C, ^{15}N heteronuclear correlation experiment which I have devised (scchnhetcor). Separation of the ^{13}C resonances of the three molecules in the asymmetric unit along the second dimension of a 2-D heteronuclear correlation experiment may also lead to an understanding of the origin and inter-relationship of the multiple peaks in the natural abundance ^{15}N spectrum of form II. Preliminary work on the 600 MHz spectrometer at Warwick University has also shown the potential for resolution enhancement of the ^{13}C CP/MAS spectra of these polymorphs.

4.12 References

1 D. M. Doddrell, D. T. Pegg, M. R. Bendall, *J. Magn. Reson.* **48,** 323-327, 1982.

2 C. J. Turner, 'Heteronuclear Assignment Techniques', *Encyclopedia of NMR*, Eds. D. M. Grant, and R. K. Harris, Wiley, **4**, 2535, 1996.

3 '*Basic One and Two Dimensional NMR Spectroscopy*', H. Friebolin, VCH 238, 1993.

4 A. Bax, R. H. Griffey, B. L. Hawkins, *J. Am. Chem. Soc.*, **105,** 7188-7190, 1983.

5 J.E.Heritage, N.Soffe, I.O.Campbell, T.J.Norwood, J.Boyd, *J. Magn. Reson.* **87** 488, 1990.

6 A.Bax, M.Ikra, L.E.Kay, D.A.Torchia, R.Tschudin, *J. Magn. Reson.*, **86**, 304, 1990.

7 J. K. M. Sanders and S. K. Hunter, *'Modern NMR spectroscopy – A guide for chemists'*, Oxford University Press, 1987.

8 S. A. Carss, Ph.D. Thesis, Durham University, 1995.

9 I. A. Whitcombe, Roche Pharmaceuticals, personal communication, March 1998.

Chapter 5

BRL61063 – A nitrogen-rich compound

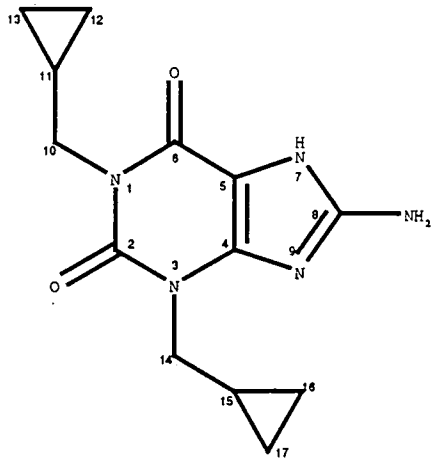

5.1 Introduction

The molecular structure of 1,3-di-(cyclopropylmethyl)-8-aminoxanthine (BRL61063) was confirmed initially by SmithKline Beecham, using a variety of techniques. The salient points are summarised in ***Table 1,*** which includes solution-state NMR information. This chapter outlines the result of solid-state NMR studies of various polymorphs of BRL61063.

Feature	Confirmation technique
Molecular formula	**Elemental analysis** **Mass spectrometry** – molecular ion and fragmentation pattern
Absolute **stereochemistry**	Single-crystal **X-ray diffraction** on the three polymorphs
Presence of **NH_2 amino** group	Single-crystal **X-ray diffraction** **IR**: 670-830, 1263, 3301, 3455 cm^{-1}. 1263 cm^{-1} band indicates this is a primary aryl amine (nujol mull) **NMR:** exchangeable proton resonance at 6.50 ppm
Presence of **NH** functionality	**IR**: absorption at 3145 cm^{-1} (nujol mull) **NMR:** exchangeable proton resonance at 11.31 ppm
Existence of a **xanthine ring** and **ring amide carbonyl** groups	**IR**: 1534, 1636, 1689 cm^{-1} with the 1636 ,and 1689 absorptions indicative of ring-amide carbonyls (nujol mull)
Position and presence of **cyclopropyl** sidechains	**IR**: 756, 1018 cm^{-1} (nujol mull) **^{1}H NMR**: multiplets at 0.29-0.48 ppm and 1.12-1.31 ppm indicate cyclopropyl ring protons. Doublets at 3.73 and 3.78 ppm are consistent with the NCH_2 methylene protons. **^{13}C NMR**: 44.1, 44.7 ppm – carbons adjacent to nitrogen. Long-range ^{13}C-^1H couplings confirm position on N(1) and N(3).

Table 1 Summary of the structure determination of BRL61063

5.2 Solution-state NMR results

5.2.1 ^{1}H NMR

Solution-state proton NMR results are consistent with the structure of BRL61063. The xanthine NH and 8-NH_2 functionalities are confirmed by the exchangeable proton resonances at 11.31 and 6.50 ppm respectively. The remaining proton resonances support the presence of two cyclopropyl sidechains, as is highlighted in ***Table 2***, below.

Assignment	Shift / ppm	No. of protons	Description
12, 13, 16, 17	0.29- 0.48	8	Multiplet
11, 15	1.12- 1.31	2	Multiplet
10, 14	3.73 3.78	2 2	Doublet, ^{3}J=7.2 Hz Doublet, ^{3}J=6.9 Hz
8-NH_2	6.50	2	Broad singlet
NH	11.31	1	Broad singlet

Table 2 Proton chemical shifts and assignments of BRL61063 (solvent DMSO-d6)

The solution-state NMR proton spectra (***Figures 1*** and ***2***) have been run (SmithKline Beecham) in DMSO-d6, and in DMSO-d6/D_2O. In the spectrum with the sample dissolved in DMSO-d6/D_2O, the signal at 11.31 ppm is absent. Furthermore, the NH_2 signal is greatly reduced in intensity. This is because these protons have been exchanged and mostly appear as part of the HOD signal at 3.62 ppm.

The peak at ~3.4 ppm in ***Figure 1*** is due to water protons in the DMSO and the peak at ~2.55 ppm is due to partially deuterated solvent.

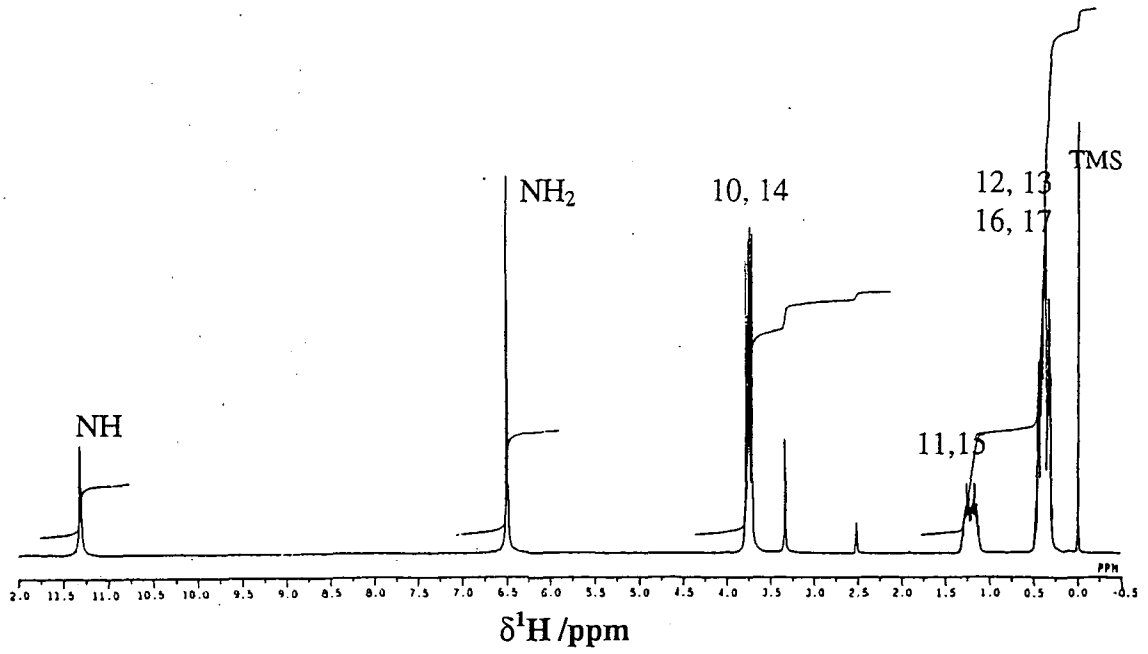

Figure 1 ^1H NMR spectrum of BRL61063 (270 MHz solvent DMSO-d6, 0.1 s rd, 400 transients) (SB)

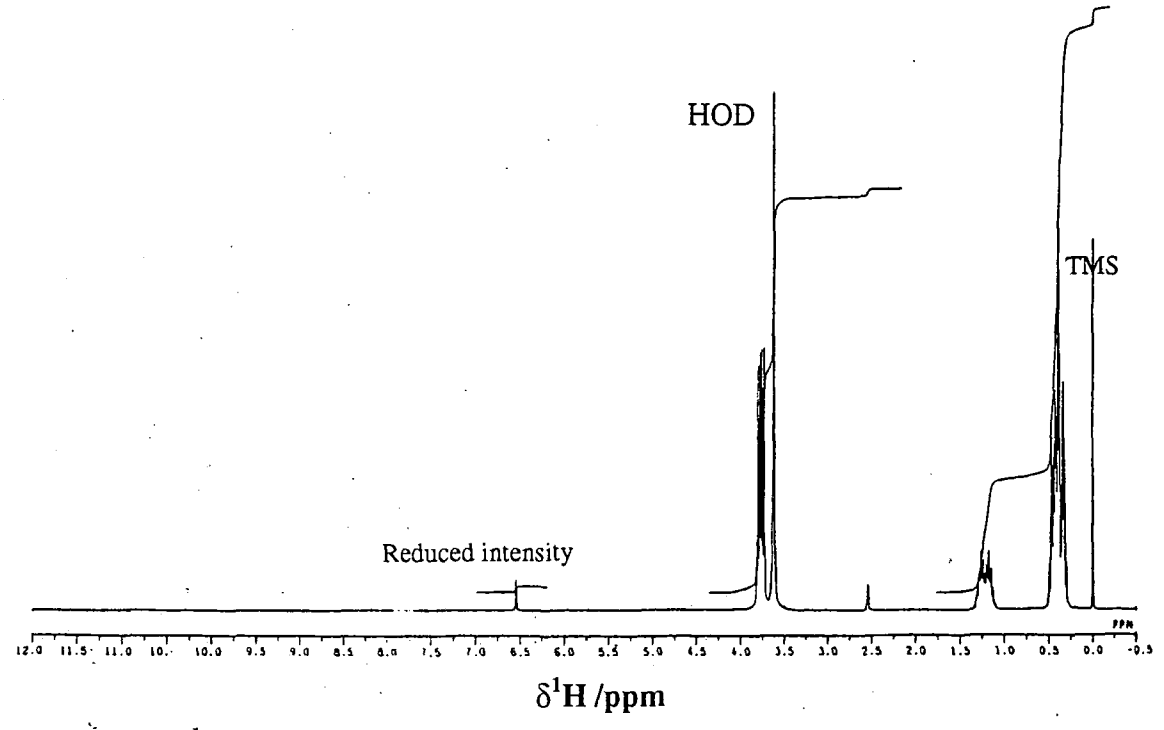

Figure 2 ^1H NMR spectrum of BRL61063 (270 MHz, DMSO-d6/ D_2O, 0.1 s rd, 400 transients) (SB)

5.2.2 ^{13}C NMR

The 67.8 MHz ^{13}C proton-noise-decoupled and DEPT-135 spectra are shown in ***Figure 3*** and the chemical shifts and assignments are summarised in ***Table 3***. Quaternary carbons were assigned on the basis of their chemical shifts and their long-range carbon-proton couplings.

Assignment		Solution-state δ^{13}C/ppm
12,13,16,17	CH_2	3.4, 3.5
11,15	CH	10.0, 10.3
10,14	CH_2	44.3, 47.1
5	N-C-C=O	101.3
4	N\ C=C N/	149.3
2	N\ C=O N/	151.1
6	N\ C=O C/	152.3
8	N\ C-NH_2 N//	154.8

Table 3 BRL61063, ^{13}C chemical shifts, and assignments (DMSO-d6)

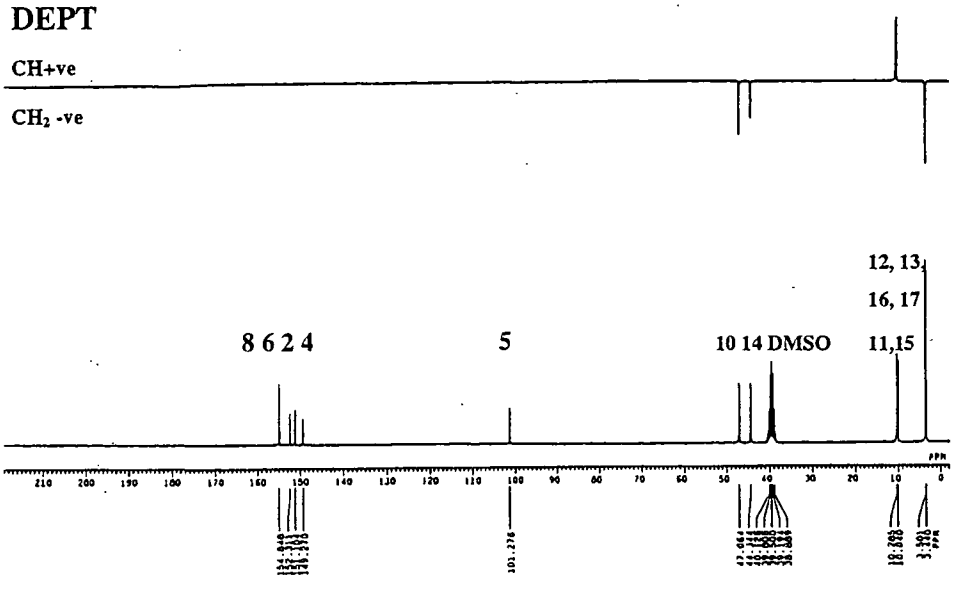

Figure 3 ^{13}C solution-state NMR spectrum (Solvent DMSO-d6, 67.80 MHz, 2000 transients, 1.5 s rd, 0.963 s acqtm) (SB).

5.2.4 ^{15}N NMR.

A solution-state natural abundance ^{15}N NMR spectrum (***Figure 4***) of BRL61063, dissolved in DMSO-d6 was acquired in Durham.

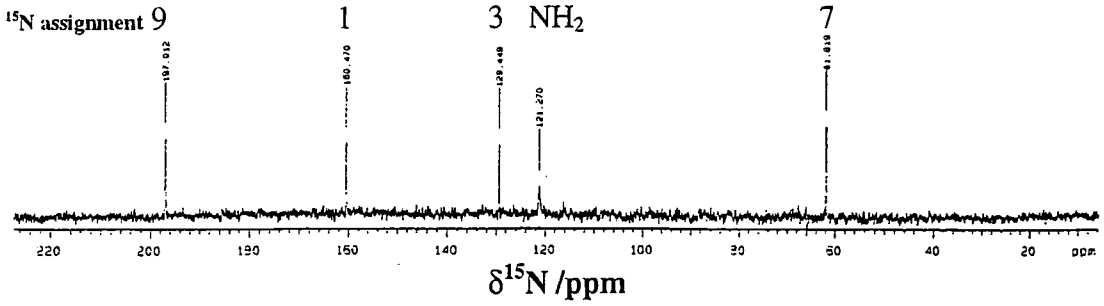

Figure 4 ^{15}N natural abundance solution-state NMR spectrum (40.532 MHz, DMSO, 1327 transients, 10 s rd, 0.998 s acqtm).

(δ ^{15}N/ ppm)	Assignment
197.01	9
160.47	1
129.45	3
121.27 (broad)	NH_2
61.82	7

Table 4 ^{15}N chemical shifts and their assignments (solvent DMSO-d6)

The resonances were assigned by comparison with the literature[1,2,3]. The resonance at 127 ppm is very broad in comparison to the other peaks. Tautomerism or the formation of NH_3^+ may cause this to occur.

5.3 ^{13}C Solid-state NMR assignment

This chapter will detail the results of experiments that have been carried out on the four polymorphs that have been introduced in chapter 3: forms 1, 2, 'D' and 'yellow'. The majority of experiments have been applied to forms 1 and 2, as these are standard batches supplied from SmithKline Beecham Pharmaceuticals and were available at the start, before recrystallisation studies revealed the other two polymorphs, form D and 'yellow'.

5.3.1 ^{13}C CP/MAS spectral acquisition and resolution enhancement (TPPM).

Parameters were optimised using the cpflip pulse sequence. The recycle delay (9 s) was optimised by measurement of the average proton T_1 values using the T1hcp pulse sequence (values for forms 1 and 2 are 2.60 ± 0.2 s). Contact times (1 ms) were optimised using variable contact time experiments. A standard MAS rate of 4 kHz was used, with an acquisition time of 51 ms, and 200 transients.

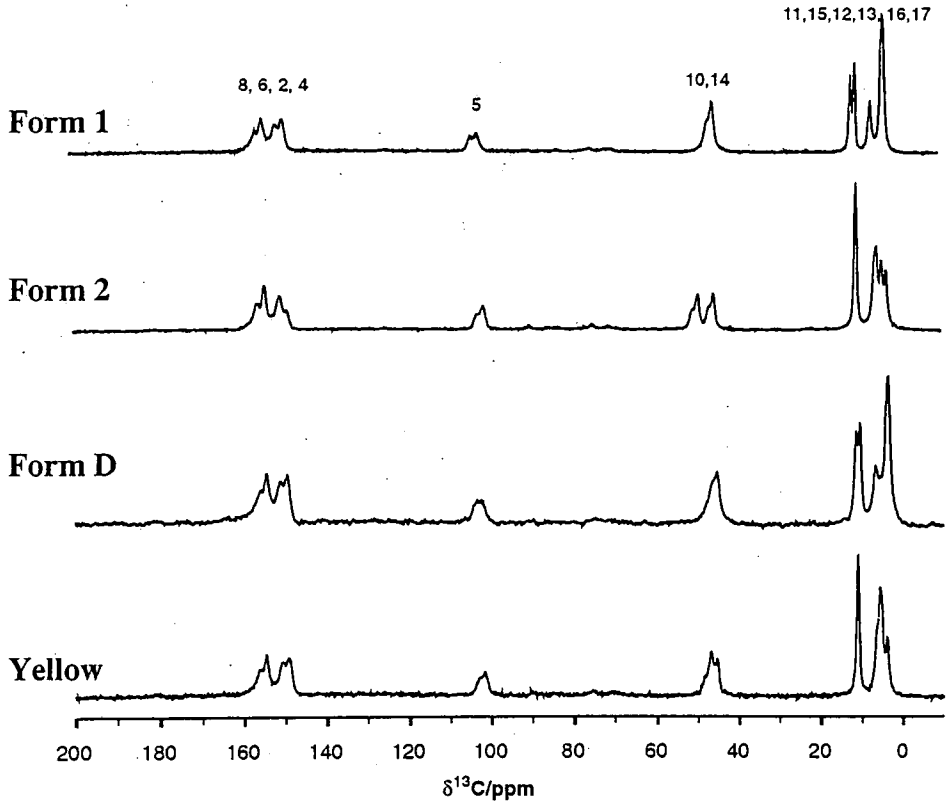

Figure 5 ^{13}C CP/MAS spectra of BRL61063 polymorphs (cp4_pm, 200 transients, 51 ms acqtm, 1.0 ms ct, 9 s rd, MAS rate 4 kHz)

The room temperature $^{1}H \rightarrow ^{13}C$ CP spectra are shown in ***Figure 5***. These spectra show several differences. That of form 2 contains two separate peaks for the C(14) and C(10) sites as opposed to the single resonance observed for the other forms. Asymmetric splittings of peaks assigned to C(8), (6), (2), (4), (5), (10) and (14) are clearly due to residual dipolar coupling (RDC) interactions with adjacent ^{14}N nuclei. This is discussed in detail in chapter 6. The splittings of resonances of C-N carbons were confirmed to be

arising from RDC interactions by observation of the spectra obtained at higher magnetic field. (Varian Unity Plus 300 MHz spectrometer), which showed reduced splittings and narrower peaks (see chapter 6).

The chemical shifts and relative intensities of the protonated carbon peaks below 20 ppm show variations between the spectra of the different polymorphs. This alludes to differences in relative orientation of the pendant cyclopropyl groups at room temperatures. These have been shown to exist by single crystal XRD for forms 1, 2 and 4 (see chapter 3).

TPPM decoupling on the proton channel is necessary to resolve individual protonated carbon resonances for the ^{13}C spectrum of form 2. Comparative spectra are shown in ***Figure 6***, below.

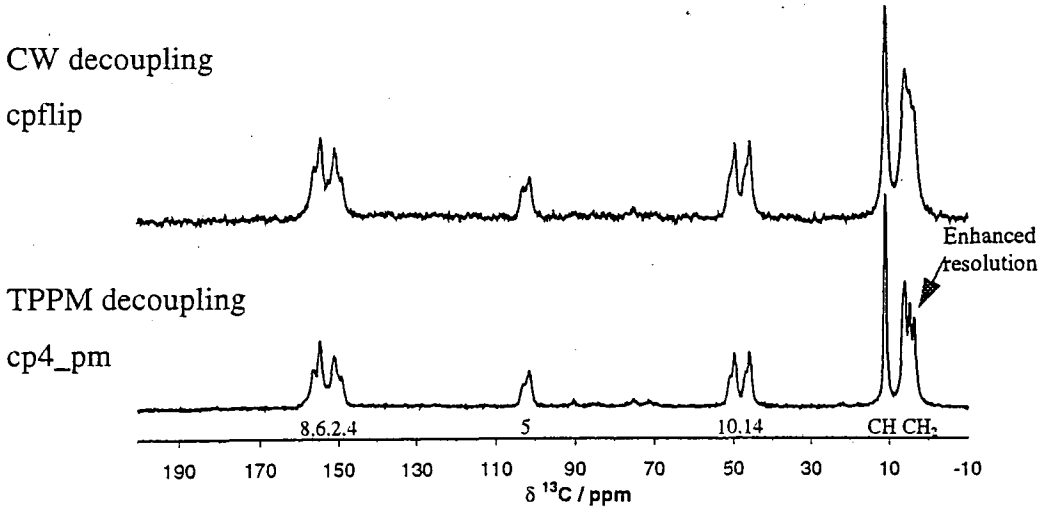

Figure 6 Improvements in the spectra of BRL61063 form 2 for CH groups on application of TPPM decoupling on protons (MAS 4 kHz, 200 transients, 51 ms acqtm, 1.0 ms ct, 9 s rd, MAS rate 4 kHz)

5.3.2 Comparison of solid- and solution-state NMR spectra.

A comparison of the ^{13}C chemical shifts with those observed in the solution state was made in order to assign the spectra in the solid state. As may be observed in ***Table 5***,

direct comparison of the solid and solution-state spectra is possible for all four polymorphs. There are no large solid-solution chemical shift differences. Asymmetric doublets exist for carbons that are bonded to ^{14}N (see chapter 6 for further discussion).

^{13}C Assignment		Solution state $\delta^{13}C$/ ppm	Solid state $\delta^{13}C$ / (± 0.2) ppm			
			Form 1	Form 2	Form D	'yellow'
12,13, 16,17	CH_2	3.4, 3.5	3.6, 6.5	3.5, 4.6, 5.9, 6.3	2.4, 3.9, 4.4, 5.3	3.6, 5.6, 6.2
11,15	CH	10.0, 10.3	10.3, 11.3	11.0	9.2, 10.2	11.1
10,14[⊗]	CH_2	44.3, 47.1	45.7	46.3, 50.1	44.9	45.4, 47.1, 48.3
5[⊗]	N-C-C=O	101.3	102.9	102.2	102.5	102.2
4	N\ C=C N/	149.3	149.6	149.3	149.3	149.3
2	N\ C=O N/	151.1	151.3, 152.9	151.1, 152.7	150.9	150.7
6	N\ C=O C/	152.3	154.5	154.7	154.4	154.8
8	N\ C-NH_2 N//	154.8	156.1	156.4	155.8	156.2
[⊗] Weighted mean position for C-N carbons exhibiting asymmetric doublets is given.						

Table 5 Comparison of solid- and solution-state ^{13}C NMR spectra.

An interesting point to note is the existence of two peaks for carbon sites (10) and (14) in the ambient solid-state ^{13}C spectra of form 2 (46.3 and 50.1 ppm). This is also true in the solution-state ^{13}C spectrum, which shows two peaks (at 44.3 and 47.1 ppm), indicating that the conformation adopted by form 2 of BRL61063 is similar to that in the solution state (see section 5.2.2). The presence of only one band for these two carbons of form 1 indicates that the two sites are rendered equivalent (or nearly so, at least) on the NMR timescale.

5.3.3 Proton spectra

Proton broadband spectra were run of the four polymorphs. Using the same conditions and parameters resulted in the spectra appearing very different. The proton spectrum of

form 1 appears very broad, whereas in forms 2, D and 'yellow' there are varying numbers of very definite, sharp peaks superimposed upon the broad baseline.

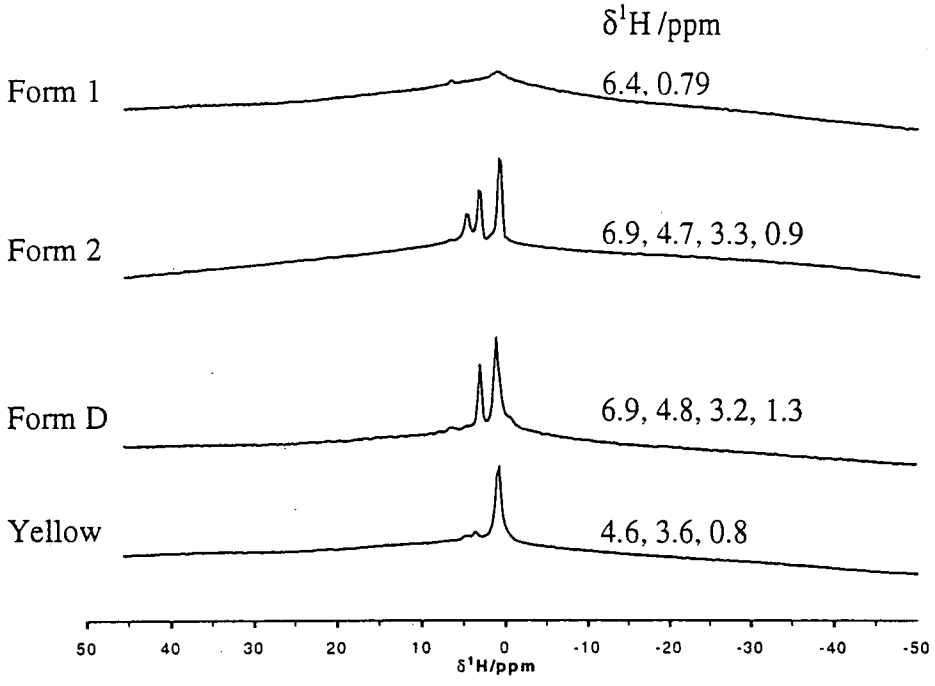

Figure 7 Proton broadband spectra of the polymorphs (1pulse, MAS 4 kHz, 9 s rd, 10.241 ms acqtm, 64 transients).

No hydrogen-bonded peaks (above 10 ppm) are evident from the solid-state results. Sharp peaks are often associated with mobile components in a sample. The possibility of inclusion of solvents in the solid structure was ruled out by DSC measurements, which show completely straight profiles with a heating rate of 10 °C per minute over the temperature range -100 to +199.4 °C. This therefore does not indicate the loss of any solvent. The most likely cause of sharp proton lines is the presence of mobile components in the samples, although the cause in these cases remains unexplained.

5.3.3.1 Proton CRAMP spectra

The proton CRAMPS spectra of forms 1 and 2 provided no extra information and showed negligible differences between the two polymorphs. No peaks indicating hydrogen bonding were observable. Spectra showed only two peaks at 1.6 ppm and 5.0 ppm for form 1 and 1.6 ppm and 4.9 ppm for form 2.

5.3.3 Spectral editing techniques

The final assignments of the ^{13}C CP/MAS spectra are summarised in ***Table 5***. However, these results have been analysed further by application of several spectral editing techniques. This has mainly involved a study of the characteristics of form 1 versus those of form 2.

5.3.3.1 Non quaternary suppression (NQS)

The ^{13}C NQS spectra for the four polymorphs are shown in ***Figure 8***. Insertion of a 50 μs delay (tau) before application of proton decoupling should leave only the quaternary and methyl carbon resonances (see chapter 2) in the ^{13}C spectrum.

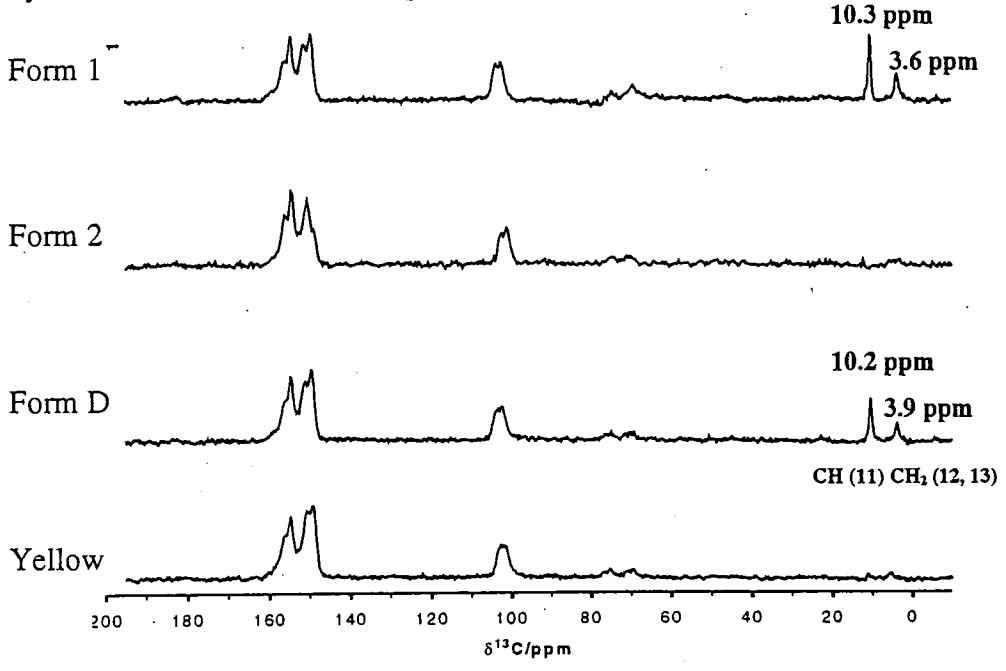

Figure 8 Comparison of NQS experiments of the polymorphs of BRL61063 (MAS 4 kHz, tau 50 us, 50 ms acqtm, 9 s rd, 1 ms ct, 200 transients, ambient temperature).

The interesting result of applying this technique to the polymorphs of BRL61063 is the fact that for forms 1 and D, signals for protonated carbons remain after the dephasing time. This infers the existence of mobility in the pendant cyclopropyl groups. This result

therefore supports the single-crystal X-ray diffraction work, where disorder caused by conformational flexing of the pendant cyclopropyl group containing C(12) and (13) has been proposed. This mobility has the effect of partially averaging the proton-carbon dipolar interactions such that the ^{13}C signal does not dephase as would be expected for rigid protonated ^{13}C resonances.

Therefore the assignment of the ^{13}C CP/MAS spectra of BRL61063 form 1 has been assisted and it is now possible to predict that those peaks remaining after the dephasing time may be assigned to CH(11) at 10.3 ppm and CH_2(12) and (13) at 3.6 ppm i.e. to the cyclopropyl group shown by XRD to be disordered. Since no crystal XRD data exist for form D, the resonances that remain after the dephasing time (at 10.2 and 3.9 ppm) have been assigned to CH (11) or (15) and CH_2 (12) and (13), or (16), and (17), respectively. This result leads to the conclusion that the pendant cyclopropyl groups in form D also exhibit mobility with similar characteristics to that observed for form 1.

5.3.3.2 ^{13}C-^{1}H WISE

WISE experiments were repeated several times for form 1 and 2 to investigate whether the sharp proton lines may be assigned to specific carbon sites. Despite many attempts, it was not possible to correlate these sharp proton lines. This may be due to the mobile carbon components possessing extremely low CP efficiency from protons.

On comparison of the two 2-dimensional stacked plots (see ***Figure 9*** and ***Figure 10***), it is possible to observe that the linewidths in the proton dimension for form 2 are much broader than those for the CH groups in form 1. This may be ascribed to the mobility of the pendant cyclopropyl groups of form 1 causing averaging of the proton-carbon dipolar interactions. In form 2 the CH_2 and CH groups may be assumed to be rigid at room temperature. A comparison of some slices through the second dimension (proton lineshapes) for specific carbon sites is shown in ***Figure 11***.

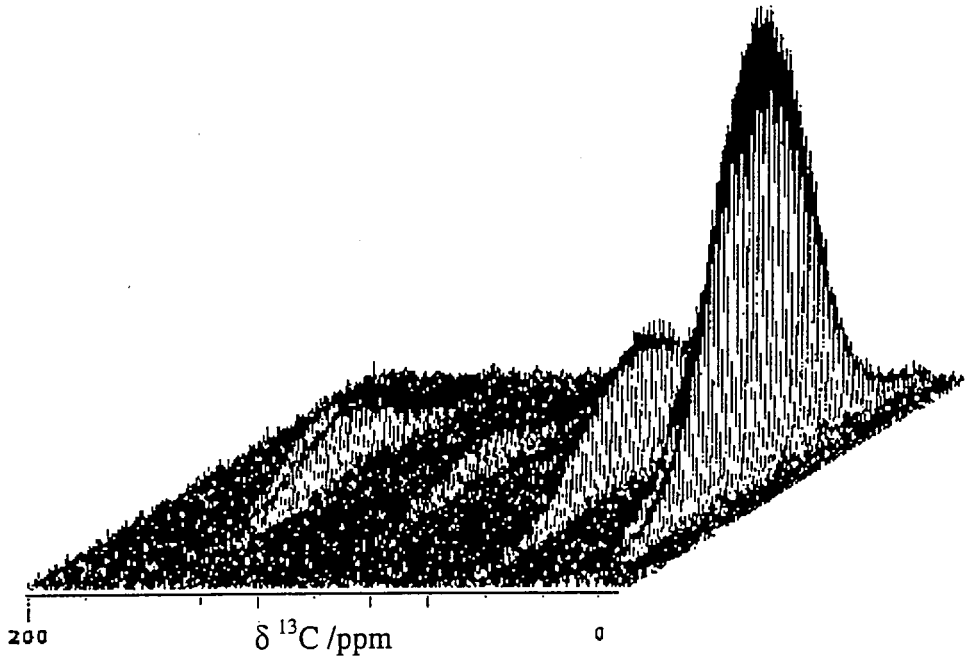

Figure 9 WISE form 1 (MAS 4 kHz, 9 s rd, 51 ms acqtm, 0.5 ms ct, 5μs dwt1, 100 transients)

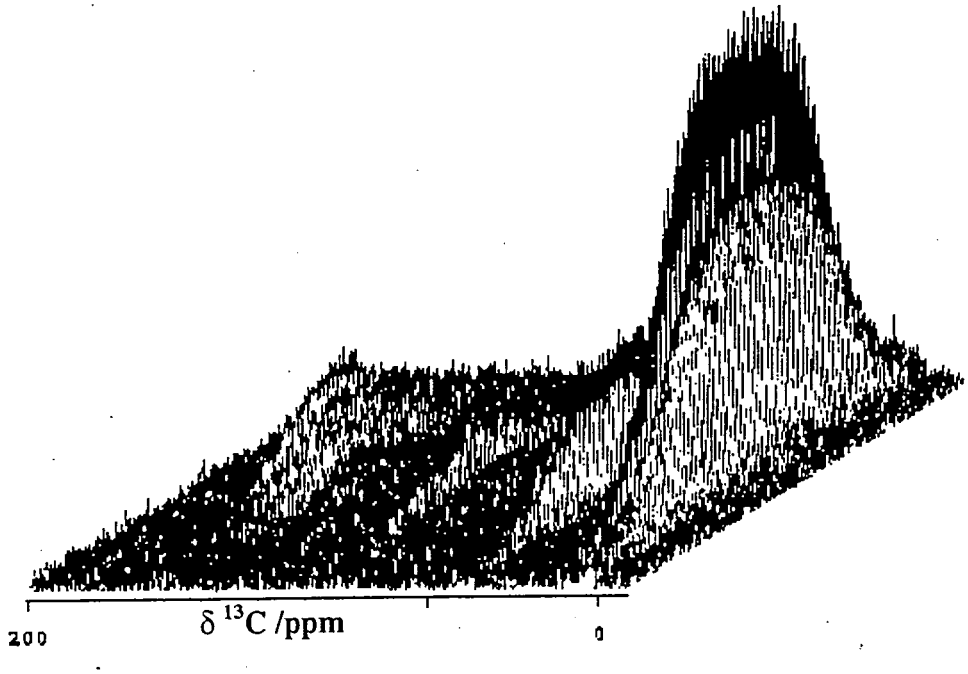

Figure 10 WISE form 2 (MAS 4 kHz, 9 s rd, 51 ms acqtm, 0.5 ms ct, 5μs dwt1, 100 transients)

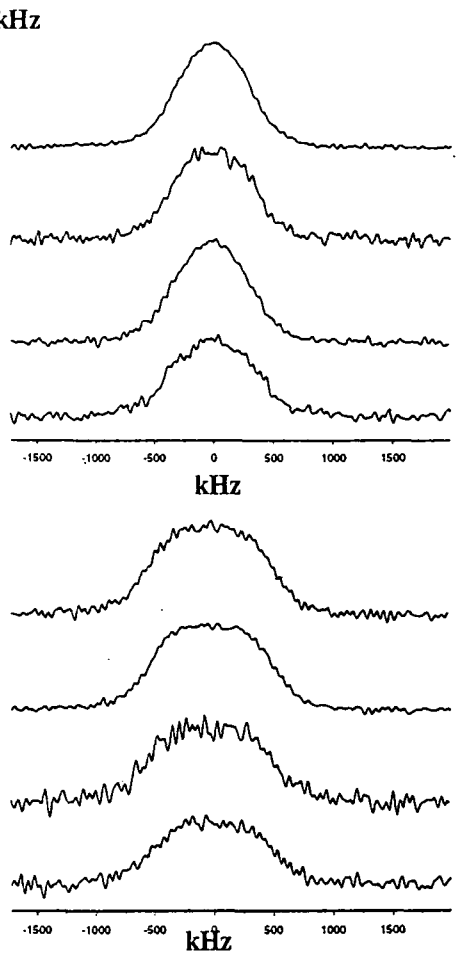

Figure 11 Slices through the proton dimension of the WISE plots for forms 1 and 2

5.3.3.3 Variable dipolar dephasing and Separated Local Field (SLF) experiments

The variable dipolar dephasing experiment has been used to distinguish between the protonated and non-protonated carbons. Therefore, the typical spectrum will contain only ^{13}C weakly coupled to protons, i.e. quaternary carbons and mobile groups such as methyls. Strongly coupled carbons are dephased during the dephasing window in which the spins evolve under the heteronuclear dipolar interactions. A 180 ° pulse is also applied to the S spins at an integer number of rotor periods, in order to remove magnetic field inhomogeneities and frequency-dependent phase shifts.

In order to obtain the results that are shown in ***Figure 12*** and ***Figure 13***, the length of the dephasing window was incremented in equal values up to a maximum of 313 μs. A

rotational echo is observed at integer values of the echo time, where the echo time is equal to the inverse of the spinning speed (250 μs).

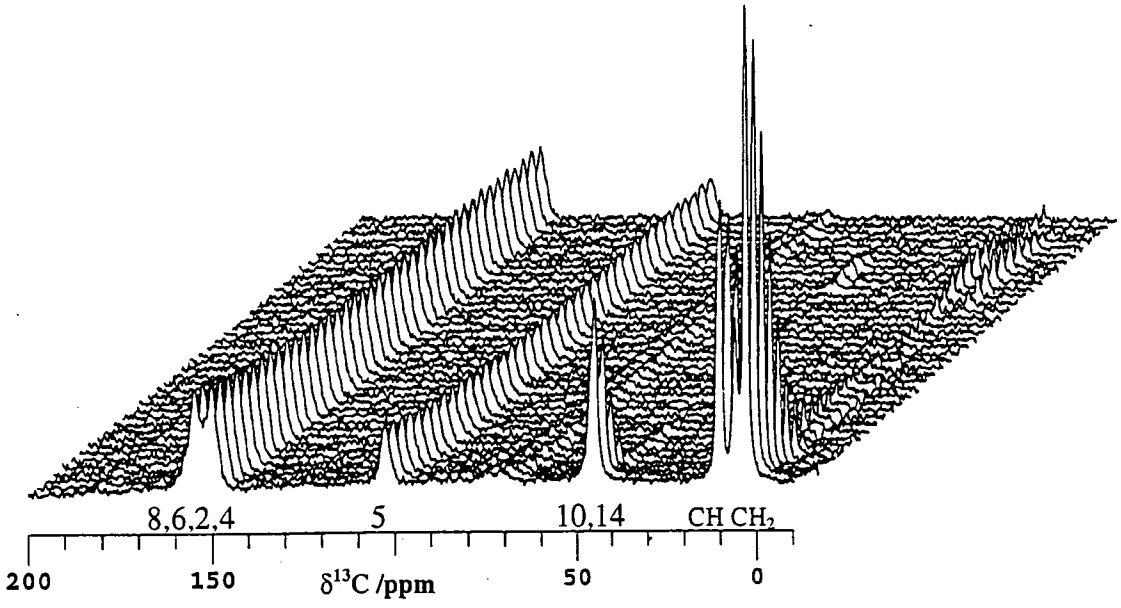

Figure 12 Variable dipolar dephasing experiment with rotational echo. BRL61063 form 1 tau incremented from 1 to 313 μs, in 40 steps of 8μs (50.329 MHz, MAS 4 kHz, 9 s rd, 51 ms acqtm, 180 transients).

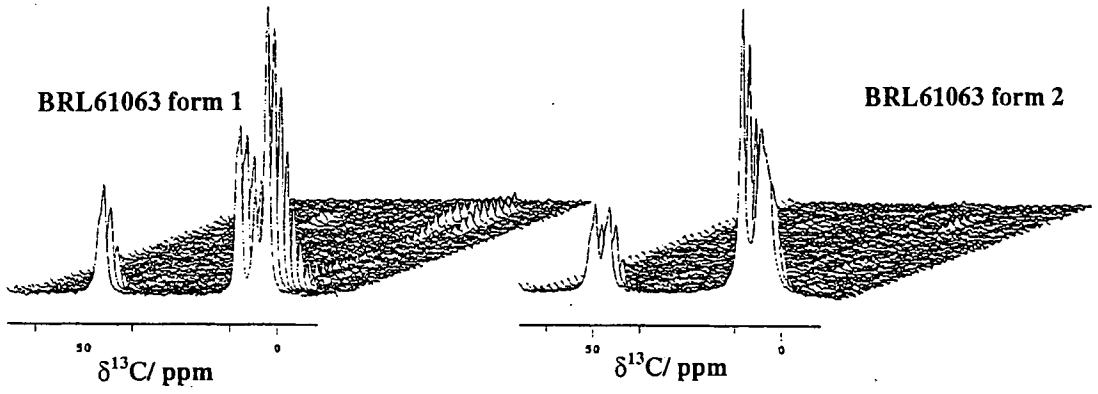

Figure 13 Comparison of aliphatic region of the ^{13}C spectra variable dipolar dephasing spectra showing differences between BRL61603 form 1 and 2 (tau incremented from 1 to 313 μs, in 40 steps of 8μs 50.329 MHz, MAS 4 kHz, 9 s rd, 51 ms acqtm, 180 transients).

The stacked plot in ***Figure 12*** shows the contrasting behaviour of the quaternary and protonated carbon sites. The quaternary carbon resonances do not dephase within the timescale of this experiment, since their large distance from ^{1}H sites cause their ^{1}H, ^{13}C dipolar coupling interactions to be weak. It should be noted that the quaternary resonance at 155 ppm is obscured at high values of tau due to the orientation of the 2-dimensional plot. The protonated carbon sites dephase rapidly in oscillatory manner and are inverted at certain dephasing times due to their ^{1}H, ^{13}C heteronuclear dipolar coupling interactions.

Figure 12 and ***Figure 13*** show a comparison of the variable dipolar dephasing experiments when applied to BRL61063, forms 1 and 2. The part of the spectrum that contains the quaternary resonances has not been included for form 2, since this appears identical in character to form 1. The difference between the two samples is the presence in the spectrum of form 1 of oscillations of the protonated carbon signals.

Oscillations of the ^{13}C resonance are caused because during the dephasing window (tau) the ^{13}C spins evolve under their chemical shifts and heteronuclear dipolar interactions. The chemical shift is refocused at the start of the acquisition time. It may therefore be expected that for an isolated ^{13}C, ^{1}H dipolar-coupled spin pair, a doublet will result in the ^{13}C spectrum due to coupling with a ^{1}H spin that is parallel and antiparallel to B_o. Therefore, in the rotating frame of the ^{13}C spins, half of the ^{13}C spins rotate clockwise and half anticlockwise, which results in a net oscillation of the ^{13}C spin magnetisation. Usually, for a ^{13}C spin in the presence of a large number of ^{1}H spins, this oscillation is not seen because the ^{13}C spin magnetisation is lost to the ^{1}H spin bath. However, for cases in which the ^{1}H, ^{1}H dipolar interaction is weakened by mobility it is possible to observe oscillations in the ^{13}C spectra before the magnetisation is lost to the protons. Rotational echoes are observed at multiples of the rotor period since at this point in time the heteronuclear dipolar interaction becomes refocused.

Therefore, the oscillations that are evident for the protonated sites in form 1 indicate the mobility of the pendant cyclopropyl groups causing a reduction of the effective strength of the dipolar interactions. This supports the results of single crystal XRD (see chapter 3).

The plot for form 2 does show some very small oscillations for the protonated carbon sites, which indicates that thermal flexing may be present in this form at ambient temperatures. This is weakly observed for all protonated sites, with no indication of a greater degree of motion present for any one site.

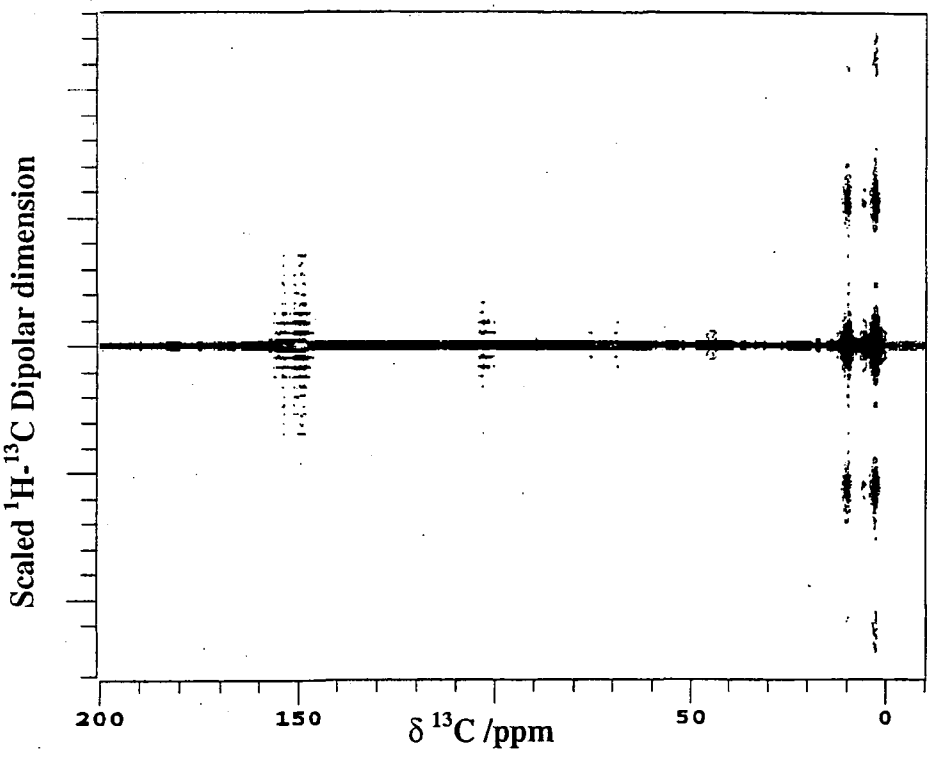

Figure 14 2D plot of SLF results on BRL61063, form 1. (MAS 4 kHz, scslf3w, 50.329 MHz, 102 ms acqtm, 1 ms ct, 9 s rd, 80 transients, WAHUHA cycle time 17.2 μs, States2d processing macro).

The separated local field technique makes use of the fact that the heteronuclear coupling between isolated ^{13}C spins and nearby protons, with decoupling of the ^{1}H-^{1}H interactions can be related to the molecular structure. This occurs since the heteronuclear dipole coupling is sensitive to the distances between the interacting nuclei as well as to the number and arrangement of protons coupling to the carbon considered.

The SLF technique was developed in its application to form 1 of BRL61063 by incorporation of M-REV8 and WAHUHA homonuclear decoupling sequences in the

dephasing window. The larger spectral width in the second dimension (33.5 kHz) provided by the WAHUHA sequence caused this to be the pulse sequence of choice for this sample. The second dimension is scaled by the WAHUHA scaling factor of 0.577 (as opposed to 0.471 for MREV-8 homonuclear decoupling). The cycle time for WAHUHA sequence used was 17.2 μs. The scaled inverse of this value is equal to the spectral width in the second dimension (dw2), which is 58 kHz as opposed to 28 kHz for MREV-8.

Figure 14 shows the 2-dimensional contour plot of the results when applied to form 1. The heteronuclear dipolar sidebands along ν_1 are separated by the carbon isotropic chemical shifts along ν_2. Hence this technique has been referred to as the 'dipshift' experiment. The envelope of the heteronuclear sideband intensities can be used to analyse the dipolar coupling for the purpose of detecting motional averaging.

Rotational echoes may be observed at integer values of the spinning frequency away from the centre of the spectrum and these are indications of the mobility of the protonated carbon sites in this polymorph. It should be noted that the peaks on either side of the quaternary carbon sites are caused by truncation of the FIDs of these sites in the second dimension.

Overall, the dipolar dephasing results and SLF spectrum in ***Figure 14*** indicate the mobility of some of the CH groups in form 1.

5.3.3.4 Inversion Recovery Cross Polarisation (IRCP) Experiment

This experiment was applied to assist with the certainty of the spectral assignment. The technique utilises the fact that doubly-protonated carbon resonances will invert more rapidly than those that have only one attached proton. Thus, it may be observed that the signals attributed to CH_2 resonances decay rapidly, whilst the non-protonated resonances do not decay to any great extent. The signals for the CH resonances also decrease, but not as rapidly as those for CH_2 groups, and display more oscillations. This behaviour is displayed in ***Figure 15***.

Figure 16 and ***Figure 17*** show interesting variations in the decay of the ^{13}C signal intensity for forms 1 and 2, which vary with degree of protonation of the carbon sites. These values and their assignments are described below and summarised in ***Table 6***. Anomalies also confirm differences in mobility of the pendant cyclopropyl groups in the two polymorphs. A combination of this information with mobility characteristics indicated by the single-crystal XRD data (see chapter 3) assists assignment of the ^{13}C spectra.

Quaternary carbon signals for both forms 1 and 2 show intensities that do not invert or reach a null point. This is true for resonances assigned to carbons (8), (6), (6), (2), (4) and (5).

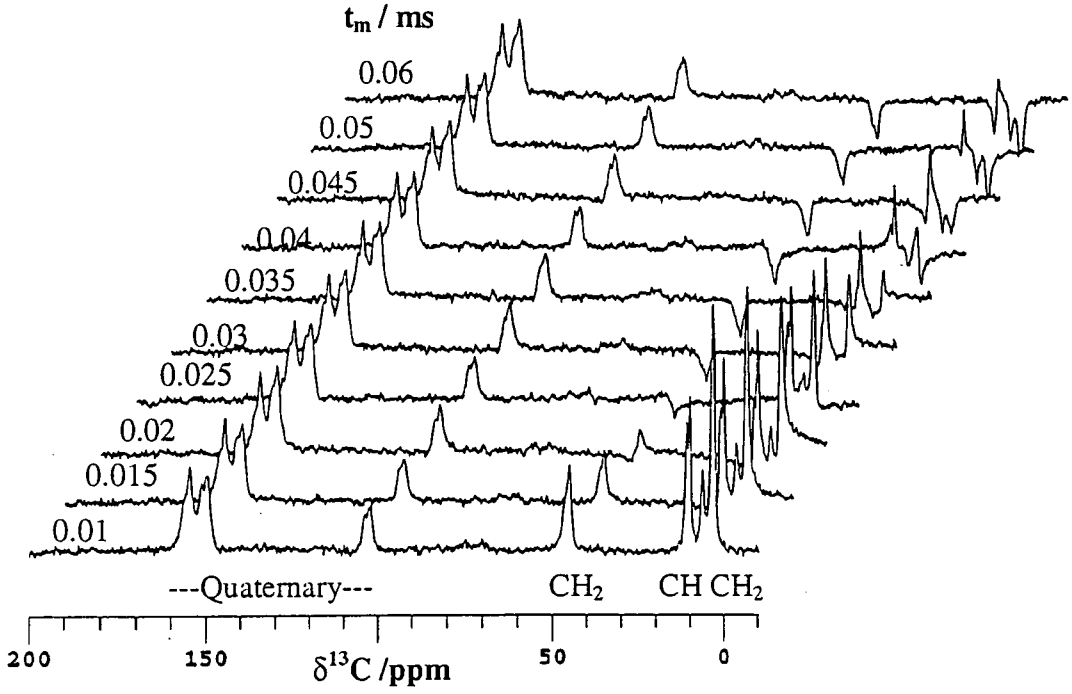

Figure 15 ^{13}C IRCP experiment BRL61063 form 1 (MAS 4 kHz, 51 ms acqtm, 9 s rd, ppfn gamircp, 1 ms ct, 32 transients).

The individual carbon signals that are assigned to C(10) and C(14) in form 2 reach null points at different times, the peak at 45.67 ppm inverting at 2/3 the time taken for the peak at 49.55 ppm to do so. The difference between the peaks indicates that there may exist some motion in the pendant group including C(10) in form 2, causing the resonance of C(10) at 49.55 ppm to invert after a greater time period. XRD data acquired at ambient

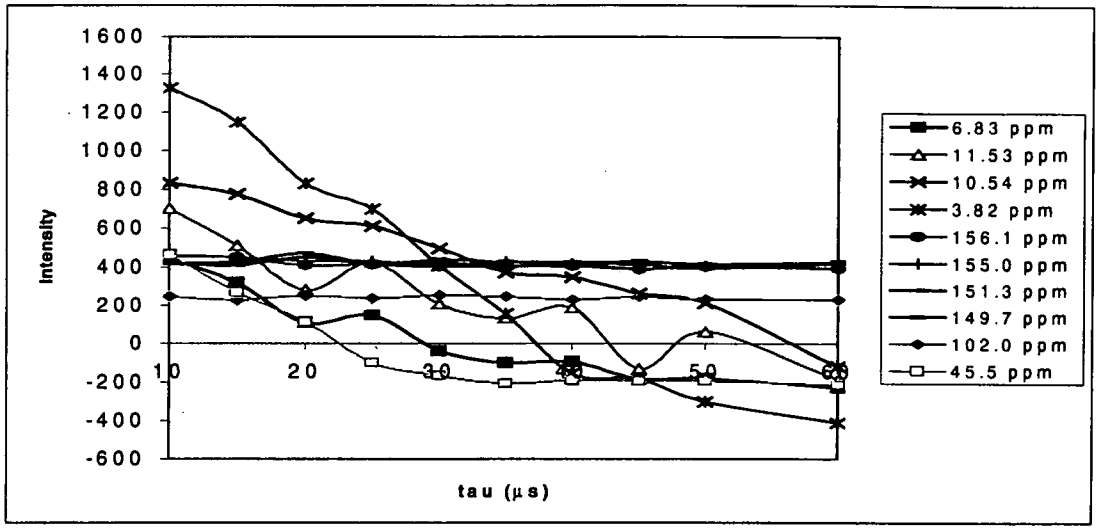

Figure 16 Plot of signal intensity versus tau for IRCP experiment (BRL61063, form 1).

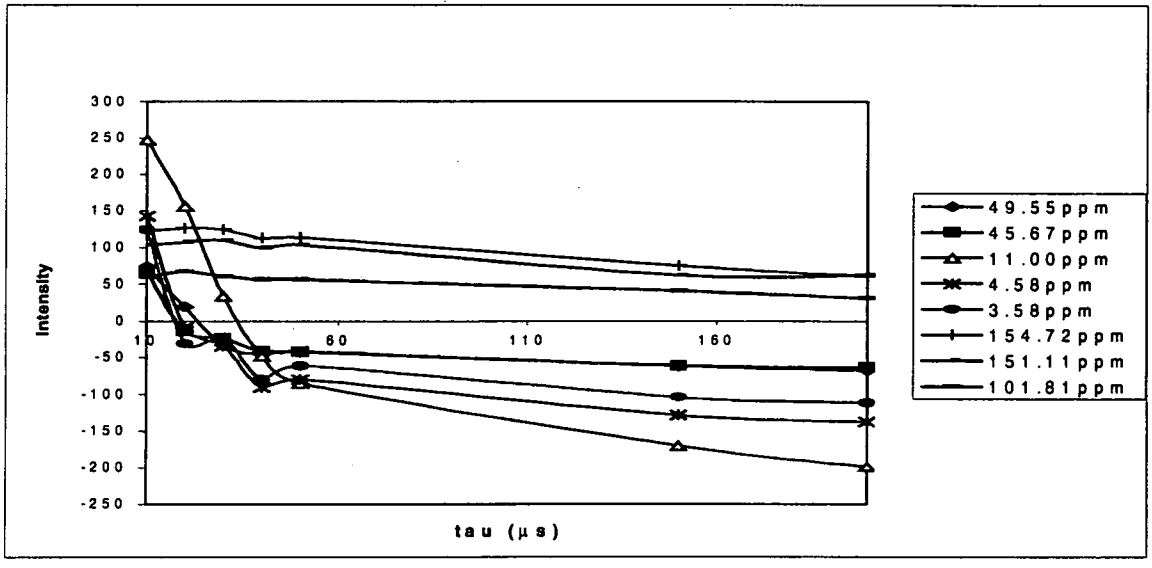

Figure 17 Plot of signal intensity versus tau for IRCP experiment (BRL61063, form 2).

^{13}C	Form 1		Form 2	
	δ ^{13}C/ ppm	Null time (µs)	δ ^{13}C/ ppm	Null time (µs)
Quaternary 8, 6, 2, 4, 5	156.1, 155.0, 151.3, 149.7, 102.0	No inversion	154.72, 151.11, 101.81	No inversion
CH_2 10, 14	C(10&14) 45.5	22.5	C(10) 49.55 C(14) 45.67	24.0 16.0
CH 15, 11	C(15) 11.53 C(11) 10.54	43.0 56.0	C(11&15) 11.00	33.5
CH_2 16, 17 12, 13	C(16&17) 6.83 C(12&13) 3.82	28.5 37.5	C(16&17) 4.58 C(12&13) 3.58	19.0 16.0

Table 6 Summary of assignments and null times in ^{13}C IRCP experiments

temperatures infer no mobility in form 2. However, it is possible that sample heating caused by MAS could cause flexing to become allowed.

Resonances arising from CH groups may be expected to invert half as quickly as those arising from CH_2 groups. This effect is illustrated by comparison of the profiles for CH groups (11) and (15) of form 2 at ~11 ppm, which invert at 33.5 μs, with the CH_2 groups assigned to carbons (16), (17), (12) and (13), which reach null points at a time of approximately half this value (17.5 μs).

However, the standard predictions are interfered with in the decay profiles of form 1 by mobility characteristics of this compound. The ^{13}C spectra of form 1 show only one resonance for both C(10) and (14) at ambient temperatures. This peak (at 45.5 ppm) inverts at 22.5 μs, which is half way between the two time values observed for the individual resonances of form 2.

Using prior knowledge (from XRD information) of the existence of conformational flexing of the C(12) (13) group in form 1 it may be predicted that the CH at 11.53 ppm (inversion time of 43 μs) is for the less mobile C(15) and that at 10.54 ppm is for C(11), the more mobile group since the inversion time for the latter is longer (56 μs). Continuing this argument the CH_2 resonance at 3.82 ppm (null time 37.5 μs) may be ascribed to the mobile C(12) and (13) resonances and the resonance at 6.83 ppm to the remaining C(16) and (17).

Comparison of the data for corresponding peaks for form 2 (which exhibits no disorder) show null times at much shorter times: 33.5 μs for C(15) and (11), 16.0 μs for C(12) and (13), and 19.0 μs for C(16) and (17). This is consistent with the rigidity of this form.

Thus the IRCP technique has been useful in the assignment of the solid-state spectra in their own right. This method has also been of considerable value for detecting the mobility in the compounds and assigning the mobile groups of the ^{13}C CP/MAS spectra.

5.4 Relaxation and quantitative parameters

A combination of T_1xcp and variable $^1H \rightarrow ^{13}C$ contact-time experiments were used to determine ^{13}C T_1, ^1H $T_{1\rho}$, plus T_{HC} values for each of the resolved ^{13}C peaks in the spectra of polymorphic forms 1 and 2. Values are shown in ***Table 7.***

From ***Table 7*** there is an obvious difference between the proton-to-carbon cross polarisation times for quaternary and protonated carbon nuclei, the values for quaternary carbons being much the longer owing to the H-C distance through space being much greater than that for a direct C-H bond. This also confirms the assignment of the ^{13}C CP/MAS spectra. It is hard to assess whether the existence of one extra hydrogen bond in form 2 is supported by the T_{HC} values, since the atoms involved exist in the complex quaternary, (8), (6), (2), (4) region. The main difference observed between the two forms is the T_{HC} time for C(10) and (14). Form 1 shows a time of 37 μs, while form 2 shows value of ~80 μs. (T_{HC} times are accurate to ± 50 μs). There seems to be no evidence of mobility for form 1 from T_{CH} values.

Form 1				Form 2			
$\delta^{13}C$ /ppm	T_{CH} (μs)	$T_1{}^{13}C$ (s)	$T_1\rho^H$ (ms)	$\delta^{13}C$ /ppm	T_{CH} (μs)	$T_1{}^{13}C$ (s)	$T_1\rho^H$ (ms)
156.1	450	94.8	17	156.4	500	-	130
154.5	600	-	15	154.7	700	36.0	130
151.3	800	-	13	151.1	900	68.7	130
149.6	800	96.0	14	-	-	-	-
104.0	500	-	19	103.2	-	-	-
102.4	100	138.5	14	101.7	700	79.5	170
-	-	-	-	49.7	78	4.4	280
46.4	37	20.2	16	-	-	-	-
-	-	-	-	45.9	80	22.0	370
11.3	106	4.7	14	11.0	94	8.7	210
10.3	100	7.7	13	-	-	-	-
6.5	53	3.8	15	6.3	67	4.1	260
-	-	-	-	5.9	-	-	-
-	-	-	-	4.6	67	3.0	260
3.6	75	1.8	14	3.5	72	5.6	240

Table 7 A summary of $^1H \rightarrow ^{13}C$ CP times, ^{13}C T_1 and ^1H $T_1\rho$ values measured from variable contact time experiments at ambient temperature.

Form 2 possesses ^{1}H $T_{1\rho}$ values that are of the order of 10 times greater than those for form 1. This may allude to the mobility differences between the two forms, since the shorter values observed for form 1 correspond to this form possessing more mobility at room temperature. If proton spin diffusion is efficient then the proton $T_{1\rho}$ values should be the same and the average value is 15 ms for form 1. The values shown for form 2 show a much greater variation, which may be due to the fact that the variable contact time experiment that was used to calculate these could only be taken to a maximum contact time of 16 ms.

The plots in ***Figure 18*** show data for form 1 and form 2 which has been extracted from analysis of the variable contact time experiments. From these plots the difference in the ^{1}H $T_{1\rho}$ values is immediately obvious. A comparison of the build-up curve showing T_{HC} also contrasts the more rapid rise in magnetisation for the protonated than the quaternary carbon site.

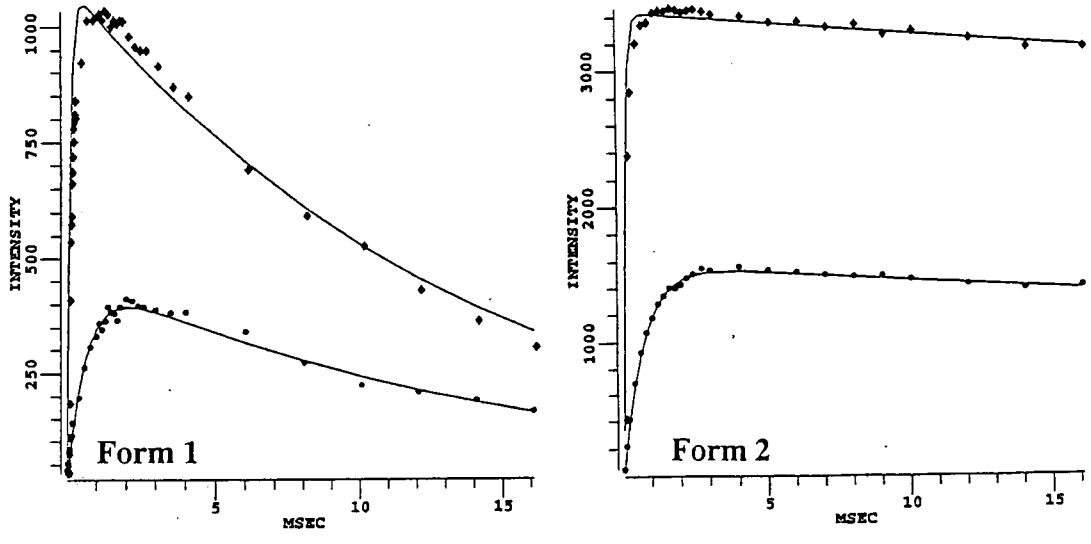

Figure 18 Sample plots of intensity versus contact time (ms) for variable contact time experiments on BRL61063 forms 1 and 2. (Dots represent quaternary C(8), diamonds represent CH (11)).

The carbon T_1 values are also shown (± 0.5 s) in ***Table 7***. There exist large variations between the T_1 values for the carbons of each polymorph. This again alludes to differences in mobility between the two forms, thus highlighting major differences between the molecular structures and inter-molecular interactions. The lower values for the protonated carbon sites of form 1 are consistent with the mobility in these groups. However, the carbon T_1 values of the quaternary signals are much greater for form 1. This is also somewhat of a puzzle, but may be caused by the T_1^C values being a function of temperature, with T_1 minima existing due to the presence of different molecular motions.

5.5 The effect of varying the temperature

The obvious progression following observation of these mobility characteristics is to try to increase or decrease the rates involved by raising or lowering the temperature of the sample. The following section describes experiments that have been carried out under variable temperature conditions whilst observing the ^{13}C spectra of the polymorphs.

5.5.1 ^{13}C CP/MAS VT

Variable temperature experiments provided interesting results, especially in the case of form 1. As can be seen in ***Figure 19***, the peak at approximately 45 ppm in the ^{13}C spectrum of form 1 gradually splits into two peaks as the temperature is decreased towards –140 °C. The two peaks that appear seem to be asymmetric doublets, with similar orientation ie. most intense peak at lowest frequency. The shifts of these most intense peaks are at 44.8 and 41.5 ppm with the less intense signals at 46.1 and 42.4ppm respectively. The corresponding signal for the solution state is assigned to the CH_2 carbons (10) and (14) on the pendant cyclopropyl groups. Therefore this alteration seems to suggest that the two groups become inequivalent with decrease in temperature. However, this is not in the sense that they are exchanging, as the bands don't broaden and merge, they just shift. The low-frequency peaks around 10 ppm also show small changes in relative intensity and chemical shift. The actual values are shown in ***Table 8***.

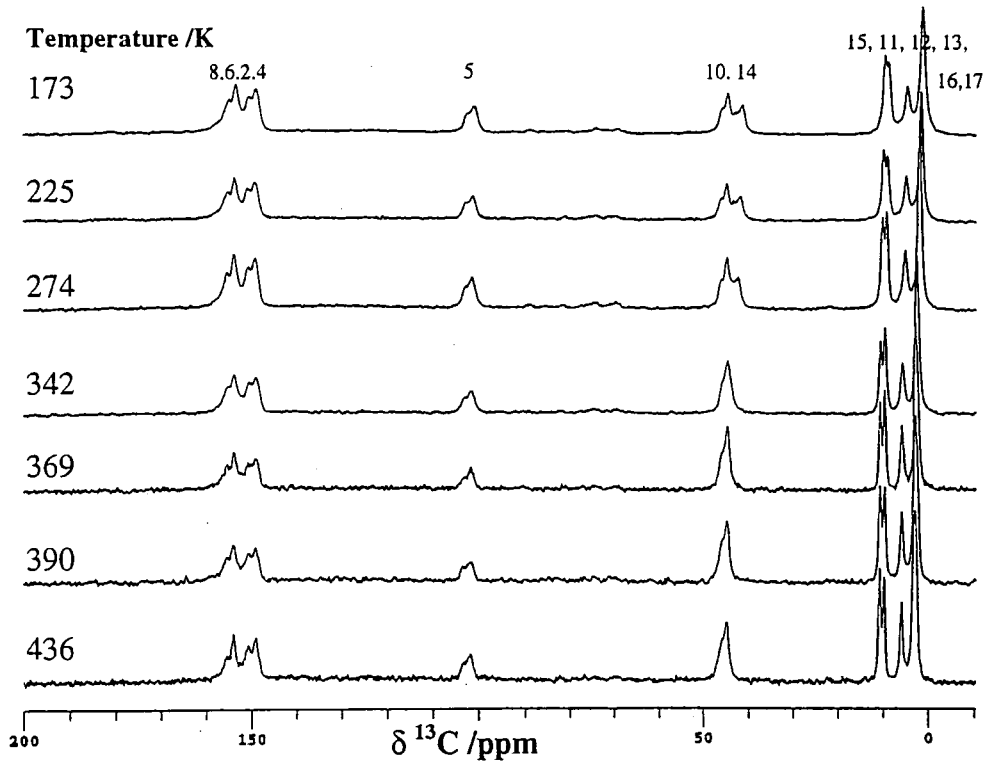

Figure 19 ^{13}C VT experiments on BRL61603 form 1 (MAS 4 kHz, cp4_pm, 1 ms ct, rd 9 s, 51 ms acqtm, 160 transients)

Temp / K	δ ^{13}C / ppm Form 1								
436	154.3	149.3	102.2	45.2		11.1	10.2	6.3	3.4
396	154.4	149.5	102.3	45.1		11.1	10.1	6.3	3.3
369	154.2	149.4	102.1	45.1		11.1	10.1	6.3	3.3
342	154.3	149.4	102.0	44.9		11.0	10.0	6.2	3.1
274	154.2	149.5	101.9	45.0	42.6	10.5	9.5	5.5	2.2
225	154.1	149.5	101.6	45.0	42.1	10.2	9.3	5.3	1.9
173	153.7	149.2	101.2	44.2	41.5	9.9	9.1	5.0	1.6
Final Δ	**-0.7**	**-0.3**	**-1.1**	**-1.0**	**-3.7**	**-1.2**	**-1.1**	**-1.3**	**-1.8**

Table 8 Chemical shift differences on alteration of temperature for ^{13}C CP/MAS spectra of BRL61063, form 1.

The changes observed in the ^{13}C spectra of form 1 are reversible when the temperature is brought back up to room temperature. However, it should be noted that the chemical shifts of the two peaks for C(10) and (14) around 50 ppm are not the same as observed in

form 2 at ambient temperatures, so that this is not a form 1-to-2 interconversion. Low temperature DSC data do not indicate a phase change in form 1.

The 'final Δ' data in ***Table 8*** show that the major change is for the C(10) and (14) peaks. The small changes in some of the other peak positions may be ascribed to a small general effect arising from the referencing on going to low temperatures.

Form 2 shows negligible changes in the ^{13}C CP/MAS spectra on subjecting the samples to lower temperatures (see ***Table 9***). At 408K, the individual C(10) and (14) peaks for form 2 are negligibly (0.2 ppm) closer together than at room temperature.

Temp / K	δ ^{13}C / ppm Form 2							
396	154.7	103.2	101.7	11.0	6.3	5.9	4.6	3.5
369	154.7	103.0	101.4	10.9	6.3	5.8	4.6	3.4
328	154.6	103.0	101.5	10.9	6.4	5.7	4.6	3.4
225	154.2	102.6	101.2	10.7	6.2	5.4	4.3	3.1
173	154.0	102.4	101.1	10.6	6.3	5.4	4.3	3.1
Final Δ	**-0.7**	**-0.8**	**-0.6**	**-0.4**	**0**	**-0.5**	**-0.3**	**-0.4**

Table 9 Chemical shift changes on alteration of temperature for ^{13}C CP/MAS spectra of BRL61063, form 2.

Subjecting 'yellow' to low temperatures causes the complex peak for C(10)(14) to appear to broaden and separate into two individual peaks (46.27 ppm and 44.85 ppm at 178 K), whilst heating the sample causes the signal to approximate to a single resonance (at 46.4 ppm at 450 K) indicating that the C(10) and (14) sites are becoming more nearly equivalent. Each of the polymorphic forms exhibit changes in the chemical shifts of the protonated carbon resonances.

5.5.2 Variable temperature dipolar dephasing experiments

Variable temperature ^{13}C NQS experiments have also been carried out on form 1 (see ***Figure 20***). These prove that the mobility of the pendant cyclopropyl group assigned

C(12) (13) does slow gradually at lower temperatures such that the CH_2 carbon resonances do not remain observable in the ^{13}C spectra after the 50 μs dephasing window. The mobility has slowed to the extent to which no signal is observed at 234 K.

The sample of 'yellow' was heated to 504 K and a ^{13}C NQS experiment was carried out. This showed peaks of low intensity appearing for the CH and CH_2 groups, as observed for the room temperature ^{13}C NQS spectra of form 1 and D, indicating that the necessary energy is present at this temperature to mobilise the pendant cyclopropyl groups in 'yellow'.

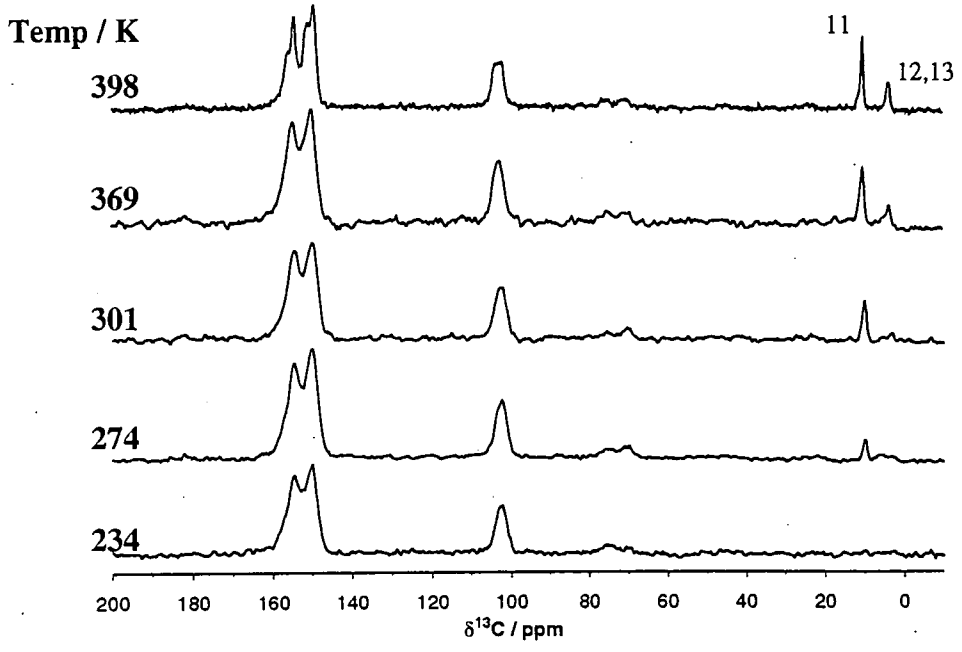

Figure 20 ^{13}C VT NQS experiments of BRL61063, form 1 (MAS 4 kHz, 9 s rd, 1 ms ct, 51 ms acqtm, anDDecho, 50 μs dephasing time, 100 transients)

5.5.1.2 Variable temperature variable contact time experiments (T_{HC} and $T_{1\rho}$).

Proton-to-carbon variable contact time experiments have been carried out at variable temperature in order to analyse the T_{HC} values and proton $T_{1\rho}$ values for individual carbon sites in form 1 and form 2.

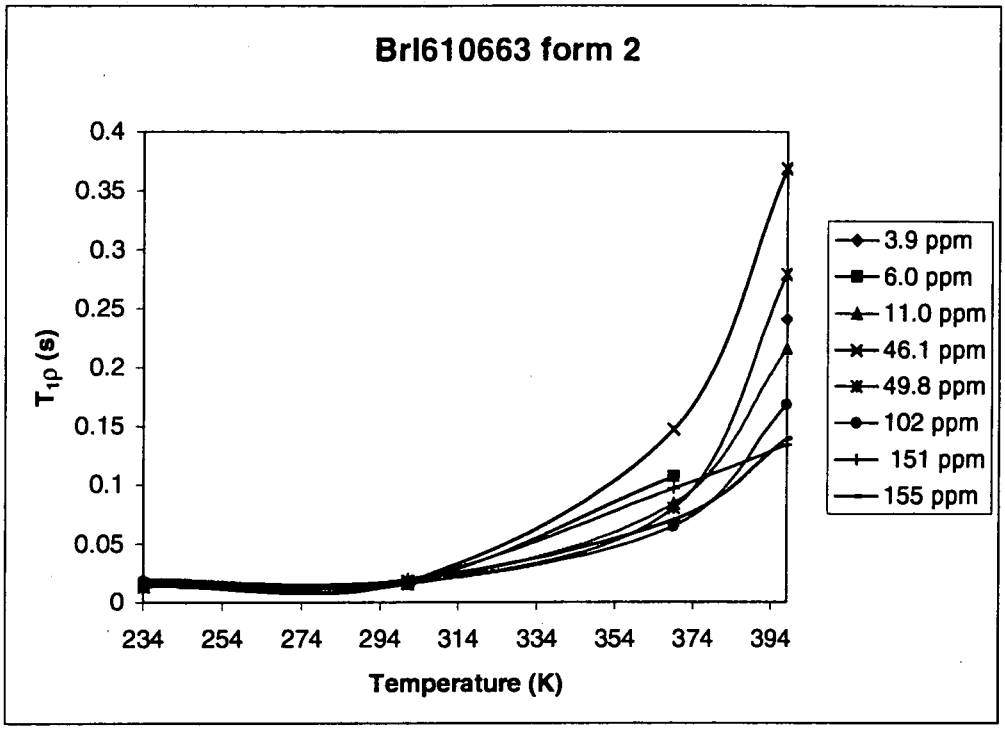

Figure 21 Comparison of $T_{1\rho}^{H}$ for BRL61063 form 2 with variation in temperature.

Variable temperature proton $T_{1\rho}$ experiments showed contrasting results for forms 1 and 2. The variation of $T_{1\rho}^{H}$ values for form 2 are shown in ***Figure 21***. This polymorph shows values of $T_{1\rho}$ that increase rapidly with increase in temperature, which is the opposite to simple behaviour. There appears to exist a broad minimum for the value of $T_{1\rho}^{H}$, which is centred around 274 K. This infers that at this temperature the motions within BRL61063, form 2 are of the same order as the equivalent frequency of the spin-locking field, which was 56 kHz. From the variation in the values of proton $T_{1\rho}$, it would appear that proton spin diffusion is not as efficient at higher temperature, although the reason for this remains unclear.

It is already predicted from XRD studies and other earlier work (NQS, dipolar dephasing, IRCP) that form 2 exists in a rigid conformation at ambient temperatures. It has also been established that the ^{13}C spectrum of form 2 shows negligible changes when the sample is subjected to a decrease in temperature. Results show that on the whole, the $T_{1\rho}^{H}$ measured for individual ^{13}C sites in form 2 decreases with decrease in temperature.

These results are interesting because although minimal changes are observed in the ^{13}C CP/MAS VT spectra within these temperature ranges (see section 5.5.1.1), the ^{15}N natural abundance spectra of form 2 show more temperature dependence (see section 5.6.3).

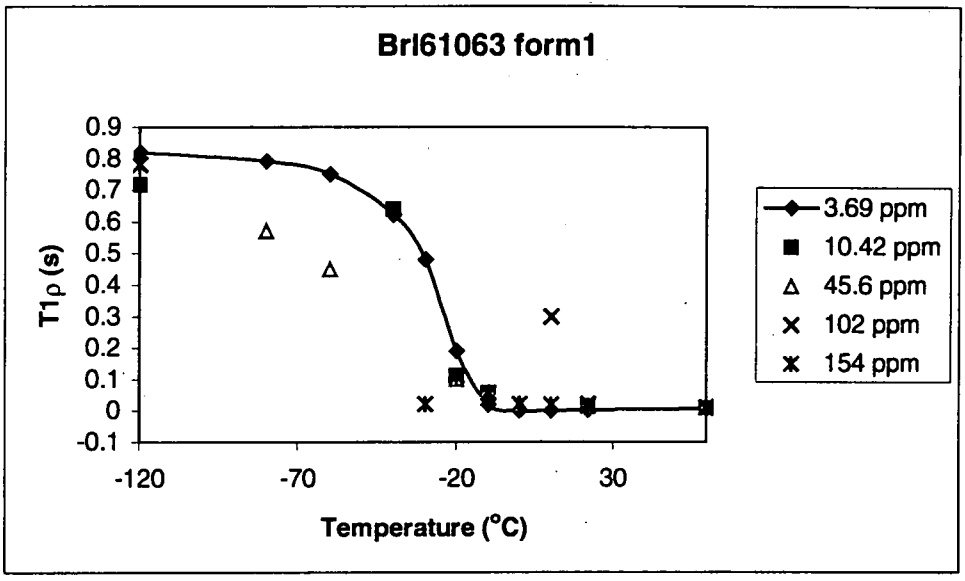

Figure 22 Comparison of $T_{1\rho}^{H}$ for BRL61063 form 1 with variation in temperature

The same proton-to-carbon variable contact time experiments were repeated on form 1, but with very different results (shown in ***Figure 22***). The lines shown on these plots have no theoretical significance and merely connect the points. In ***Figure 22***, where data points were of dubious quality they have been removed. The is trend shown by connecting the data points for the peak at 3.60 ppm and in so far as it is possible to observe trends for other points, they parallel this.

The trend in $T_{1\rho}^{H}$ with temperature variation for form 1 opposes that observed for form 2 in that the value of $T_{1\rho}^{H}$ is very high at low temperature, but decreases with increase in temperature, appearing to reach a minimum at 409-436 K, which is the expected behaviour for a simple case on the low-mobility side of a $T_{1\rho}$ minimum.

These results are particularly interesting because when approaching low temperatures (234 K) that the ^{13}C CP/MAS VT spectra show separate peaks for C(10) and (14), indicating that the sample is approaching the rigid limit and that the two sites are then

rendered inequivalent. The ^{13}C CP/MAS VT NQS spectra also indicate the decreasing mobility of the CH_2 groups, since the CH and CH_2 signals for C(13) and C(11) and (12) do not appear in the dipolar dephasing spectra at temperature ranges below 234 K.

The minimum $T_{1\rho}^{H}$ values are 0.008 ms and 0.015 ms for form 1 and 2, respectively. Whilst the value of $T_{1\rho}^{H}$ exists at its minimum at ambient temperatures for form 2, form 1 exists above this point at ambient temperatures.

No definite trends appear in the proton-to-carbon CP times on alteration of temperature.

5.5.2 Variable Temperature Proton CRAMPS

No significant changes in the proton CRAMP spectra are observed by subjecting the samples of form 1 and 2 to 260 K.

5.6 ^{15}N CP/MAS spectra

The large number of nitrogen sites in BRL61063 makes the polymorphs very interesting to study. Standard natural abundance ^{15}N spectra were obtained using cross polarisation from protons, with MAS and HPPD during the acquisition time.

The room temperature ^{15}N CP/MAS spectra of the four polymorphs are shown in ***Figure 23,*** and the shifts of the individual resonances are compared with those obtained in the solution-state in ***Table 10***. Assignment of the solid-state spectra was made on comparison with the solution-state spectra and the literature[4,5]. Comparison of solution- and solid-state spectra required conversion between the referencing scales used (as outlined in chapter 2).

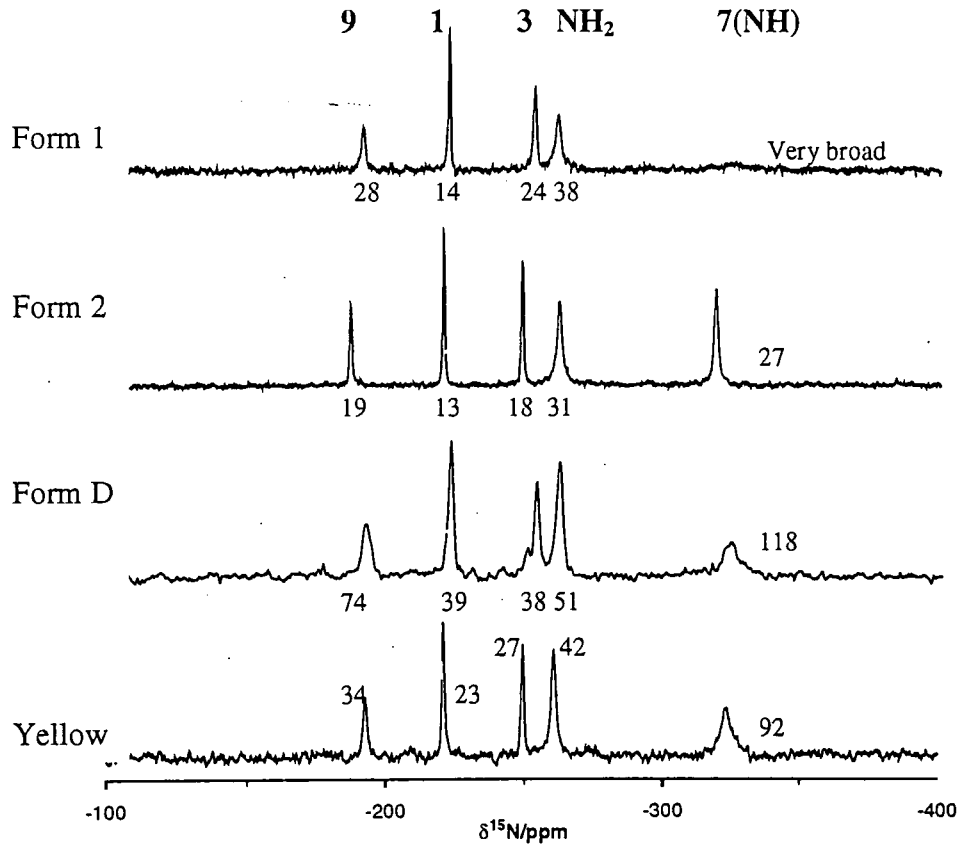

Figure 23 ^{15}N CP/MAS spectra of the four polymorphs (Cpflip, 4 kHz MAS, 204 ms acqtm, 9 s rd, 1 ms ct, 9680 transients) figures indicate $\Delta\nu_{1/2}$ /Hz.

Form 1		Form 2		Form D	Yellow	^{15}N Site	$\delta^{15}N$/ppm Solution state
$\delta^{15}N$ /ppm	Corrected*	$\delta^{15}N$ /ppm	Corrected*	$\delta^{15}N$ /ppm	$\delta^{15}N$ /ppm		
-191.1	**190.3**	-186.4	**195.0**	-192.5	-192.9	**9**	**197.01**
-221.7	**159.7**	-219.6	**161.8**	-220.7	-220.7	**1**	**160.47**
-252.6	**128.8**	-248.0	**133.4**	-249.5	-249.5	**3**	**129.45**
-261.0	**120.4**	-261.4	**120.0**	-260.6	-260.6	**NH_2**	**121.27**
-325	**56.4**	-318.3	**63.1**	-323.2	-323.5	**7**	**61.82**
* shifts converted (see chapter 2) to allow comparison with solution-state spectra.							

Table 10 Comparison of solid- and solution-state ^{15}N spectra of BRL61063.

It is very interesting at this stage to note the variation in the appearance of the resonance of the NH(7) site. This varies from extremely broad in form 1 to very sharp in form 2, to varying degrees of broadness in form D and 'yellow'.

5.6.1 Assignment of the ^{15}N spectra of forms 1 and 2 using IRCP

Assignment of the ^{15}N CP/MAS spectra was confirmed using comparison with solution-state assignments plus a combination of the IRCP and NQS techniques. The IRCP technique was used since in theory, resonances arising from the doubly-protonated nitrogen atoms should invert earlier than those for the singly-protonated nitrogen sites.

Figure 24 shows a stacked plot of the ^{15}N CPIR experiment carried out on form 2. It is clear that the resonance assigned to the NH_2 group at -261 ppm decreases to zero intensity in half the time in which the NH signal at -318 ppm does. The times involved are 85 and 170 μs for the NH_2 and the NH peaks, respectively.

The graphical plots in ***Figure 25*** and ***Figure 26*** show individual signal intensity versus time for the ^{15}N IRCP experiments carried out on form 1 and form 2. The mobility characteristics of form 1 influence the decay profiles observed such that the NH_2 resonance achieves its null point later than the NH resonance. However, the low intensity, broad nature of the NH(7) resonance may cause this to be an erroneous result.

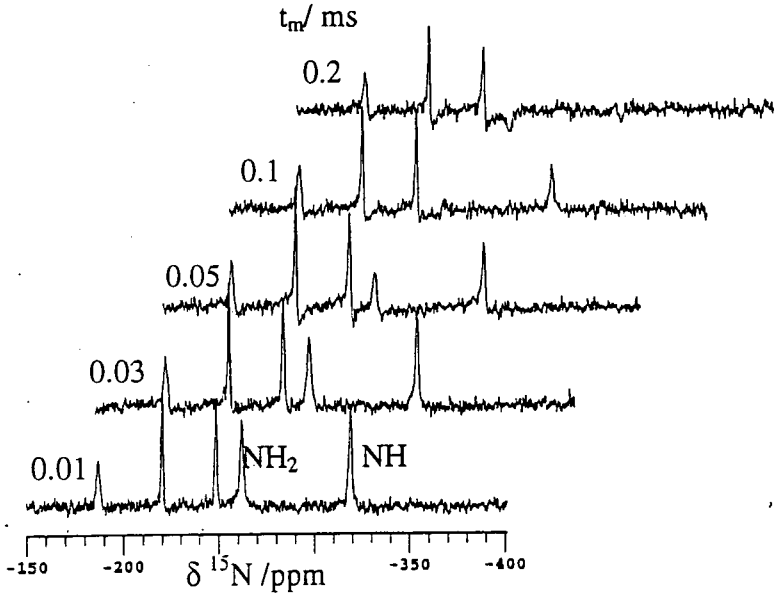

Figure 24 BRL61603 form 2 ^{15}N IRCP experiment (ppfn gamircp, MAS 4 kHz, ct 2ms, 102 ms acqtm, 9 s rd, 1680 transients).

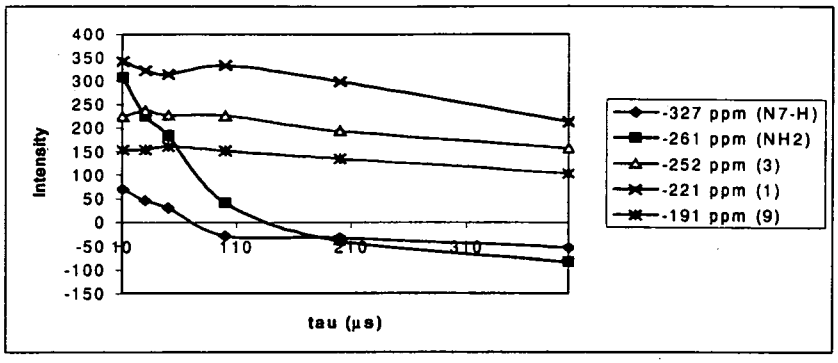

Figure 25 Form 1: Graph showing intensity versus time for the N15 IRCP experiment

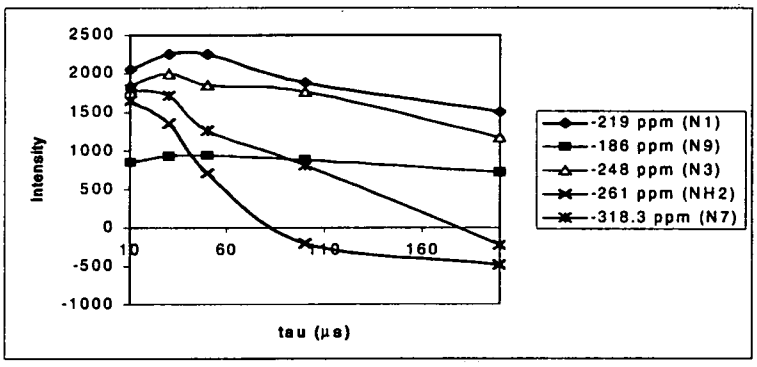

Figure 26 Form 2: Graph showing peak intensity with time for IRCP experiment.

5.6.3 ^{15}N Variable temperature experiments

The established mobility characteristics of the polymorphs of BRL61063 and the broad signal for the NH_2 site in form 1 provoked an interest into finding the reason why the resonance was indeed absent at ambient temperature.

The natural abundance ^{15}N spectra of form 1 were recorded with decreasing temperature (see ***Figure 27***). The broad peak at ~-325 ppm sharpens up dramatically with increasing relative peak height compared to the other peaks in the spectrum. The relative intensity and chemical shift of some of the other resonances also alter with decrease in temperature.

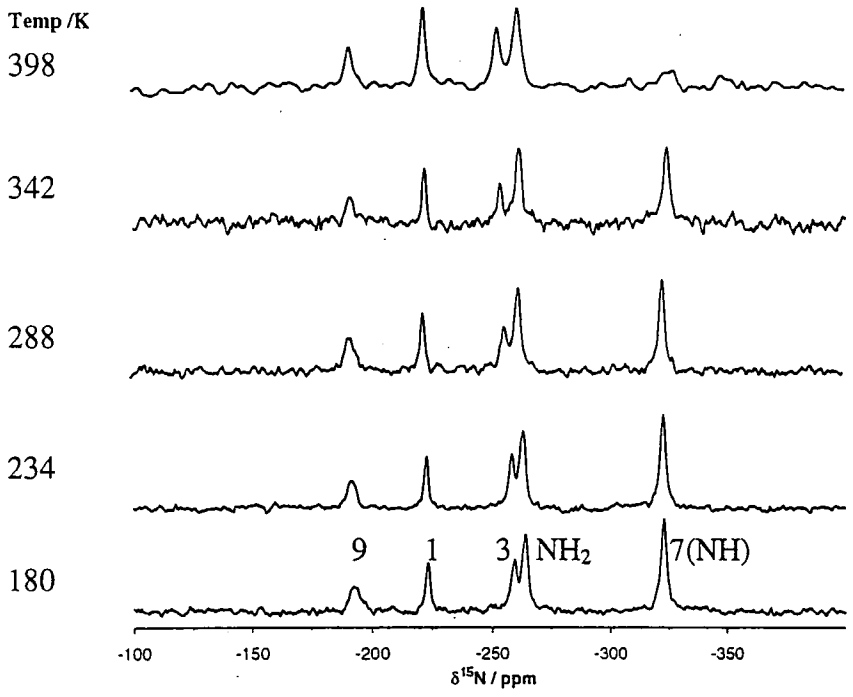

Figure 27 BRL61063 form 1 VT ^{15}N (MAS 4 kHz, cpflip, 1 ms ct, rd 9 s, 154 ms acqtm, 1024 transients).

Dipolar dephasing experiments were carried out on ^{15}N for form 1 at low temperature (133 K), leaving a dephasing window of 200 μs to allow the protonated nitrogen sites to dephase. This technique confirmed the assignment of the NH and NH_2 resonances as the peak at -261 ppm decreased in intensity, but not completely. This would be consistent with an NH_2 group that is slightly mobile. The peak at –325 ppm decreased to zero intensity after the dephasing time, indicating that this resonance may indeed be assigned to a NH group.

A selective population inversion experiment was carried out for form 1 at low temperatures (253, 223, and 193 K) on the 300 MHz Varian Unity Plus spectrometer in order to investigate the possibility of proton exchange occurring between the two protonated ^{15}N sites (-261 and –325 ppm). The peak at –261 ppm was inverted and the filename of the pulse program was cpnoesyps. Mixing times used were as follows: 253 K and 193 K: $1x10^{-5}$, 0.4, 0.8, 1.6, 3.2, 6.4 s; 223 K: $1x10^{-5}$, 0.8 s. The conclusion was that this phenomenon is not occurring on a NMR-observable time scale.

In a continuing effort to explain the room temperature broadening of the resonance at -325ppm, the possibility of interference of the applied proton decoupling power and/or the magic angle spinning rate with the broadening mechanism was investigated, by observing the spectrum whilst varying these factors systematically. All experiments were carried out on the 300 MHz Varian spectrometer. No effect causing narrowing of the resonance was observed when altering either parameter through the range of MAS rates (4.5, 4.0, 3.5 kHz) and decoupling powers ('dipolr' settings used: 1700, 1100, 600). These experiments were acquired at a set temperature of 25°C, where the resonance at -325 ppm is extremely broad, so that any narrowing would be immediately obvious.

Subjecting the sample of form 1 to low temperatures and acquiring the ^{15}N CP/MAS spectra, showed the sharpening up of the peak at –327 ppm. The resolution enhancement of this peak, plus the NH2 peak at –261 ppm does not alter greatly below 342 K indicating that the structure of form 1 remains identical below this temperature.

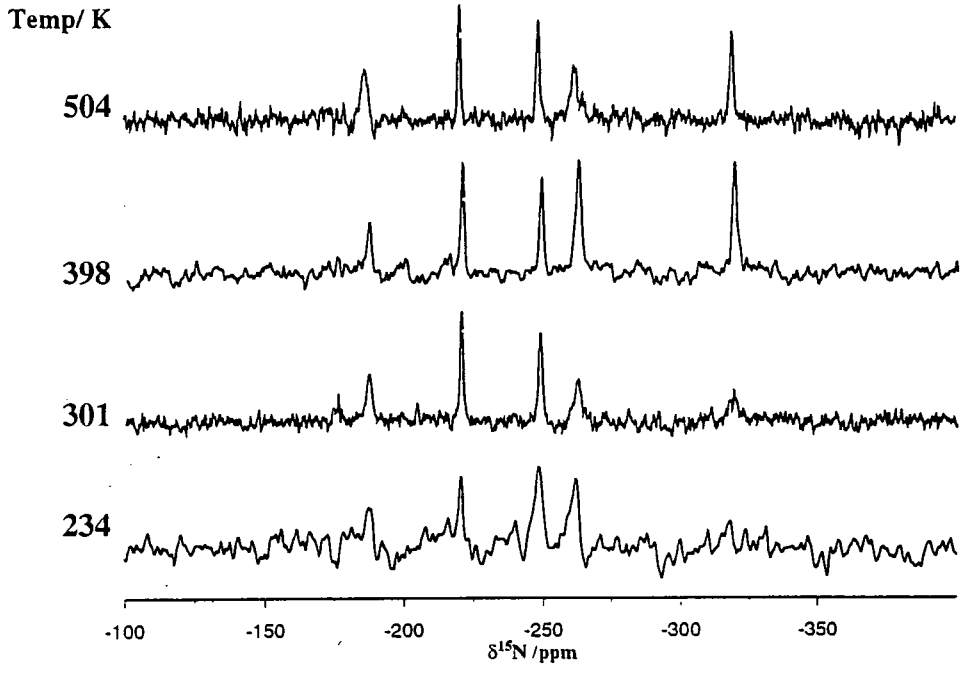

Figure 28 BRL60163 form 2 VT ^{15}N (MAS 4 kHz , cpflip, 1 ms ct, rd 9 s, 154 ms acqtm, 800 transients).

The ^{15}N variable temperature spectra of form 2 are shown in ***Figure 28***. This polymorph shows the exact opposite behaviour to form 1 in that the resonance at –325 ppm broadens

significantly upon decrease of temperature. With decrease in temperature it has been shown that there is an associated decrease of $T_{1\rho}{}^{H}$. The cause of the loss of this resonance is still not clear, although possibilities of mobility in the hydrogen bonding or local exchange at this nitrogen site may play a part.

5.6.3.1 VT ^{15}N NQS experiments

The dipolar dephasing technique was also applied to the ^{15}N spectra. The technique was only altered from carbon in that a dephasing window of 200 μs was used (rather than 50 μs, which is used for ^{13}C). At room temperature, after a dephasing time of 200 μs, form 1 showed complete loss of the sharp NH signal at –322.9 ppm, but the signal at -264.0 ppm decayed only in part, to approximately 1/3 its initial intensity. This effect has been observed by Apperley[6] in a compound which experiences proton 'hopping' between two sites in the molecule. For form 1 at 180 K, complete dephasing of both these protonated signals appears to take place, and each is absent in the ^{15}N NQS spectrum (see ***Figure 29***).

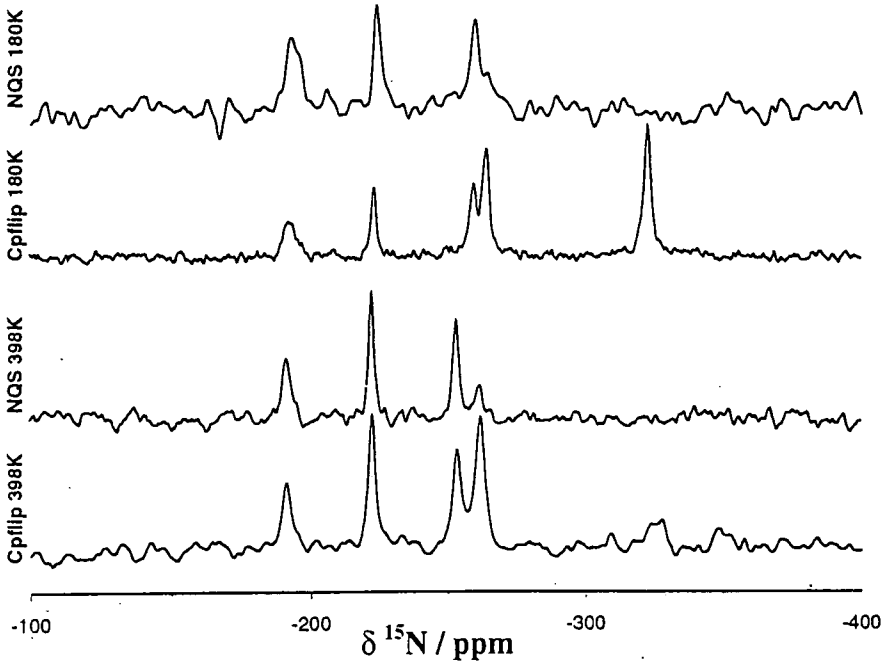

Figure 29 ^{15}N dipolar dephasing spectra of BRL61063 form 1 at two temperatures (MAS rate 4 kHz, 1000 transients, 9 s rd, 1 ms ct, anDDecho 200 μs dephasing time).

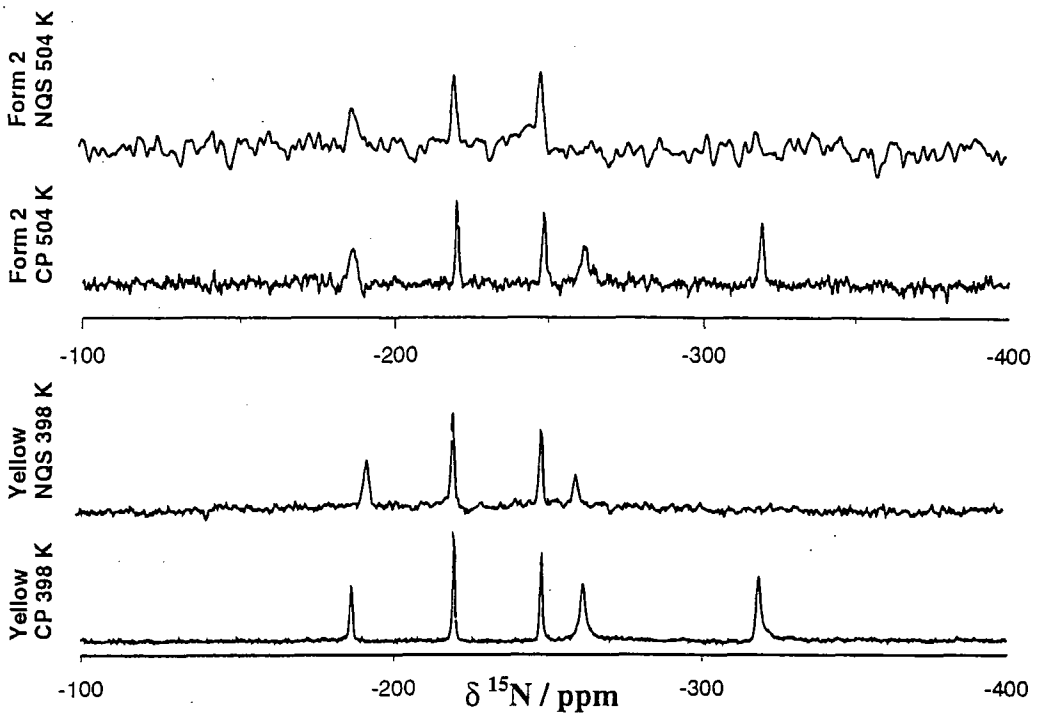

Figure 30 Comparison of Cpflip and NQS spectra for 'yellow' and form 2 (MAS rate 4 kHz, 1 ms ct, 9 s rd, Cpflip and anDDecho, 200 μs dephasing time).

The technique was also applied to some of the other polymorphic forms at various temperatures. Spectra for form 2 (at high temperature) and 'yellow' (just above ambient temperature) are shown in ***Figure 30***.

Yellow showed similar results to form 1 at room temperature, with the NH signal disappearing completely and the NH_2 signal decreasing in intensity. It appears that the decrease in intensity for the NH_2 signal of form 1 is greater than that observed for 'yellow' although the poorer signal-to-noise ratio of the spectra for form 1 means that this spectrum is not as clear.

On application of the NQS technique to form 2, neither the NH nor the NH_2 resonance remains in the final spectrum at high temperature indicating that the rigidity of the molecular structure of form 2 is stable to 504 K.

5.7 Conclusions

BRL61063 has provided a system that may be considered as containing form 1 as the disordered or mobile limit, and form 2 as the rigid limit. Recrystallisation work has been successful in reproducing forms 1 and 2, plus two other samples, named 'D' and 'yellow', which show somewhat different solid-state NMR and powder XRD data. These two samples appear to be intermediate in character between forms 1 and 2, with form D approximating to the mobile limit seen for form 1, whilst 'yellow' shows characteristics that infer greater similarity with the structure of form 2.

Whilst ATR-FTIR and DSC data appear to be inadequate for differentiating between the polymorphic forms of BRL61063, PXRD traces do show significant differences between all four samples. The question as to whether samples 'D' and 'yellow' are in fact the polymorphs named 'form 3' and 'form 4' originally produced by SmithKline Beecham Pharmaceuticals remains unclear due to incomplete characterisation of the original polymorphs ('3' and '4') by available techniques.

The single-crystal X-ray diffraction data for polymorphs 1, 2, and 4 have been usefully compared with and supported by solid-state NMR results. The extension of the molecular framework and hydrogen-bonding information into long-range space, beyond the unit cell, during the latter part of this Ph.D. has also provided a framework on which it is possible to postulate causes for effects observed in the NMR results.

The main subject areas that have been addressed by solid-state NMR techniques in this chapter vary greatly from those presented in chapter 4 due to the nature of the polymorphs of BRL61063. The three main areas that have been considered included probing the mobility and disorder characteristics, the effects of varying temperature, together with relaxation time analysis and comparison.

NMR has been able to show the effect of temperature variation on some of the polymorphs, most notably form 1, which shows disorder in its C(12)(13) pendant cyclopropyl groups at ambient temperatures. The ^{13}C CP/MAS spectra of this form show accidental equivalence of the resonance for C(10) and (14) at ambient temperatures. On decreasing the temperature, these resonances become inequivalent (as is observed for form 2 at ambient temperatures) and the motion of the CH and CH_2 groups has been proved to decrease by application of solid-state NMR spectral editing techniques.

The variation in the hydrogen-bonding characteristics of the forms is marked. Both the amide hydrogen atoms in form 2 are involved in intermolecular hydrogen bonds with two partners of a dimer. This bonding holds the NH_2 groups in form 2 in a rigid, planar conformation. In form 1, where the amide hydrogen atoms are not necessarily involved in strong hydrogen bonds, the NH_2 group is free to rotate. This fact is proven by ^{13}C NMR NQS experiments on the nitrogen sites, which show that rotation of the NH_2 group causes rapid modulation of the dipolar coupling interactions. The involvement of the N(9) position in an intermolecular hydrogen bond, giving rise to the close proximity of a hydrogen atom, is also alluded to by solid-state NMR spectral editing results for the polymorphs.

Application of the novel TPPM decoupling sequence for proton decoupling is necessary in order to resolve the resonances of the aliphatic carbon sites in the ^{13}C spectra of form 2. Also, since every sp_2 carbon site is bonded directly to at least one nitrogen atom, complex residual dipolar coupling characteristics result (see chapter 6).

Questions still remain as to the cause of the sharp proton lines for form 2 as opposed to form 1, as these are more usually observed when there is a mobile component in a sample. Wideline separation experiments failed to associate these narrow proton resonances with any carbon sites in the molecules, which may be explained by the poor CP efficiency of mobile sites. DSC and solution-state NMR have ruled out the existence of pseudopolymorphism or solvate formation in these systems.

The inter-form variation in the proton $T_{1\rho}$ values at ambient temperatures prompted their measurement at variable temperatures. This has revealed interesting comparisons between form 1 and form 2, which are consistent with the varying degrees of motional disorder in the compounds.

I would like to propose that there is potential for colour polymorphism in the BRL61063 polymorphic system and I have summarised the pale colours exhibited by the forms in the schematic below. This phenomenon[7] has been observed for small organic molecules before, and has been associated with the degree of electron delocalisation within molecular structures, which arises from the degree of overlap of orbitals relating to conformational differences between functional groups in the different polymorphs.

	Form 1	'D'	'Yellow'	Form 2
Disordered	----------→	----------→	----------→	---------- **Rigid**
Colour:	White	white	pale yellow	very pale pink

The question as to the characteristics of the disorder in the cyclopropyl groups of form 1 at ambient temperatures has been addressed using solid-state NMR techniques. The existence of ^{13}C resonances in the spectra that result from the dipolar dephasing techniques infers that these groups are moving and thus averaging the heteronuclear dipolar interactions at room temperatures. This motion slows to a rate that is not observable in the NQS spectra at lower temperatures. At this point it may be assumed that the lower energy conformation is adopted, with the cyclopropyl groups across the channels existing in their edge-to-non-parallel-edge (see chapter 3) conformation.

Areas for future work on this system should most definitely include a variable-temperature single-crystal X-ray study of the polymorphs, especially looking at form 1 at low temperatures, to investigate the way in which the occupancies of the disordered positions change at low temperature and what exactly drives the disorder characteristics in form 1.

5.8 References

1 S. Berger, S. Braun, H. O. Kalinowski, *'NMR spectroscopy of the non-metallic elements'*, Wiley, Chapter 4, 191, 1996.

2 G. C. Levy, R. L. Lichter, *'Nitrogen-15 NMR spectroscopy'*, Wiley, 1979.

3 J. Mason, Encyclopedia of NMR, *'Nitrogen NMR'*, Ed.s D. M. Grant and R. K. Harris, Wiley, **5**, 3227, 1996.

4 G. A. Webb, *Annual reports on NMR spectroscopy,* Academic Press, **16**, 187, 1985.

5 G. A. Webb, M. Witanowski, L. Stefaniak, *'Annual reports on NMR spectroscopy'*, Academic Press, **18**, 1986.

6 D. C. Apperley, University of Durham Industrial Research Laboratories, Mountjoy Research Centre, personal communication.

7 G. A. Stephenson, T. B. Borchardt, S. R. Byrn, J. Bowyer, C. A. Bunnell, S. V. Snorek, L. Yu, *J. Pharm.Sci.*, **84**, 11, 1385, 1995.

Chapter 6

Residual Dipolar Coupling.

Resolution enhancement – extracting conformational information from broadened lines

6.1 Introduction

In the previous chapters it has been shown that the lineshapes of ^{13}C nuclei that are directly bonded to ^{14}N (quadrupolar) nuclei may display broadening or asymmetric doublets in their ^{13}C CP/MAS spectra. These effects may be ascribed to a phenomenon which has been referred to as 'residual dipolar coupling' (RDC) and is so-called because second-order quadrupolar effects are transferred to the spin-1/2 spectra by dipolar interactions. Although this effect provides an added complication in the NMR spectra of solids, its manifestation also portrays a useful source of molecular information[1] that is not obtainable from solution-state NMR.

The residual dipolar coupling[2] phenomenon may arise in solid-state spectra when any quadrupolar nucleus is coupled to a spin-½ nucleus[3,4,5]. Examples include the isotopes of halogens such as ^{35}Cl and ^{37}Cl[6,7] plus ^{79}Br and ^{81}Br[8,9], all of which have nuclear spin quantum numbers of I= 3/2. Whereas an adjacent ^{14}N (I=1) nucleus causes formation of an asymmetric doublet[10,11] for the adjacent spin-½ nucleus, the greater I values of these halogen nuclei cause more extensive splitting of the resonance, causing asymmetric quartets to be formed. However, for the purpose of this chapter, only the (^{13}C, ^{14}N (I= 1))[12] case will be discussed since this is the system which has been of the greatest relevance within this Ph.D. research area.

6.1.1 From where do these asymmetric lineshapes arise?

The first observations of an asymmetric lineshape in a ^{13}C CP/MAS NMR spectrum of a compound containing a ^{13}C-^{14}N bond were reported by Kundla and Lippmaa[13] in 1979. The authors observed a resonance in their ^{13}C spectra that consisted of an asymmetric doublet that could be assigned to a C-N group. They also noted that the magnitude of this splitting possessed an inverse dependence on the magnetic field. This is contrary to the relationship expected for J-coupling. Thus, it was concluded that the splitting was arising from a dipole-dipole interaction with the ^{14}N nucleus having a quadrupole interaction of comparable magnitude to the Zeeman interaction.

In the solution state, ^{13}C nuclei immediately adjacent to ^{14}N nuclei generally give rise to a singlet in the ^{13}C NMR spectrum. An exception is the case of isonitriles ($R—N^{+}\equiv C^{-}$)[14] where a 1:1:1 triplet arises as a consequence of J-coupling to the ^{14}N spin-1 nucleus. Whereas in solids the isotopic substitution of the ^{14}N nucleus for ^{15}N would cause this multiplet to collapse to a singlet, in solution-state the J-coupling effects would not disappear, but just become scaled by the ratios of the gyromagnetic constants $\gamma^{14}N/\gamma^{15}N$.

RDC therefore involves the transmission of quadrupolar effects to the spin-½ nucleus being observed through the magnetic dipolar interaction between the two nuclei. This in turn depends upon the inter-nuclear distance. It is also possible to observe longer-distance effects[15] since the interactions are transmitted through space, not through chemical bonds.

6.1.2 Applications of RDC phenomena

There is particular interest in the (^{13}C, ^{14}N) system due to its obvious relevance in biological systems[16]. The observation of a splitting in the α-carbon resonance of amino-acids[17,18,19] such as alanine[20] has been utilised to set the magic angle in the experimental adjustments[21]. Deviations of ±4 ° from the magic angle (54.7 °) give rise to broader spectra and thus cause the apparent disappearance of the asymmetric doublet. However, modern techniques of setting the magic angle are more accurate than this one.

6.2 Theory

It has already been established that MAS results in substantial narrowing of resonances in the solid state via its ability to average out anisotropic interactions to their corresponding isotropic values. This occurs since these interactions are weak as compared with their Zeeman interactions. However, interesting deformations of the resonances of spin-½ nuclei that are directly bound to quadrupolar nuclei (i.e. nuclear spin > ½) may frequently be observed in solid-state CP/MAS NMR spectra. These asymmetric splittings, or 'non-Lorentzian broadening effects' are caused by the residual dipolar coupling between ^{13}C and adjacent, quadrupolar ^{14}N (I =1), which can not be completely averaged out by rapid MAS.

6.2.1 How are second order quadrupolar coupling effects transferred to scalar-coupled nuclei?

The asymmetric splittings induced by ^{14}N nuclei on those signals of ^{13}C nuclei to which they are spatially close arise from the fact that the ^{14}N eigenstates are not pure Zeeman states (***Figure 3***) but are determined by the Zeeman-quadrupole Hamiltonian, incorporating terms C and D of the dipolar Hamiltonian. The Zeeman states $|+1\rangle$, $|0\rangle$, $|-1\rangle$ are therefore mixed, leaving a dipolar interaction (^{13}C, ^{14}N) with an angular dependence different to the familiar $(3\cos^2\theta - 1)$ which affects the energies of the spin states. Therefore, MAS is unable to average this coupling to zero since it has an angular dependence other than $(3\cos^2\theta - 1)$ leading both to the splitting and broadening of the ^{13}C signals. Applying a first-order approximation, an asymmetric splitting of the ^{13}C resonance into two signals of relative area 2:1 is predicted.

The following section outlines the perturbation approach that has been used (by Olivieri[22]) for the study of quadrupole-induced multiplicities in solid state NMR. The discussion will be restricted to the (I= ½, S = 1) case as for ^{13}C, ^{14}N.

6.2.1.1 The Quadrupole Hamiltonian

Nuclei with spin greater than ½ possess, in addition to the magnetic moment, an electric quadrupole moment. This may be pictorially represented as a 'cigar', or 'prolate' shape whereby positive charge exists above the poles and a positive charge defect results around the equator. Therefore, such a particle does not have a resultant dipole moment, it behaves in a manner similar to an arrangement of four charges known as a quadrupole.

The Quadrupole Hamiltonian may be expressed as:

$$\hat{H}_Q = \left(e^2 q_{z'z'} Q\right)\left(3\hat{S}_{z'}^2 - \hat{S}^2\right) / 4S(2S-1)$$

This may then be expressed in frequency terms, for a spin-1 nucleus such as ^{14}N:

$$h^{-1}\hat{H}_Q = (e^2 q_{z'z'} Q / 4)(3\hat{S}_{z'}^2 - \hat{S}^2)$$

where $e^2 q_{z'z'} Q/h$ is known as the quadrupole coupling constant, χ. This depends upon the nucleus (through eQ) and on the distribution of electrons in its surroundings (through $eq_{z'z'}$). Since electrons in s orbitals have spherically symmetric charge distributions, nuclear quadrupole moments are not sensitive to them. However, since p orbitals show axial symmetry along the orbital axis, it is lack of symmetrical occupancy of these orbitals that is primarily responsible for the $e^2 q_{z'z'}$ factor. χ values may be obtained through nuclear quadrupole resonance spectroscopy, and for ^{14}N these may range from 1-5 MHz.

Since the equation above is expressed as a function of the operator $\hat{S}_{z'}$ acting along the main axis z' of the efg, it is necessary to express it in the Zeeman frame as a function of the operators $\hat{S}_{x,\ y,\ z}$ defined in the frame where the z axis is coincident with B_o. After manipulation of the equation, the result may be expressed as an alphabetical expansion:

$$h^{-1}\hat{H}_Q = \left(\frac{\chi}{4}\right)\left(\hat{A}_Q + \hat{B}_Q + \hat{C}_Q + \hat{D}_Q + \hat{E}_Q + \hat{F}_Q\right)$$

Where:

$$\hat{A}_Q = 3\hat{S}_z^2\cos^2\theta - \hat{S}^2$$

$$\hat{B}_Q = (3/2)(\hat{S}_+\hat{S}_- + \hat{S}_-\hat{S}_+)\sin^2\theta$$

$$\hat{C}_Q = (3/2)(\hat{S}_+\hat{S}_z + \hat{S}_z\hat{S}_+)\sin\theta\cos\theta\exp(-i\phi)$$

$$\hat{D}_Q = (3/2)(\hat{S}_-\hat{S}_z + \hat{S}_z\hat{S}_-)\sin\theta\cos\theta\exp(i\phi)$$

$$\hat{E}_Q = (3/4)(\hat{S}_+^2)\sin^2\theta\exp(-2i\phi)$$

$$\hat{F}_Q = (3/4)(\hat{S}_-^2)\sin^2\theta\exp(2i\phi)$$

6.2.1.2 The Dipolar Hamiltonian

The classical energy due to the interaction of two magnetic vector moments, μ_1 and μ_2, separated by distance r is:

$$E = \left(\frac{\mu_0}{4\pi}\right)\left(\frac{1}{r^3}\right)\left[\mu_1\cdot\mu_2 - \frac{3(\mu_1\cdot r)(\mu_2\cdot r)}{r^2}\right]$$

If μ is replaced as a function of the spin operators, the corresponding quantum mechanical Hamiltonian for the dipolar coupling between the I and S spins will be:

$$\hat{H}_D = \left(\frac{\mu_0}{4\pi}\right)\left(\frac{\gamma_I\gamma_S\hbar^2}{r^3}\right)\left[\hat{I}\cdot\hat{S} - \frac{3(\hat{I}\cdot r)(\hat{S}\cdot r)}{r^2}\right]$$

Dividing by frequency units gives:

$$h^{-1}\hat{H}_D = D\left[\hat{I}\cdot\hat{S} - \frac{3(\hat{I}\cdot r)(\hat{S}\cdot r)}{r^2}\right] \qquad D = \left(\frac{\mu_0}{4\pi}\right)\left(\frac{\gamma_I\gamma_S h}{4\pi^2 r^3}\right)$$

where D is the dipolar I, S coupling constant. (D is approximately 716 Hz for a typical directly-bonded ^{13}C, ^{14}N spin pair around 1.45 Å apart.)

The Dipolar Hamiltonian may also be described by an alphabetic expansion. This is useful since in calculations it is necessary to express the products $\hat{I} \cdot \hat{S}$, $\hat{I} \cdot r$ and $\hat{S} \cdot r$ as a function of the corresponding Cartesian components: $\hat{I} \cdot r = \hat{I}_x r_x + \hat{I}_y r_y + \hat{I}_z r_z$.

If the r direction is given by angles θ and ϕ, then

$r_x = r \sin\theta \cos\phi$

$r_y = r \sin\theta \sin\phi$

$r_z = r \cos\theta$

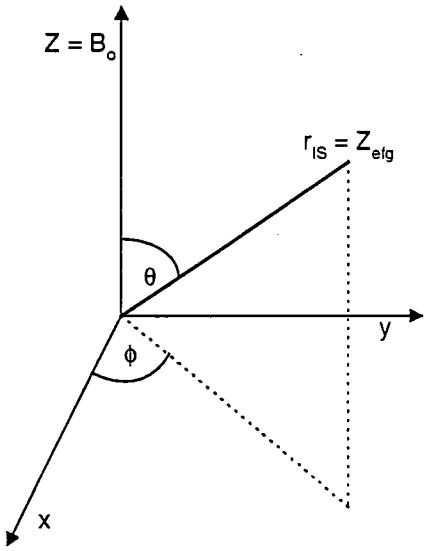

Figure 1 Zeeman coordinate frame x,y,z and location of the internuclear vector r and the z axis of the efg at the quadrupolar nucleus.

Thus the equation may now become represented in the following alphabetical form, similar to the expansion shown for the quadrupolar Hamiltonian:

$$h^{-1}\hat{H}_D = D(\hat{A}_D + \hat{B}_D + \hat{C}_D + \hat{D}_D + \hat{E}_D + \hat{F}_D)$$

where terms $\hat{A}$ to $\hat{F}$ may be derived as follows:

$$\hat{A}_D = \hat{I}_Z \hat{S}_Z (1-3\cos^2\theta)$$
$$\hat{B}_D = -(1/4)(\hat{I}_+ \hat{S}_- + \hat{I}_- \hat{S}_+)(1-3\cos^2\theta)$$
$$\hat{C}_D = -(3/2)(\hat{I}_+ \hat{S}_Z + \hat{I}_Z \hat{S}_+)\sin\theta\cos\theta\exp(-i\phi)$$
$$\hat{D}_D = -(3/2)(\hat{I}_- \hat{S}_Z + \hat{I}_Z \hat{S}_-)\sin\theta\cos\theta\exp(i\phi)$$
$$\hat{E}_D = -(3/4)(\hat{I}_+ \hat{S}_+)\sin^2\theta\exp(-2i\phi)$$
$$\hat{F}_D = -(3/4)(\hat{I}_- \hat{S}_-)\sin^2\theta\exp(2i\phi)$$

6.2.1.3 Perturbation Theory[14]

This approach is a powerful tool that can be used to solve, to a good degree of approximation, problems in which the Hamiltonian can be decomposed into two parts: $\hat{H} = \hat{H}_O + \hat{H}_P$, where $\hat{H}_O$ is the main Hamiltonian and $\hat{H}_P$ is the perturbing Hamiltonian such that, if these are proportional to a and b, respectively, $a>>b$.

Supposing we know that the eigenfunctions of $\hat{H}_O$ are $|\psi_i\rangle$, perturbation theory allows us to expand the eigenvalues E_i of $\hat{H}$ as follows:

$$E_i = {}^{O}E_i(a) + {}^{1}E_i(b) + {}^{2}E_i(b^2/a) + \ldots$$

${}^{0}E_i$, ${}^{1}E_i$ and ${}^{2}E_i$ are approximations of the zero, first, and second order to E_i.

If no perturbation were present, the zero-order value, ${}^{0}E_i$, is the energy the system would have and this depends linearly upon a. Successive n[th]-order corrections, ${}^{n}E_i$ depend on (b^n/a^{n-1}) and decrease as n increases.

According to this theory:

$${}^{0}E_i = \langle \psi_i | \hat{H}_O | \psi_i \rangle$$
$${}^{1}E_i = \langle \psi_i | \hat{H}_P | \psi_i \rangle$$
$${}^{2}E_i = \sum_{j \neq i} \frac{\langle \psi_i | \hat{H}_P | \psi_j \rangle \langle \psi_j | \hat{H}_P | \psi_i \rangle}{({}^{0}E_i - {}^{0}E_j)}$$

6.2.1.4 Solution of the Zeeman and Dipolar Hamiltonians

The Zeeman Hamiltonian for two non-interacting spins can be shown as

$$E = -\mu_0 \cdot B_0 = -\mu_Z \cdot B_0$$

If the z axis is selected as parallel to B_0, one can obtain the analagous quantum mechanical equation by replacing the classical vector, μ, with the operator $\mu\hbar\hat{I}$ (or $\mu\hbar\hat{S}$ for the S spins). Therefore, when only I spins are present, the Zeeman Hamiltonian is:

$$\hat{H}_Z = -\gamma\hbar\hat{I} \cdot B_0 = -\gamma\hbar B_0 \hat{I}_Z$$

If both I and S spins are present, this becomes:

$$\hat{H}_Z = -\gamma_I \hbar B_O \hat{I}_Z - \gamma_I \hbar B_O \hat{S}_Z$$

This may be divided by Planck's constant to give the frequency Hamiltonian:

$$h^{-1}\hat{H}_Z = -\nu_I \hat{I}_Z - \nu_S \hat{S}_Z$$

where $\nu = \frac{\gamma B_0}{2\pi}$ is the resonance frequency of each nucleus.

The spin functions $|m_I\rangle$ and $|m_S\rangle$, which form the basis sets for I and S spins, are eigenfunctions of the spin operators $\hat{I}_Z$ and $\hat{S}_Z$, respectively. Appropriate eigenfunctions can be constructed as products of the individual spin functions as follows:

$$|\psi_1\rangle = |\tfrac{1}{2},1\rangle$$
$$|\psi_2\rangle = |\tfrac{1}{2},0\rangle$$
$$|\psi_3\rangle = |\tfrac{1}{2},-1\rangle$$
$$|\psi_4\rangle = |-\tfrac{1}{2},1\rangle$$
$$|\psi_5\rangle = |-\tfrac{1}{2},0\rangle$$
$$|\psi_6\rangle = |-\tfrac{1}{2},-1\rangle$$

i.e. in general, $|\psi_i\rangle = |m_I, m_S\rangle$ (where $I = {}^{13}C$ and $S = {}^{14}N$).

Thus, if the Zeeman Hamiltonian acts on the six eigenfunctions above, six equations of the form $h^{-1}\hat{H}_Z|\psi_i\rangle = |\upsilon_i\psi_i\rangle$ result, from which $E_i = h\upsilon_i$ are the allowed energies. Thus, for level 1, with spin function $|\tfrac{1}{2},1\rangle$, the energy becomes $-\frac{\nu_I}{2}-\nu_S$. For level two (spin function $|\tfrac{1}{2},0\rangle$), the energy becomes $-\frac{\nu_I}{2}$. Carrying on this derivation, it can be proved that the spectra of both the *I* and *S* nuclei consist of single lines, centred at ν_x, where x is *I* or *S*.

Next, we can add the possibility of a mutual interaction through the dipolar coupling, $\hat{H}_D$. A complete Hamiltonian for this would therefore be:

$$h^{-1}\hat{H} = h^{-1}(\hat{H}_Z + \hat{H}_D) = -\nu_I\hat{I}_Z - \nu_S\hat{S}_Z + D\left[\hat{I}\cdot\hat{S} - \frac{3(\hat{I}\cdot r)(\hat{S}\cdot r)}{r^2}\right]$$

Therefore, since the value of D is of the order of kHz and the Zeeman frequencies, ν_S and ν_I, are MHz, we now therefore have a Hamiltonian that can be split into two parts, $\hat{H}_Z$ and $\hat{H}_D$ (the perturbation).

Using perturbation theory, a first-order approximation to the allowed energies may be found by correcting the zero-order energies (i.e. in absence of the perturbation) with $\langle\psi_i|\hat{H}_D|\psi_i\rangle$, where $|\psi_i\rangle$ are the eigenfunctions of $\hat{H}_Z$.

Only the alphabetic $\hat{A}_D$ term, the so-called 'secular' term of the alphabetic expansion of the Dipolar Hamiltonian produces a non-vanishing value of $\langle\psi_i|\hat{H}_D|\psi_i\rangle$. This is because $|\psi_i\rangle = |m_I, m_S\rangle$ are eigenfunctions of the product $\hat{I}_Z\hat{S}_Z$, but not of any of the other operator products of the alphabetical expansion, terms $\hat{B}_D$ to $\hat{F}_D$.

Therefore, the first-order approximation is called the 'secular approximation' and the allowed energies may then be calculated, for example:

$$\begin{aligned} \nu_1 &= -\frac{\nu_I}{2} - \nu_S + \langle \psi_1 | \hat{A}_D | \psi_1 \rangle \\ &= -\frac{\nu_I}{2} - \nu_S + \langle \tfrac{1}{2},1 | \hat{I}_Z \hat{S}_Z (1 - 3\cos^2\theta) | \tfrac{1}{2},1 \rangle \\ &= -\frac{\nu_I}{2} - \nu_S + D\frac{(1-3\cos^2\theta)}{2} \end{aligned}$$

The other allowed energies and transitions may also be calculated in this way. The spectra may now be expected to be a 1:1:1 triplet for I and a 1:1 doublet for S, each with spacing of $D(1\text{-}3\cos^2\theta)$.

6.2.1.5 The effect of Magic Angle Spinning

Next, the effect of MAS has to be taken into account. All the above discussion calculations assumed a single crystal. However, in a microcrystalline sample (the usual case) all orientations of θ are present giving broad and complex lines. By rotation at 54.7 ° (the magic angle) the chemical shift anisotropy is averaged and, by rotating faster than the value of *D* (the Dipolar Coupling constant) the term $(3\cos^2\theta - 1)$, collapses to zero, removing the dipolar coupling contribution.

Therefore, the next step is to take the quadrupolar Hamiltonian into account as this causes the complication in the spectra of spin-½ nuclei directly bonded to ^{14}N since, unlike the dipolar Hamiltonian, spinning at the magic angle does not average out all of the terms and contributions to the lineshape to zero.

The complete Hamiltonian for two spins, *I* and *S*, both interacting with a magnetic field, B_o, mutually coupled through magnetic dipole-dipole interactions, and including the interaction of *S*-spins with the surrounding electric field gradient is:

$$h^{-1}\hat{H} = h^{-1}\left(\hat{H}_Z + \hat{H}_D + \hat{H}_Q\right).$$

Both $\hat{H}_D$ and $\hat{H}_Q$ consist of alphabetic expansions:

$$h^{-1}\hat{H} = -\nu_I \hat{I}_Z - \nu_S \hat{S}_Z + D(\hat{A}_D + \hat{B}_D + \hat{C}_D + \hat{D}_D + \hat{E}_D + \hat{F}_D) + \left(\frac{\chi}{4}\right)(\hat{A}_Q + \hat{B}_Q + \hat{C}_Q + \hat{D}_Q + \hat{E}_Q + \hat{F}_Q)$$

Therefore, perturbation theory may again be used, this time taking $\hat{H}_Z$ as the main Hamiltonian (~14 MHz for ^{14}N in a field B_o ~4.7 T), and the sum $(\hat{H}_D + \hat{H}_Q)$ as the perturbation (D ~716 Hz, and χ ~3 MHz). Now, by applying first order perturbation theory as before, energy levels result that are perturbed because of the quadrupolar interaction. However, these are caused by the secular terms $\hat{A}_Q$ and $\hat{B}_Q$, but no net effect is observed on the transition frequencies $\nu_{1\text{-}4}$, $_{2\text{-}5}$, and $_{3\text{-}6}$ because the effect is only upon the *S* transition frequencies, not on those corresponding to *I* and therefore the effects cancel out. Therefore, we must continue to explore second-order effects using perturbation theory. Following on from the equation described in section 6.2.1.3, the second-order perturbation term may be taken as:

$$^2E_i = \sum_{j \neq 1} \frac{\langle \psi_i | \hat{H}_D + \hat{H}_Q | \psi_j \rangle \langle \psi_j | \hat{H}_D + \hat{H}_Q | \psi_i \rangle}{^0E_i - ^0E_j}$$

In this case, the '*C* and *D*' term of the quadrupole Hamiltonian is the one in which the contributions in $D\chi$ do not vanish. Since these terms are sensitive to *I* spins (combined with quadrupolar contributions) it is from calculation of the effect of these terms on the energies that the lineshapes of RDC resonances may be derived since MAS cannot remove these second-order shifts on the *I* lines due to their not possessing a factor $(3\cos^2\theta\text{-}1)$.

Also, the angular dependence of the microcrystallites' orientations causes the individual components of the resulting lineshape to be inhomogeneously broadened, forming powder patterns. Since $\nu_{1\rightarrow4} = \nu_{3\rightarrow6}$ are both shifted from the unperturbed υ_I resonance by half the shift obtained for $\upsilon_{2\rightarrow5}$, and in the opposite direction the final I(^{13}C) line will be

an asymmetric doublet with a splitting dependent upon the $\tilde{C}_Q$ and $\tilde{D}_Q$ terms (see ***Figure 2***). The weighted average resonance position will be the true chemical shift, ν_c.

J coupling can affect the residual dipolar coupling pattern inferred upon the spin-½ spectra, but for the ^{13}C, ^{14}N case, the J_{NC}^{iso} value is negligible.

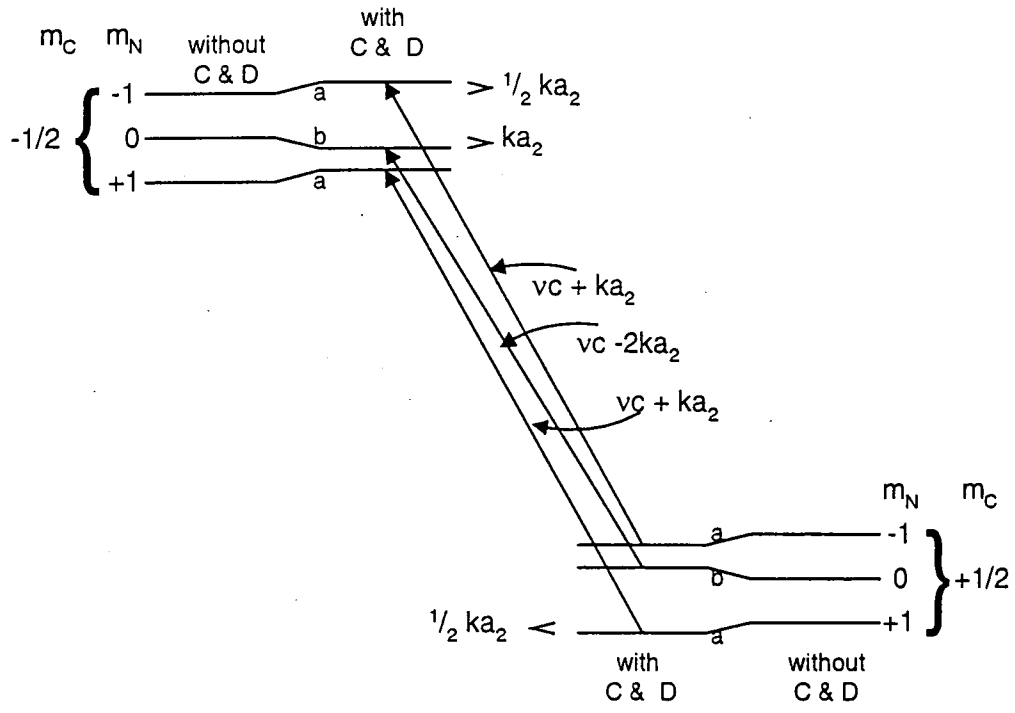

Figure 2 Energy Level diagram illustrating second-order quadrupolar (I=1) effects transferred to spin-1/2 spectra.

From ***Figure 2*** it is evident that two of the transitions are degenerate and therefore a 2:1 doublet is predicted. Factors C and D are higher-order terms of the dipolar Hamiltonian. The magnitudes of the second-order energy shifts a and b are ½ ka_2 and ka_2 respectively, where the factor k depends upon angular terms, so each part of the spectrum is a powder pattern. Therefore, resonances occur with intensity ratio 1:2 at $\nu_C - 2ka_2$ and $\nu_C + ka_2$, respectively.

The splitting pattern of a spin-1/2 nucleus bonded directly to a ^{14}N nucleus is shown in ***Figure 3***, which shows the effect of simultaneous coupling to three adjacent ^{14}N atoms.

The bracketed numbers e.g. (± 1) indicate the energy levels between which the transitions are taking place to form a particular resonance. In a.) no splitting occurs, in b.), RDC to one ^{14}N gives rise to an asymmetric doublet with splitting of 3a. This pattern is propagated through c.) and d.) with splitting magnitudes of 3b and 3c, respectively. For simplicity, this scheme assumes the same sign of splitting for all ^{14}N centres. (Peak positions in d.) are, from highest to lowest frequency: a+b+c, a+b-2c, a-2b+c, a-2b-2c, b-2a+c, b-2a-2c, -2a-2b+c, -2a-2b-2c.

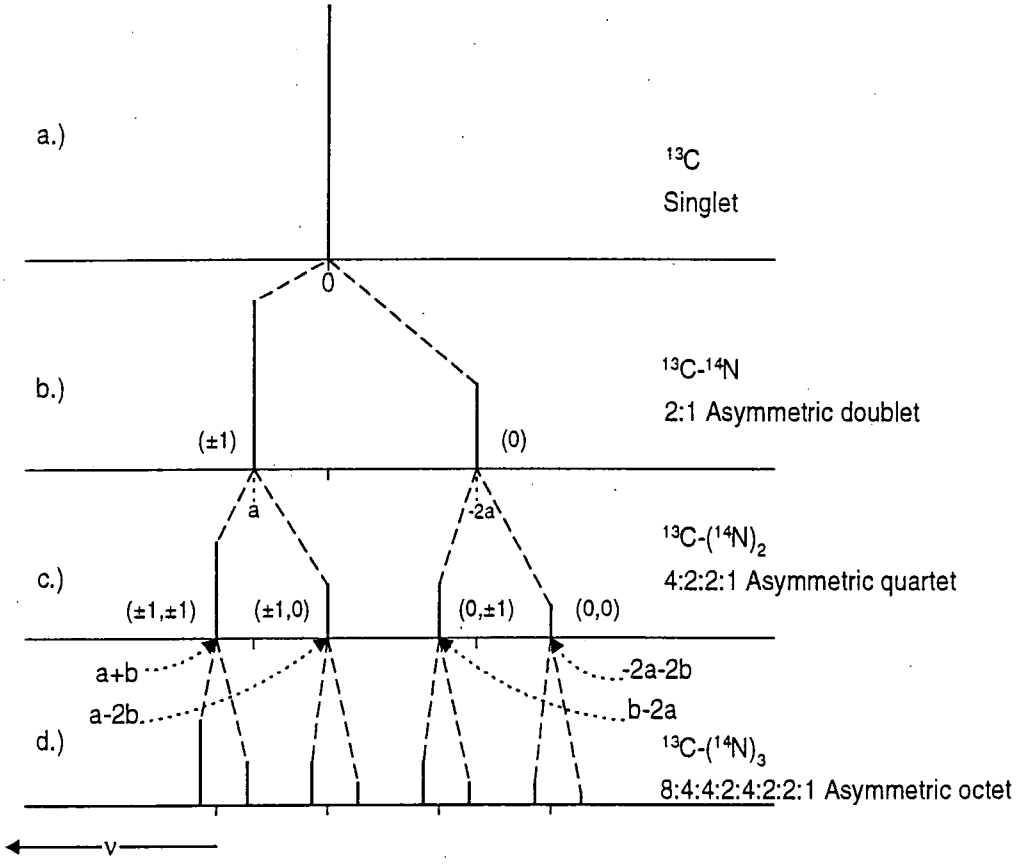

Figure 3 'Stick' spectra illustrating successive splitting of the carbon signal under the influence of three residual (^{13}C, ^{14}N) dipolar couplings (not to scale).

The residual splitting depends on a variety of molecular and structural factors including: the quadrupole coupling constant (χ); the orientation of the internuclear vector r_{CN} in the PAS of the efg given by the polar and azimuthal angles β^D and α^D; the asymmetry

parameter of the efg tensor (η); the dipolar coupling constant (D) and the Zeeman frequency of the ^{14}N (Z_N).

The theory behind the RDC phenomenon is now well understood[14]. Perturbation theory[8] has been used to produce the equation for the splitting magnitude equation. This approach is particularly relevant to the analysis of the RDC situation where the Zeeman interaction is considered to be large enough so the ^{14}N quadrupole Hamiltonian can be treated as a perturbation. Using theoretical methods, it is also possible to simulate[23,24,25,26] the powder bandshapes for nuclei bound to quadrupolar nuclei.

The splitting of the asymmetric doublet may be given by the equation[16]:

$$s = \left(\frac{9}{20}\right)\left(\frac{D\chi}{Z_N}\right)\left[\left(3\cos^2\beta^D - 1\right) + \eta\sin^2\beta^D\cos 2\alpha^D\right]$$

$\chi = \dfrac{e^2 Q q_{zz}}{h}$ = Quadrupolar coupling constant

η = Asymmetry parameter of the efg tensor

$Z_N = \gamma_N B_0/2\pi$ = Zeeman frequency of ^{14}N in the applied field

$D = \dfrac{\gamma_C \gamma_N h}{4\pi r_{CN}^3}$ = Dipolar coupling constant

α^D, β^D = The polar and azimuthal angles that define the orientation of the internuclear vector in the principal axis system of the efg at ^{14}N. (See ***Figure 4.***)

Thus, s can be estimated if all the geometric (β^D, α^D, r_{CN}) and energetic (χ, η, Z_N) factors are known. It should be noted that this research has proved extremely challenging due to the fact that very few, if any, of these factors are known for the compounds being studied within this Ph.D. research.

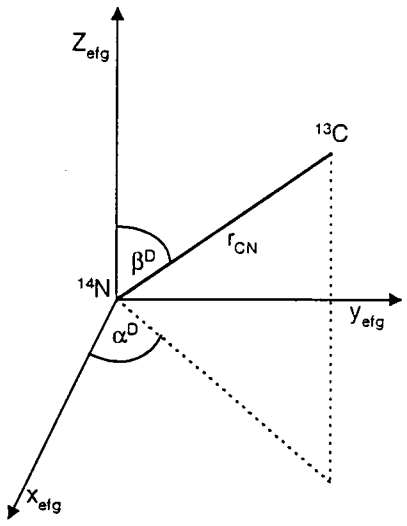

Figure 4 Definition of the Euler angles α^D β^D (γ^D=0) orienting the ^{13}C, ^{14}N internuclear vector in the ^{14}N efg PAS.

Thus, it has been established that the appearance of spectra depends upon the size of the quadrupolar interaction and the orientation of the efg tensor with respect to the internuclear vector, r_{CN}. The processes that may influence the magnitude and orientation of the efg tensor at a ^{14}N atom may include molecular motion, phase transitions, plus formation or breaking of hydrogen bonds and conformational changes.

6.3 C-13 spectra

The potential for extraction of molecular and structural information from ^{14}N residual dipolar coupling effects in ^{13}C CP/MAS spectra provides the impetus for the rigorous analysis of the ^{13}C spectra. Thus, it is the main aim of this chapter to relate the ^{13}C bandshapes to absolute and relative structural differences in the two main polymorphic systems studied.

These provide an interesting contrast, from BRL55834, which contains one ^{14}N location, to BRL61063, which possesses five separate ^{14}N sites. The differences in the manifestation of the RDC effects in the ^{13}C CP/MAS spectra of the polymorphic forms of these systems, combined with the corresponding lack or existence of crystallographic

data, also provide interesting 'footholds' on which to develop the analysis, and validate any conclusions that may be drawn.

In the following sections I will attempt the complex analysis of the ^{13}C spectra that are influenced by adjacent ^{14}N nuclei.

6.3.1 BRL55834

There are large differences between the way in which residual dipolar coupling effects are manifested in the ^{13}C CP/MAS spectra of the two polymorphic forms of BRL55834 (see ^{13}C spectra, chapter 4). In the spectra of form II of BRL55834, the crystallographic splitting of the peaks (caused by the existence of three molecules in the asymmetric unit) is further complicated by asymmetric doublets, which are observed for the resonances assigned to carbon locations 14, 18 and 4. However, the corresponding resonances in the spectra of form I show only a broadening, because any splitting is of much smaller magnitude.

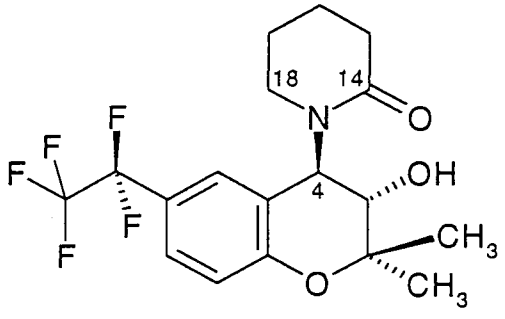

Figure 5 Molecular diagram of BRL55834 showing the numbering of atoms immediately adjacent to the ^{14}N

6.3.1.1 BRL55834 Form I

Surprisingly, no residual dipolar splitting is visible for the resonances of C(14), (4) and (18) in the spectra of form I, possibly because of unfavorable angles α^D and β^D. However, these resonances are significantly broadened in comparison to the remaining peaks in the

spectrum (see ***Table 1***). This indicates the existence of a value of 's' that is too small to be resolved at our operating field (B_0).

Assignment	Shift / ppm	$\Delta\nu_{1/2}$ / Hz
C (14)	172.9	80
C (4)	52.7	110
C (18)	42.3	124

Table 1 Summary of residual dipolar coupling phenomena exhibited in the ^{13}C CP/MAS spectra of BRL55834, form I.

6.3.1.2 BRL55834 Form II

C13 CP/MAS spectra of form II are much more complicated due to the fact that the residual dipolar splittings are superimposed upon a spectrum that possesses complex crystallographic splitting patterns (see ***Table 2***). These factors combine to produce a spectrum that may have almost fifty different peaks, of which not all are resolvable, due to overlap. The resonances assigned to C(14) are fairly well separated, and provide an interesting case for analysis and comparison with previous results quoted in the literature.

A comparison of the observed splittings (*s*) for form II was made with those quoted in the literature[27,28] for the ribonucleoside molecules cytidine and uridine (***Figure 6***). The 'N(1)' atoms in those compounds show a similar chemical configuration to the N(13) present in BRL55834. It is assumed that the z axis of the quadrupole tensor points along the lone pair orbital which is taken to be perpendicular to the NR_3 group (assumed to be essentially planar), therefore causing the angle β^D to be 90°. The asymmetry parameter is assumed to be zero, implicitly causing the angle α^D to be irrelevant. The individual $r_{N\text{-}C}$ values were taken from data for the appropriate N-C distances in the ribonucleosides and χ is taken to be approximately –3 MHz[28] (see ***Table 3***).

Assignment	Weighted mean isotropic shift /ppm	Comments
14	178.0, 173.4, 171.2	Three sets of asymmetric doublets are visible of which one is particularly well separated, and to higher frequency than the other two – due to H-bonding of the carbonyl in one of the molecules?
4	55.4-51.8 (range)	One broad, composite peak is visible.
18	43.5-39.3 (range)	One broad, composite peak is visible.

Table 2 Summary of the residual dipolar coupling phenomena exhibited in the ^{13}C CP/MAS spectra of BRL55834, form II.

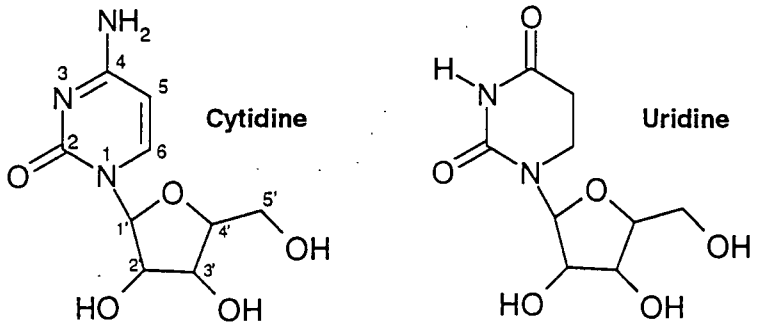

Figure 6 Numbered molecular diagrams of ribonucleoside molecules used to compare ^{14}N residual dipolar coupling effects with those observed in BRL55834.

Reference molecule	^{13}C-^{14}N	$^{13}C^{a}$	r_{C-N}/ Å	β^{D}	s/ Hz Literature	s/ Hz Experimental
Cytidine[b]	C(2)-N(1)	14	1.379	90	78	83
	C(6)-N(1)	18	1.368	90	79.5	95
	C(1)-N(1)	4	1.497	90	60.5	65
Uridine[c]	C(2)-N(1)	14	1.371	90	86	83
	C(6)-N(1)	18	1.369	90	86.5	95
	C(1)-N(1)	4	1.490	90	67	65

[a] Identifies the ^{13}C-N bond in BRL55834 most similar or the given C-N bond in the reference molecule. [b] Cytidine N(1): χ = -3 MHz, η = 0. [c] Uridine N(1): χ = -3.28 MHz, η = 0. [d] In all cases quoted, s is positive (i.e. a 1:2 doublet is seen). [e] This work.

Table 3 Comparison of ^{13}C, ^{14}N residual dipolar splittings (s) at 50 MHz for selected ribonucleosides and form II of BRL55834.

The splitting magnitudes for form II seem to be of similar order to those given in the literature (see ***Table 3***), although the larger values observed in our experiments seem to suggest that our χ values may be slightly greater, or to imply that C-N bond lengths in BRL55834 may be shorter than those extracted from the literature. The most extreme difference is for the C(18)-N bond which therefore is probably significantly shorter than the N(1)-C(6) bond in the two ribonucleosides. Of course, the relevant ^{13}C signals are powder patterns, so that the values of *s* are subject to significant errors (*ca.* ±4 Hz).

The observation of three asymmetric doublets of 2:1 intensity for the C(14) resonance for form II may be explained by the existence of three molecules in the crystallographic asymmetric unit (as mentioned in chapter 4).

6.3.2 BRL61063

Due to the presence of five nitrogen atoms within the molecular structure of BRL61063, the splitting that may be attributed to residual dipolar coupling of individual carbon atoms is much more involved than in BRL55834, where there are only three carbons that are directly affected by the singular ^{14}N nucleus.

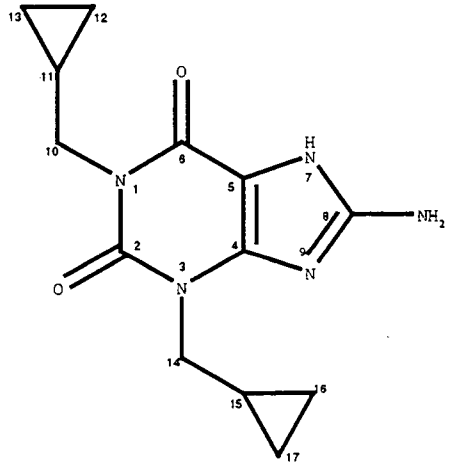

Figure 7 Structure and atomic numbering of BRL61063

As may be observed from ***Figure 7***, carbon atoms (5), (6), (10) and (14) are adjacent to one nitrogen atom, whilst (2) and (4) are adjacent to two nitrogen atoms, and carbon (8) is

directly bonded to three nitrogen atoms. This therefore potentially confers a much greater degree of complexity on the ^{13}C spectra, and residual dipolar splitting patterns will be much more complex. ***Figure 3*** shows the splitting effect of more than one ^{14}N atom upon the resonance of a ^{13}C atom.

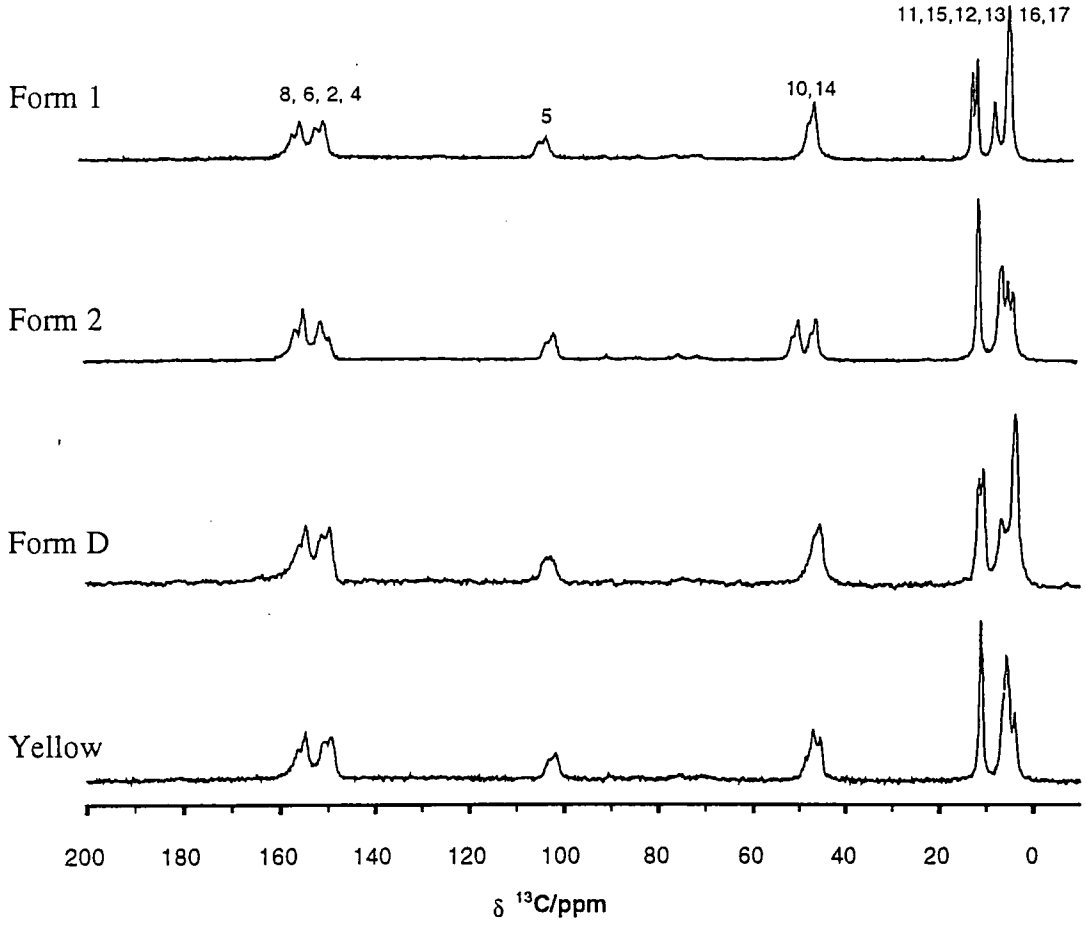

Figure 8 Comparison of ^{13}C spectra of the four polymorphs of BRL61063 showing asymmetric doublets for carbon atoms 10, 14 and 5. (50.329 MHz, 1 ms ct, 9 s rd, cp4_pm, 4 kHz MAS, 220 transients).

The more complex splitting which is caused by coupling to multiple nitrogen atoms is virtually impossible to resolve due to peak overlap. A knowledge of interatomic distances from X-ray crystallography for some polymorphs of BRL61063 (see chapter 3) provides a

factor that allows comparisons to be made with splitting magnitudes that are quoted in the literature.

The ^{13}C CP/MAS spectra of the polymorphs of BRL61063 demonstrate that the ^{13}C resonances for carbons (8), (6), (2), (4), (5), (10) and (14) each show asymmetric broadening effects. The resonances that are the more simple to analyse are those for carbons (5), plus (10) and (14), each of which shows an asymmetric 1:2 doublet with the highest intensity peak at lowest frequency, caused by coupling to a single ^{14}N nucleus.

Carbon site (5)

A summary of the splittings observed for carbon (5) in BRL61063 and a comparison with the literature values quoted using the ribonucleoside molecule, uridine (see **Figure 6**) is presented in ***Table 4***. Literature values suggest a splitting of ~90 Hz, which is fairly close to the splittings observed in each form for C(5) (~70 Hz). (Initially a comparison was made with the C(5) location in adenosine and guanosine, but this suggested the existence of negligible splittings, and since N(7) is obviously protonated in BRL61063, and therefore possesses a different relative orientation of the efg, it was decided to compare this with the protonated N(3) site in uridine instead.) The difference between the experimentally observed splittings and the literature values may be attributed to geometrical differences between a six- and a five-membered ring.

Uridine	χ/ MHz	η	$r_{C\text{-}N}$/ Å	β^D/ °	α^D/ °	S/ Hz				
						Literature	Form 1	Form 2	Form D	'Yellow'
C(4)-N(3)	-2.71	0.46	1.38	90	63.4	89	77	79	70	67
C(2)-N(3)			1.37	90	63.4	91				

Table 4 Comparison of literature and experimental values for s/ Hz for C(5) using the N(3) atom of the ribonucleoside molecule, uridine.

Carbon sites (10) and (14)

Splitting of the asymmetric doublets may be measured for carbons 10 and 14. In form 2 these resonances are separate and have splitting magnitudes of 63 and 51 Hz, respectively (see ***Table 5***). In the spectra of form 1, *s* is 53 Hz, and in 'form 3', 56 Hz. It is difficult to measure the splitting in 'yellow' due to an unclear splitting pattern existing. Carbons (10) and (14) are adjacent to N(1) and (3), respectively. From single-crystal XRD these carbon-nitrogen bond lengths are known to be similar both within each polymorph and between the individual polymorphic forms. The only exception is for the $r_{C(14)\text{-}N(3)}$ bond distance, which has a maximum value of 1.486 Å in form 2, yet is 1.476 Å in form 4 and only 1.461 Å in form 1. This variation of 0.025 Å will alter D by 35 Hz and therefore, due to the direct dependence of *s* upon D, it may be expected to cause a noticeable difference in the coupling effects. This does appear strikingly obvious on comparison of the spectra. For form 2, the added complication/ simplification (depending upon how one thinks of it) exists in that the two ^{13}C resonances exist as separate asymmetric doublets. This phenomenon may allude to mobility differences, with these pendant cyclopropyl groups being less mobile than those in form 1 and thus becoming individually resolvable upon the NMR timescale for form 2. The splittings for these groups are of the same sense i.e. 1:2 with the higher intensity peak at lower frequency.

C(1')-N(1)	χ/ MHz	η	$r_{C\text{-}N}$/ Å	β^D/ °	α^D/ °	s/ Hz (± 4 Hz)				
						Literature	Form 1	Form 2	Form D	'Yellow'
Cytidine	-3	0	1.497	90	-	60	53	63	56	unclear
Uridine	-3.28	0.02	1.49	90	-	67		51		

Table 5 Comparison of literature and experimental values for s/ Hz for C(10) and C(14) using the C(1')-N(1) data of uridine and cytidine.

It has been suggested[22,27] that NR_3 groups possess values of χ of the order of –3 MHz with the z axis pointing along the lone pair orbital. In view of the small values of η

adopted for these situations, the exact locations of the x and y axes become unimportant (see ***Figure 10d***).

The experimental data therefore agree quite well with the data observed for the 'sugar' (NR_3) sites in uridine and cytidine (see ***Table 5***). The larger splitting for the lower frequency asymmetric doublet in form 2 suggests that this may be assigned to the group with the lower $r_{C\text{-}N}$, i.e. C(10)-N(1).

Carbon sites (8), (6), (2) and (4)

The complex splitting pattern expected for carbons 8, 6, 2, and 4 is virtually impossible to resolve as the resonances, each of which are split by one, two or three adjacent ^{14}N atoms occur within a small range and thus overlap each other. However, the pattern does appear as two asymmetric doublets, the splitting of which may be measured. An interesting point may be noted in that, whilst the pattern exists as a 1:2:1:2 pattern for forms 1, '3' and 'yellow', form 2 shows an apparent 1:2:2:1 pattern. This indicates at least a variation in the relative orientation of the efg tensor with respect to the PAS of the molecule in form 2. This may be induced by hydrogen bonding, as X-Ray data for form 2 lead us to believe that form 2 does exhibit intermolecular hydrogen bonding of a very different nature to form 1 as both amide protons are involved in hydrogen bonds in form 2. However, it is not clear which particular carbon resonance this effect on the spectrum may be attributed to.

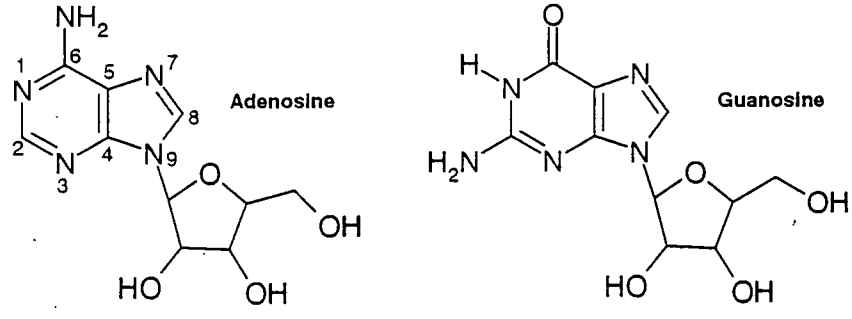

Figure 9 Structure of two ribonucleoside molecules used to compare parameters for RDC with BRL61063.

The data that are known for the ribonucleoside molecules adenosine and guanosine (***Figure*** 9), will be used to compare with results observed in the spectra of BRL61063.

It has been suggested[16] that the splitting conferred upon a carbon nucleus directly bound to a N atom similar to N(9) in BRL61063 (such as C(4) and (8)) may be expected to be negligible due to the special orbital arrangement around this type of nitrogen location (see ***Table 6***). The principal z axis of the efg at imino nitrogens in heterocyclic compounds has been located in the plane of the molecule, directed towards the lone pair and with χ negative. In the gas phase, the y axis for pyridine and imidazole has been proposed to be perpendicular to the molecular plane. However, ***Figure 10c*** shows the most probable orientation of the principal axes in -N= groups in solid imidazole and nucleoside bases. In these molecules, the x and y axes are interchanged owing to the presence of hydrogen bonding. Therefore this orientation infers an angle β^D between 50° and 60°. For these values of β^D the term $(3\cos^2\beta^D - 1)$ becomes small, and hence the splittings *s* induced by these types of nitrogens are taken to be very small and thus may be neglected.

C(5)-N(7)	χ/ MHz	η	r_{CN}/ Å	β^D/ °	α^D/ °	s/ Hz (± 4 Hz)				
						Literature	Form 1	Form 2	Form D	'Yellow'
Adenosine	-3.2	0.16	1.386	52	90	-3	Can not be resolved			
Guanosine	-3.15	0.47	1.385	51.7	90	2				

Table 6 Comparison of literature and experimental values for s/ Hz for the expected C(4)-N(9), and C(8)-N(9) splittings in BRL61063.

Since the geometry and measured bond lengths in BRL61063 do not deviate much from those observed in guanosine and adenosine, it may be derived that the splitting pattern, though not resolvable in the ^{13}C CP/MAS spectra of BRL61063, will be identical to that expected from comparison with the literature. These factors may be influenced by the

donation of a hydrogen onto the N(9) lone pair in BRL61063, this may be effected by the intermolecular hydrogen bonding to the N(9) site in form 2.

This therefore leaves the splitting pattern of carbon (8), which is surrounded by three nitrogen atoms, to be predicted. Consultation of the literature shows that a large s value should exist for coupling to an NH_2 group (130 Hz is suggested for a C-N bond length of 1.34 Å). Analysis of crystallographic data from the polymorphs of BRL61063 shows that the C-N bond varies between forms (1.357, 1.344, 1.352Å for forms 1, 2 and 4, respectively), with the shorter bond length corresponding with the greater degree of hydrogen bonding from the amide protons. Once again, coupling to N(9) should result in negligible splitting of the carbon resonance due to the reasons described above. Finally, the splitting caused by coupling to N(7) should be of a magnitude of approximately 80 Hz. This discussion is summarised in ***Table 7*** below and ***Figure 11***.

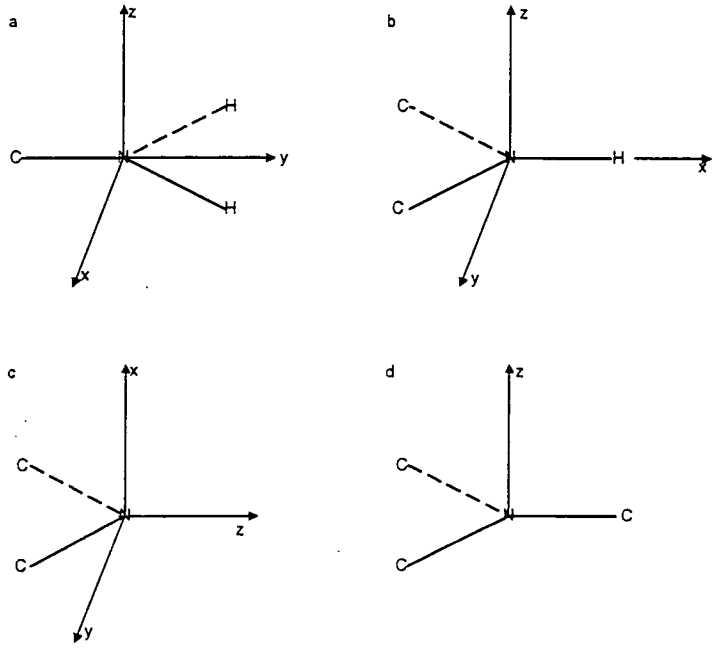

Figure 10 Vector diagrams showing proposed orientations of the quadrupole tensors at the different ^{14}N sites present in the ribonucleosides used. a.) –NH_2, b.) –NH, c.) -N=, and d.) –N- (sugar) groups[16].

BRL61063	**Literature**[§]	**χ/MHz**	**η**	**r_{CN}/ Å**	**β^D/ °**	**α^D/ °**	**s/ Hz***
C(8)-NH_2	G C(2)-NH_2	-3.3	0.5	1.342	90	90	140
	A C(6)-NH_2	-3.15	0.29	1.332	90	90	125
C(8)=N(9)	G C(8)-N(7)	-3.2	0.16	1.305	52	90	-3.5
	A C(8)-N(7)	-3.15	0.29	1.308	51.7	90	2.5
C(8)-NH(7)	G C(8)-N(9)	-3	0	1.374	90	-	80
	A C(8)-N(9)	-3	0	1.362	90	-	78
§ Literature values for: G = guanosine, A = adenosine, * = ± 4 Hz							

Table 7 Literature values that may be compared with experimental spectra in order to predict splitting for carbon (8) in BRL61063.

Therefore, the effective splitting pattern for C(8) may be predicted as a 1:2:2:4 quartet with a large separation (~100s of Hz) between the weighted mean of the two asymmetric 'doublets', which in turn should have a splitting of approximately 80 Hz. This is shown in a schematic (not to scale) below.

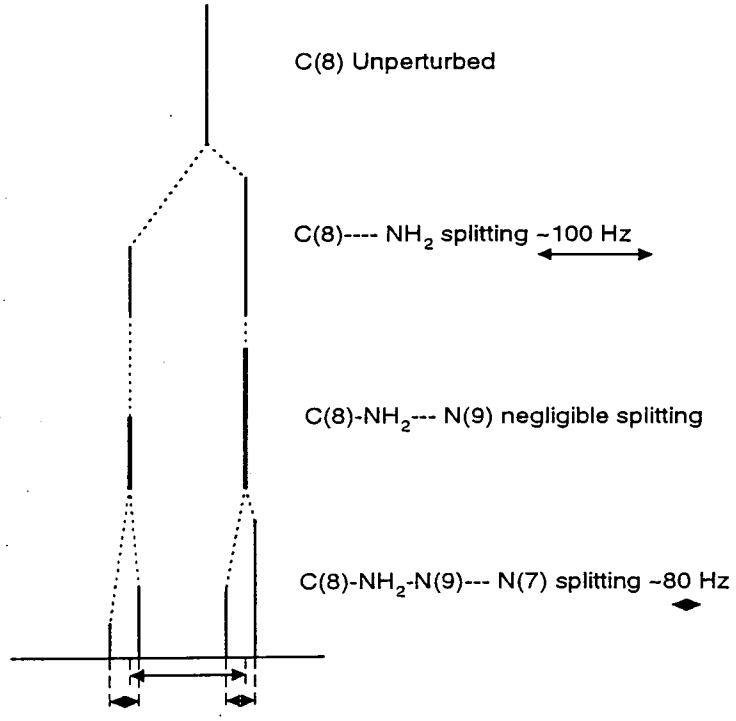

Figure 11 Schematic showing proposed successive splitting of the $^{13}C(8)$ resonance in BRL61063 (not to scale).

The properties of the ^{13}C spectra in this region (around 160 ppm), except for C(8) are summarised in ***Table 8***, below. The linewidth of each 'doublet' may not be broad enough to incorporate a C-NH_2 RDC-induced splitting, yet the separation between the weighted mean of the doublets seems also to be too large to represent this coupling. However, if the C-NH_2 actually becomes C=NH_2^+ then the splitting has been reported to become of the order of 250 Hz (Garcia *et al*). This is possibly quite unlikely, so it may be concluded that the resonance attributed to C(8) is 'hidden' amongst the broadened signals in this region. 300 MHz ^{13}C/CPMAS spectra (see section on high field operation) show two peaks (both of which are quite broad, and can be taken to be composite) in this region, indicating that carbon environments (8), (6), (2) and (4) are indeed resonant at very close frequencies, in two pairs of signals.

Form	Apparent splitting	Splitting/ Hz (± 4 Hz)		
		High ν 'doublet'	Low ν 'doublet'	Inter-doublet'*
1	1:2:1:2	84	87	240
2	1:2:2:1	87	86	300
D	1:2:1:2	66	90	267
Yellow	1:2:1:2	71	69	271

Table 8 Comparison of doublet and inter-doublet splitting in the 50 MHz ^{13}C CP/MAS spectra of BRL61063 polymorphs. (*Difference between weighted mean of individual doublets)

Therefore the region of resonances at around 160 ppm may be taken to consist of the following parts: C(8) - a 1:2:2:4 quartet; C(6) - a 1:2 doublet; C(2) – a 1:2:2:4 quartet; C(4) – a 1:2 doublet. It may be assumed, therefore, that the peaks around 160 ppm are a superposition of C(8), (6) (2) and (4), with the low intensity (due to splitting) of C(8) and C(2) causing low intensity 'baseline noise' and C(6) and C(4) causing the doublets that rise above the other signals. If this is the case, I would expect C(6) to exist at higher frequency than C(4). Therefore, the change in the sense of this doublet in form 2 may indeed allude to the presence of hydrogen bonding to N(9) in this form as predicted by the XRD data (see chapter 3) as this would cause a change in the relative orientation of the efg and thus, quite possibly, the sense of the doublet's splitting.

The result of this detailed analysis therefore goes to prove that this type of information can provide an insight into the chemical conformation and structure of a molecule. On examination of the data in ***Table 8*** the greatest splitting between the weighted mean of the two doublets may be observed for form 2. This is reasonable in that this is the form in which the C-NH_2 bond distance is the shortest, and which forms two hydrogen bonds from the amide hydrogen atoms. This also supports the theory that the N(9) position is involved in intermolecular hydrogen bonding, also helping to explain the ^{15}N CP/MAS spectra of form 2, which shows different spectral characteristics for this location to that of form 1 due to CP dynamics from the nearby proton.

6.4 Modulation and removal of the RDC effect

Despite the extra information that is contained within RDC distortions in the spectra of spin-½ nuclei, it would be desirable to have the option of being able to remove these broadening and splitting effects. This would be especially useful in cases where a large number of peaks in close spectral proximity cause difficulty in the resolution and assignment of individual resonances.

It should be mentioned that, by nature of processes occurring in the molecular structure of some molecules, residual dipolar coupling effects are either modulated or not observed or eliminated. This is because the observation of the linewidths may be influenced by the relaxation behaviour of the quadrupolar nucleus. This effect may range from line broadening in the region of slow and intermediate relaxation, to line narrowing due to 'self decoupling' for rapidly relaxing nuclei.

The following section summarises the molecular and experimental methods by which the RDC effects may be modulated or removed.

6.4.1 Molecular/ Natural methods of modulating RDC interactions

6.4.1.1 Self-decoupling[29,30,31]

Provided that the spin-lattice relaxation time (T_1) of the ^{14}N nucleus is sufficiently long, asymmetric doublets may be observed. However, proton transfer[29,30,32] in solids may be accompanied by corresponding jumps in the ^{14}N efg main axis. These jumps are able to shorten the T_1 (^{14}N) to a point where the expected splittings will collapse. An example is that of solid 3,5-dimethylpyrazole. Both protons are involved in a triple proton transfer and therefore both sites possess a very short T_1. Also, in the case of solid arylazonaphthols[33,34], rapid solid-state interconversion between the keto-hydrazone and the enol-azo tautomers cause there to be an absence of RDC effects in the spectra, again due to hydrogen transfer.

6.4.1.2 Isotopic replacement

By isotopically enriching the ^{14}N (I=1) sites with ^{15}N (I = ½), the molecular nature of the substance is not altered, but the quadrupolar nucleus is replaced with a spin-½ nucleus. Thus, for a 100% enrichment of the nitrogen sites, all residual dipolar coupling effects upon the ^{13}C spectra will be removed.

It has been previously mentioned that the effect of isotopic enrichment on the solution-state spectrum will result in quite different effects, since indirect (J) coupling effects will then become observable between the ^{15}N and the spin-½ nuclei.

Figure 12 shows the ^{13}C CP/MAS spectrum of a sample in which 100 % isotopic enrichment of the N(13) location was made (see chapter 4). Although it may be observed that residual dipolar coupling artifacts are no longer detectable in the spectrum, the changes in the resonances in the whole carbon spectrum seem to suggest that a new polymorph has been created. Further discussion of this topic may be found in chapter 4. Therefore, in this case, the asymmetric doublets have been removed by isotopic

substitution of the nitrogen site, but the result has caused further complications in the analysis of the system.

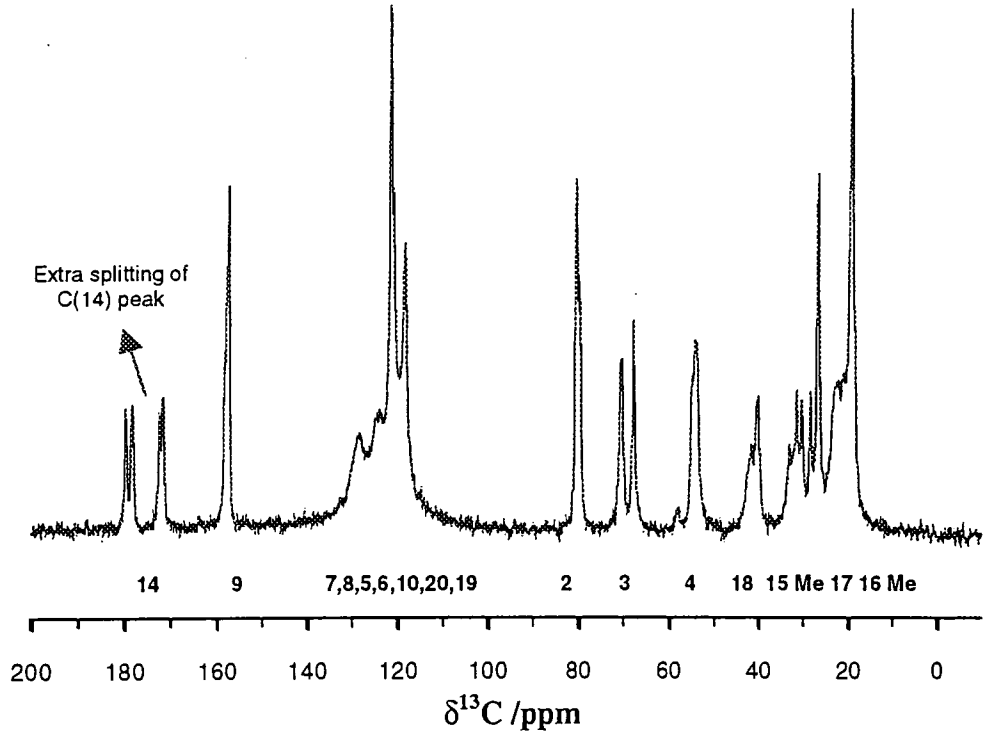

Figure 12 ^{13}C CP/MAS spectrum of [^{15}N]BRL55834. (50.329 MHz, 10 ms ct, 3 s rd, 400 transients, cp4_pm, 100ms acqtm)

6.4.1.3 Spherical electronic symmetry

When a quadrupolar nucleus exists in a spherically symmetrical environment, such as a cubic or octahedral environment (e.g. the NH_4^+ ion), this causes the quadrupolar coupling constant, χ to equal zero. Therefore the value of s collapses to zero and no residual dipolar splitting exists for the resonances of adjacent nuclei.

6.4.2 Experimental methods of modulating RDC interactions.

6.4.2.1 Variation of the magnetic field.

Due to the inverse dependence of RDC upon the magnetic field, it is possible to reduce this splitting to an irresolvable value by operation at a higher magnetic field. Of course, it

is also possible to increase the observed splitting by operation at a lower magnetic field, and many measurements were made using lower field magnets in the past [10, 24, 35].

By increasing B_o, this lowers the ratio of the quadrupolar to the Zeeman interaction and therefore decreases the transferred second-order effects. Thus the asymmetric doublet splitting decreases and the two components move towards the weighted average isotropic resonance value. This therefore has the same effect in solids as the effect of 100% isotopic enrichment (^{15}N) of the nitrogen location.

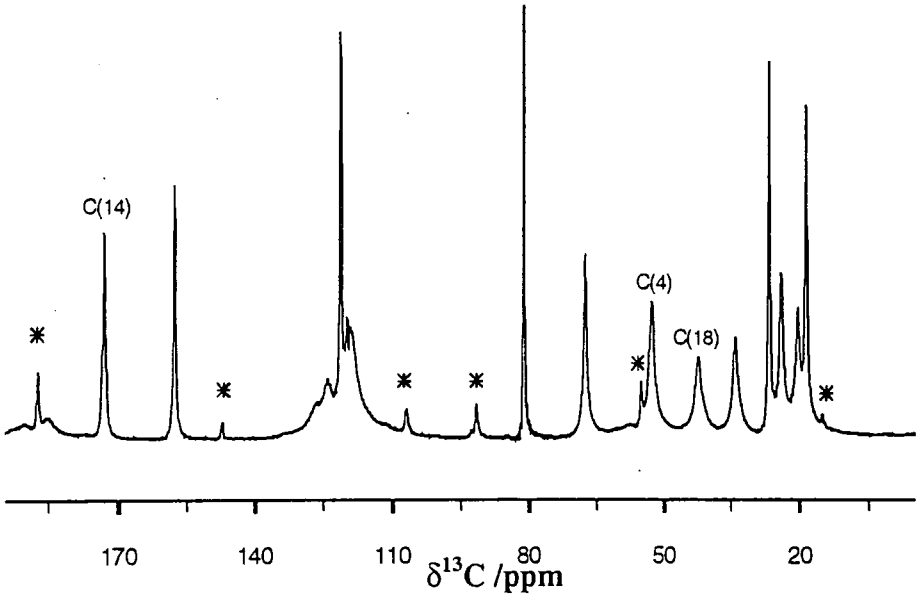

Figure 13 300 MHz ^{13}C CP/MAS spectrum of BRL55834 form I with carbons adjacent to ^{14}N indicated. (* = ssb) (4 kHz MAS, 10 ms ct, 3 s rd, 100 ms acqtm, 400 transients, 75 MHz)

(***Figure 13*** and ***Figure 14***) show the effect of acquiring ^{13}C CP/MAS spectra at 300 MHz on the RDC effects in the spectra of BRL55834 forms I and II. The ^{13}C CP/MAS spectrum of form 1 shows the narrowing of the C(14), (4) and (18) resonances, although the C(4) and (18) resonances appear broader than the other carbon resonances as these are CH_2 groups. The 300 MHz spectrum of form II, shows narrowing of these resonances as well, with the collapse of the asymmetric doublets towards the weighted mean chemical shift position this causes the existence of three peaks for C(14) to become more clear.

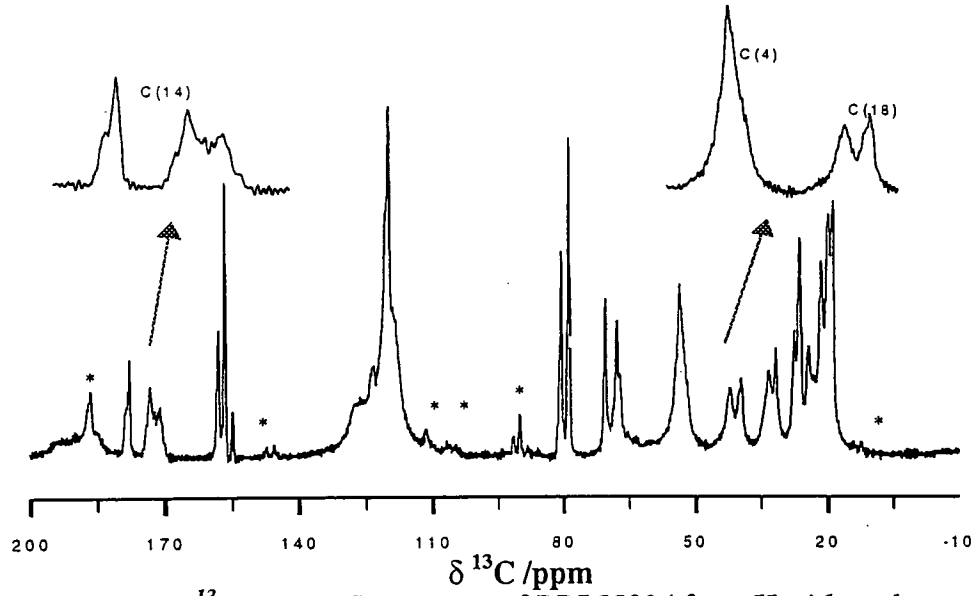

Figure 14 300 MHz ^{13}C CP/MAS spectrum of BRL55834 form II with carbons adjacent to ^{14}N indicated. (= ssb) (4 kHz MAS, 10 ms ct, 3 s rd, 100 ms acqtm, 400 transients, 75 MHz)*

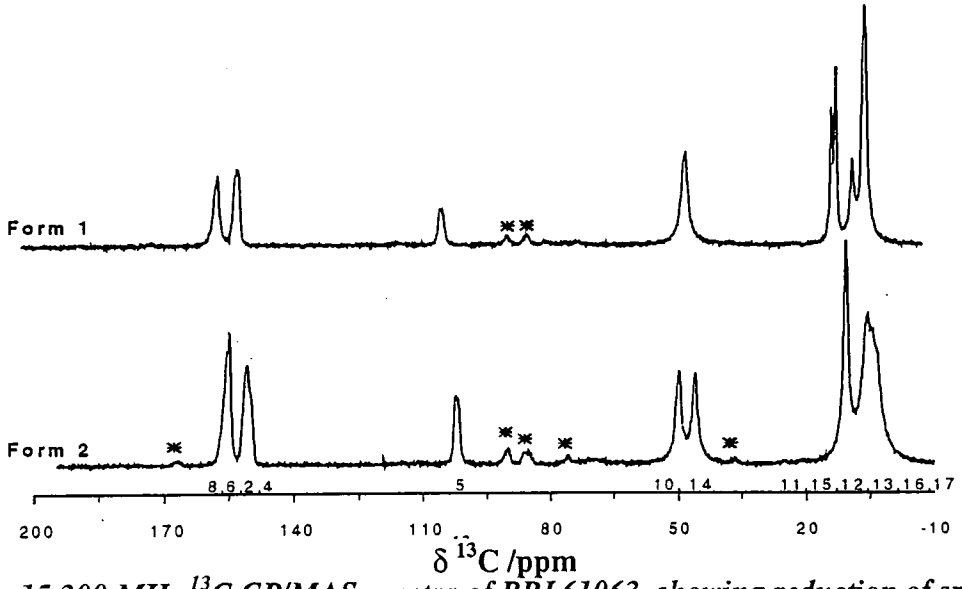

Figure 15 300 MHz ^{13}C CP/MAS spectra of BRL61063, showing reduction of splitting values to give isotropic peaks. (4 kHz MAS, 1 ms ct, 9 s pd, 100 ms acqtm, 384 transients, ^{13}C freq. 75 MHz)

Figure 15 shows the effect of operating at higher field for BRL61063, forms 1 and 2. In this case, it appears that all peaks that previously exhibited asymmetric doublets now appear as resonances at their weighted mean positions. Carbon sites (8), (6), (2) and (4) now appear to exhibit accidental equivalence, appearing as two, broadened peaks.

6.4.2.2 Decoupling ^{14}N – a novel technique

In the same way in which decoupling proton and fluorine, both individually and simultaneously has helped to improve the resolution of the ^{13}C CP/MAS spectra, it was decided to attempt to decouple ^{14}N with the aim of reducing or removing completely the asymmetric couplings caused by residual dipolar coupling to this nucleus by ^{13}C. This was a challenge because the technique has never previously been attempted in the literature (as far as I have ascertained) due to the problems[36] associated with ^{14}N (its quadrupolar nature, plus the 'experimental' problem which is its low frequency - 14.4 MHz at 4.7 T).

Therefore, a significant amount of preparation (over the space of approximately 12 months) had to be made before even the first simple experiment could be carried out.

6.4.2.2.1 Preparation

The HXY (HML) probe was chosen, with the aim of carrying out a $^{13}C\{^{1}H\}\{^{14}N\}$ CP/MAS experiment. This probe (as mentioned in Chapter 2) has a set of replaceable traps and capacitors that enable different frequency ranges to be used on each of the High, Medium and Low channels. Currently available combinations were not suitable for such low-frequency operation as is required for ^{14}N. Thus, the probe, amplifier and filter set up had to be adapted for the purposes of this experiment.

Filters – The ^{15}N 20 MHz low pass filter that is currently used for REDOR experiments was tested and found to be suitable for the ^{14}N frequency.

Probe capacitors and traps – With the assistance of Allen Palmer (Chemagnetics, now Varian), and Barry Say (Durham) the required set up was calculated. The required values are not manufactured by Varian and therefore we had to contact an electronics company called 'Phase Components' to get several capacitors around these values to be supplied. Due to voltage considerations and the internal geometry of the probe, I then worked with

the electrical workshop at Durham University to shape, fit and attach these together so that they would fit into the probe and accept the powers. Finally, we tested various top and bottom capacitor combinations using the mobile oscilloscope setup. Eventually, a suitable combination was isolated, which allowed the probe to be tuned to the required frequencies.

6.4.2.2.2 Experimental

A standard set up was initiated (see Chapter 2), shimming and setting the proton 90 power with PDMSO, followed by setting the ^{1}H-^{13}C match and referencing using adamantane. The magic angle was set using KBr. A sample of NH_4NO_3 was made up in purified water and placed into a glass insert before using its spectrum to set a ^{14}N 90° pulse. The set up that was used for the first set of experiments is shown in ***Table 9***, below.

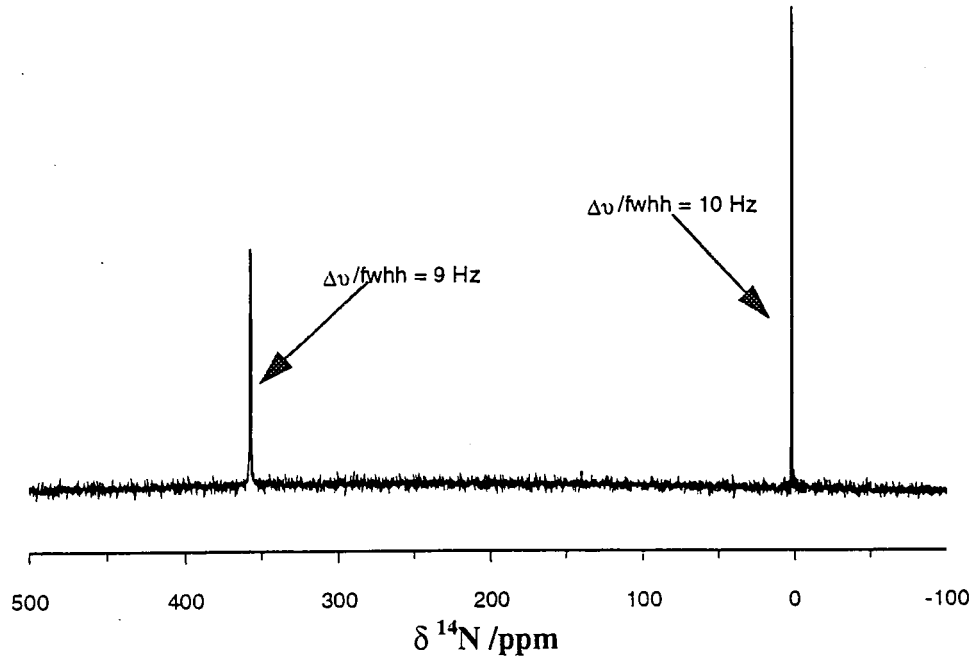

Figure 16 ^{14}N spectrum of ammonium nitrate (liquid) obtained on HFX probe. (No MAS, 1pulse, ^{14}N @ 14.458 MHz, 5.0 s rd)

Nucleus	Channel	Amplifier	Conditions	Power/W	Filter/MHz
^{1}H	2	CE	5 μs proton 90 ° pulse	31	200 LP
^{13}C	3	Bruker	Match (5 μs)	79	51 LP
^{14}N	1	Middle AMT	9 μs ^{14}N 90 ° pulse	145	20 LP
Probe's internal setup: Trap = 47 pF large; C_{Top} = 390 pF; C_{Bottom} = 330 pF A blue, 100 low-pass filter was also placed on the receiver cable before the preamplifier.					

Table 9 Experimental set up for the ^{14}N decoupling experiment.

6.4.2.2.3 Results

Finally, once the experimental conditions had been set up, solid glycine was used to test the efficiency of ^{14}N decoupling. The lineshape arising from the carbon atom directly adjacent to the nitrogen location was examined. Under 'normal' conditions, with proton-to-carbon CP and proton decoupling, an asymmetric doublet may be observed with a linewidth (fwhh) of 88 Hz. Upon application of ^{14}N decoupling tuned to 13.9 MHz this linewidth, measured in the same way, decreases. This decrease is due to the reduction of the residual splitting, *s*, brought about by the partial decoupling of the ^{14}N, thus the components move towards the weighted mean isotropic shift for the nucleus. (***Figure 17***).

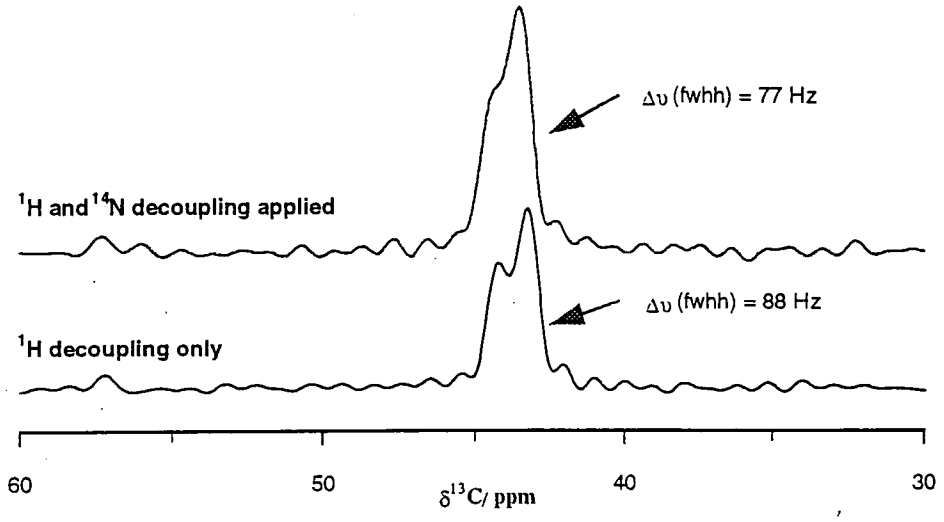

Figure 17 ^{13}C CP/MAS spectra of glycine, carbon adjacent to nitrogen site. (3 kHz MAS, ^{14}N @ 13.9 MHz, uscp2dec, 1.5 ms ct, 3.0 s rd, 20 ms acqtm, 20 transients).

Thus, it appeared that for a ^{14}N decoupling power of 145 Watts, and decoupling frequency of 28 kHz, a 10 % reduction in the splitting may be obtained for glycine, spinning at 3 kHz.

Following on from the partial success of the ^{14}N decoupling on glycine, I made a similar investigation of the effect upon my two polymorphic systems. Using a standard approach I acquired the CP/MAS spectra with only ^{1}H, and then both ^{1}H and ^{14}N decoupling. Then, by comparing the fwhh linewidths (full width at half height) it was possible to make an assessment of whether or not the decoupling of the ^{14}N had been effective. Importantly, some sort of control was introduced by taking measurements of the fwhh (Hz) of other resonances in the spectrum and thus comparing the absolute resolution of spectra resulting from each experiment (with or without ^{14}N decoupling) to check that the results were truly comparable.

6.4.2.2.3.1 BRL61063 Form 2

Form 2 was chosen in preference to form 1 since more pronounced asymmetric lineshapes are observed, especially for carbons (10), (14) and (5). An investigation was

MAS rate	**4 kHz**			**6 kHz**			**7 kHz**		
Assignment	**Linewidth (fwhh) / Hz (± 3 Hz)**								
	{H}	{H}{N}	% reduction	{H}	{H}{N}	% reduction	{H}	{H}{N}	% reduction
8, 6, 2, 4	155	134	16	151	127	19	192	129	49
	343*	331*	4	142	138	3	441*	367*	20
5	132	115	15	161	124	30	Broad	Broad	-
10	107	104	3	100	102	-2	112	98	14
14	107	84	27	100	100	0	112	103	9
Control$_{(CH_n)}$	50	50	0	50	50	0	57	57	0
Average$^{\nabla}$			13			10			23

Accuracy – all fwhh values accurate to ± 2 Hz.

* whole band width measured as individual doublet not resolved to baseline to allow measurement of fwhh.

$^{\nabla}$ Average percentage reduction on application of ^{14}N decoupling, only for C peaks adjacent to N atoms.

Table 10 BRL61063 form 2. A comparison of the effectiveness of application of ^{14}N decoupling field on ^{13}C resonances affected by RDC effects.

carried out over three different spinning speeds: 4, 6, and 7 kHz and interesting variations could be observed between spectra acquired at each of these spinning speeds.

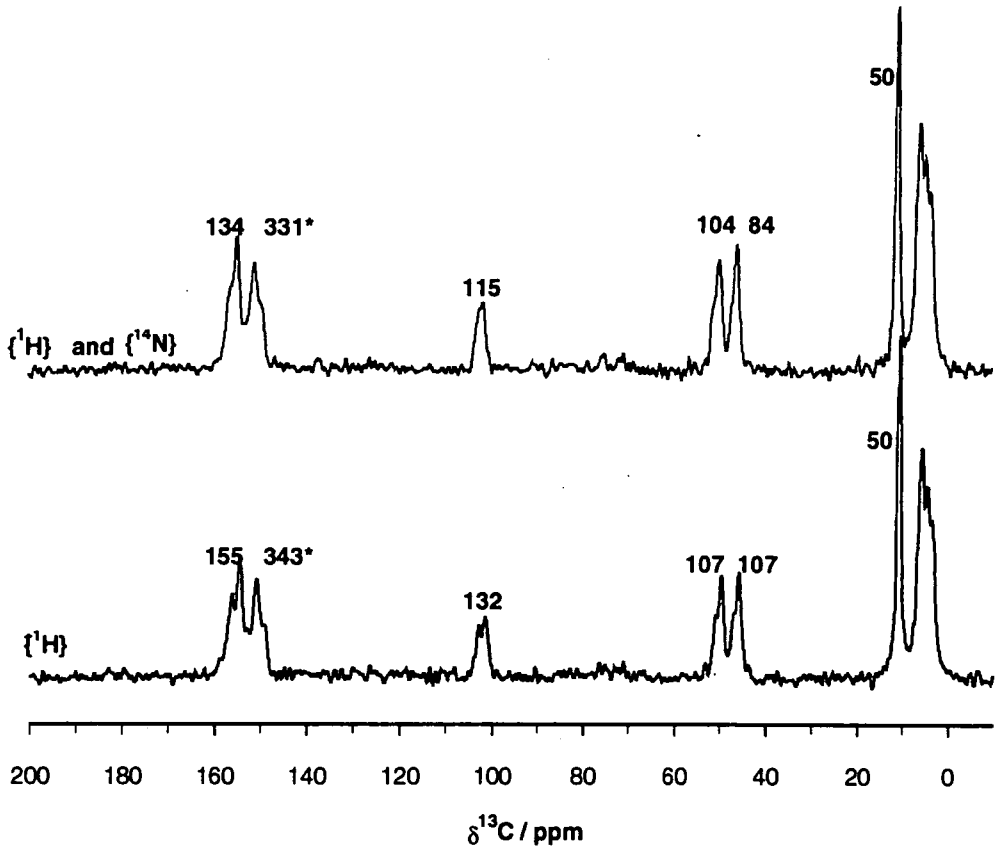

Figure 18 ^{13}C CP/MAS spectra of BRL61063 form 2, with and without ^{14}N decoupling indicating bandwidths (fwhh) /Hz. (Numbers in red refer to C adjacent to ^{14}N, * indicates whole bandwidth, not just doublet).(MAS 4 kHz, 200 transients, 1.0 ms ct, 9 s rd, 20 ms acqtm).

Discussion

Results seem to be fairly variable, yet there appears to be a reduction in bandwidth on application of decoupling. Interesting variations in efficiency occur for the more mobile groups, possibly inferring interference effects upon effective decoupling when operating at different spinning speeds. The results are believable since the 'control' resonances showed no alteration in their linewidths between experiments.

If nothing else, application of a ^{14}N decoupling field may assist the assignment of ^{13}C resonances directly adjacent to ^{14}N nuclei by comparison of the linewidths.

6.4.2.2.3.2 BRL55834 Forms I and II

The results of applying ^{14}N decoupling whilst acquiring the ^{13}C CP/MAS spectra of the two forms of BRL55834 were very interesting. For both forms, 'control resonances' for carbons that are not directly bonded to the ^{14}N were selected and their linewidths (fwhh) were measured and found to be constant for both experiments (i.e. with and without ^{14}N decoupling). However, most of the resonances corresponding to carbon atoms (14), (4) and (18) showed a decrease in fwhh on application of ^{14}N decoupling. This may be assumed to be due to the reduction of the splitting of the asymmetric doublet.

Assignment	Linewidth (fwhh) / Hz (± 3 Hz)					
	Form I			Form II		
	{^{1}H}	{^{1}H}{^{14}N}	% reduction	{^{1}H}	{^{1}H}{^{14}N}	% reduction
14	64	53	**21**	46 153	53 186	**-14** **-17**
4	87	74	**18**	164	142	**15**
18	105	87	**21**	231	222	**4**
Control C*	(3) 47	47	**0**	(9) 40	40	**0**
Control C*	(17) 63	63	**0**	(2) 42	42	**0**
* carbon resonance used as controls in brackets						

Table 11 Comparison of fwhh/ Hz of individual linewidths for the two polymorphs of BRL55834 with and without ^{14}N decoupling.

The only exception to this observation was for the multiple resonances observed for C(14) in the spectra of form II. This may be caused by a lack of resolution of the lines, causing noise to be incorporated into the linewidth, especially for the peak at higher frequency. Also, the peak at lower frequency has been recognised to consist of two, individual asymmetric doublets. If the sense of the residual dipolar splitting is opposed in each of these doublets, causing the composite line to exist as the sum of 2:1 and 1:2 asymmetric doublets, then as the splitting reduces due to ^{14}N decoupling, each doublet will 'close' towards their respective weighted mean, isotropic shift value. This will therefore cause movement of the weighted mean of the two separate doublets in opposite

directions, away from each other, and thus broaden the composite lineshape. The results are summarised in ***Table 11***.

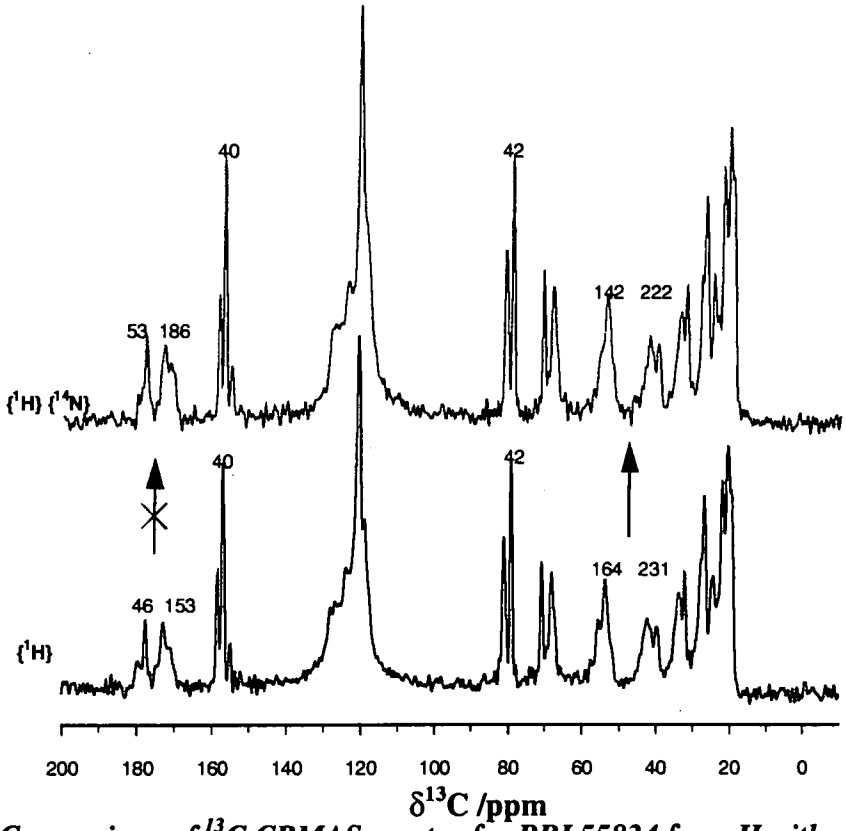

Figure 19 Comparison of ^{13}C CPMAS spectra for BRL55834 form II with and without ^{14}N decoupling. (MAS 5 kHz, 10 ms ct, 3s rd, 400 transients, 20 ms acqtm).

6.4.2.2.3 Discussion of the efficiency of the ^{14}N decoupling technique

Effective decoupling ^{14}N involves consideration of the complex interplay of many parameters, including the magnitude of the quadrupolar and dipolar coupling constants of the nitrogen nucleus, plus its relaxation time.

During the course of experimentation an interesting frequency shift phenomenon appeared in the ^{13}C $\{^{14}N\}$ CP/MAS spectra. This section describes briefly my observations, followed by recommendation of an experiment to probe the origin of the effect.

Observations – The frequency shift effect

Once the probe had been tuned to the ^{14}N frequency and thus had been set up as described in earlier sections in order to acquire ^{13}C $\{^{14}N\}$ spectra, an experiment was then carried out in which the ^{14}N decoupling frequency was arrayed. The aim of this experiment was to establish the optimum ^{14}N decoupling frequency for each sample. However, when 'on tune' at 14.4 MHz, the ^{13}C spectra appeared to broaden and loose resolution. There also appeared to be a frequency shift of approximately 5 ppm of the whole spectrum at this position of the decoupler frequency. On alteration of the decoupler to frequency values greater and lower than the 'on tune' position, the ^{13}C resonances sharpened up and the whole spectrum returned to the correctly referenced chemical shift measured without ^{14}N decoupling.

Various origins of this 'frequency shift effect' may exist, and sample heating or a Bloch-Siegert effect at the 'on-tune' position has been considered. However, the shift did not alter in magnitude upon variation of the effective ^{14}N decoupling power applied to the sample. This would be expected if the shift was attributed to a Bloch-Siegert effect, which in any case would be theoretically anticipated to be negligibly small.

The proposed experiment

It may be possible to distinguish the cause of the shift as being related to a probe heating effect or a NMR effect by making up a mixed sample in a CMX rotor of two compounds, one containing nitrogen sites (e.g. glycine) and one that does not (e.g. adamantane). It would be sensible to separate these samples by placing one of them in a glass ampoule within the rotor and packing the other around this. Next, acquire the ^{13}C CP/MAS spectra with and without ^{14}N decoupling and array the frequency of the decoupler on either side of the 'on tune' position. If the ^{13}C spectra of both compounds exhibit a frequency shift effect then the cause may be attributable to sample rf heating effects. The heating produced may be calibrated by use of techniques that are outlined in chapter 2. If the ^{13}C spectra of only the, nitrogen-containing compound alters and the adamantane resonances remain in the same chemical shift position then the frequency shift may be attributed to a nuclear magnetic resonance effect.

6.5 Conclusions

It has been shown that the transferred effects of quadrupolar (I=1) nuclei into the spectra of adjacent spin-½ nuclei can be a useful source of conformational information in solid-state NMR. This has been confirmed for compounds for which crystallographic data may or may not be available.

Results for BRL55834 lead us to believe that the conformation about the single nitrogen location in the two polymorphs is very different in form I and form II. For BRL61063, the involvement of the N(9) location in an inter-molecular hydrogen bond infers negligible RDC-induced splitting of the resonances of the adjacent ^{13}C atoms corresponding with this crystallographic data. Therefore, this shows that the conformational information that can be derived from solid-state NMR supports results of X-ray crystallography.

Attempts to remove and analyse the effect have opened up other substantial areas of research such as ^{14}N decoupling, whilst synthesis of an ^{15}N-enriched sample has caused the formation of a new polymorph!

Overall, ^{14}N decoupling appears to have been at least partially successful, although work still needs to be continued to improve the technique. This can be simply improved in the first instance by using a different amplifier set up to facilitate longer acquisition times. I also foresee that phase modulation of the decoupler, using a sequence such as TPPM (see chapter 2) should improve the decoupling efficiency.

I am grateful to Barry Say and Eric Hughes for their practical help with the implementation of the ^{14}N decoupling technique and Barry for the useful discussions on how to probe the cause of the frequency shift effect in the ^{13}C CP/MAS spectra.

In the future I feel that the residual dipolar coupling effect holds great potential for obtaining original information concerning the molecular conformation of small organic molecules. I feel that the incorporation of solid-state NMR RDC data into molecular modelling packages and genetic algorithm techniques would optimise the efficiency of using this type of data to obtain structural information about molecules that do not form good quality crystals suitable for single-crystal X-ray diffraction studies.

6.5 References

1 A. C. Olivieri, L. Frydman, L. E. Diaz, *J. Magn. Reson.*, **75**, 50, 1987.

2 A. C. Olivieri, R.K.Harris, *Progr. Nucl. Magn. Reson. Spectrosc.*, **24**, 435, 1992.

3 A. C. Olivieri, *Magn. Reson. in Chem.*, **34**, 365, 1996.

4 A. C. Olivieri, *J. Magn. Reson.*, **81**, 201, 1989.

5 R. K. Harris, P. Jonsen, K. J. Packer, *Magn, Reson. in Chem.*, **23**, 7, 1985.

6 S. A. Carss, *Ph.D. Thesis,* Durham University, 1995.

7 S. H. Alarcon, A.C. Olivieri, S. A.Carss, R. K. Harris, M. J. Zuriaga, G. A. Monti, *J. Magn. Reson.*, A, **116**, 244, 1995.

8 R. K. Harris, A. C. Olivieri, *Prog. Nucl. Magn. Reson. Spectrosc.* **24**, 435, 1992.

9 S. H. Alarcon, A .C. Olivieri, S. A. Carss, R. K. Harris, *Magn. Reson. in Chem.*, **33**, 603-606, 1995.

10 A. Naito, S. Ganapathy, C. A. McDowell, *J. Magn. Reson.*, **48**, 367, 1982.

11 M. Chippendale, A. Mathias, S. Aujla, R. K. Harris, K. J. Packer, B. J. Say, *J. Chem. Soc. Perk. Trans. 2,* 1357, 1993.

12 C. A. McDowell, Encyclopedia of NMR 'MAS ^{13}C lineshapes: the effect of 14N', Eds. D. M. Grant and R. K. Harris, Wiley, **5**, 2901, 1996.

13 E. Lipmaa, M. Alla, H. Raudf, R. Telaar, I. Heinmua, E. Kundla, *Proc. 20th Cong. Ampere,* Tallin, p87 Springer, Berlin, 1979.

14 P. Grondona, A. C. Olivieri, *Concepts in Magn. Reson.*, **5**, 319, 1993.

15 S. Opella, M. H. Frey, J. C. S. *Chem. Com.* 1980.

16 A. C. Olivieri, L. Frydman, M. Grasselli, L. E. Diaz, *Magn. Reson. in Chem.* **26**, 281, 1988.

17 C. J. Groombridge, R. K. Harris, K. J. Packer, B. J. Say, S. F. Tanner, *J. Chem. Soc. Chem. Comm.*, 174, 1980.

18 M. H. Frey, S. J. Opella, *J. Chem. Soc. Chem.Comm.*, 474, 1980.

19 M. D. Hollingsworth, N. Cyr, *J. Chem. Soc. Chem. Comm.*, 578, 1990.

20 A. Naito, S. Ganapathy, K. Akasaka, C. A. McDowell, *J. Chem. Phys.*, **74**, 6, 1981.

21 N. Zumbulyadis, P. M. Hendrichs, R. H. Young, *J. Chem. Phys.*, **75**, 4, 1981.

22 A. C. Olivieri, *Concepts in Magn. Reson.*, 279, 1996.

23 B. H. Suits, J. Sepa, D. White, *J. Magn, Reson. A.* **120**, 88, 1996.

24 A. C. Olivieri, L. Frydman, M. Graselli, L. E. Diaz, *Magn. Reson. in Chem.*, **26**, 615, 1988.

25 C. G. Hoelger, F. Aiguilar-Parrilla, J. Elguero, O. Weintraub. S. Vega, H. H. Limbach, *J. Magn. Reson. A.*, **120**, 46, 1996.

26 K. Eichele, R. E. Wasylishen, *Solid State Nucl. Magn. Reson.*, **1**, 159, 1992.

27 A. C. Olivieri, L. Frydman, M. Grasselli, L. E. Diaz, *Magn. Reson. Chem.* **26**, 281, 1985.

28 A. C. Olivieri, L. Frydman and L. E. Diaz, *J. Magn. Reson.*, **75**, 50, 1987

29 A. C. Olivieri, *J. Chem. Soc. Perk. Trans. 2, 85,* 1989.

30 S. H. Alarcon, A. C. Olivieri, P. Jonsen, *J. Chem. Soc. Perk. Trans. 2, 1993.*

31 S. H. Alarcon, A. C.Olivieri, A. Nordon, R.K.Harris, *preprint.*

32 A. C. Olivieri, *J. Chem. Soc. Perk. Trans. 2*, 85, 1990.

33 A. C. Olivieri, R. B. Wilson, I. C. Paul, D. Y. Curtin, *J. Am. Chem. Soc.* **111,** 5525, 1989.

34 R. K. Harris, P. Jonsen, K. J. Packer, *Magn. Reson. in Chem.*, **24**, 977, 1986.

35 J. Roschester, U. Berg, M. Pierrot, J. Sandstrom, *J. Am. Chem. Soc.*, **109**, 492, 1987.

36 G. Jeschke, M. Jansen, *Angew. Chem. Int. Ed.*, **37**, 1282, 1998.

Appendix

Research conferences attended

NMR of solids and solid-like materials, NMR discussion group of the RSC. University College, London, 19th December 1995.

Summer school on NMR of solids, University of Durham, 16-20th September, 1996.

NMR of inclusion and molecular recognition phenomena in solids and liquids, NMR discussion group meeting. University of Birmingham, 15th April 1997.

13th RSC International Conference on NMR, Exeter, 6-11th July 1997.

British Pharmaceutical Conference, polymorphism symposium, Scarborough, 18th September, 1997.

39th Experimental NMR Conference, Asilomar, Pacific Grove, California, 22-27th March 1998.

RSC National Congress, polymorphism symposium, and Young Researchers' meeting Durham, 6-9th April 1998.

*39th Meeting of Nobel Laureates in Chemistry, Lindau, Germany, June 24-29th 1998.
*Attended as one of 8 students selected by the Royal Society of Chemistry from all over the UK to attend the meeting and meet the 23 laureates who were present!

Oral Presentations

Group talks – presented one per term on research or literature for three years.

Poster Presentations

ICI Poster competition, University of Durham, 18th December 1996.

13th RSC International Conference on NMR, Exeter, July 1997.

Experimental NMR Conference (ENC), Asilomar, Pacific Grove, California, USA, March 1996.

RSC Annual Congress, Polymorphism symposium and Young Researchers Meeting*, Durham, April 4-9th 1998.

* Young researchers prize awarded for poster in the solid-state section.

Publications

'NMR and polymorphism of a piperidinone-substituted benzopyran with fluorinated sidechain.' S. C. Campbell, R. K. Harris, M. J. Hardy, D. C. Lee, D. J. Busby, *J. Chem. Soc. Perkin Trans. 2.*, 1913, 1997.

Research conducted outside the department

Solution-state NMR of Brl55834. SB pharmaceuticals, Harlow. 1 week, December 1995.

Solid-state Raman spectroscopy of mixtures of Brl55834. SB pharmaceuticals, 'The Frythe', Welwyn, 1 week, May 1996.

Chemometric analysis of solids Raman of mixtures. SB pharmaceuticals, 'The Frythe', Welwyn, 1 week, June 1996.

Radioisotopic labelling of Brl55834. SB pharmaceuticals, Harlow, 1 week, June 1997.

Crystal structure determination from powder X-ray diffraction data. Birmingham University School of Chemistry, 1 week, June 1998.

Research colloquia, seminars and lectures given by invited speakers

1995

October 11 Prof. P. Lugar, Frei Univ Berlin, FRG
Low Temperature Crystallography

October 13 Prof. R. Schmutzler, Univ Braunschweig, FRG.
Calixarene-Phosphorus Chemistry: A New Dimension in Phosphorus Chemistry♦

October 18 Prof. A. Alexakis, Univ. Pierre et Marie Curie, Paris,
Synthetic and Analytical Uses of Chiral Diamines

October 25 Dr.D.Martin Davies, University of Northumbria
Chemical reactions in organised systems.

November 1 Prof. W. Motherwell, UCL London
New Reactions for Organic Synthesis

November 3 Dr B. Langlois, University Claude Bernard-Lyon
Radical Anionic and Psuedo Cationic Trifluoromethylation

November 8 Dr. D. Craig, Imperial College, London
New Stategies for the Assembly of Heterocyclic Systems

November 15 Dr Andrea Sella, UCL, London
Chemistry of Lanthanides with Polypyrazoylborate Ligands

November 17 Prof. David Bergbreiter, Texas A&M, USA

Design of Smart Catalysts, Substrates and Surfaces from Simple Polymers

November 22 Prof. I Soutar, Lancaster University
A Water of Glass? Luminescence Studies of Water-Soluble Polymers.

November 29 Prof. Dennis Tuck, University of Windsor, Ontario, Canada
New Indium Coordination Chemistry

December 8 Professor M.T. Reetz, Max Planck Institut, Mulheim
Perkin Regional Meeting

1996

January 10 Dr Bill Henderson, Waikato University, NZ
Electrospray Mass Spectrometry - a new sporting technique♦

January 17 Prof. J. W. Emsley , Southampton University♦
Liquid Crystals: More than Meets the Eye

January 24 Dr Alan Armstrong, Nottingham Univesity
Alkene Oxidation and Natural Product Synthesis

January 31 Dr J. Penfold, Rutherford Appleton Laboratory,
Soft Soap and Surfaces

February 7 Dr R.B. Moody, Exeter University
Nitrosations, Nitrations and Oxidations with Nitrous Acid

February 12 Dr Paul Pringle, University of Bristol
Catalytic Self-Replication of Phosphines on Platinum(O)

February 14 Dr J. Rohr, Univ Gottingen, FRG

Goals and Aspects of Biosynthetic Studies on Low Molecular Weight Natural Products

February 21 Dr C R Pulham , Univ. Edinburgh
Heavy Metal Hydrides - an exploration of the chemistry of stannanes and plumbanes

February 28 Prof. E. W. Randall, Queen Mary & Westfield College
New Perspectives in NMR Imaging♦

March 6 Dr Richard Whitby, Univ of Southampton
New approaches to chiral catalysts: Induction of planar and metal centred asymmetry

March 7 Dr D.S. Wright, University of Cambridge
Synthetic Applications of Me_2N-p-Block Metal Reagents

March 12 RSC Endowed Lecture - Prof. V. Balzani, Univ of Bologna
Supramolecular Photochemistry♦

March 13 Prof. Dave Garner, Manchester University
Mushrooming in Chemistry

April 30 Dr L.D.Pettit, Chairman, IUPAC Commission of Equilibrium Data
pH-metric studies using very small quantities of uncertain purity

October 9 Professor G. Bowmaker, University Auckland, NZ
Coordination and Materials Chemistry of the Group 11 and Group 12 Metals : Some Recent Vibrational and Solid State NMR Studies♦

October 14 Professor A. R. Katritzky, University of Gainesville,University of Florida, USA Recent Advances in Benzotriazole Mediated Synthetic Methodology

October 16 Professor Ojima, Guggenheim Fellow, State University of New York at Stony Brook. Silylformylation and Silylcarbocyclisations in Organic Synthesis

October 22 Professor Lutz Gade, Univ. Wurzburg, Germany
Organic transformations with Early-Late Heterobimetallics: Synergism and Selectivity

October 22 Professor B. J. Tighe, Department of Molecular Sciences and Chemistry, University of Aston
Making Polymers for Biomedical Application - can we meet Nature's Challenge? Joint lecture with the Institute of Materials

October 23 Professor H. Ringsdorf (Perkin Centenary Lecture), Johannes Gutenberg-Universitat, Mainz,
Germany
Function Based on Organisation

October 29 Professor D. M. Knight, Department of Philosophy, University of Durham
The Purpose of Experiment - A Look at Davy and Faraday

October 30 Dr Phillip Mountford, Nottingham University
Recent Developments in Group IV Imido Chemistry

November 6 Dr Melinda Duer, Chemistry Department, Cambridge
Solid-state NMR Studies of Organic Solid to Liquid-crystalline Phase Transitions

November 12 Professor R. J. Young, Manchester Materials Centre, UMIST
New Materials - Fact or Fantasy?

Joint Lecture with Zeneca & RSC

November 13 Dr G. Resnati, Milan
Perfluorinated Oxaziridines: Mild Yet Powerful Oxidising Agents

November 18 Professor G. A. Olah, University of Southern California, USA
Crossing Conventional Lines in my Chemistry of the Elements♦

November 19 Professor R. E. Grigg, University of Leeds
Assembly of Complex Molecules by Palladium-Catalysed Queueing Processes

November 20 Professor J. Earnshaw, Deptartment of Physics, Belfast
Surface Light Scattering: Ripples and Relaxation♦

November 27 Dr Richard Templer, Imperial College, London
Molecular Tubes and Sponges

December 3 Professor D. Phillips, Imperial College, London
"A Little Light Relief" -

December 4 Professor K. Muller-Dethlefs, York University
Chemical Applications of Very High Resolution ZEKE Photoelectron Spectroscopy

December 11 Dr Chris Richards, Cardiff University
Sterochemical Games with Metallocenes

1997

January 15 Dr V. K. Aggarwal, University of Sheffield
Sulfur Mediated Asymmetric Synthesis

January 16 Dr Sally Brooker, University of Otago, NZ
Macrocycles: Exciting yet Controlled Thiolate Coordination Chemistry

January 21 Mr D. Rudge, Zeneca Pharmaceuticals
High Speed Automation of Chemical Reactions

January 22 Dr Neil Cooley, BP Chemicals, Sunbury
Synthesis and Properties of Alternating Polyketones♦

January 29 Dr Julian Clarke, UMIST
What can we learn about polymers and biopolymers from computer-generated nanosecond movie-clips?

February 4 Dr A. J. Banister, University of Durham
From Runways to Non-metallic Metals - A New Chemistry Based on Sulphur

February 5 Dr A. Haynes, University of Sheffield
Mechanism in Homogeneous Catalytic Carbonylation

February 12 Dr Geert-Jan Boons, University of Birmingham
New Developments in Carbohydrate Chemistry

February 18 Professor Sir James Black, Foundation/King's College London
My Dialogues with Medicinal Chemists

February 19 Professor Brian Hayden, University of Southampton
The Dynamics of Dissociation at Surfaces and Fuel Cell Catalysts

February 25 Professor A. G. Sykes, University of Newcastle

	The Synthesis, Structures and Properties of Blue Copper Proteins
February 26	Dr Tony Ryan, UMIST
	Making Hairpins from Rings and Chains♦
March 4	Professor C. W. Rees, Imperial College
	Some Very Heterocyclic Chemistry
March 5	Dr J. Staunton FRS, Cambridge University
	Tinkering with biosynthesis: towards a new generation of antibiotics
March 11	Dr A. D. Taylor, ISIS Facility, Rutherford Appleton Laboratory
	Expanding the Frontiers of Neutron Scattering
March 19	Dr Katharine Reid, University of Nottingham
	Probing Dynamical Processes with Photoelectrons
October 8	Prof. E. Atkins, Department of Physics, University of Bristol
	Advances in the control of architecture for polyamides: from nylons to genetically engineered silks to monodisperse oligoamides
October 15	Dr. R. Mark Ormerod, Department of Chemistry, Keele University
	Studying catalysts in action
October 21	Prof. A. F. Johnson, IRC, Leeds
	Reactive processing of polymers: science and technology
October 22	Prof. R.J. Puddephatt (RSC Endowed Lecture), University of Western Ontario Organoplatinum chemistry and catalysis

October 23 Prof. M.R. Bryce, University of Durham, Inaugural Lecture
New Tetrathiafulvalene Derivatives in Molecular, Supramolecular and Macromolecular Chemistry: controlling the electronic properties of organic solids

October 29 Prof. Bob Peacock, University of Glasgow
Probing chirality with circular dichroism

October 28 Prof. A P de Silva, The Queen's University, Belfast
Luminescent signalling systems"

November 5 Dr Mimi Hii, Oxford University
Studies of the Heck reaction

November 11 Prof. V Gibson, Imperial College, London
Metallocene polymerisation

November 12 Dr Jeremy Frey, Department of Chemistry, Southampton University
Spectroscopy of liquid interfaces: from bio-organic chemistry to atmospheric chemistry♦

November 19 Dr Gareth Morris, Department of Chemistry, Manchester Univ.
Pulsed field gradient NMR techniques: Good news for the Lazy and DOSY♦

November 20 Dr Leone Spiccia, Monash University, Melbourne, Australia
Polynuclear metal complexes

November 25 Dr R. Withnall, University of Greenwich
Illuminated molecules and manuscripts

November 26 Prof. R.W. Richards, University of Durham, Inaugural Lecture
A random walk in polymer science♦

December 2 Dr C.J. Ludman, University of Durham
Explosions♦

December 3 Prof. A.P. Davis, Department. of Chemistry, Trinity College Dublin.
Steroid-based frameworks for supramolecular chemistry

December 10 Sir Gordon Higginson, former Professor of Engineering in Durham and retired Vice-Chancellor of Southampton Univ. 1981 and all that.

December 10 Prof. Mike Page, Department of Chemistry, University of Huddersfield
The mechanism and inhibition of beta-lactamases

October 27 Prof. Warren Roper FRS. University of Auckland, New Zealand

1998

January 14 Prof. David Andrews, University of East Anglia
Energy transfer and optical harmonics in molecular systems♦

January 20 Prof. J. Brooke, University of Lancaster
What's in a formula? Some chemical controversies of the 19th century

January 21 Prof. David Cardin, University of Reading♦

January 27 Prof. Richard Jordan, Dept. of Chemistry, Univ. of Iowa, USA.
Cationic transition metal and main group metal alkyl complexes in olefin polymerisation

January 28 Dr Steve Rannard, Courtaulds Coatings (Coventry)
The synthesis of dendrimers using highly selective chemical reactions

February 3 Dr J. Beacham, ICI Technology
The chemical industry in the 21st century

February 4 Prof. P. Fowler, Department of Chemistry, Exeter University
Classical and non-classical fullerenes

February 11 Prof. J. Murphy, Dept of Chemistry, Strathclyde University

February 17 Dr S. Topham, ICI Chemicals and Polymers
Perception of environmental risk; The River Tees, two different rivers

February 18 Prof. Gus Hancock, Oxford University
Surprises in the photochemistry of tropospheric ozone

February 24 Prof. R. Ramage, University of Edinburgh
The synthesis and folding of proteins

February 25 Dr C. Jones, Swansea University
Low coordination arsenic and antimony chemistry

March 4 Prof. T.C.B. McLeish, IRC of Polymer Science Technology, Leeds University. The polymer physics of pyjama bottoms (or the novel rheological characterisation of long branching in entangled macromolecules)

March 11 Prof. M.J. Cook, Dept of Chemistry, UEA
How to make phthalocyanine films and what to do with them♦

March 17 Prof. V. Rotello, University of Massachusetts, Amherst The interplay of recognition & redox processes - from flavoenzymes to devices

March 18 Dr John Evans, Oxford University. Materials which contract on heating (from shrinking ceramics to bullet proof vests)

I just couldn't resist putting this at the end of my thesis ... it's as close as I'll ever get!

Dr Helen Pain CChem MRSC
Membership Development Officer
The Royal Society of Chemistry
Science Park Milton Rd
Cambridge CB4 4WF

Dear Susan

Meeting of Nobel Laureates in Chemistry Lindau, Germany - 29 June to 3 July 1998

Every three years since 1954, Chemistry Nobel Laureates of all nationalities have gathered together in the island town of Lindau, off the German shore of Lake Constance, for a 'celebration' of Chemistry. They are joined by some 500 Chemistry students who come from universities across Germany. This year, for the first time, the organising committee has asked the Royal Society of Chemistry to invite ten students from the UK.

I would like to invite you as one of the ten students who will get the chance to meet the famous names of the Chemistry world, all expenses paid. Amongst the distinguished guests who have been invited to attend are Sir Harry Kroto, Professor Herbert Brown and Professor Rudolf Mossbauer. The meeting will take the form of a conference with a series of talks being given by the invited speakers. I understand that there will also be plenty of social events and a chance to do some networking with the Laureates.

I should be very grateful if you could let me know as soon as possible whether or not you would like to attend this very special event as a representative of the UK's chemistry community. As spaces are limited to ten, I will need to submit the final list of attendees by 28 April. Please do not hesitate to contact me should you require any further information.

Best wishes
Helen

My program for the meeting of Nobel Laureates, signed and autographed!

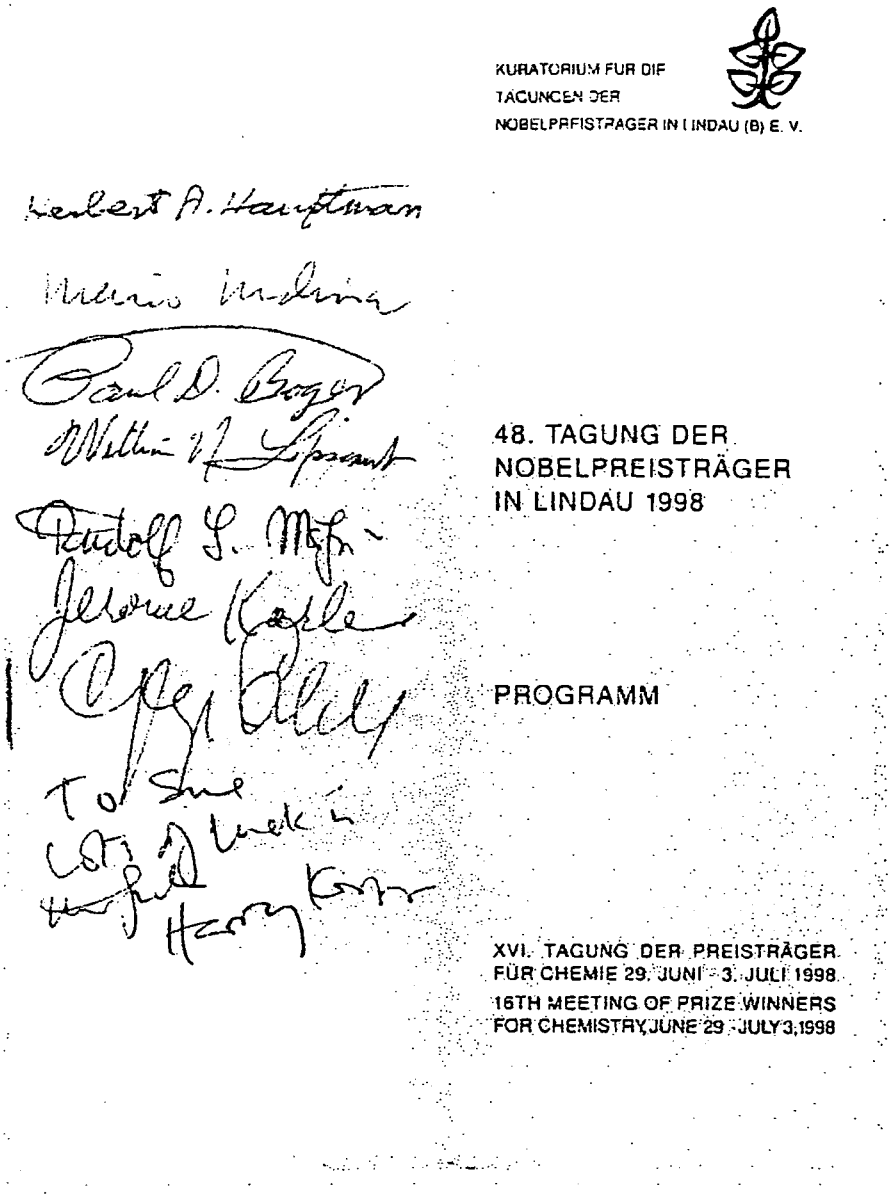

Name, year, and reason for winning the Nobel prize:

Herbert A. Hauptman and **Jerome Karle** (1985) for the development of direct methods for the determination of crystal structures; **Mario Molina** (1995) for atmospheric chemistry, particularly concerning the formation and decomposition of ozone; **Paul D. Boyer** (1997) for elucidation of the enzymatic mechanism underlying the synthesis of ATP (adenosine triphosphate); **William N. Lipscomb** (1976) for his studies on the structures of boranes illuminating problems of chemical bonding; **Rudolf L. Mossbauer** (1962-physics) for discovery of the 'Mossbauer effect' – the recoilless nuclear resonance absorption of γ radiation ; **George Olah** (1994) for his contribution to carbocation chemistry; **Harry Kroto** (1996) for the discovery of fullerenes.